ATTENUATION OF LEAKY MODES
AND
FILTERING TECHNIQUES
IN
GRADED INDEX MULTIMODE FIBRES

by

Halil Tanyer Eyyuboglu, B.Sc., M.Sc.

A Doctoral Thesis
Submitted in partial fulfilment of the requirements for the
award of Doctor of Philosophy of the
Loughborough University of Technology

October 1981

Supervisor: C Wilson, MSc, PhD.
Department of Electronic and Electrical
Engineering

To my sister Ayşe

LIST OF SYMBOLS

1. Latin Letters

A) Capitals

A, A_i	:	1st argument of Confluent Hypergeometric function
Ai	:	Airy function of first kind
A_n	:	normalized amplitude
B, B_i	:	2nd argument of Confluent Hypergeometric function
Be	:	Beta function
Bi	:	Airy function of second kind
B_s	:	source brightness
$C_1, C_2 .. C_n$		constants
C_k^n	:	Binomial coefficient
D	:	differential operator
Da	:	Dawson's integral
Db	:	integral function
D_q	:	integral function
Ep, Ep1, Ep2	:	argument of Airy functions
Eu	:	Euler's constant
F, F_i	:	transverse field function
G, G_i	:	longitudinal field function
$H_1 \ldots H_n$	:	combination of Bessel functions
H, H_m	:	Hankel function (Bessel 3rd kind)
I, I_m	:	modified Bessel function (1st kind)
I_{np}	:	integral function

J, J_m : Bessel function (1st kind)

K, K_m : modified Hankel function (modified Bessel 2nd kind)

L, L_p^n : Laguerre polynomial

M, M_i : Confluent Hypergeometric Function (1st kind)

N : number of modes in a fibre

P : power

$P_1, P_2 .. P_n$ used to denote cluster of terms

R, R_1 : radius of curvature for laser beam

$S_1, S_2 .. S_n$ scalar functions

S_p : sum notation

T : transmission coefficient

T_f : Fresnel reflection coefficient

U, U_i : derivative of Confluent Hypergeometric function w.r.t. first two arguments

Uh : Confluent Hypergeometric function (2nd kind)

V : normalized frequency of fibre

W : (1) transverse field function, (2) general function

X : function representing the characteristic equation

Y, Y_m : Bessel function (2nd kind)

Z_o : impedance of free space

B) Small Letters

a : core radius

b : cladding radius

c : jacket radius

d : distance

d/d(r,x etc)	:	differentiation with respect to
e, exp	:	exponential
f	:	radial source (LED) intensity parameter
fl	:	focal length
g	:	source directionality
h, h(r)	:	gradient function of core profile
i	:	integer, 1(2) HE(EH) modes
j	:	imaginary number $\sqrt{-1}$
k	:	integer used for summation
k_o	:	wave number of free space
k_m	:	mode radial parameter
k_r	:	ray radial parameter
ℓ	;	azimuthal mode number (integer)
$\overline{l}$	:	azimuthal ray parameter
m	:	azimuthal mode number (integer)
n	:	radial order of TEM modes (integer)
n(r)	:	refractive index distribution
n_1	:	refractive index at the core centre
n_2	:	refractive index of cladding
n_3	:	refractive index of jacket
p	:	radial order of fibre modes
q	:	core profile parameter
q_1	:	jacket profile parameter
r, r_1, r_2, r_3	:	radial variable
r_o	:	radial displacement
r_n	:	normalized radial variable

s	:	ratio of phase parameters (cladding to jacket)
s, s_1	:	laser beamwidth
s_o	:	narrowest width of laser beam
s_f	:	fibre spot size
t	:	(1) time variation, (2) general variable
u	:	phase parameter inside core
v	:	phase parameter inside jacket
w	:	phase parameter inside cladding
x	:	(1) distance along x coordinate (2) general variable
y	:	(1) distance along y coordinate (2) general variable
z	:	(1) axial distance (2) general variable
z_p	:	ray period

2. Greek Letters

α	:	attenuation coefficient
α_a	:	rotation angle of y-z plane
α_{mp}	:	excitation coefficient of modes
$\bar{\beta}$	:	axial phase parameter (ray)
β	:	axial phase parameter (mode)
β_1, β_2	:	normalized phase parameter (mode)
β_a	:	rotation angle of x-z plane
γ	:	refractive index difference between core and cladding
γ_1	:	refractive index difference between cladding and jacket
Γ	:	Gamma function
Γ_1	:	incomplete Gamma function

δ_1, δ_2	:	refractive index ratios
$\partial/\partial(r, \phi$ etc)	:	partial differentiation with respect to
Δ	:	refractive index difference between core and cladding
Δ_1	:	refractive index difference between cladding and jacket
$\varepsilon(r)$	:	permittivity distribution
ε_o	:	permittivity of free space
ε_1	:	permittivity at the core centre
ε_2	:	permittivity of cladding region
ε_3	:	permittivity of jacket region
η	:	power coupling efficiency
η_t	:	total power coupling efficiency
ν	:	order of Bessel functions (non-integer)
θ, θ_o	:	angle w.r.t. z axis
θ_c	:	critical angle
λ	:	wavelength in free space
μ_o	:	permability of free space
ϕ	:	azimuthal angle
ψ_p	:	phase angle
ψ, ψ_1	:	azimuthal angle
ψ	:	logarithmic derivative of Gamma function (Psi function)
ω	:	radiation (angular) freqiency

Notes: 1. Definitions of parameters $P_1 \ldots P_n$ are such that they will hold till redefined.

2. (a) For graphs plotted on the computer, subscripts are indicated by '_', i.e. r_o,
   (b) the same meanings of symbols apply for these graphs except (1) Greek letters are written with English pronunciation (2) the ray parameter $\bar{T}$ is denoted by capital L.

Abbreviations

Abs	:	absolute value
int	:	integer part
Im	:	imaginary part, also indicated by subscript 'm'
L.H.S.	:	left hand side
N.A.	:	numerical aperture
nor.	:	normalized
R.H.S.	:	right hand side
Re	:	real part, also indicated by subscript 'r'
w.r.t.	:	with respect to

CONTENTS

ACKNOWLEDGEMENTS

I would like to express my gratitude to the following people who contributed in the preparation of this work.

To Dr C Wilson for his continuous guidance and encouragement.

To Dr P J Stevens for helping in the initiation of the research programme.

To the people of STL (Standard Telecommunications Labs., ITT Research Centre in the UK) for their kind permission to enable me to gain practical experience in optical fibre and terminations. In particular I am indebted to Dr M Chown, Mr J Leach for the supply of the fibres which were used in the experiments.

To my dear parents and brothers without whose moral support the work would not have been possible.

To Dr G Evans (Mathematics Department, Loughborough University of Technology) for the loan of his subroutine which was used in the simulation of a number of important functions.

To the Head of the Department who kindly provided the necessary equipment.

To the members of staff in the mechanical workshop of the Electronic and Electrical Engineering Department for their assistance in the mechanical fabrication of the various items used in the experimental part of the project. I would also like to express my thanks to the people in the Chemistry Department.

I owe a great deal to a sincere friend who, due to his modesty, wishes to remain anonymous for the invaluable help in the evaluation of the 8 x 8 matrix.

To the Post Office of Turkey (PTT) who provided the financial assistance.

To Mrs J Smith for typing the manuscript and correcting the mistakes.

Finally I would like to mention the moral encouragement received from Miss V Gouldeli at the beginning of the research.

SYNOPSIS

This work is an investigation of leaky ray (mode) attenuation in graded multimode fibres.

In contrast to slab or rectangular dielectric waveguides, cylindrical fibres possess leaky modes which greatly modify their propagation properties. The power carried by such modes eventually diminishes to zero, thus adding no useful contribution to the signal transmission over fibre channels. Suitable filtering techniques are therefore proposed.

For a proper understanding of the problems involved the presentation of a detailed propagation theory is essential.

In the mathematical treatment, ray analysis and an approximate form of mode theory are given separately. The former leads to a pictorial representation that is easy to comprehend. The rigorous aspects of propagation on the other hand, have to be handled by mode theory. Where permissible, comparisons are made.

This is followed by a study of fibre excitation by various types of sources.

Finally experiments are carried out to test the validity of some of the theoretical derivations.

INTRODUCTION

The advent of high quality optical fibres has brought new dimensions to the field of communications. With attenuation figures down to 1 dB/km and bandwidths approaching GHz (1,2), there is certainly a great deal of attention being devoted to this new technology. In order to realize the impact, one needs only to look at the diversity of areas in which optical fibres have found application (3,4).

Despite the rapid progress since 1968, specifications still remain to be improved more and more.

Unlike the other types of guided transmission mediums such as coaxial cables or metallic waveguides, the transfer of signal from the source to the fibre (similarly from one fibre into the adjacent one) involves fine geometrical and mechanical accuracy. When micrometric tolerances are envisaged, it is easy to predict the resulting increase in the cost and complexity of systems employing optical fibres.

Therefore research has been conducted in an attempt to reduce losses and acquire acceptable coupling efficiencies.

Prior to the formulation of the problem, some basic knowledge of optical fibres will be presented.

a) Optical Fibres:

Normally fibres consist of two cylindrical layers, the inner part named core, the outer the cladding. The desired transmission takes place through the core, whereas the cladding provides a non-variant interface and protection against oxidisation and mechanical stress.

Optical fibres may be classified into two groups according to the refractive index profile; step index and graded index.

After light is launched into the fibre, it is collectively carried between the modes that the fibre can support. Since each mode is assigned a different propagation velocity, intersymbol interference may occur at the output. Single mode fibres are used to increase data rates. Another method in this direction is to control the grading of the refractive index in the core such that mode delay differences are equalized.

There are three known sources of dispersion in fibres, modal, mentioned above, material and waveguide dispersion. Clearly the first one is not experienced in single mode fibres.

Material dispersion arises because light sources do not radiate at a single frequency but comprise a finite spectrum of frequencies. The refractive index of the material being frequency dependent, ascribes to each frequency component a different velocity of propagation.

Waveguide dispersion (or delay distortion) is related to the dispersive nature of waveguides to which optical fibres belong.

A report previously submitted by the author gives adequate coverage of these topics (5).

In the fabrication of the fibre, purified silica is generally used being suitably doped during the process to establish the correct grading and the refractive index values.

Graded index fibres have assumed a position in practice as a compromise between step index and single mode fibres. Compared with the former, they offer much higher bandwidths, while owing to their size, simultaneously avoiding the stringent alignment requirements of single mode fibres.

b) Formulation of the Problem

Consider two fibres that are to be spliced. Obviously for the most efficient transmission, it would be expected that the receiving fibre intercepted all the light radiated from the first fibre. From basic principles, a number of approaches may be adopted.

The solid angle under which the light is emitted from the end face of a fibre is determined by the numerical aperture of the fibre, the launching angle on the source side and the degree of homogeneity in the fibre. Assuming full illumination by the source, then all possible rays (modes) would be excited. With a limited angle of incidence, only certain types of modes would come into existence. In both instances however mode conversion inside the fibre itself will occur, if it contains inhomogeneities such as geometrical deformation axially or in transverse directions, or variations in refractive index profile axially. Mostly this is seen to be from low order modes to the higher ones (6).

Omitting this phenomenon, propagation would proceed in the following manner. The refracting rays would be extracted almost immediately leaving solely guided and leaky rays. Next the leaky rays would gradually radiate out from the cladding at a rate depending on their skewness. Finally the light emerges from the end face being a combination of trapped and leaky rays. In the event of multimode step index fibres, it is possible to identify the bound and leaky rays on the far field radiation pattern as the inner and outer regions respectively.

One way in which to ensure that the second fibre can capture the maximum amount of light is to place it as close as possible to the transmitter. Apart from the evident physical reason, this would have the advantage of moving the rays with small emission angle further down towards the core centre. For the case of graded index fibres, they then impinge upon areas where the numerical aperture for trapping is wider. In passing, it is worth

noting that bringing the fibres closer would also increase the reflections from the ends. This is normally minimized by using index matching liquid (7).

It is equally possible to formulate other techniques, for instance the utilization of a lens in the interfacing medium to focus the light on the entrance of the coupled fibre. This, however, causes additional alignment problems and also adds to cost.

Nevertheless, regardless of the method applied, one obstacle is still present. That is the existence of leaky rays. Because all leaky modes of the first fibre would continue to be leaky upon launching into the second fibre.

The persistence of leaky rays primarily related to fibre length and other characteristics. The attainment of a steady state condition may require a fibre length of several kilometres (8). Hence for a long-haul transmission network such as a telephone system, leaky rays may not be of major importance. In short distance communication on the other hand, their effect must be taken into account.

To summarize, leaky rays (modes) represent either the portion of the light power that would eventually be lost in the transmission, or the unwanted modes which merely serve to increase signal distortion.

To appreciate the scale of the problem, the reader is referred to Table A which lists a series of coupling measurements, taken at STL. The alignment was made through the probe of a 1 μm step motor driven micropositioner. Both the launching end of the first fibre and the exit end of the coupled fibre were mode stripped terminations. These were basically jewelled-ferrule structure with extension tubes of approximately 7.5 cm. To provide the filtering, the bare fibre inside the tube was embedded in epoxy. But from the readings, it is not difficult to observe that this was really unsatisfactory.

TABLE (A)

Receiving Fibre

Transmitter Diameter (micro m.)	47	48	49	50	51	52	Diameters measured with scanning eye piece
47	(13.28)	10.76	10.64	11.02	11.24	10.95	47.075
48	10.90	(21.50)	12.04	14.89	15.53	14.10	48.425
49	10.31	11.25	(14.79)	11.75	11.76	11.79	48.95
50	10.71	13.84	11.95	(19.63)	14.24	12.45	49.725
51	11.03	14.99	12.14	14.39	(21.30)	13.59	50.625
52	10.86	13.95	11.92	13.68	14.19	(16.74)	51.3

Notes : 1) Figures are in 'micro W'

2) Dioganal figures in brackets indicate power levels obtained by coupling the fibre straight into optometer

3) Source : LED , Detector : Optometer from United Detector Tech.

Thus, a proper filtering scheme would have to be devised.

c) Conclusions

From the preceding, it is seen that two methods to control the presence of leaky modes in fibres, may be suggested. One is to make arrangements on the launching side such that leaky modes are not excited. This choice furthermore limits the type of source to be used.

As generally known lasers have outputs which are very nearly Gaussian. Axial launching from such a source will excite certain types of modes alone. If the beam radius of the laser is comparable in magnitude with the spot size of the fibre, most of the power will be concentrated in the low order modes.

Light emitting diodes (LEDs) present quite a different picture. It is relatively more difficult to collimate the radiation from an LED. For an incoherent illumination such as that of an LED, the power is distributed uniformly amongst all the modes of the fibre. A probable approach to decrease the power going into leaky rays would be to confine the maximum of incidence subtended at the fibre face to the meridianally defined numerical aperture. This could be successfully applied to step index fibres. Unfortunately for graded index fibres bound and leaky rays have an overlapping angular region in which both types of rays are equally accepted.

A second method is to filter leaky modes after they have entered the fibre. This is accomplished by placing the fibre in a dielectric medium where refractive index is higher than that of the cladding. A variety of chemical fluids may be used for this purpose. However, care must be taken to ensure that the transmission properties of guided modes remain unaltered.

It is the objective of this study to utilise the latter technique for analysing the effect of leaky modes.

In order to gain a deeper understanding of the subject, a detailed propagation theory must now be introduced. From this, the framework relevant to excitation and mode filtering will be derived.

d) Introduction to Theory of Propagation in Fibres

It has long been established that two complementary approaches may selectively be used in the theoretical treatment of optical phenomenon.

Geometrical ray theory is a powerful tool affording a conceptual aid for a number of optical problems. Being a simple procedure, it contains large approximations and only gives the macroscopically correct interpretation. Generally speaking, its validity is restricted to the ratio of the system components to the wavelength of light. As this ratio increases, the effects of the assumptions of the macroscopic theory diminish, thus the accuracy increases.

Mode theory is based upon Maxwell's equations. Inevitably it produces more complete descriptions for all types of optical observations. In the limit of a few wavelengths, the ray analysis can no longer quantify the propagation in fibres adequately. Hence the mode theory has to be invoked for such cases.

Even then however, it is extremely rare to find the precise forms of the wave equations being preserved. Very frequently perturbations are carried out to result in much simplified derivations. This is due to the fact that exact solutions are incredibly complex in essence and time consuming to compute, whereas reduced formulas often yield satisfactory results.

Before embarking upon mathematical details, an attempt is made to eludicate two issues of central importance:

1. The dividing line between mode theory and ray analysis.

2. Different assumptions entailed in the derivations.

Fundamental knowledge suggests that ray representation is ultimately the solutions to Maxwell's equations with the uniform plane wave approximation, i.e. when the wavefront has zero curvature. One way to achieve this is to let the wave number approach infinity.

However in this the representation does not take into account the phase information. The introduction of the phase information into the ray picture leads to a set of discrete modes of propagation. The quantization is such that rays with common labels constitute the same mode.

A physical interpretation of this would be to imagine the radiation output of a waveguide falling onto a plane positioned across its end face. Each geometrical line that could be conceived to extend from the waveguide to the plane (within the limits of numerical aperture) might be regarded as a single ray, while the density of these consistently grouped would nominate a particular mode.

A mode is able to retain its unique characteristics provided that it is not disturbed by other modes travelling within the same confinement.

It is well known that the properties of single mode fibres exclusively match those of coherent sources. This is because the desired transmission in such fibres occurs in the fundamental mode alone. Therefore here the use of mode theory would be indispensible.

On the other hand both coherent and incoherent sources might be equally considered suitable for multimode fibres. Normally the adoption of coherent excitation would accompany the aim of concentrating more power into the fibre. Under specific circumstances, the launching parameters may be refined to generate a restricted number of modes or even one mode. In order to express the uniqueness

of the individual modes, a more rigorous solution of Maxwell's equations is necessary and that essentially means mode theory. With the increase in the number of modes, the wavelength dependence conferred from the beam of incidence is progressively destroyed. Consequently the descriptions of the modes approach the plane wave condition.

The case of incoherent excitation is readily resolved since the source itself now radiates in a wide range of modes.

The discussion of the second part can perhaps be best initiated by referring to dyadic Green's function which formulates completely the problem of source excited field in an arbitrary dielectric environment (9). From these it is feasible to proceed to all specialized configurations.

The reduction of the general formula to the practical fibre medium is accomplished by recognizing the important fact that the maximum numerical value of the refractive index in the core is very close to that of the cladding. In this situation, the fields can be constructed from scalar wave functions. Despite the great deviation that might be found (refractive index of the core twice of the cladding), the accuracy of this assumption is remarkable (10% maximum error) (10).

Such fibres possess a mechanism of weak guidance of the modes, hence the nomenclature 'weakly guiding fibres' was given.

Depending on the type of mode under investigation, other assumptions may be envisaged. The neglect of the cladding boundary is one of them for instance when dealing with low order modes. Also very frequently, the cladding will be considered to extend to infinity in the case of two layered structures. Obviously each level of approximation may call for a new mathematical approach. These are to be elaborated in the forthcoming sections.

The subject of ray analysis has extensively been covered in a number of sources. Thus for a majority of items, it will suffice to present brief accounts only. Branching in a particular direction will be conducted according to its relevance to the rest of the work.

Despite the wide availability of literature, the treatment of mode theory has somewhat been confusing and not well understood. There is the extra complication that the characteristic equation becomes extremely difficult to handle upon the addition of the outer jacket. Therefore it was decided to devote more space to mode theory.

CHAPTER I

GEOMETRICAL RAY THEORY

1.1 Elementary Analysis

For ease of comprehension, the presentation is firstly on step index fibres.

A general ray striking the core-cladding interface is characterized by angles θ, Ψ as shown in Figure 1.1. The projection of the incident ray on fibre cross-section defines the angle Ψ. A further angle θ_n is indicated which is related to θ and Ψ by the equation at the bottom of the illustration.

If $\Psi = \pi/2$ implying that the ray projection passes through the core centre, then the ray is said to be meridional, otherwise it is skew where Ψ becomes a measure of skewness.

The behaviour of the rays in the fibre will depend on the angles of incidence. Referring to Figure 1.1a, the critical angle may be expressed as:

$$\theta_c = \text{Cos}^{-1} \frac{n_2}{n_1} \tag{1.1}$$

where n_2 and n_1 denote the refractive index values for cladding and core respectively.

Taking the simple case $\Psi = \pi/2$, the rays will be trapped inside the core provided that

$$\theta < \theta_c \ (\text{i.e. } \text{Cos}^{-1} \frac{n_2}{n_1}) \tag{1.2}$$

and when

$$\theta > \theta_c \tag{1.3}$$

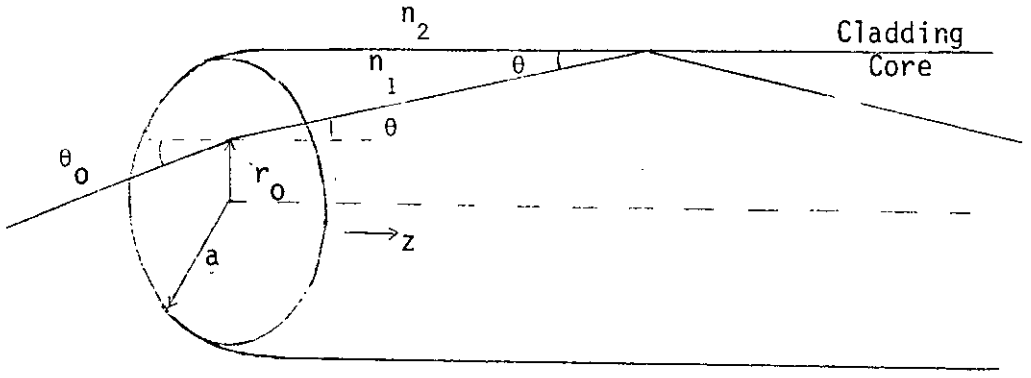

(a) Ray on Fibre Front Face

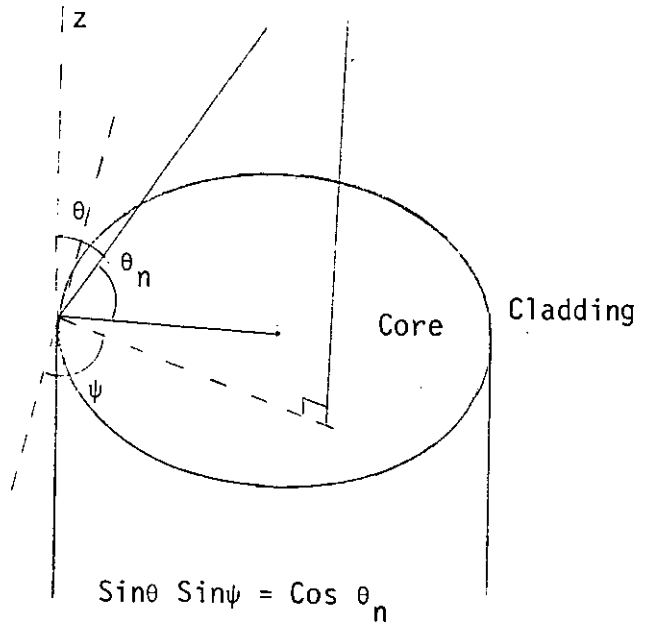

Fig.1.1(b) Cross-sectional View on Incidence at the Boundary

they will be refracted.

With skew rays, equation 1.2 still holds. For total refraction however, additional requirements prevail when $\theta > \theta_c$ but simultaneously

$$\theta_n > \pi/2 - \theta_c \tag{1.4}$$

then the ray is partially trapped, i.e. leaky. Only the set of conditions

$$\theta > \theta_c \quad \text{and} \quad \theta_n < \pi/2 - \theta_c \tag{1.5}$$

lead to completely refracting rays.

It is this second group of rays which has widely enjoyed the attention of many authors. By now with the aid of the models developed, the full effect of leaky rays can be incorporated into the simple ray picture.

Separate numerical aperture (N.A.) equations may be written:

$$\text{N.A.} = n_1 \operatorname{Sin}\theta_c = (n_1^2 - n_2^2)^{\frac{1}{2}} \text{ for meridional rays} \tag{1.6}$$

$$\text{N.A.} = (n_1^2 - n_2^2)^{\frac{1}{2}}\left[1 + \left(\frac{(r_o/a)\operatorname{Sin}\Psi_1}{1+(r_o/a)\operatorname{Cos}\Psi_1}\right)^2\right]^{\frac{1}{2}} \text{ for skew rays} \tag{1.7}$$

where $\Psi_1 = \text{Cos}^{-1} [-(r_o/a) \text{ Cos } \Psi] + \Psi$ and r_o is the radial distance from the core centre on fibre entrance (Figure 1.1a).

The acceptance angle of meridional rays is constant across the fibre end face, while that of skew rays is a function of radial position in addition to the expected dependence on the skew angle.

For a closer examination, graphs are plotted for the numerical aperture equation (see Figure 1.2) where the variations against both parameters (Ψ and r_o) are displayed.

The next natural step seems to be the introduction of the N.A. expression of graded index fibres, so that comparisons can be made.

$$\text{N.A.} = (n_1^2 (r_o) - n_2^2)^{\frac{1}{2}} \tag{1.8}$$

$$\text{N.A.} = \left[\frac{n_1^2(r_o) - n_1^2}{1 - (r_o/a) \text{ Cos}^2 \Psi}\right]^{\frac{1}{2}} \tag{1.9}$$

Again the upper formula is for meridianal rays alone and the lower to cover all rays. The fibre is assumed to have a profile of

$$n(r) = n_1 [1 - 2\Delta (r/a)^q]^{\frac{1}{2}} \quad \text{when } r \leq a$$

$$n(r) = n_1 (1 - 2\Delta)^{\frac{1}{2}} = n_2 \quad \text{elsewhere} \tag{1.10}$$

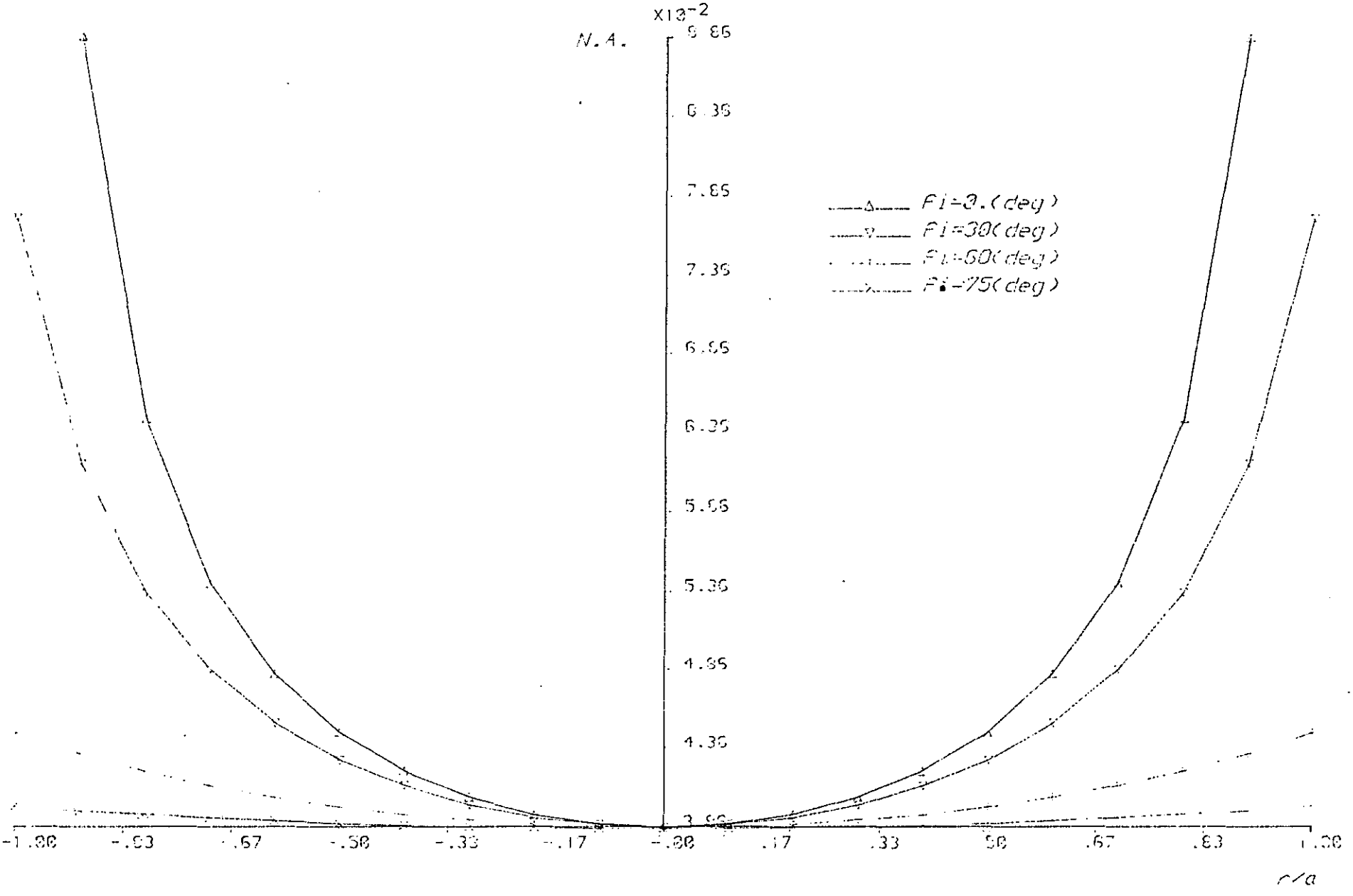

Fig. 1.2 Variation of Numerical Aperture For Step Index Fibre

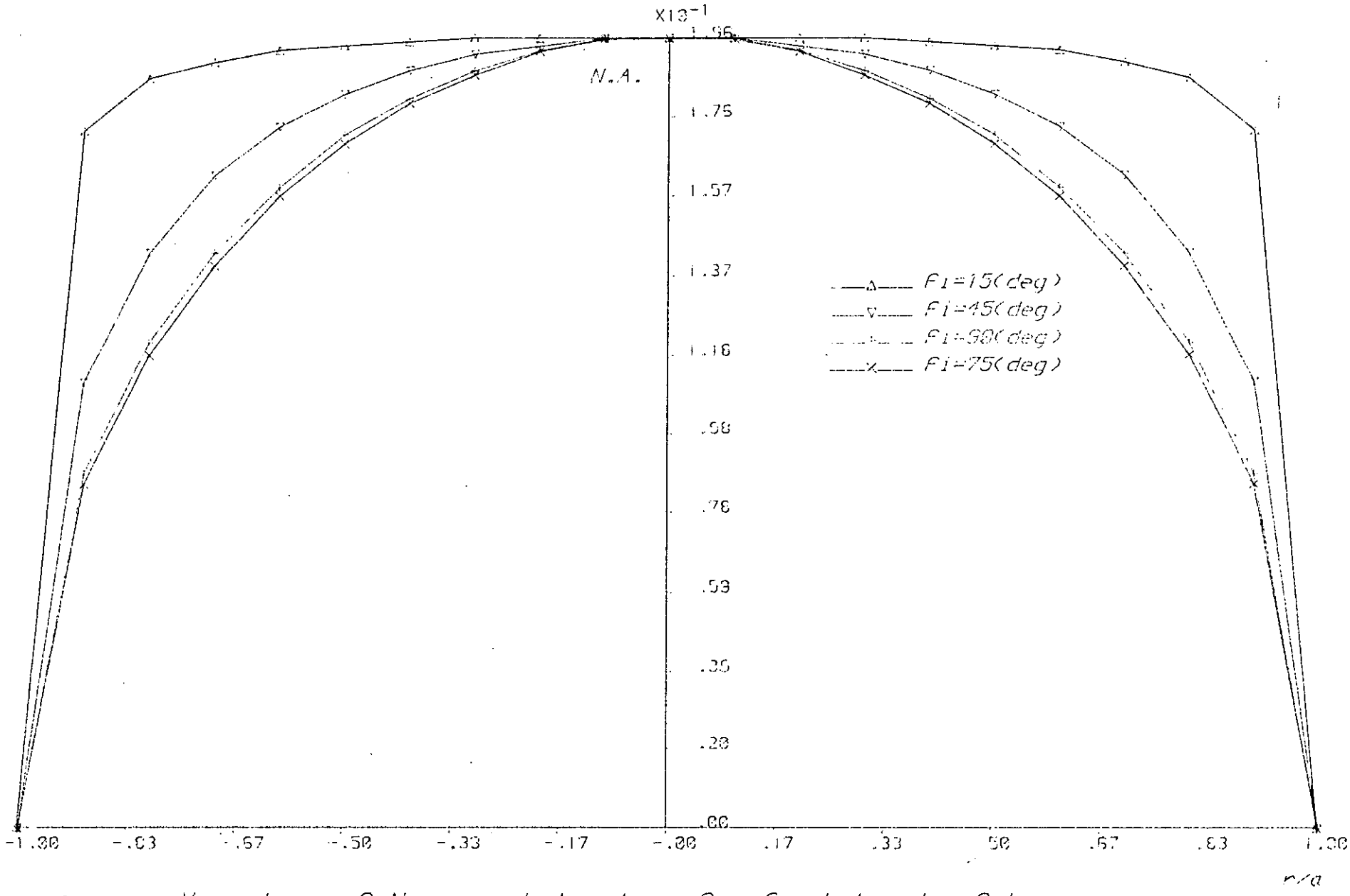

Fig. 1.3 Variation of Numerical Aperture For Graded Index Fibre

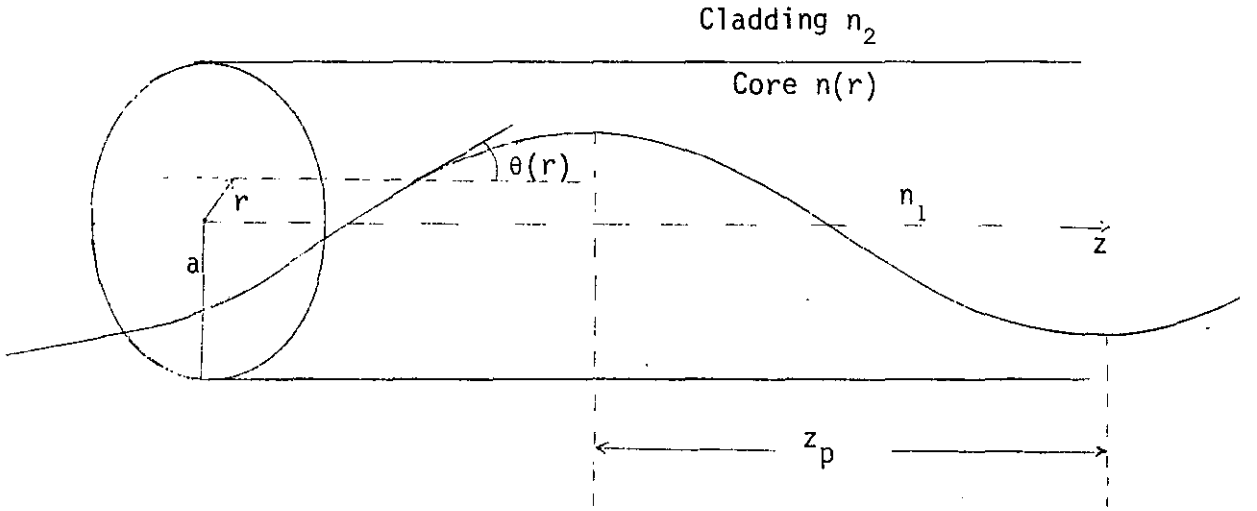

(a) Propagation in Fibres of Graded Index

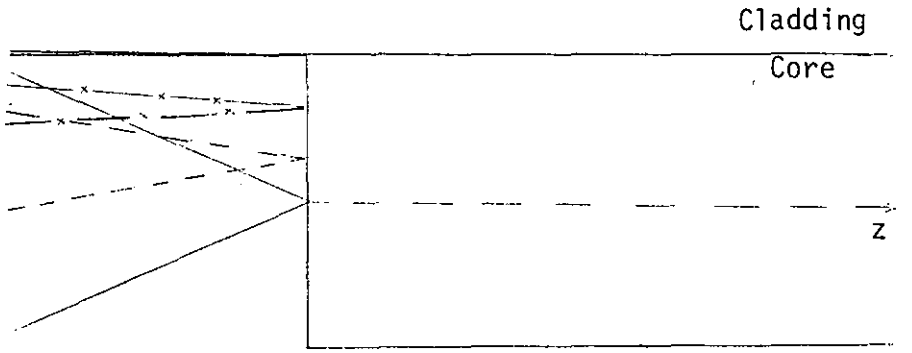

Fig. 1.4(b) Variation of N.A. over Entrance Face

where the new term introduced may be related to the critical angle by $2\Delta = \mathrm{Sin}^2\theta_c$. n_1 is the refractive index value of the core centre. q denotes the profile parameter such that q = 2 for parabolic case.

In this instance owing to the gradient, the numerical aperture also changes radially. This is shown schematically in the drawing of Figure 1.4b. The graphs in Figure 1.3 depict the numerical aperture as functions of r_o and Ψ.

From the above survey, the important conclusions may be summarized as: (a) step index fibres are capable of collecting more light than their counterparts graded index fibres, (b) the acceptance angle of skew rays in fibres with step index profile is always greater than that of meridianal rays, (c) by contrast, the maximum numerical aperture of a graded index fibre is $2\Delta n_1$ occurring at the centre of the core. As the position moves into the fibre's periphery, the acceptance angle decreases monotonically and reaches zero at the core-cladding interface.

1.2 In-Depth Analysis

In graded index fibres, because of the radial slope in the index of refraction, the trajectory traversed by the ray is no longer straight, but becomes helical instead (see Figure 1.4a).

The electromagnetic field on the grounds of geometrical optics may be synthesized in locally plane waves (1). By orientating the cylindrical coordinates suitably, the phase integral via the use of eikonal equation reveals two quantities which are constant along the ray path. These are

$$\overline{\beta} = n(r)\ \mathrm{Cos}\,\theta\,(r) \qquad (1.11)$$

$$\bar{\ell} = (r/a)\ n(r)\ \mathrm{Sin}\,\theta(r)\ \mathrm{Cos}\,\Psi(r) \qquad (1.12)$$

where the angles $\theta(r)$ and $\Psi(r)$ have their previous meanings and (r) indicates the radial dependence. $\bar{\beta}$ and $\bar{\ell}$ constitute the modal equivalence of axial (β) and azimuthal (ℓ) components of the wave.

It is easily recognised that $\bar{\ell} = 0$ for meridional rays.

Adopting the profile of equation 1.10, a consistency requirement may be derived by demanding r remain positive as $\Psi \to 0$.

Thus

$$\gamma^2\, r_n^{q+2} - (n_1^2 - \bar{\beta}^2)\, r_n^2 + \bar{\ell}^2 = 0 \qquad (1.13)$$

where alternative definitions

$$r_n = r/a \qquad \text{and} \qquad \gamma = (n_1^2 - n_2^2)^{\frac{1}{2}}$$

are used.

When the derivative of 1.13 is set to zero, an upper limit is fixed for $\bar{\ell}^2$.

$$\bar{\ell}^2_{max} = q \left(\frac{n_1^2 - \bar{\beta}^2}{q+2}\right)^{1+\frac{2}{q}} \left(\frac{2}{\gamma^2}\right)^{2/q} \qquad (1.14)$$

It is now feasible to categorize the rays into:

1. Guided: $$n_2 \leq \bar{\beta} \leq n_1$$
$$0 \leq \bar{l} \leq \bar{l}_{max} \qquad (1.15)$$

2. Leaky: $$\max\,[0,(n_1^2 - \gamma^2 q/2)^{\frac{1}{2}}] \leq \bar{\beta} \leq n_2$$
$$(n_2^2 - \bar{\beta}^2)^{\frac{1}{2}} \leq \bar{l} \leq \bar{l}_{max} \qquad (1.16)$$

3. Refracting: Any positive and real values of $\bar{\beta}$, $\bar{l}$ obeying:

$$\bar{\beta}^2 + \bar{l}^2 \leq n_2^2 \qquad (1.17)$$

This classification is also illustrated in Figure 1.5 as what is called the $\bar{\beta}$ - $\bar{l}$ domain*. Subject to the consistency requirement, the area to the right of $\bar{l}_{max}$ represents the physically unrealizable rays.

The $\bar{\beta}$ - $\bar{l}$ diagram has proven to be an invaluable aid in studying rays of all types, but especially leaky ones. Further reference to the diagram will be made later.

A certain function $k_r(r)$ associates $\bar{\beta}$ and $\bar{l}$ in the following manner

$$k_r(r) = [n^2(r) - \bar{\beta}^2 - (a\,\bar{l}/r)^2]^{\frac{1}{2}} \qquad (1.18)$$

This delineates the motion of the ray in the transverse directions

---

* Note that in this and the subsequent graphs $\bar{l}$ is shown as L for easier identification.

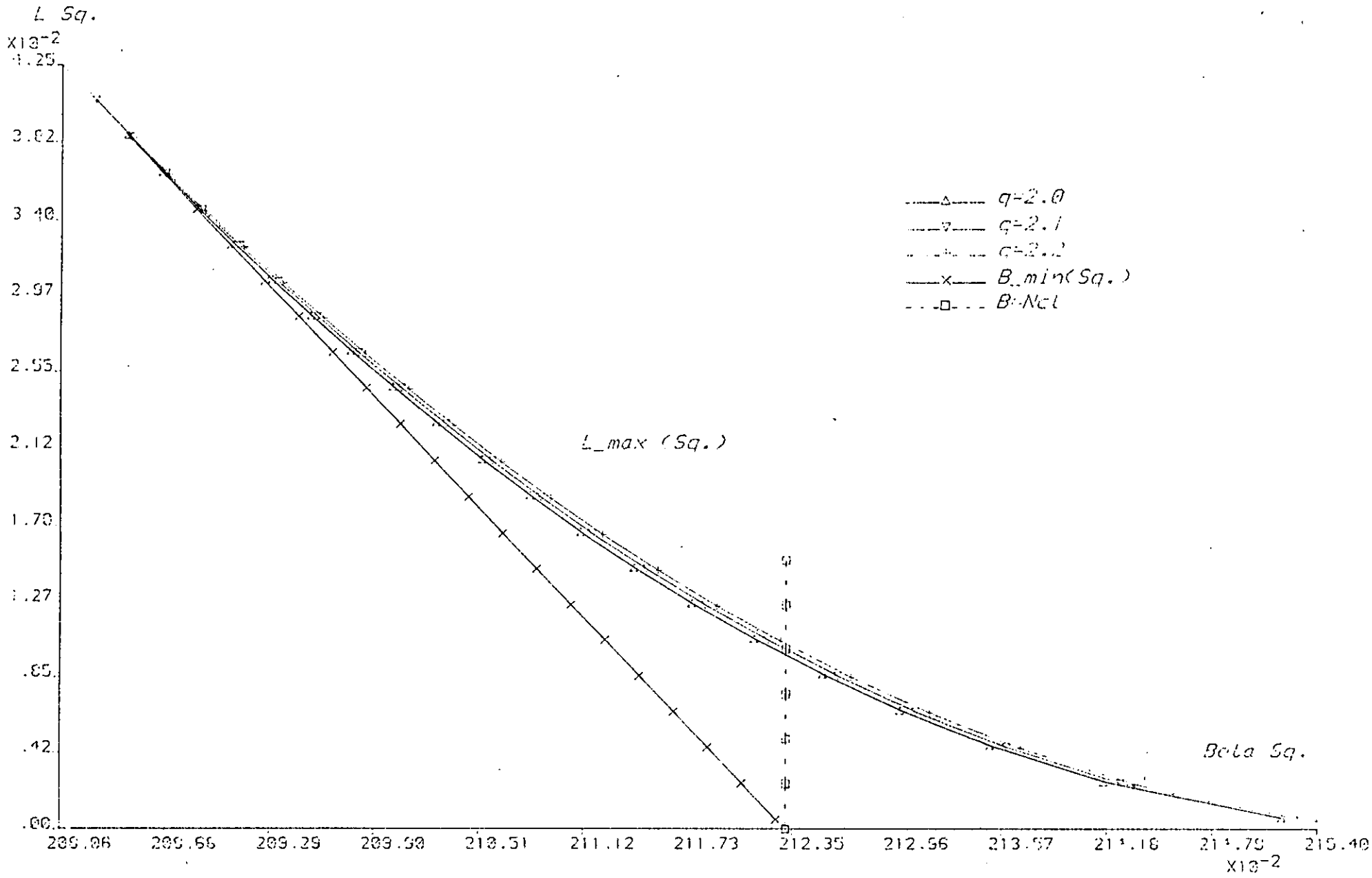

Fig. 1.5 Ray Parameters For different profile values

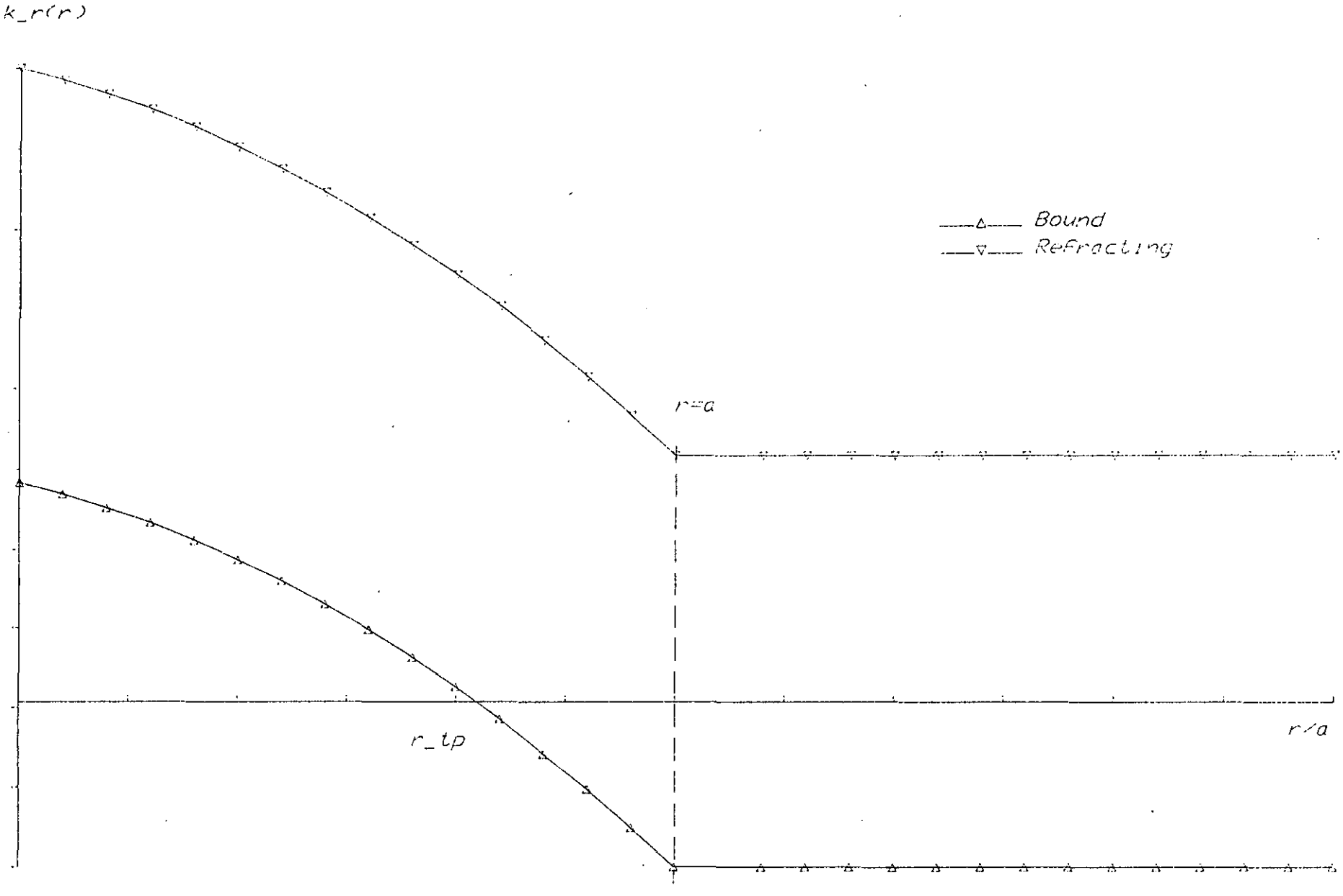

Fig. 1.6 Plots of Meridional ray Domains

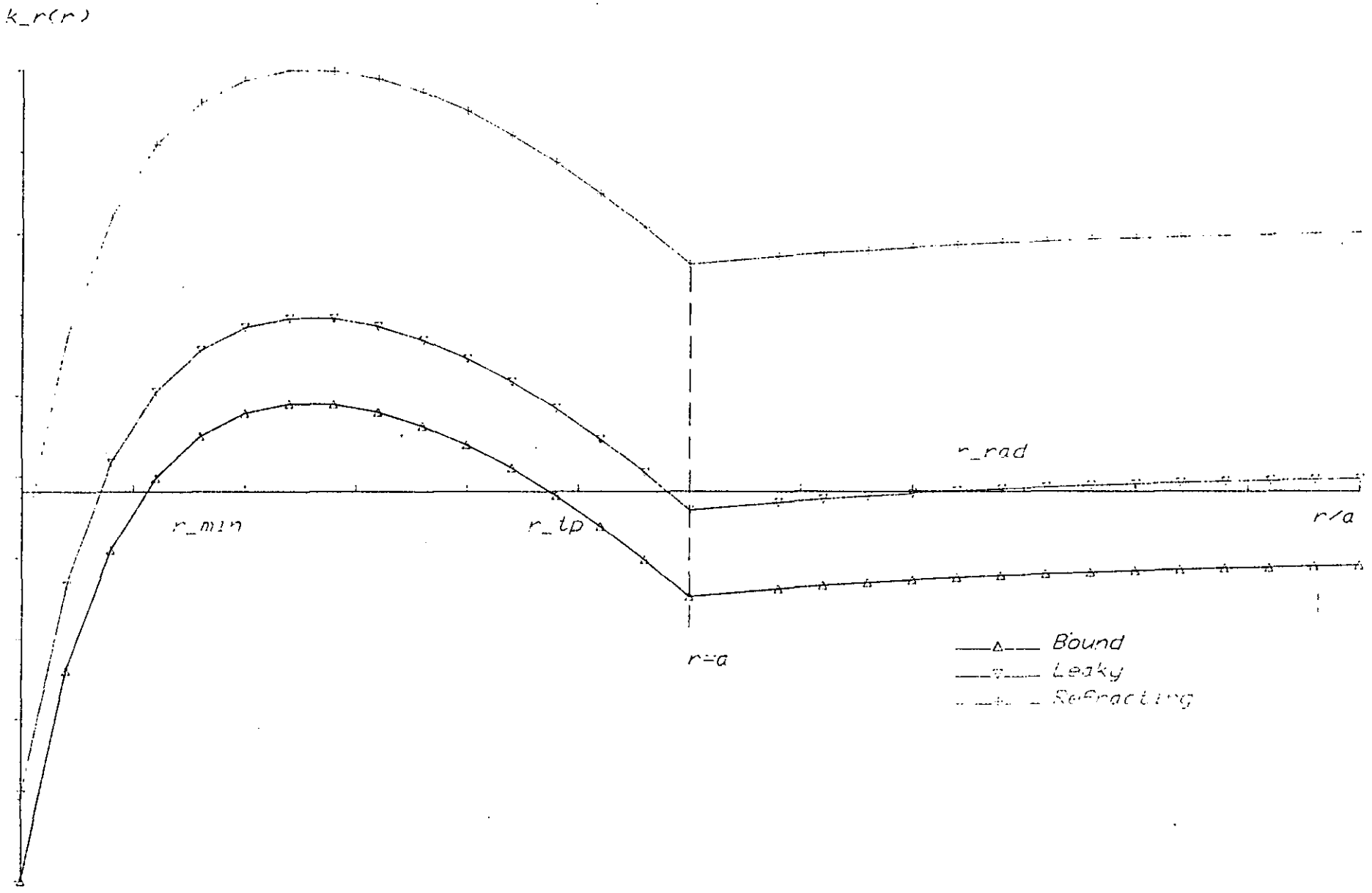

Fig. 1.7 Plots of Skew ray Domains

with respect to the longitudinal axis, may thus be regarded as the radial component. Plotting $k_r(r)$ for different values of $\bar{\beta}$ and $\bar{l}$ reveals the existence of several crossing points. A general ray, skew leaky, will have three of such points, while a refracting ray will never reach the r axis (Figures 1.6 and 1.7). The first two roots (r_{min}, r_{tp}) define a zone within which the ray travels in the fibre. The most outer point locates the emergence of the leaky ray after having tunnelled through the region of evenescence.

The two areas $0 < r < r_{min}$ and $r_{tp} < r < r_{rad}$ will be seen as black bands if viewed under a microscope, and are sometimes referred to as caustics (2).

It is with this familiar process of electromagnetic tunnelling that leaky rays lose a fraction of their transmitted power to radiation. Expressions to compute their attenuation have been described in various works (3-5). To facilitate a proper understanding on the subject however, the wave equation must be introduced at this stage.

1.3 Wave Equation and Leaky Ray Attenuation

The scalar wave equation in cylindrical coordinates is:

$$\frac{d^2 S_1}{dr^2} + \frac{1}{r} \frac{d S_1}{dr} + k_o^2 [n^2(r) - \bar{\beta}^2 - \bar{l}^2 (a/r)^2] S_1 = 0 \qquad (1.19)$$

S_1 defines the field distribution and $k_o = 2\pi/\lambda$ is the wave number λ being the wavelength. The collection of terms in the brackets may immediately be identified as $k_r(r)$.

After carrying out the transformation $S_2 = S_1 r^{\frac{1}{2}}$

$$\frac{d^2 S_2}{d r^2} + k_o^2 \left[n^2(r) - \bar{\beta}^2 - \left(\bar{l}^2 - \frac{1}{(2k_o a)^2}\right)(a/r)^2\right] S_2 = 0 \tag{1.20}$$

The term $1/(2ka)$ is small compared to $\bar{l}$, therefore may be dropped so that

$$\frac{d^2 S_2}{d r^2} + k_m^2(r)\, S_2 = 0 \tag{1.21}$$

here $k_m(r) = k_o\, k_r(r)$

However even with this omission, it is extremely difficult to formulate a closed solution to 1.21 for a general q profile, unless certain constraints are imposed.

One such case is the Airy function uniform approximation.

By subsequent alteration of equation 1.21 to a new variable Ep and a function $S_3(6)$

$$Ep\,(Ep')^2 = k_m^2 \tag{1.22a}$$

$$S_3 = (Ep')^{\frac{1}{2}}\, S_2 = (k_m^2/Ep)^{\frac{1}{4}}\, S_2 \tag{1.22b}$$

prime denotes differentiation with respect to r.

The differential equation then reads

$$\frac{d^2 S_3}{d\, Ep^2} + [Ep + \frac{1}{4\ (Ep')^2}\ ]S_3 = 0 \qquad (1.23)$$

An accurate representation in terms of Airy functions is permissible if

$$\frac{1}{4\ (Ep')^2} << Ep \qquad (1.24)$$

Accepting the above condition to hold well, upon rearranging the substitutions

$$S_2 = \frac{Ep^{\frac{1}{4}}}{k_m^{\frac{1}{2}}} C_1[Ai\ (-Ep) \mp j\ Bi\ (-Ep)] \qquad (1.25)$$

where C_1 is a constant, Ai and Bi are Airy functions described in Appendix B.

The relationship between Ep and $k_m(r)$ may be expressed via a single integral

$$Ep = [(3/2)\int k_m(r)\ dr]^{2/3} \qquad (1.26)$$

Finally the transmission coefficient, which is the ratio of the power lost into the cladding to the total incident power on

the interface from the derivation discussed in Appendix A, is

$$T = \frac{4}{\pi^2} \frac{P_3}{P_4^2 + P_5^2} \tag{1.27}$$

where

$$P_4 = P_2 \,(Ai1\, Ai2 - Bi1\, Bi2) - P_3 \,(Ai1\, Ai2' - Bi1\, Bi2')$$

$$- Ai1'\, Ai2 + Bi1'\, Bi2 \tag{1.28a}$$

$$P_5 = P_2 \,(Ai1\, Bi2 + Bi1\, Ai2) - P_3 \,(Ai1\, Bi2' + Bi1\, Ai2')$$

$$- Bi1'\, Ai2 - Ai1'\, Bi2 \tag{1.28b}$$

$$Ai1 = Ai\,(Ep1),\ Ai2 = Ai(Ep2),\ Bi1 = Bi(Ep1),\ Bi2 = Bi(Ep2)$$

The derivative of Airy functions are distinguished by the prime sign, while the definitions of P_2, P_3

$$P_2 = - Ep1^{\frac{1}{2}} \left[(Ep1^{-3/2} + Ep2^{-3/2})/4 - \gamma^2/(2ak_0\, P_1^3)\right] \tag{1.29a}$$

$$P_3 = (Ep1/Ep2)^{\frac{1}{2}} \tag{1.29b}$$

and

$$P_1 = (\bar{\beta}^2 + \bar{1}^2 - n_2^2)^{\frac{1}{2}} \tag{1.30}$$

Ep1 and Ep2 are the definite integrals of 1.26 with the corresponding limits r_{tp} to a and a to r_{rad}.

With the solution outlined so far, it becomes necessary to test the region of validity. The extra term present in equation 1.23 is 1/4 $(Ep')^2$ or from 1.22a

$$\frac{1}{4(Ep')^2} = \frac{Ep}{4\ k_m^2} \tag{1.31}$$

It is easy to verify that k_m and Ep tend towards zero simultaneously. This occurs at the division between tunnelling and refracting rays. Irregularities would therefore be observed in this neighbourhood.

A particular method to ensure a smooth transition between the two sectors is given in Ref 4, i.e. linearizing both sides of the interface. The same result will be attained by taking the limiting values of P_2 and P_3.

There is a serious drawback however to the solution of Ref 4. For the majority of rays, the turning point r_{tp} is situated close to the boundary, though the radiation caustic may be further away. The act of linearization will then decrease the Ep2 values drastically. Thus, the transmission coefficient would appear to be larger than it actually is.

In this report, the Airy function representation stated here will be adopted as a reasonable fit, since it provides the best resolution in the region of weakly leaky rays.

Another approach, greatly simplified, yet effective, is the well known WKB expression which is an exact solution of the differential equation (7).

$$\frac{d^2 S_2}{dr^2} + [k_m^2 + \frac{k_m''}{2k_m} - (\frac{k_m'}{k_m})^2 (3/4)] S_2 = 0 \qquad (1.32)$$

prime means d/dr.

This equation differs from that of 1.21 via the last two terms.

The representation is;

$$(WKB)\ S_2 = \frac{C_1}{k_m^{\frac{1}{4}}} e^{\mp j \int k_m dr} \qquad (1.33)$$

Following the presently explained steps leads to

$$T_{WKB} = \exp\ (-\ 2 \int_{r_{tp}}^{r_{rad}} k_m\ dr) \qquad (1.34)$$

Alternatively this may be obtained directly by invoking the asymptotic forms of Airy functions in 1.27.

Due to the difference between the limits vanishing the WKB procedure is expected to fail for highly leaky rays. The transmission coefficient in this instance approaches unity. Furthermore, the WKB based field expressions are very inaccurate in the vicinity of caustic (8).

Now to deduce the attenuation coefficient it is convenient to write the power flow in the fibre as

$$P(z) = P(0)\ e^{-\alpha z} \qquad (1.35)$$

where $P(0)$ is the initial power supplied by the source. $P(z)$ thus accounts for the power at a position z on the fibre axis. In order that α measures the attenuation per unit length, it must be coupled to T through

$$\alpha = \frac{T}{z_p} \tag{1.36}$$

with z_p being the axial distance between successive reflections (Figure 1.4 a).

The power left in a particular ray after having travelled a certain distance z could be calculated from 1.35. To get the overall attenuation, a summation over all rays would be needed such that

$$P_{tot}(z) = \int_{\bar{\beta}} \int_{\bar{T}} P(0)\, e^{-\alpha(\bar{\beta},\, \bar{T})z}\, d\bar{\beta}\, d\bar{T} \tag{1.37}$$

where the limits of the integration are to be determined by the excitation conditions. If full excitation is applied, they cover the entire $\bar{\beta}$ - $\bar{T}$ domain defined by the fibre parameters.

In general, the individual power associated with each ray may be different. However it has been established that incoherent sources distribute their power equally amongst the fibre modes (9,10) and this state is reached rapidly with coherent sources when the total number of propagating modes exceeds 10 or so (Ref. Chapter III).

Thus within the confines of geometrical optics, the integral in 1.37 remains valid. To continue with T expressed in terms of Airy functions is quite cumbersome. As already pointed out

T_{WKB} formula may be used to an advantage.

A suitable strategy has recently been developed to this effect (11-13). The underlying philosophy is to neglect the contribution of strongly attenuated rays, since they die out in a short interval from the launching end.

Such an upper bound is fixed by letting

$$\exp\ (-\ T\ z/z_p) = 1 \tag{1.38}$$

or, after taking the log of both sides

$$\ln\ T + \ln\ (z/z_p) = 0 \tag{1.39}$$

To proceed analytically, the ray period of a parabolic fibre may be taken as an example. From Appendix A this is seen to be

$$z_p = \bar{\beta}\, a\pi/\gamma \tag{1.40}$$

However, the range of variation for $\bar{\beta}$ throughout the ray domain concerned is very small. Hence $\bar{\beta}$ may be set to its maximum value i.e. n_2*.

Moreover, the T as a WKB approximation may be further simplified by avoiding the integration over the core region. This choice is justified provided that the separation between the radiation point

---

* Note that the authors mentioned in the references have used $\bar{\beta} = n_1$

and the core-cladding boundary is appreciably larger than that of the turning point. A better compromise might be to employ the expansion explained in Appendix A to acquire

$$T_{core} = \exp\left(-2\left[\frac{k_o a\,(\bar{\beta}^2 + \bar{T}^2 - n_2^2)^{\frac{1}{2}}}{(q\,\gamma^2 - 2\,\bar{T}^2)}\right]\right) \qquad (1.41)$$

In keeping with the conventions of Colin Pask (12), the following parameters will be written

$$\bar{\beta}_n = \frac{(n_2^2 - \bar{\beta}^2)}{\gamma^2\,(q/2)} \qquad (1.42a)$$

$$\bar{l}_n = (2/q)^{\frac{1}{2}}\,\bar{T}/\gamma \qquad (1.42b)$$

On adding the exact expression for the cladding to 1.41 and making the necessary substitutions, equation 1.39 becomes

$$2(\bar{l}_n^2 - \bar{\beta}_n)^{\frac{1}{2}} + \ln\left[\frac{\bar{\beta}_n}{(\bar{l}_n + (\bar{l}_n^2 - \bar{\beta}_n)^{\frac{1}{2}})^2}\right]^{\bar{l}_n} - \frac{(\bar{l}_n^2 - \bar{\beta}_n)^{3/2}}{(1 - \bar{l}_n^2)}$$

$$+ \ln\frac{(z/z_p)}{k_o a\,\gamma\,(2q)^{\frac{1}{2}}} = 0 \qquad (1.43)$$

Now the integral of 1.37 via the new variables is

$$P_t \propto \int_0^1 d\,\bar{\beta}_n \int_{\bar{\beta}_n^{\frac{1}{2}}}^{\left(\frac{2 + q\,\bar{\beta}_n^2}{2 + q}\right)^{(2+q)/2q}} e^{-T z/z_p}\, d\,\bar{T}_n \qquad (1.44)$$

The normalizing tunnelling ray power at z = 0 is found to be

$$P_t(0) \alpha \left(\frac{2}{2 + 3q} \right) \left(\frac{1}{2 + q} \right)^{(2+q)/2q} .$$

$$[(2 + q)^{(2+3q)/2q} - 2^{(2+3q)/2q}] - 2/3 \qquad (1.45)$$

To evaluate the P_t at a specified z by means of the proposed method, the limits must be the roots of equation 1.43. Calling these $\bar{\beta}_r$ and $\bar{1}_r$

$$\frac{P_t(z)}{P_t(0)} = \frac{1}{P_t(0)} \left(\frac{2}{2 + 3q} \right) \left(\frac{1}{2 + q} \right)^{(2+q)/2q} .$$

$$[(2 + q\ \bar{\beta}_r)^{(2+3q)/2q} - 2^{(2+3q)/2q}] - \frac{1}{P_t(0)} \int_0^{\bar{\beta}_r} \bar{1}_r \, d\, \bar{\beta}_n$$

(1.46)

Hence, it should be less difficult to work with the above integral than the full attenuation factor.

Before moving on, some numerical examination of what has so far been presented will be given.

1.4 Numerical Results (1)

The algorithm techniques employed in the evaluations of Airy and all other functions encountered in the thesis are contained in Appendix B.

The fibre parameters (supplied by STL) were

$n_1 = 1.47028$

$n_2 = 1.45709$

$a = 25\ \mu m$

$b = 62.5\ \mu m$ (outer radius)

The profile value approximated to 2.1 when the dip was considered and 2.2 otherwise (see Figure 1.8). The wavelength was that of a red laser source $\lambda = 632$ nm.

The computations undertaken were extended to the whole of $\bar{\beta}$ - $\bar{l}$ domain with special emphasis on weakly leaky rays. Two groups were considered, one comprising lines of regular intervals throughout the range, the other concentrating on the lower part of the range. Figure 1.9 displays the specific numerical values chosen. The magnitudes adopted for $\bar{l}$ were such that they corresponded to the nearest integer counterparts of the azimuthal mode numbers.

The first calculation was that of T given in equation 1.27. This is labelled as Prog. A3. Figures 1.10 and 1.11 show the variation of the transmission coefficient against $\bar{\beta}^2$ and θ (the angle of incidence). The values occupying the bottom end of the curves could not be accommodated into the graphs with their actual magnitudes. Table 1.1 lists a selection of these.

The smallest attenuation is to be found close to the interface $\bar{\beta} = n_2$. A sharp rise is then experienced with T becoming roughly 0.5 at the next boundary. Finally far away, in the refrac-

ting ray region, the upper limit of unity is approached.

Though this is the typical behaviour exhibited whichever $\overline{l}$ is chosen, the bulk of the slowly attenuating rays are located around the intersection of $\overline{\beta} = n_2$ and $\overline{\beta}_{max}$ line. Thus a mapping of equi-transmission coefficients would resemble that of Figure 1.12 (the significance of this mapping may also be appreciated from equation 1.39).

Figures 1.13 and 1.14 display the success of the WKB formula. On average, the relative error between T_{Airy} and T_{WKB} was observed to be 10%.

It was possible to confirm that the attenuation would increase even for slight increments in q i.e. q = 2.1, q = 2.2 (Table 1.2).

The second programme that was run used the form of T put forward in Ref 4 (Prog. A1). As previously established, this method afforded highly underestimated results. The origin of this large deviation may visually be examined from the graphs of Ep1 and Ep2 in Figure 1.15.

Hence by omitting the linearization on the cladding side, a new equation was deduced (Appendix A), which retrieved the usual values of T (Prog. A2). The corresponding computations are shown in Figures 1.16 and 1.17, while the curves in Figures 1.18 and 1.19 compare the calculated figures from Prog. A2 and A3. One attractive feature of the former representation was that it was able to cope more adequately with the irregularities found in the vicinity of strongly leaky rays.

The condition $Ep >> Ep/(4 k_m^2)$ while containing the correct interpretation for the Airy function solution to hold well, does not yield the right order of the error.

The error terms both for the core and the cladding were determined (Table 1.3) based on the derivations of Appendix A.

The next step was to obtain the overall attenuation in the fibre. This was accomplished in two ways. One was via numerical integration over the whole of $\overline{\beta}$ - $\overline{T}$ domain utilizing the transmission coefficient in the exact form. The other was via numerical integration again but using the reduced T_{WKB} formula (equation 1.46). The results are 0.27966 (exact), 0.30679 (WKB) for z = 10m and q = 2. As seen the two figures agree favourably.

For the full attenuation factor, programmes A3 and A1 had to be combined so that the latter could provide the gradual extension up to the refracting ray boundary.

Using the WKB expression, the variation of power propagated along the fibre axis was evaluated. This is shown in Figure 1.20 for a number of q values. In a publication , Love and Pask (11) commented that the leaky ray power would decrease more rapidly for step index fibres than for the parabolic ones, a prediction that would appear to be a contradiction to the behaviour depicted in Figure 1.20.

The discrepancy here arises as a result of the ray period parameter. Figure 1.21 displays the same variation when z_p is properly taken into consideration, i.e. its value is deduced from the integration formula given in Appendix A. Thus, in the beginning the rate of decay for strongly graded profiles must be higher (remember that each curve is normalized with respect to its input power). Further on however, as the effect of z_p becomes negligibly small, the remaining power tends to fall at a slower rate for greater q values since such fibres have initially captured more tunnelling rays.

STANDARD TELECOMMUNICATION LABORATORIES LTD.
LONDON ROAD, HARLOW, ESSEX. CM17 9NA

	SIGNAL	Mic mm	Z m.m	θ_i^c
A	1.377	31.35	13.79	20 91
C	1.030	27.43	9 97	24 03
D	1 026	27 37	9 81	24 09
F	1 373	31 30	13.74	20 95

Numerical Aperture (C,A) = 0·196

" " (D,F) = 0·197

MEAN = 0·1965

SiO_2 AT 632·8nm = 1·45709

ON BASIS OF INDEX AT "A" = 1·45709

INDEX AT "C" = 1·47028

$\Delta = \frac{C-A}{A} \times 100\% = 0·905\%$

Fig 1.8

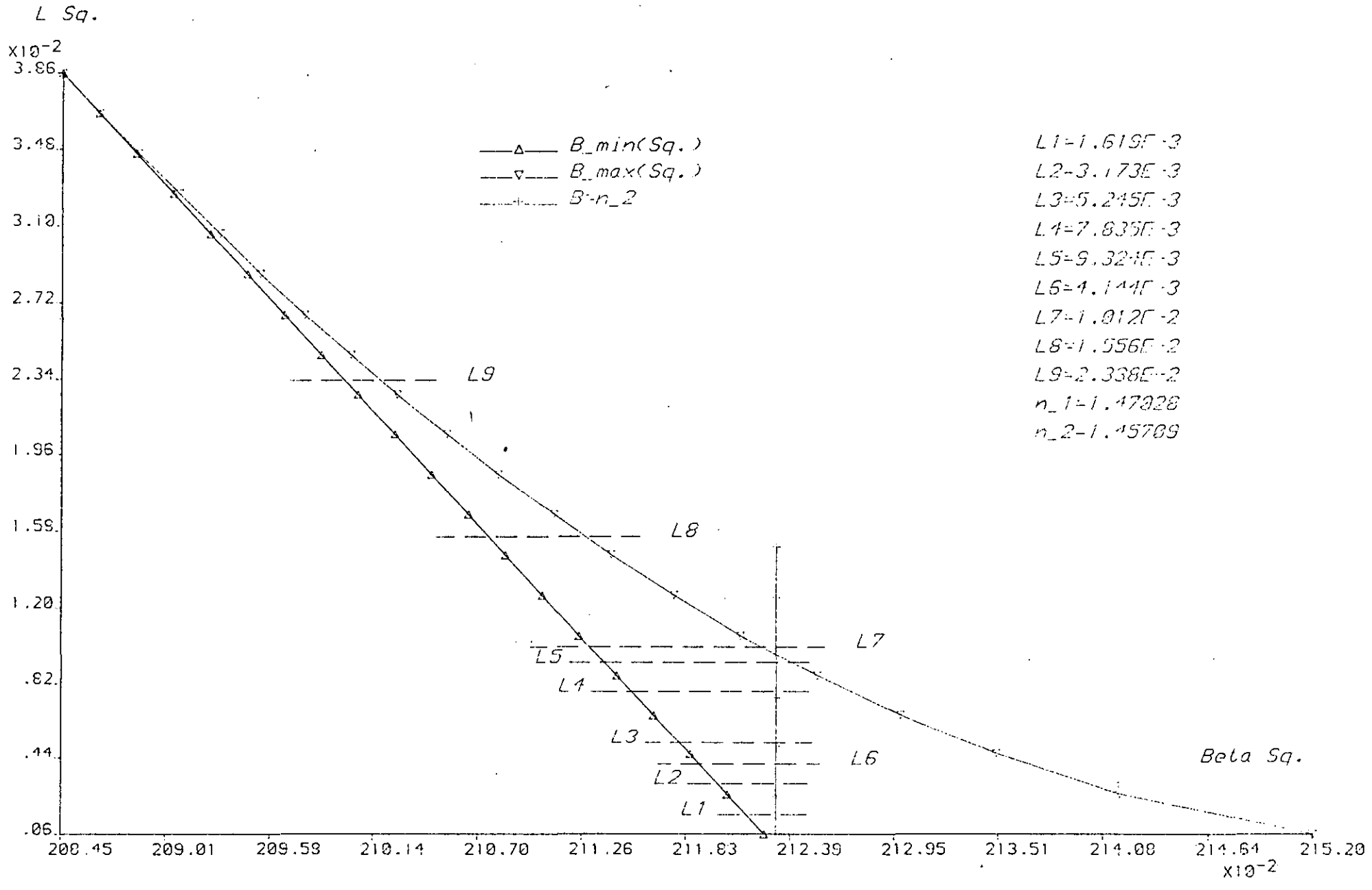

Fig. 1.9 Graph displays the L values chosen For computation(q=2)

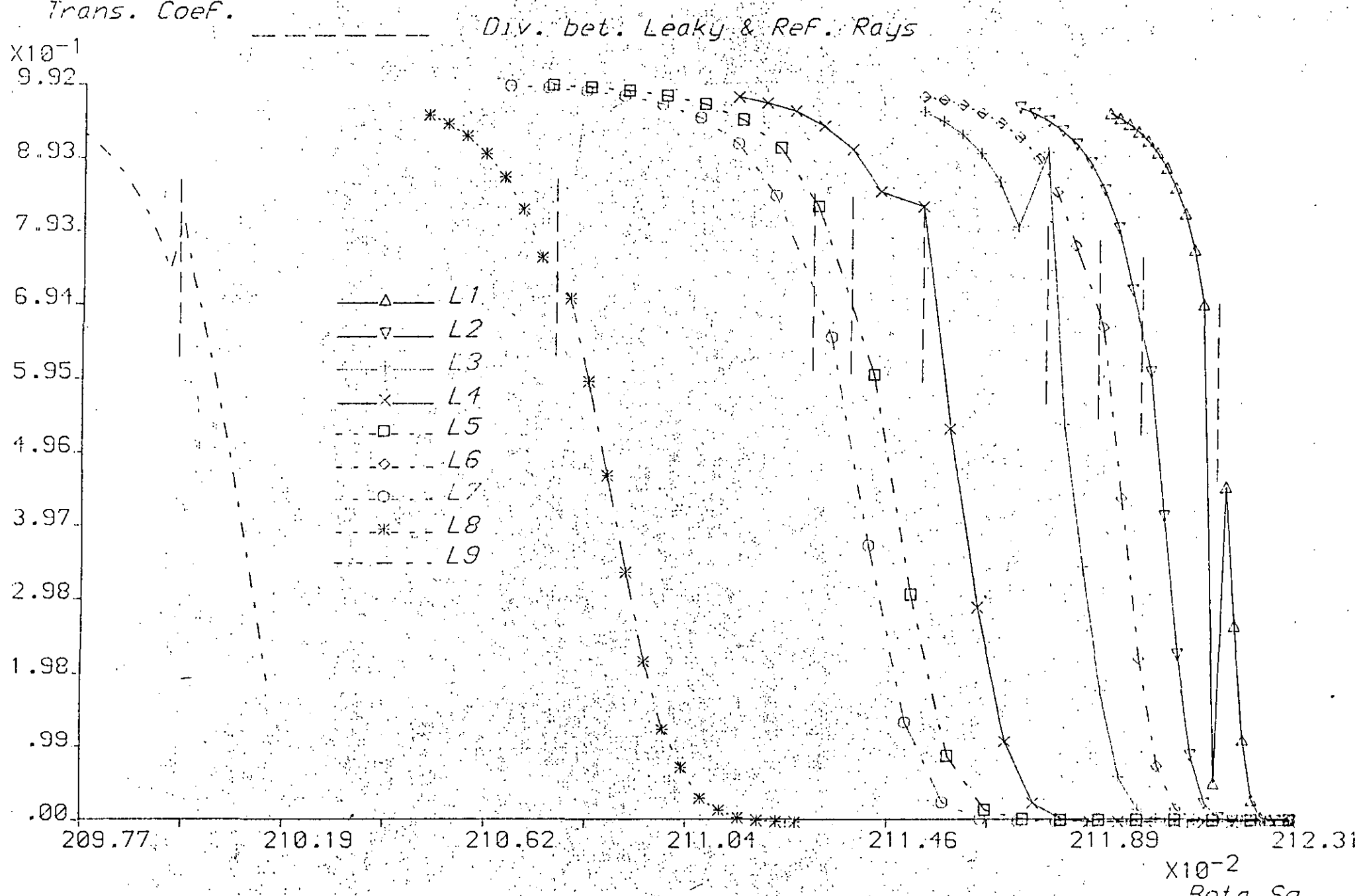

Fig.1.10 Transmission Coefficient with Ep2 Analytic(Prog.A3, q=2.0)

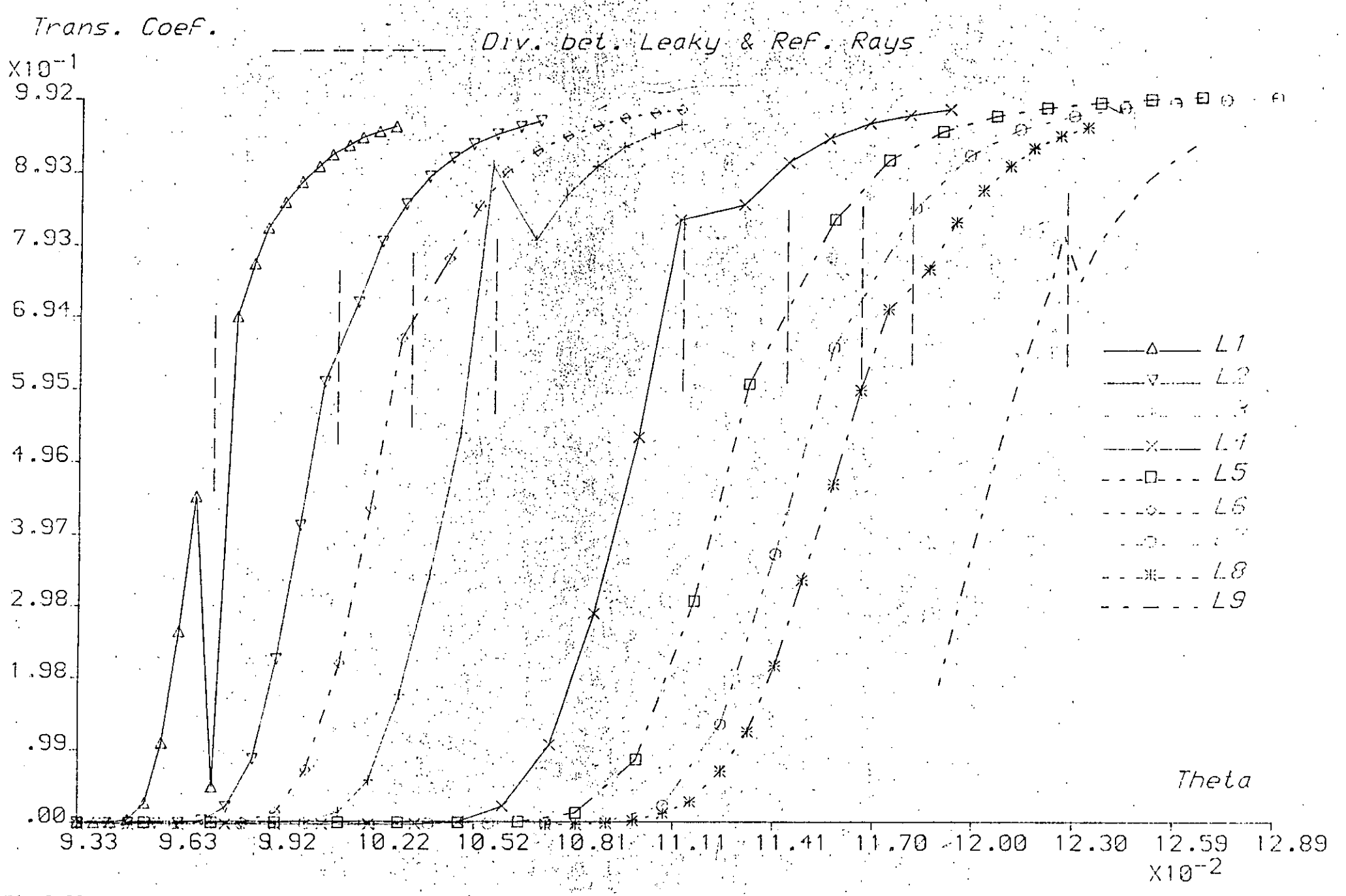

Fig.1.11 Transmission Coefficient with $E_p 2$ Analytic(Prog.A3, q=2.0)

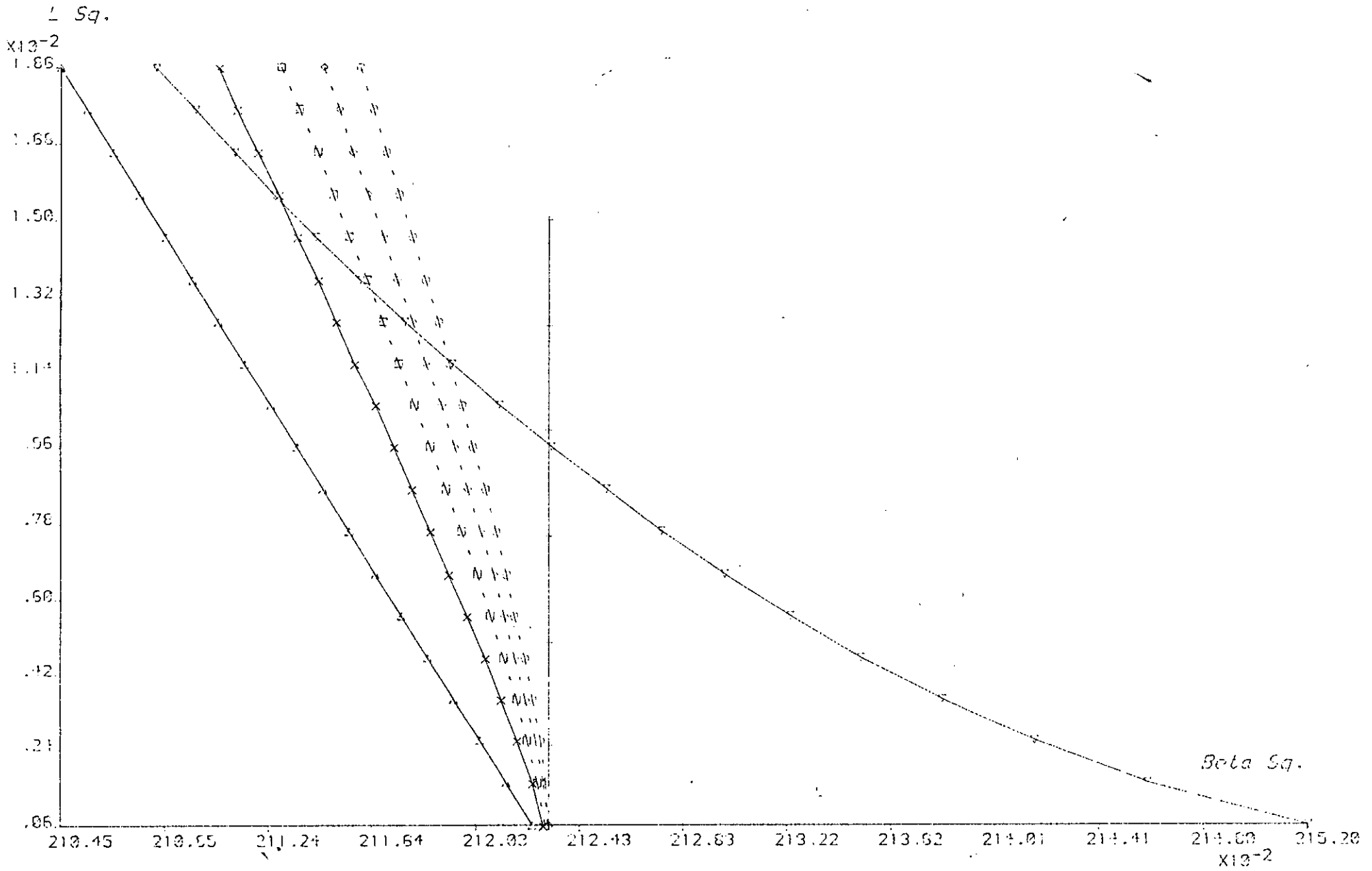

Fig. 1.12 Distribution of Equi-Transmission Coefficient values in the ray Domain

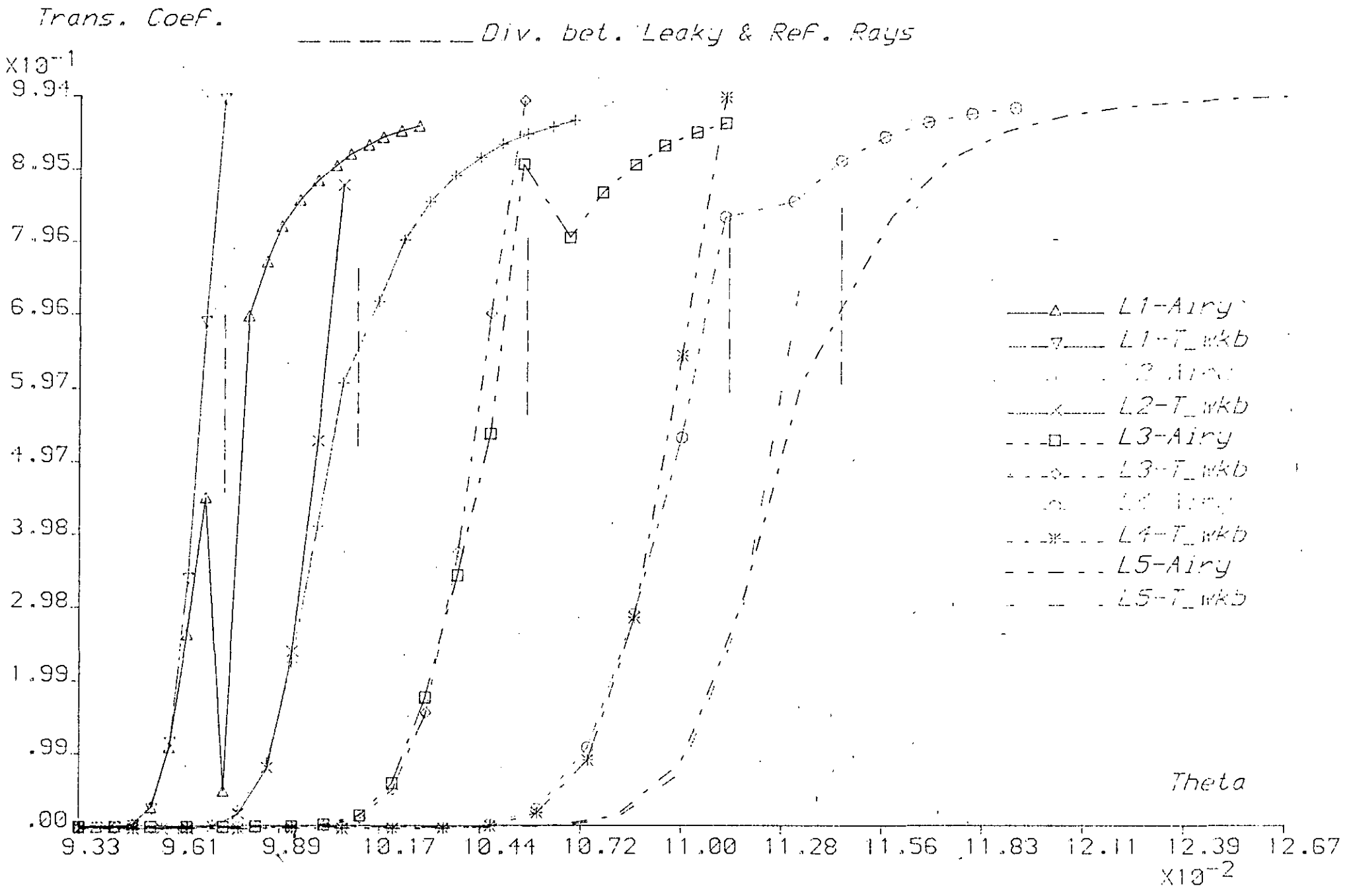

Fig. 1.13 T_wkb Approximation of Transmission Coefficient (Prog. A3, q=2.0)

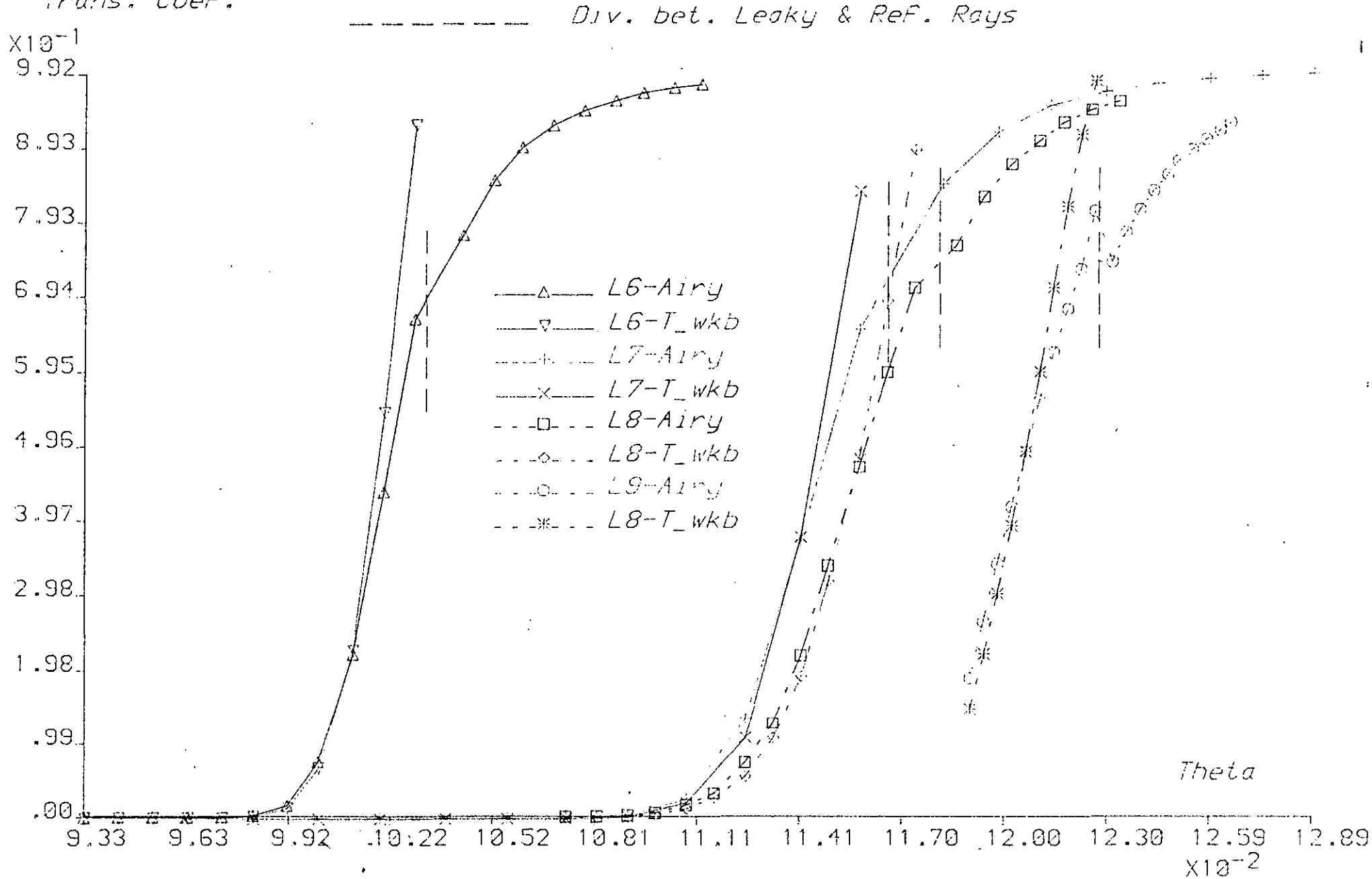

Fig. 1.14 T_wkb Approximation of Transmission Coefficient (Prog. A3, q=2.0)

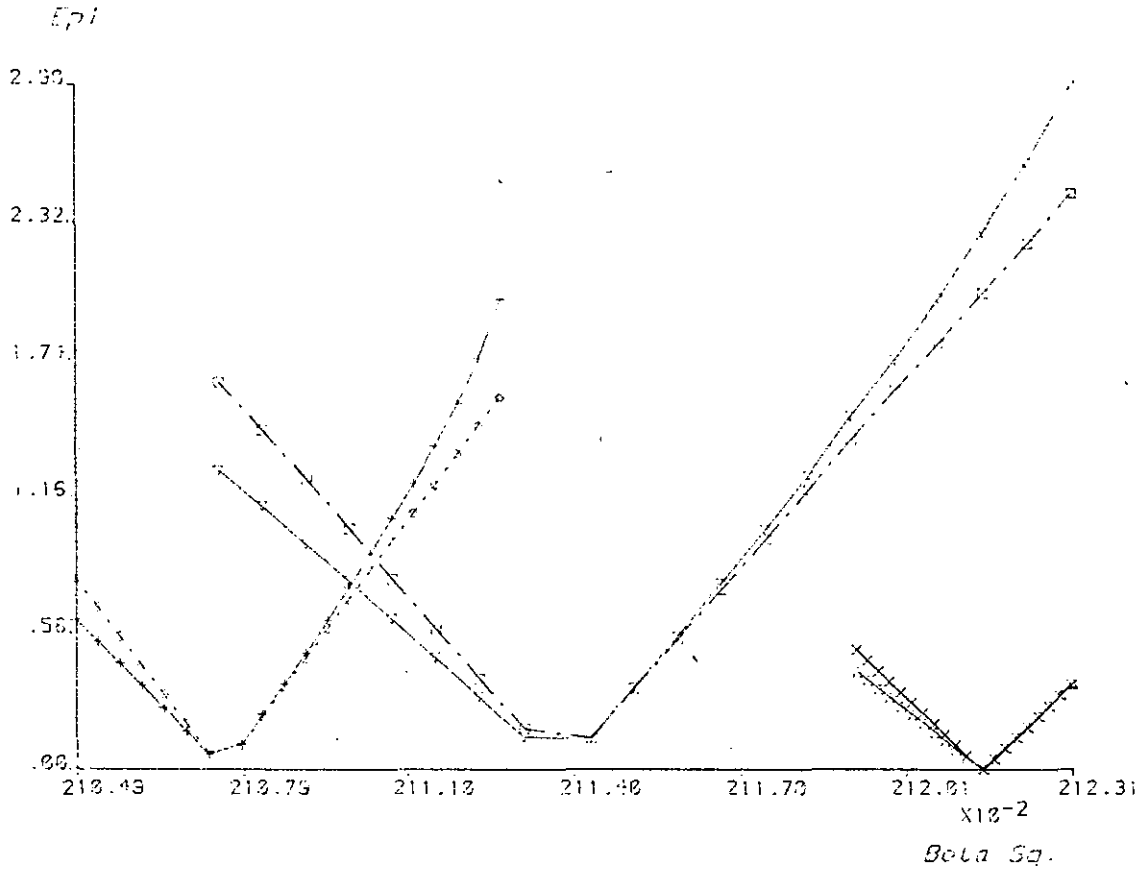

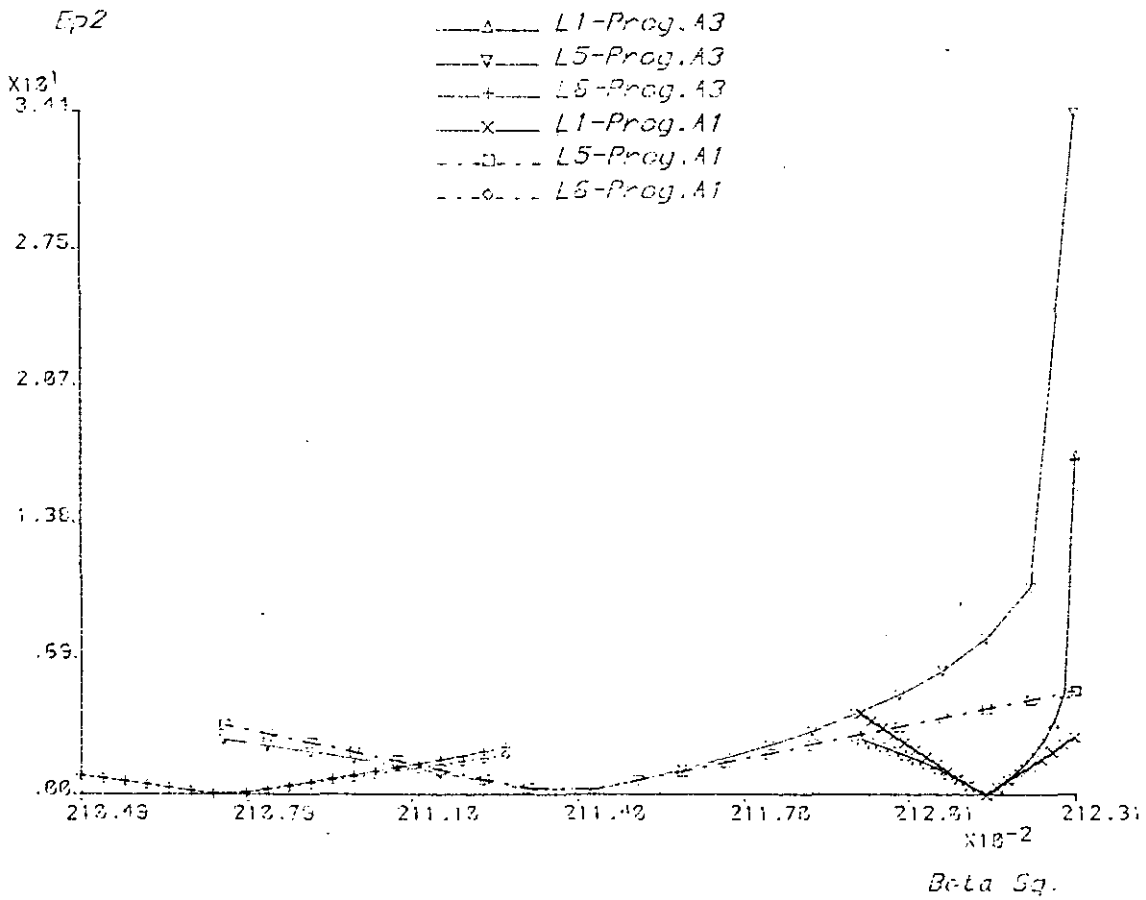

Fig. 1.15 Variation of Ep1 & Ep2 from Programmes A3, A1

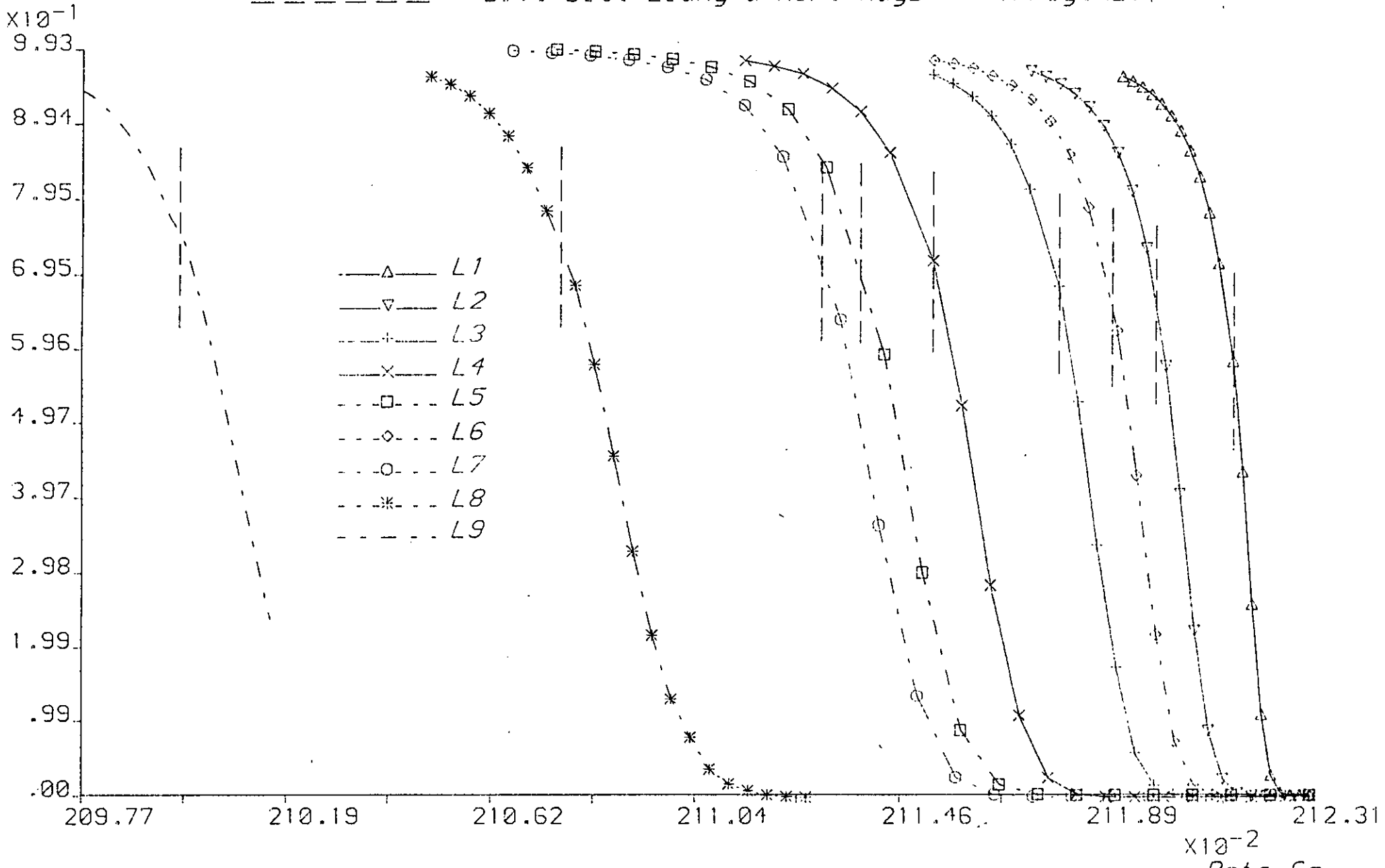

Fig. 1.16 Transmission Coefficient with EP1 Linearized and EP2 Analytic

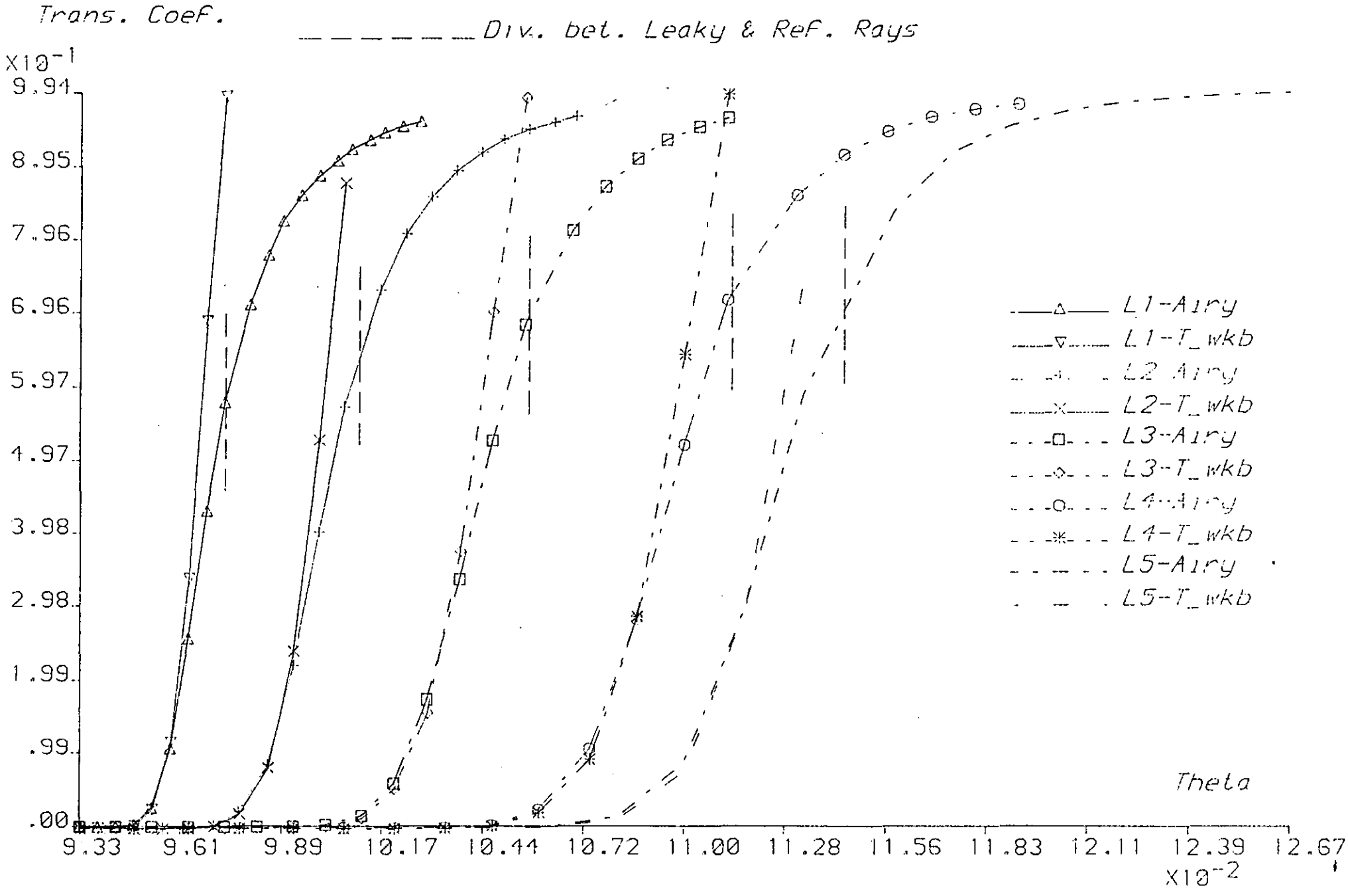

Fig. 1.17 T_wkb Approximation of Transmission Coefficient(Prog.A2)

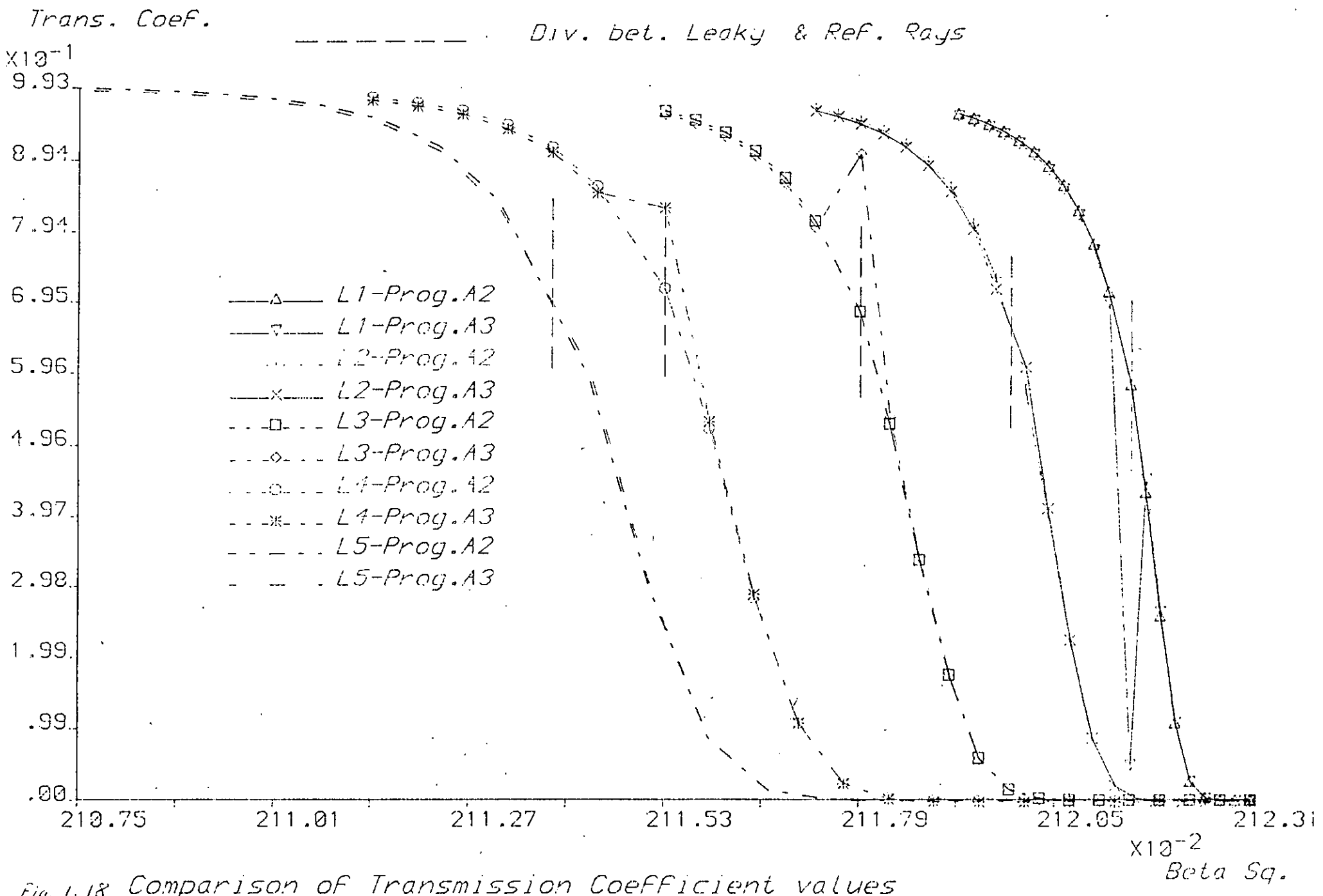

Fig. 1.18 Comparison of Transmission Coefficient values

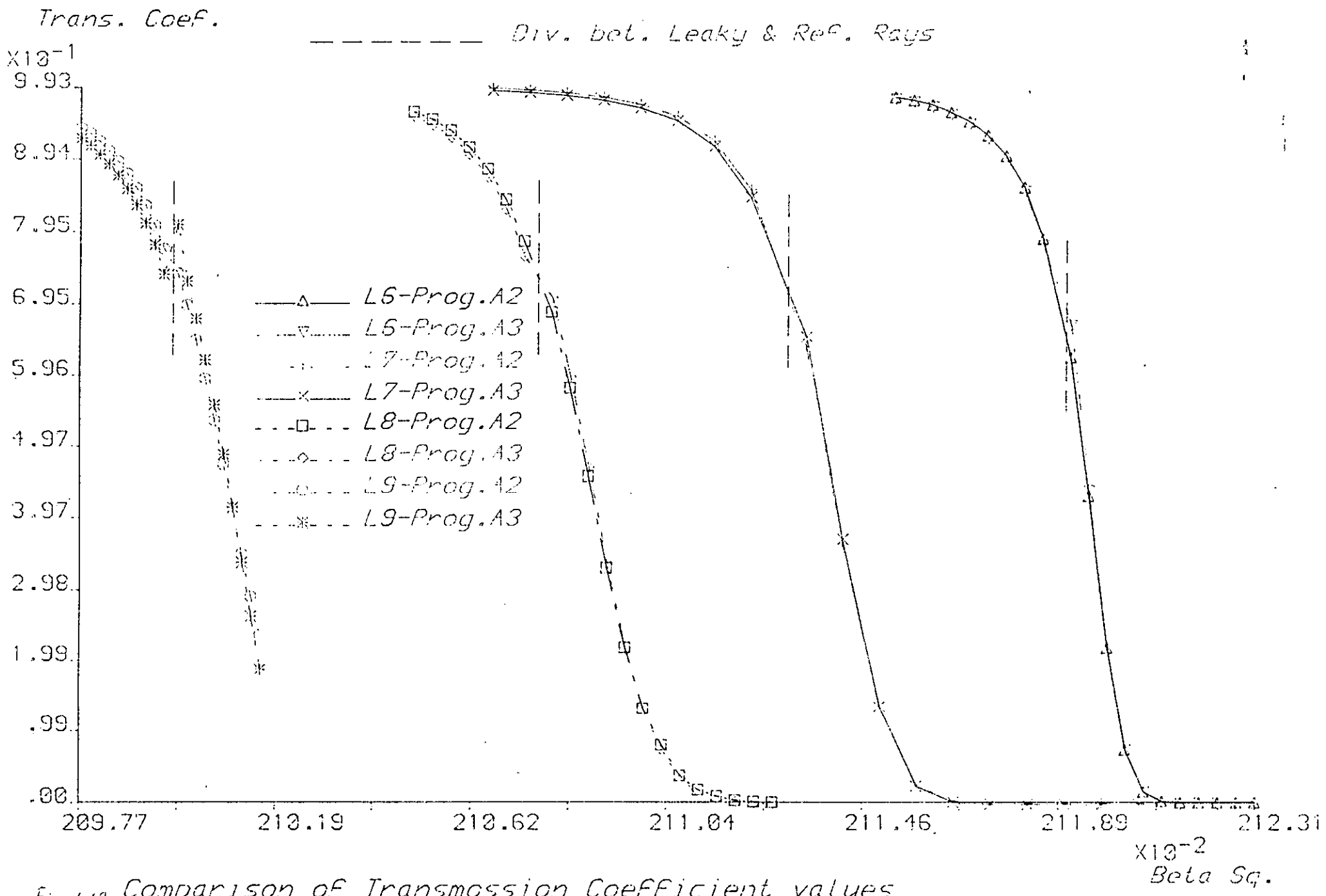

Fig. 1.13 Comparison of Transmossion Coefficient values

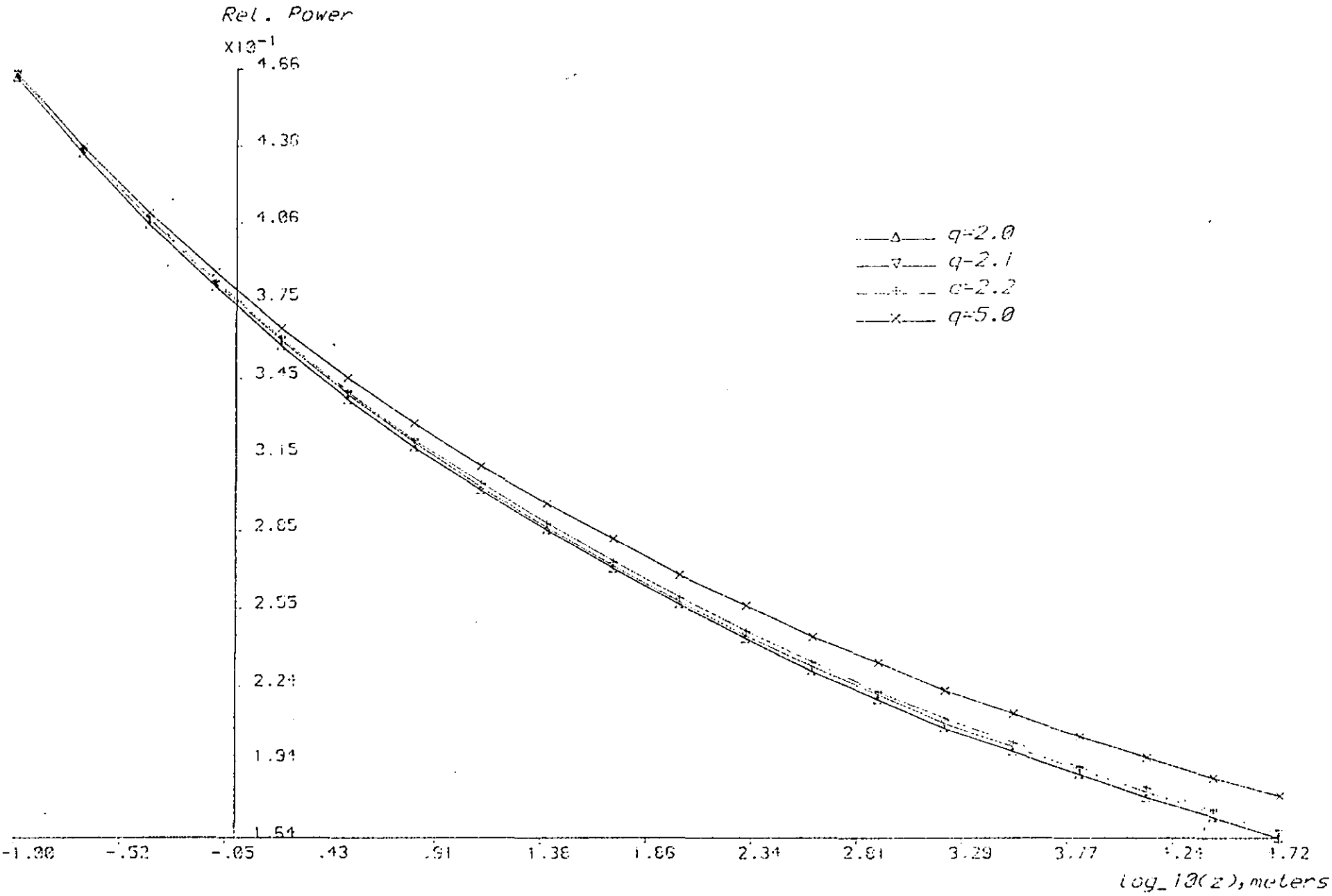

Fig. 1.20 Variation of Leaky ray power along Fibre axis using wkb Expression

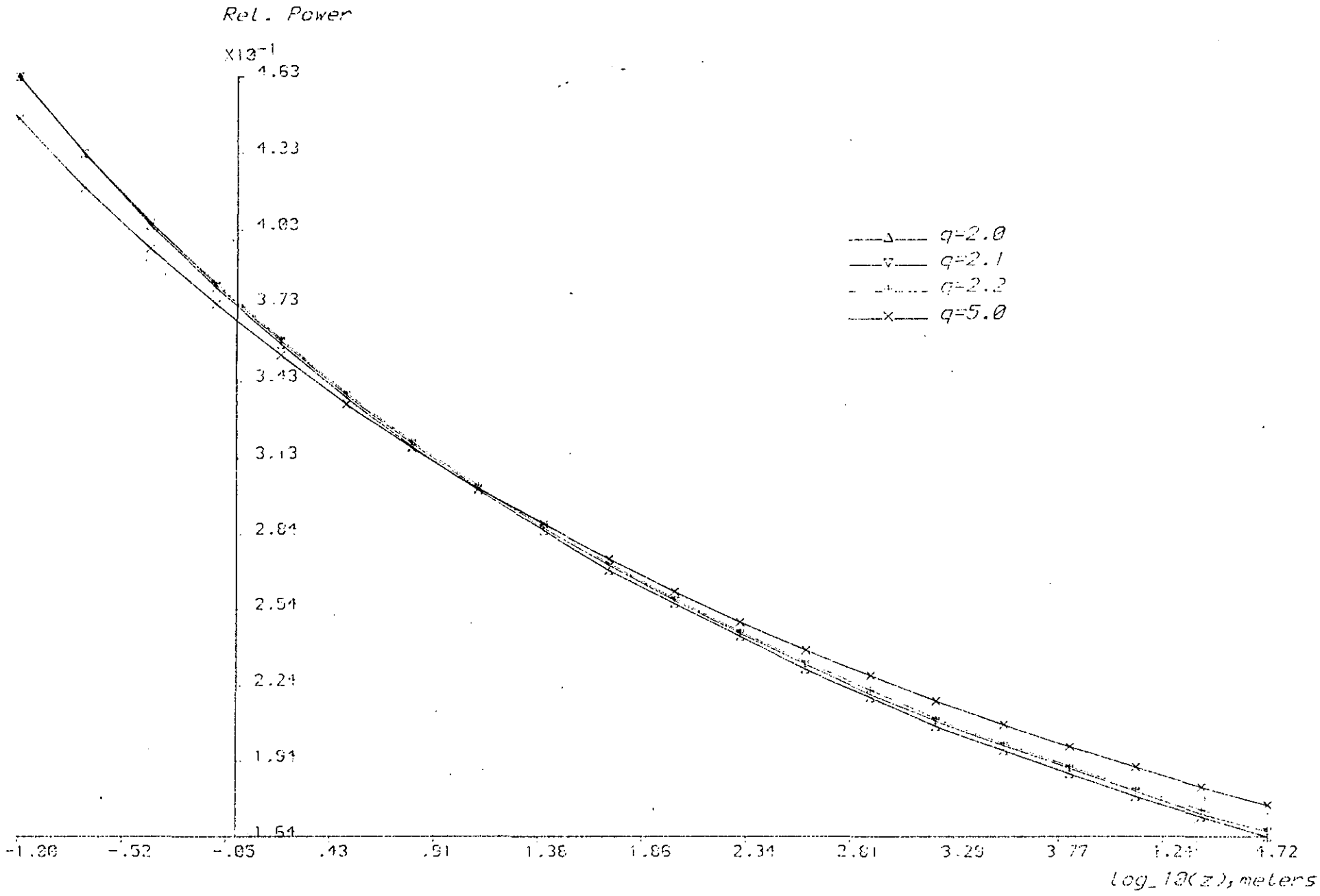

Fig. 1.21 Variation of Leaky ray power along fibre axis with z_p accounted for

TABLE (1.1)

Values of Trans. Coeff. for L Sq. = 0.1619D-02 q = 2.0

T	T_wkb	B Sq.	Ep1	Ep2	Th.	r_rad	r_tp
0.2077D-42	0.1803D-42	2.1231	0.3659	17.5617	0.0933	183.624	0.978
0.1822D-06	0.1607D-06	2.1229	0.3204	5.1100	0.0938	2.845	0.981
0.1041D-03	0.9026D-04	2.1227	0.2750	3.6035	0.0943	2.012	0.983
0.3052D-02	0.2774D-02	2.1225	0.2297	2.6466	0.0948	1.643	0.986
0.2646D-01	0.2536D-01	2.1223	0.1845	1.9278	0.0953	1.423	0.989
0.1080D 00	0.1167D 00	2.1221	0.1394	1.3447	0.0958	1.272	0.992
0.2617D 00	0.3382D 00	2.1219	0.0943	0.8503	0.0963	1.162	0.994
0.4484D 00	0.6866D 00	2.1217	0.0493	0.4188	0.0968	1.075	0.997
0.5141D-01	0.9911D 00	2.1215	0.0044	0.0334	0.0973	1.006	1.000
0.6931D 00		2.1212	0.0628	0.4757	0.0980	0.923	1.004
0.7671D 00		2.1210	0.1075	0.7812	0.0985	0.878	1.006
0.8165D 00		2.1208	0.1521	1.0644	0.0989	0.839	1.009
0.8524D 00		2.1206	0.1967	1.3288	0.0994	0.805	1.012
0.8791D 00		2.1204	0.2412	1.5772	0.0999	0.774	1.014
0.8996D 00		2.1202	0.2856	1.8115	0.1004	0.747	1.017
0.9155D 00		2.1200	0.3300	2.0335	0.1008	0.723	1.020
0.9281D 00		2.1198	0.3743	2.2446	0.1013	0.700	1.022
0.9383D 00		2.1196	0.4185	2.4461	0.1017	0.680	1.025
0.9466D 00		2.1194	0.4626	2.6388	0.1022	0.661	1.028
0.9534D 00		2.1192	0.5067	2.8236	0.1027	0.644	1.030

Div. between Leaky & Ref. rays at B Sq. = 2.12149 Theta = 0.0973

TABLE (1.1)
(contiued)

Values of Trans. Coeff. for L Sq. = 0.1012D-01 q = 2.0

T	T_wkb	B Sq.	Ep1	Ep2	Th.	r_rad	r_tp
0.1296D-22	0.1242D-22	2.1221	3.0473	10.5440	0.0963	3.309	0.718
0.1098D-15	0.1047D-15	2.1213	2.6382	8.1605	0.0982	2.423	0.791
0.1464D-11	0.1390D-11	2.1205	2.3172	6.5983	0.1001	2.002	0.825
0.1154D-08	0.1093D-08	2.1197	2.0265	5.4122	0.1019	1.745	0.851
0.1812D-06	0.1686D-06	2.1189	1.7544	4.4455	0.1038	1.566	0.874
0.9771D-05	0.8832D-05	2.1181	1.4956	3.6240	0.1056	1.434	0.894
0.2515D-03	0.2113D-03	2.1173	1.2471	2.9061	0.1073	1.330	0.913
0.3115D-02	0.2751D-02	2.1165	1.0069	2.2663	0.1091	1.245	0.931
0.2533D-01	0.2171D-01	2.1157	0.7736	1.6875	0.1108	1.175	0.947
0.1362D 00	0.1109D 00	2.1149	0.5462	1.1580	0.1125	1.116	0.963
0.3706D 00	0.3771D 00	2.1141	0.3240	0.6689	0.1141	1.065	0.978
0.6520D 00	0.8367D 00	2.1133	0.1063	0.2140	0.1158	1.020	0.993
0.8440D 00		2.1121	0.2126	0.4151	0.1182	0.962	1.014
0.9137D 00		2.1113	0.4207	0.8045	0.1198	0.929	1.027
0.9493D 00		2.1105	0.6257	1.1733	0.1213	0.899	1.040
0.9675D 00		2.1097	0.8277	1.5239	0.1229	0.872	1.053
0.9784D 00		2.1089	1.0269	1.8582	0.1244	0.846	1.065
0.9849D 00		2.1081	1.2237	2.1779	0.1259	0.823	1.077
0.9890D 00		2.1073	1.4180	2.4844	0.1274	0.802	1.089
0.9917D 00		2.1065	1.6102	2.7788	0.1289	0.783	1.101

Div. between Leaky & Ref. rays at B Sq. = 2.11299 Theta = 0.1166

TABLE (1.2)

Values of Trans. Coeff. for L Sq. = 0.5245D-02 q = 2.0

T	T_wkb	B Sq.	Ep1	Ep2	Th.	r_rad	r_tp
0.9839D-84	0.9102D-84	2.1231	1.3100	27.4266	0.0933	277.725	0.915
0.4445D-16	0.4099D-16	2.1227	1.2060	8.9946	0.0943	3.621	0.922
0.7212D-11	0.6601D-11	2.1223	1.1028	6.9063	0.0953	2.560	0.929
0.6437D-08	0.5840D-08	2.1219	1.0004	5.5905	0.0963	2.091	0.936

Values of Trans. Coeff. for L Sq. = 0.5245D-02 q = 2.1

T	T_wkb	B Sq.	Ep1	Ep2	Th.	r_rad	r_tp
0.1090D-83	0.1017D-83	2.1231	1.2610	27.4266	0.0933	277.725	0.920
0.4852D-16	0.4520D-16	2.1227	1.1610	8.9946	0.0943	3.621	0.927
0.7761D-11	0.7190D-11	2.1223	1.0618	6.9063	0.0953	2.560	0.933
0.6829D-08	0.6287D-08	2.1219	0.9632	5.5905	0.0963	2.091	0.940

Values of Trans. Coeff. for L Sq. = 0.5245D-02 q = 2.2

T	T_wkb	B Sq.	Ep1	Ep2	Th.	r_rad	r_tp
0.1193D-83	0.1123D-83	2.1231	1.2164	27.4266	0.0933	277.725	0.924
0.5241D-16	0.4934D-16	2.1227	1.1200	8.9946	0.0943	3.621	0.931
0.8275D-11	0.7761D-11	2.1223	1.0244	6.9063	0.0953	2.560	0.937
0.7190D-08	0.6715D-08	2.1219	0.9293	5.5905	0.0963	2.091	0.943

TABLE (1.3)

Error Terms of Trans. Coeff. for L Sq. = 0.4144D-02 q = 2.0

k_r(a) Sq.	ET(r\a)	ET(r)a)	Rel. Err.(1)	Rel. Err.(2)	B Sq.
0.4144D-02	-0.4483D-05	0.4130D-05	-0.1082D-02	0.9966D-03	2.1231
0.3744D-02	-0.4424D-05	0.4671D-05	-0.1182D-02	0.1248D-02	2.1227
0.3344D-02	-0.4366D-05	0.4698D-05	-0.1306D-02	0.1405D-02	2.1223
0.2944D-02	-0.4310D-05	0.4690D-05	-0.1464D-02	0.1593D-02	2.1219
0.2544D-02	-0.4255D-05	0.4670D-05	-0.1673D-02	0.1836D-02	2.1215
0.2144D-02	-0.4201D-05	0.4646D-05	-0.1960D-02	0.2167D-02	2.1211
0.1744D-02	-0.4147D-05	0.4620D-05	-0.2378D-02	0.2649D-02	2.1207
0.1344D-02	-0.4089D-05	0.4594D-05	-0.3042D-02	0.3418D-02	2.1203
0.9439D-03	-0.4010D-05	0.4568D-05	-0.4248D-02	0.4839D-02	2.1199
0.5439D-03	-0.3758D-05	0.4543D-05	-0.6908D-02	0.8351D-02	2.1195
0.1439D-03	0.1003D-04	0.4518D-05	0.6969D-01	0.3139D-01	2.1191
0.4561D-03	-0.4322D-05	0.4483D-05	-0.9477D-02	0.9829D-02	2.1185
0.8561D-03	-0.3923D-05	0.4460D-05	-0.4583D-02	0.5210D-02	2.1181
0.1256D-02	-0.3838D-05	0.4439D-05	-0.3056D-02	0.3534D-02	2.1177
0.1656D-02	-0.3787D-05	0.4418D-05	-0.2287D-02	0.2668D-02	2.1173
0.2056D-02	-0.3744D-05	0.4398D-05	-0.1821D-02	0.2139D-02	2.1169
0.2456D-02	-0.3704D-05	0.4378D-05	-0.1508D-02	0.1783D-02	2.1165
0.2856D-02	-0.3666D-05	0.4359D-05	-0.1284D-02	0.1526D-02	2.1161
0.3256D-02	-0.3629D-05	0.4341D-05	-0.1115D-02	0.1333D-02	2.1157
0.3656D-02	-0.3593D-05	0.4323D-05	-0.9829D-03	0.1183D-02	2.1153

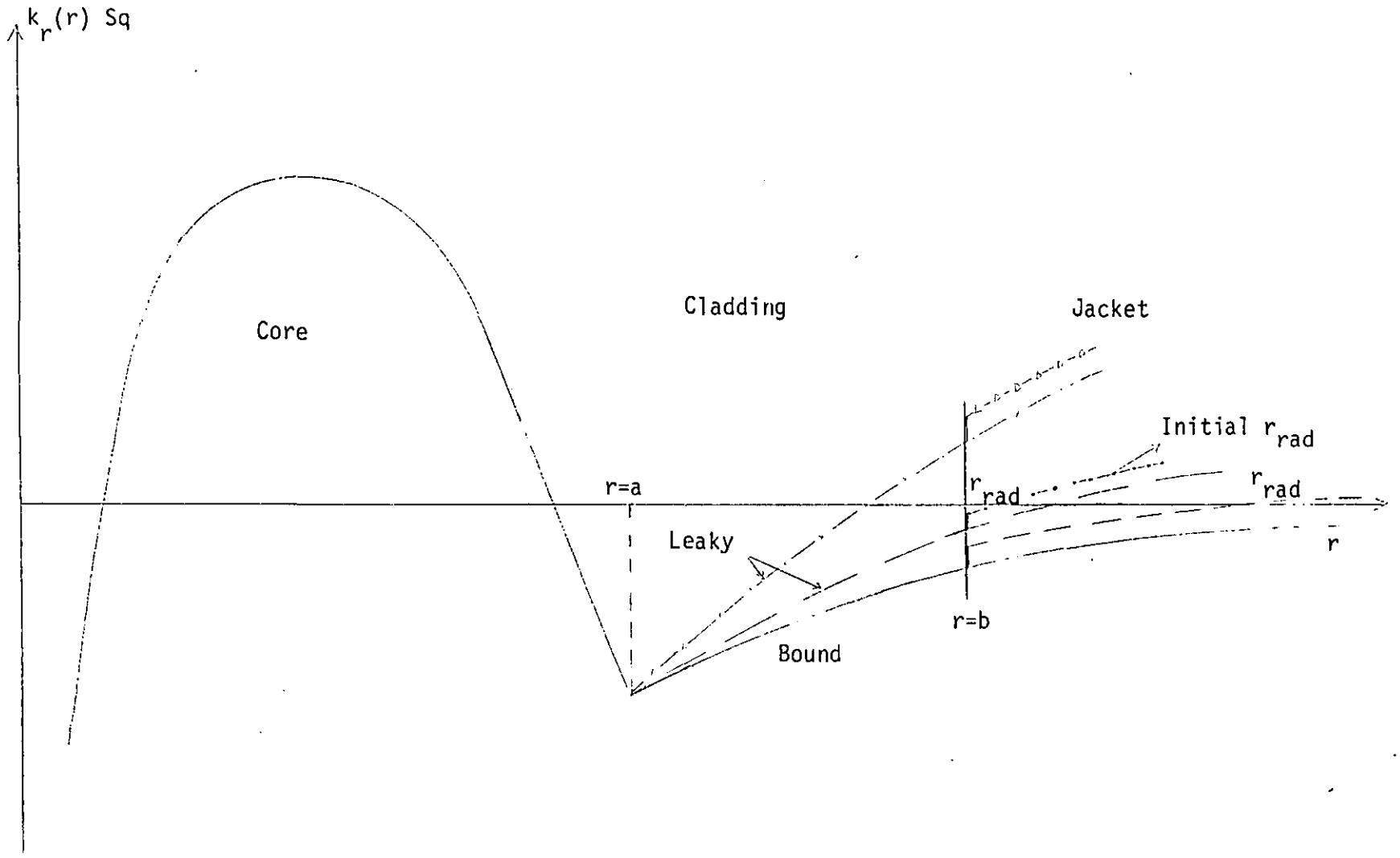

Fig. 1.22 Illustration of Filtering Concept

1.5 Filtering Theory

With the knowledge of the preceding two sections on a single cladded fibre, it should now be relatively straightforward to advance the fundamentals of filtering.

It will be recollected from the diagrams of $k_r(r)$ that the criterion for a ray to radiate a portion of its energy stipulated that $r_{tp} < \infty$, a requirement not fulfilled by any of the guided rays. Leaky rays on the other hand always possess a radiation point no matter how remote. The wider the tunnelling depth, the less attenuated the ray becomes. Hence, the object must be to narrow the zone of evenescence in order to speed up the tunnelling phenomenon. One idea that immediately suggests itself is to surround the fibre with an additional layer, usually called the jacket. Clearly, to serve its purpose, the refractive index of this outer material has to be higher than that of the cladding.

Excluding the already refracting rays, the new situation may be quantified as follows:

1. Those rays with $\overline{\beta} \geq n_3$ where n_3 denotes the index of refraction for the jacket will continue to be loss-free.

2. In the interval $n_2 \leq \overline{\beta} \leq n_3$ will be the rays originally trapped but which have now been converted into leaky ones.

3. Finally, beyond $\overline{\beta} \geq n_2$, the existing tunnelling rays will have their attenuation increased.

The graph in Figure 1.22 supplies the necessary pictorial representation.

The transmission coefficient may now be rearranged to read:

$$T = T_{core} + T_{cladding} + T_{jacket} \qquad (1.47)$$

Since the fields in the cladding are disrupted, T in this region will be bounded by the outer radius. T_{jacket} accounts for the continuation of the evenescent rays into the jacket.

To arrive at an expression for T via the scalar wave equation would mean the construction of a double boundary-value problem. As one might surmise, this would be a futile exercise bearing in mind the enormous difficulties to be faced. T_{WKB}, as demonstrated by the computations provided an adequate description. Adopting it to the case of filtering would need a few amendments.

Since the jacket gives rise to a discontinuity in the cladding profile, the Fresnel transmission coefficient (T_f) must be included in the equations (14).

Therefore it may be written that

$$T = \exp\left(-2 \int_{r_{tp}}^{r_{rad}} k_m(r)\, dr\right) T_f \qquad (1.48)$$

where the integral, in accordance with the shifted location of the radiation point, will also cover the area underneath the jacket.

The full attenuation may likewise be inferred upon inserting equation 1.48 into 1.39.

Despite its practical simplicity, the outlined technique will not achieve the desired goal. This is because, although the existing rays are caused to radiate within a shorter distance, new ones are generated. Thus the overall ratio of powers in the fibre may not have changed greatly. Furthermore, this balance is restored at the expense of the trapped rays.

Therefore, efforts should be concentrated on two aspects. One is the design of efficient filtering schemes. The second is

to minimize the interference on the characteristics of the guided ray domain.

So far the only parameter controllable has been assumed to be the refractive index in the outer material. For instance, it may be envisaged to vary the cladding thickness. Indeed, the forthcoming calculation will show that hardly any noticeable difference, can be observed if one is constrained to the specifications of commercially available fibres.

Theoretically this may be explained by referring to equation 1.46. The integral here traces along the type of rays which commonly have the outer caustics positioned at approximately 1.5 times the core radius, and if, say, the cladding has a diameter twice that of the core, which is usual in present-day fibres, then the jacket layer will not be capable of altering the transmission properties in the required manner.

Hence, a reduced dimension for the cladding is inevitable.

In order to satisfy the other criteria, some kind of grading of the jacket may be proposed. Let this be:

$$n_3(r) = n_2\left(1 + 2\Delta_1 \left(\frac{r-b}{c-b}\right)^{q_1}\right)^{\frac{1}{2}} \text{ for } a \leq r \leq c \qquad (1.49)$$

b = cladding radius, c = jacket radius

such that the profile is monotonically increasing first but is to be suitably terminated at a radial distance c, bringing the refractive index back to the cladding level (see Figure 1.23). The problem is then to adjust the parameters Δ_1, q_1 to obtain a reasonable jacket size and simultaneously accelerate the filtering.

To prevent a particular ray from leaking out, the $k_r(r)$ must never cross the r axis i.e.

$$n_3(r) - \bar{\beta}^2 - \bar{l}^2 \left(\frac{a}{r}\right)^2 < o \text{ for } b < r < \infty \qquad (1.50)$$

Obviously, this condition cannot be met for all rays simultaneously. By choosing a convenient starting point in the ray domain, for instance the intersection of $\beta = n_2$ and $\bar{l}_{max}$, will define a new boundary between the guided and leaky rays as depicted in Figure 1.23.

For the two methods elaborated above, total power loss may be calculated from

$$P_{tot} = \frac{P_{tr} + P_{br}}{P_t + P_b} \qquad (1.51)$$

with P_{tr} and P_{br} denoting modified powers contained in tunnelling and trapped rays respectively, while P_t and P_b describe the same parametersprior to any filtering.

1.6 Numerical Results (2)

Initially, to study the effect of an outer layer on individual rays, a programme was devised using the previously arranged values. Some of the results are displayed in Table 1.4. A drastic reduction of the attenuation coefficient is to be observed for weakly leaky rays. Hardly any deviation occurs however as one moves further towards the other side of the domain. In fact a slight increase is found due to the existence of the jump introduced in the cladding. Instructions were drawn up to deal with the different ray types separately. Although, in practical implementation, the number of such cases amounted to six, they may be summarized as three distinct groups:

1. Those rays possessing the radiation point before the jacket boundary.

2. Rays whose radiation point coincided with the boundary, and

3. Those rays which radiated from the jacket itself.

The above was then converted into a subroutine to solve the corresponding equation of 1.46 to obtain the overall attenuation.*

Figure 1.24 shows the variation of total power (i.e. equation 1.51) as the refractive index of the jacket is altered. As expected, the power decreases with increasing index of refraction.

Investigating this behaviour separately for leaky and guided rays reveals that the power reduction is accomplished solely owing to the latter (Figure 1.25). This also confirms the claims put forward in the theoretical treatment. In the graphs of leaky rays, the difference from the initial power is stated instead of absolute values which did not change much.

Varying the cladding thickness was considered next. Figure 1.26 depicts the situation for a range of distances on the fibre axis. From these, two important conclusions emerge.

The first one is that in order to realize an efficient filtering process, the cladding radius must be small enough so that the jacket may exert an appreciable influence on the extension of the evenescent region. Secondly, even if the cladding does not shrink in size, an outside layer will ultimately produce some degree of filtering, but its effect will not be felt over short lengths. The steeper slope of the curve for z = 100m clearly demonstrates this.

The results obtained from the study of a graded jacket are shown in Figure 1.27. It is seen that profiling of the jacket

---

* Because of the purely numerical nature of this evaluation no analytic forms were supplied in the text. Some details are nevertheless mentioned in Appendix A.

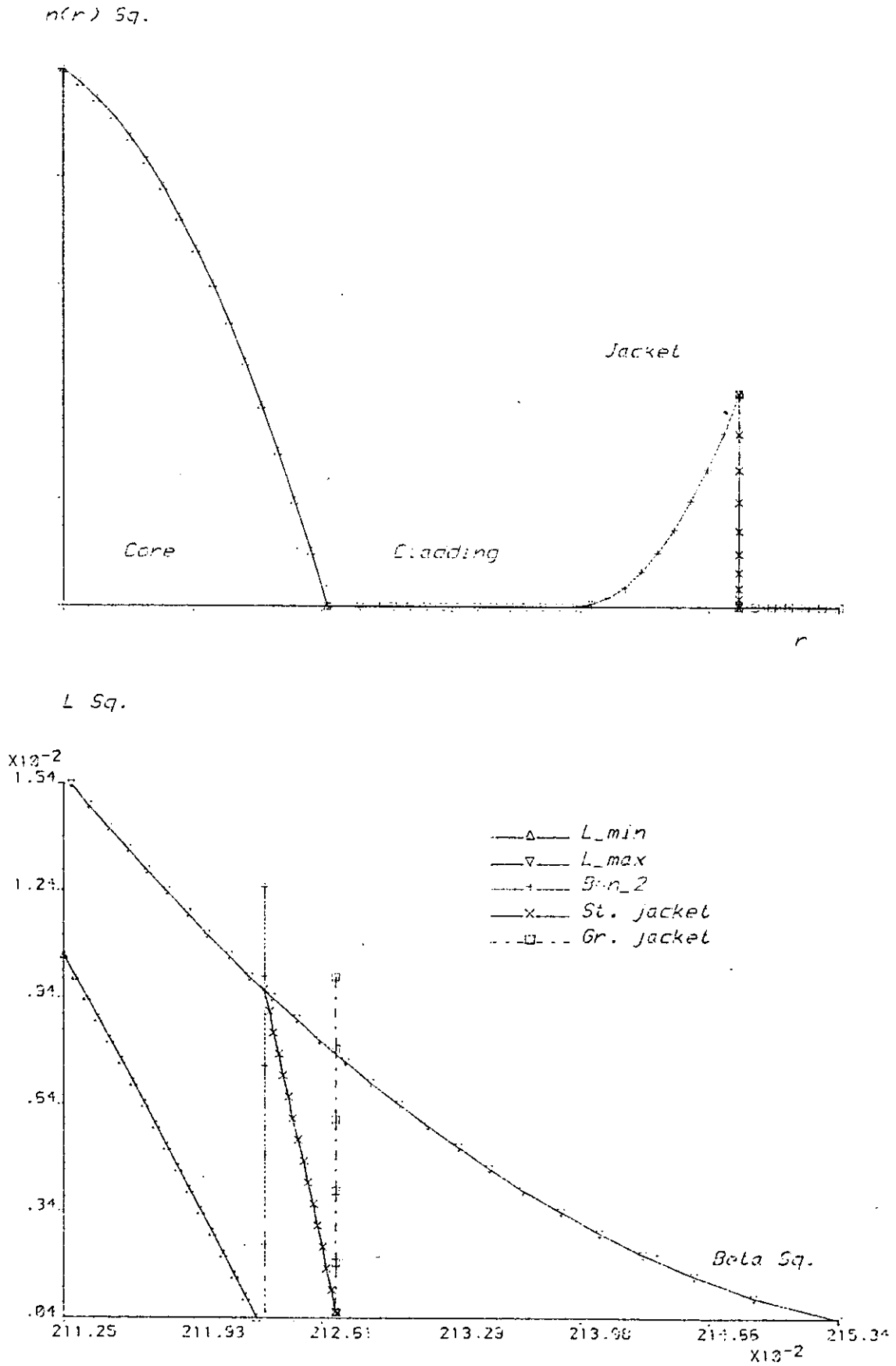

Fig. 1.23 Illustration of filtering with graded jacket

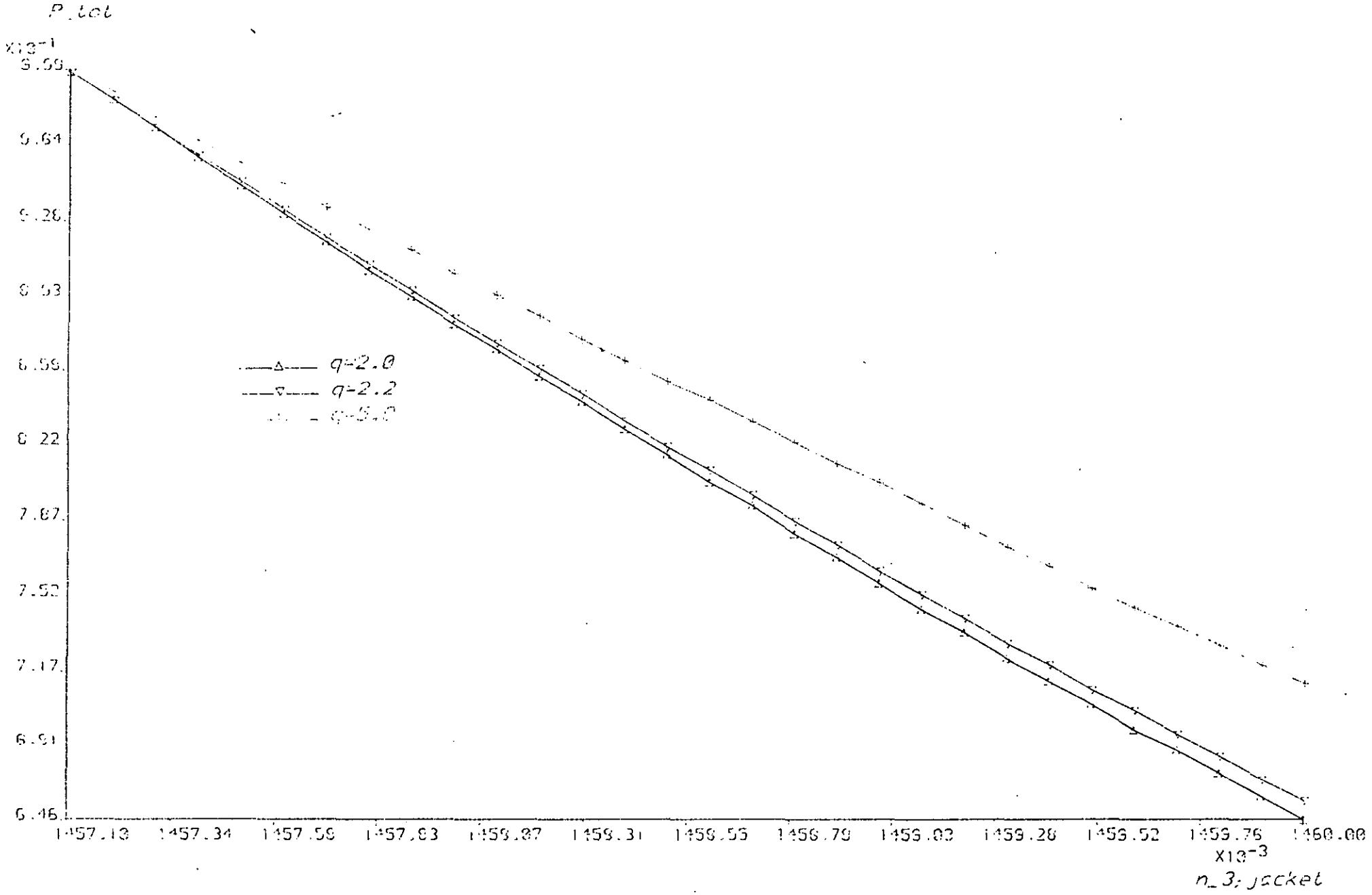

Fig. 1.24 Filtering effects on Total power due to refractive index of jacket(z=13m)

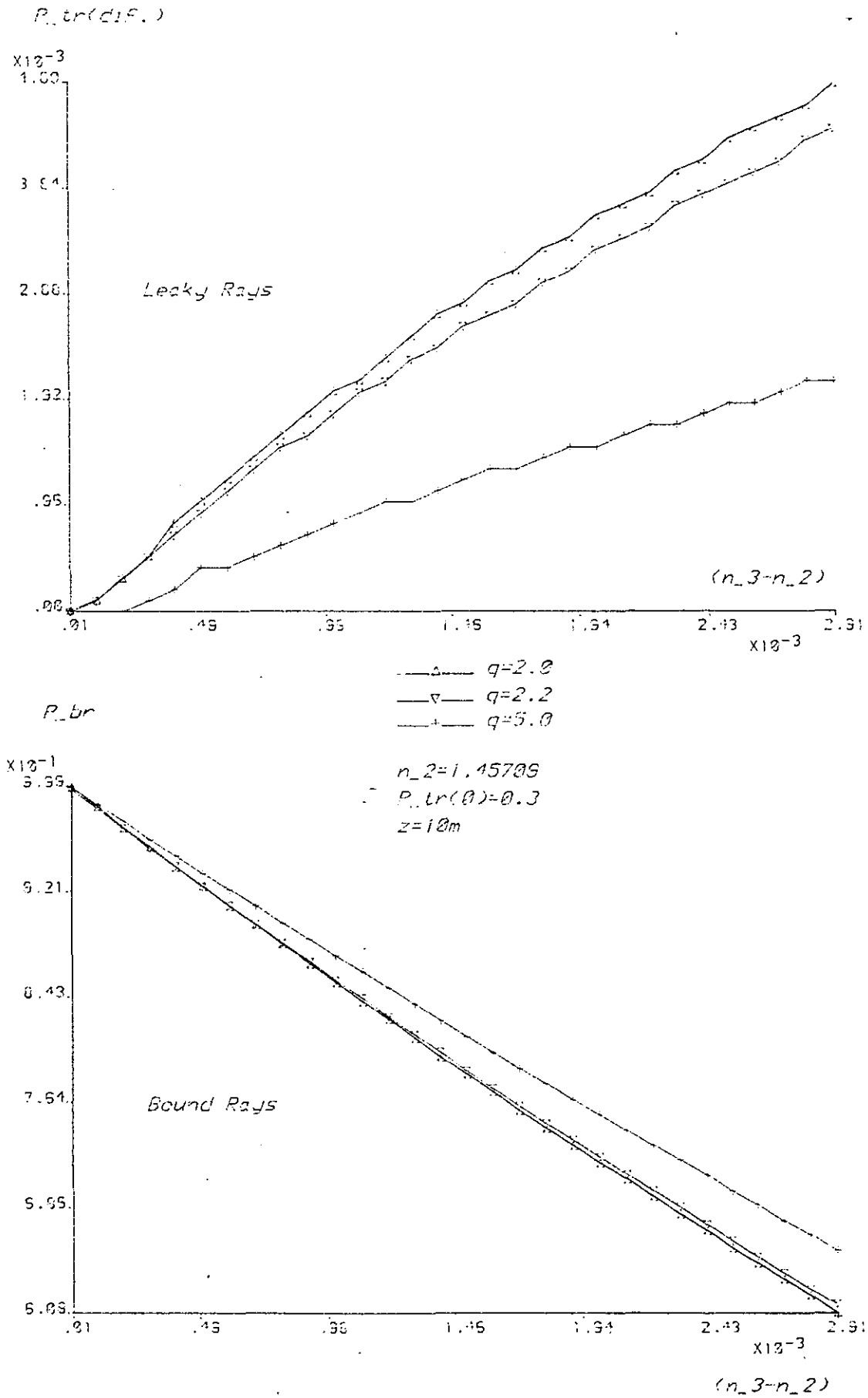

Fig.12S Variation of power with refractive index of jacket

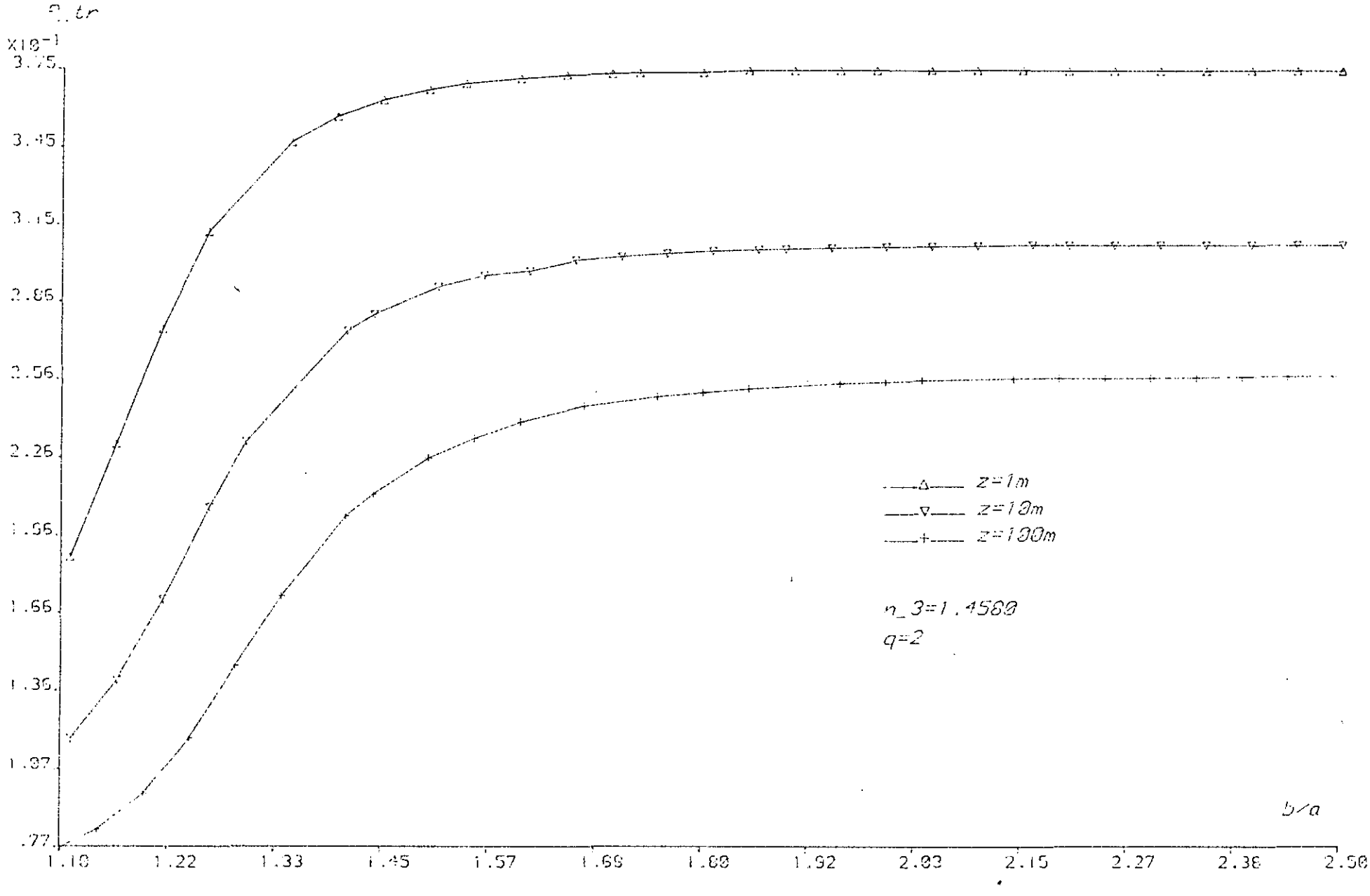

Fig. 1.26 Filtering effects due to varying cladding thickness

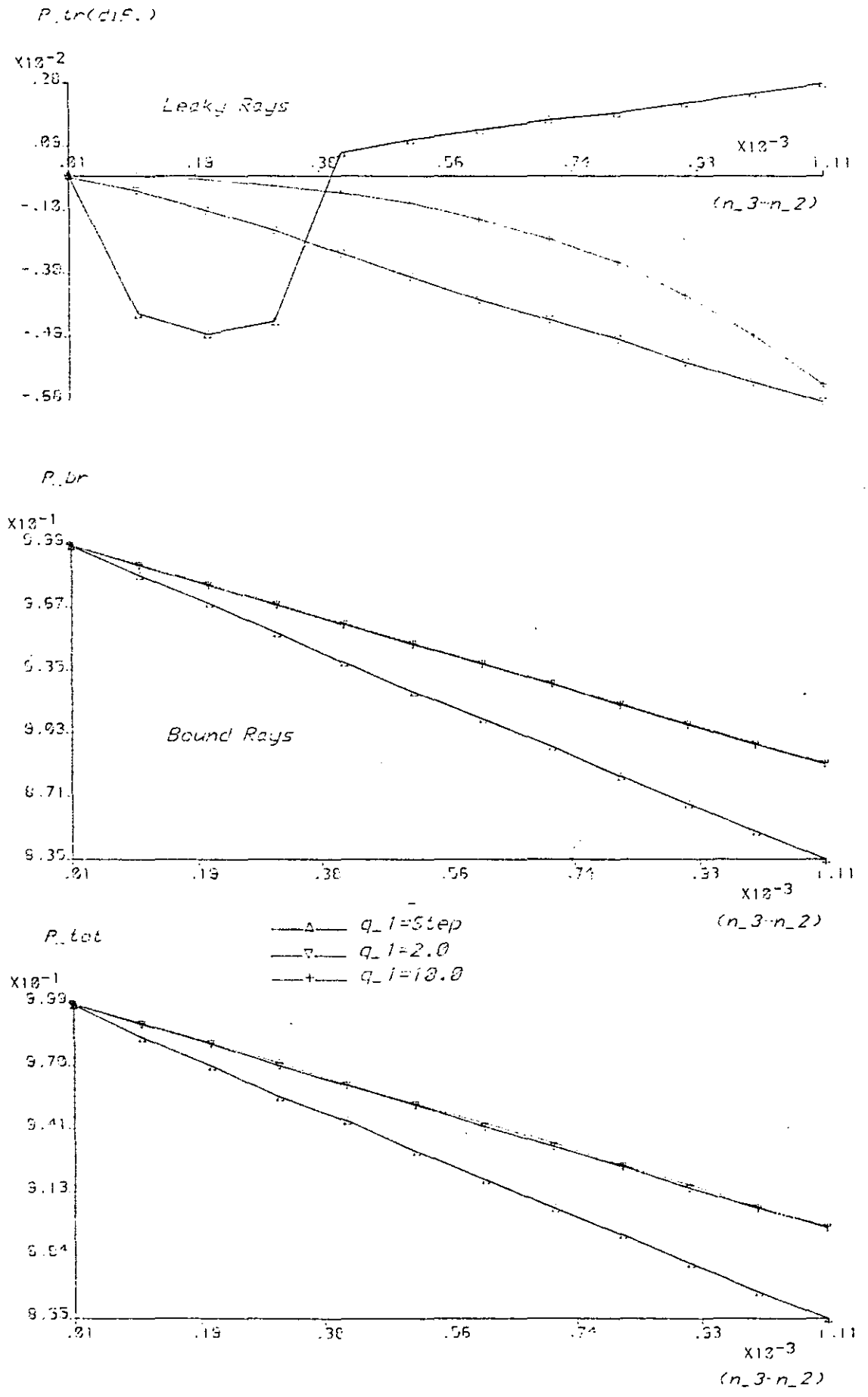

Fig. 1.27 Filtering effects with graded jacket(b=1.7*a, z=10m)

TABLE (1.4)

Transmission Coefficient values with jacket

L Sq. = 0.7835D-02 q = 2.0 n_3 = 1.4576

Initial T_wkb	New T_wkb	Initial r_rad	New r_rad	Beta Sq.
0.4413-107	0.2319D-19	339.442	2.544	2.1231
0.2066D-20	0.6431D-17	3.613	2.531	2.1225
0.6006D-14	0.6700D-14	2.555	2.508	2.1219
0.2951D-10	0.2951D-10	2.086	2.086	2.1213
0.1029D-07	0.1029D-07	1.807	1.807	2.1207
0.8205D-06	0.8205D-06	1.616	1.616	2.1201
0.2515D-04	0.2515D-04	1.475	1.475	2.1195
0.3903D-03	0.3903D-03	1.366	1.366	2.1189
0.3601D-02	0.3601D-02	1.278	1.278	2.1183
0.2185D-01	0.2185D-01	1.205	1.205	2.1177
0.9275D-01	0.9275D-01	1.143	1.143	2.1171
0.2855D 00	0.2855D 00	1.090	1.090	2.1165
0.6423D 00	0.6423D 00	1.043	1.043	2.1159
0.9945D 00	0.9945D 00	1.002	1.002	2.1153

will achieve a uniform filtering of the leaky ray though the actual amount still remains insignificant. In order to realize refractive index values up to 1.4581, the maximum cladding thickness that could be selected was 1.7a. It is also interesting to observe that for such a cladding radius, the step jacket provides filtration only when n_3 differs slightly from n_2.

1.7 Discussion (1)

In this chapter, the theoretical model of propagation in the fibres was constructed using the ray analysis.

The presentation was in two parts. Initially a double layer structure consisting of a core and a cladding was considered. Equations relating to the attenuation of leaky rays were derived both in terms of Airy functions and WKB approximations.

Some works on the topic have already been mentioned. Additionally, it is possible to enumerate others which deal with more specific aspects (15-20).

The cladding that usually has a higher intrinsic loss than the core material is reported to further increase the leaky ray attenuation, although its effect is mainly constrained to rays lying close to the refracting ray boundary (16). Another interesting study (17) identifies six different sources of losses in the fibre.

Perhaps, the most important case would be the investigation of asymmetries in the fibre cross-section. This is known to lead to a reduction in the ratio of tunnelling to bound ray power (20).

Through the calculations of this chapter, it was demonstrated that the Airy function formulation adequately described the behaviour of individual leaky and refracting rays across the entire $\overline{\beta}$-$\overline{T}$ domain.

When however, the overall attenuation is to be determined, the rather involved nature of this analysis prevents its full utilization.

The rest of the mathematical treatment was therefore conducted employing the WKB expression.

From a method previously applied to core-cladded fibres, a theory aimed at the filtration of rays with an outer jacket was developed.

In the literature there is a frequent reference to experimental arrangements using mode strippers to remove the unwanted radiation from the fibre (21, 22, 23). Though the ultimate purpose is not clearly stated*, it is logical to assume that such an assembly should preferentially affect the rays belonging to the leaky group.

It was shown in this work that compared with the amount of power extracted from the bound ray region, this procedure leaves the leaky rays almost unaltered. The computations confirmed that, to achieve any reasonable degree of filtering, the cladding thickness would have to be smaller than that of currently available commercial fibres. Obviously the extreme of reducing the dimensions of the cladding is to introduce a jump of the interface. Studies of this type are undertaken in (5, 14).

The effects of varying the cladding radius were also considered in (24, 25). Reference (25) gives the calculation of excess loss of guided rays caused by the outer layer.

---

* To make an exact quotation, 'Mode strippers were used to remove the light travelling in the cladding' (21). Whether this is due to initial launching into the cladding or the general existance of leaky rays, is not explained.

CHAPTER II

MODE THEORY

Fundamentally optical investigation on the basis of electromagnetic wave theory presents a formidable task. Mathematical development of the theory manifests itself as quite a topic on its own. Difficulties also arise in attempting to ascribe a physical meaning to the constructed model.

Despite the drawbacks, some of the complexity may promptly be alleviated by considering the practical design of fibres. The most important property which leads to major simplification is the small refractive index difference between the core and the cladding. This condition is principally dictated by low dispersion requirements. However it in retrospect helps the theoretical treatment.

From the point of view of technological limitations, the exact solutions of Maxwell's Equations for an arbitrary dielectric medium still remains an academic curiosity. This does not however mean that such strides are futile . On the contrary, a sound judgement on the quality of usable forms can only be made by referring back to the most complete representations. Therefore, the logical place to start would seem to be the Maxwell Equations themselves.

2.1 Derivation of Field Equations

The well known Maxwell's Equations are

$$\nabla \times \vec{E} = - j\omega \mu_0 \vec{H} \qquad (2.1)$$

$$\nabla \times \vec{H} = j\omega \varepsilon_o \varepsilon \vec{E} \tag{2.2}$$

$\vec{E}$ and $\vec{H}$ are the electric and magnetic field vectors respectively. $\nabla \times$ denotes the curl operator. The remaining quantities are

ω = frequency of radiation
$\varepsilon_o(\mu_o)$ = permittivity (permeability) of vacuum
ε = permittivity of propagation medium

Assuming the dependence $e^{j(\omega t - m\phi - \beta z)}$ where m (integer) is the azimuthal mode number, β propagation constant and t shows the time variation, then via the use of the curl operator, the following will be obtained:

$$j\omega \varepsilon_o \varepsilon E_z = \frac{1}{r} \frac{\partial}{\partial r} (r H_\phi) + \frac{jm}{r} H_r \tag{2.3}$$

$$j\omega \varepsilon_o \varepsilon E_\phi = -j\beta H_r - \frac{\partial}{\partial r} H_z \tag{2.4}$$

$$j\omega \varepsilon_o \varepsilon E_r = j\beta H_\phi - \frac{jm}{r} H_z \tag{2.5}$$

$$-j\omega \mu_o H_z = \frac{1}{r} \frac{\partial}{\partial r} (r E_\phi) + \frac{jm}{r} E_r \tag{2.6}$$

$$-j\omega \mu_o H_\phi = -j\beta E_r - \frac{\partial}{\partial r} E_z \tag{2.7}$$

$$-j\omega\,\mu_o\,H_r = j\,\beta\,E_\phi - \frac{jm}{r}\,E_z \qquad (2.8)$$

Thus, this set provides all three components of E (or H) in terms of the other. By subsequent substitutions, it is possible to reduce to the requested differential equation for one of them. Conventionally E_z (or H_z) is chosen for the purpose.

In what follows (unless otherwise stated), prime will specify differentiation w.r.t. r.

Hence on rearranging 2.3 to 2.8*

$$E_z'' + \left[\frac{1}{r} - \frac{\varepsilon'\beta^2}{\varepsilon(k_o^2\varepsilon - \beta^2)}\right] E_z' + \left(k_o^2\,\varepsilon - \beta^2 - \frac{m^2}{r^2}\right) E_z$$

$$= -j\,\frac{\omega\,\mu_o\,\beta\,m\,\varepsilon'}{\varepsilon r\,(k_o^2\,\varepsilon - \beta^2)}\,H_z \qquad (2.9)$$

while for H_z

---

* For a complete description of the mathematical derivations in this chapter, the reader may consult Appendix A.

$$H_z'' + \left[\frac{1}{r} - \frac{\varepsilon' k_o^2}{\varepsilon(k_o^2\varepsilon - \beta^2)}\right] H_z' + \left(k_o^2\varepsilon - \beta^2 - \frac{m^2}{r^2}\right)H_z =$$

$$= j\frac{\omega \varepsilon_o \beta m \varepsilon'}{r(k_o^2\varepsilon - \beta^2)} E_z \qquad (2.10)$$

These are the familiar coupled differential equations.

Any further eliminations will produce a differential equation of fourth order which is cumbersome to handle. Some simplifications may be effected at this stage.

Introducing the permittivity distribution of the medium

$$\varepsilon(r) = \varepsilon_1(1 - h(r)) \qquad (2.11)$$

$\varepsilon_1 = n_1^2$ is the relative permittivity on the core centre. $h(r)$ defines the profile function and is terminated at the cladding interface so that

$$\varepsilon(a) = \varepsilon_1 (1 - 2\Delta) = \varepsilon_2 = n_2^2 \text{ (cladding refractive index)}$$

The various terms in 2.9 and 2.10 may now be rewritten (after dropping the subscript r) as

$$\frac{\varepsilon' \beta^2}{\varepsilon(k_o^2 \varepsilon - \beta^2)} = -\frac{h' k_o^2 \varepsilon_1}{k_o^2 \varepsilon - \beta^2} + \frac{h'}{1 - h} \simeq -\frac{h' k_o^2 \varepsilon_1}{k_o^2 \varepsilon - \beta^2} \qquad (2.12)$$

$$\frac{\omega \mu_0 \beta m \epsilon'}{\epsilon r(k_0^2\epsilon-\beta^2)} = -(\frac{1}{1-h})[\frac{\omega \mu_0 \beta m h'}{r(k_0^2\epsilon - \beta^2)}] \simeq -Z_0 [\frac{k_0 \beta m h'}{r(k_0^2\epsilon - \beta^2)}] \quad (2.13)$$

$$\frac{\omega \epsilon_0 \beta m \epsilon'}{r(k_0^2\epsilon - \beta^2)} = -\frac{\epsilon_1}{Z_0} [\frac{k_0 \beta m h'}{r(k_0^2\epsilon - \beta^2)}] \quad (2.14)$$

$Z_0 = (\mu_0/\epsilon_0)^{\frac{1}{2}}$, intrinsic impedance of free space.

Kurtz and Streifer (1) demonstrated that the axial components may then approximately be expressed by:

$$E_z = C_1 G_1 - C_2 G_2 \quad (2.15)$$

$$H_z = \frac{j}{Z_0} \epsilon_1^{\frac{1}{2}} (C_1 G_1 + C_2 G_2) \quad (2.16)$$

C_1, C_2 = constants

From Appendix A, the transverse fields are seen to be (radial components omitted)

$$E_\phi = -\frac{1}{k_0^2\epsilon - \beta^2} [\frac{\beta m}{r} (C_1 G_2 - C_2 G_2) + k_0 \epsilon_1^{\frac{1}{2}} (C_2 G_2' + C_2 G_2')] \quad (2.17)$$

$$H_\phi = -\frac{j \epsilon_1^{\frac{1}{2}}}{Z_0(k_0^2\epsilon - \beta^2)} [\frac{\beta m}{r} (C_1 G_1 + \beta G_2) + k_0 \epsilon_1^{\frac{1}{2}} (1-h)(C_1 G_1' - \beta G_2')] \quad (2.18)$$

The coupling terms in Equations 2.9 and 2.10 will vanish if an homogeneous cladding is considered.

Therefore, the solutions in this region are

$$\text{(Modified Hankel Function) } K_m = K_m(wr/a) = K_m((\beta^2 - k_o^2\epsilon_2)^{\frac{1}{2}}r) \tag{2.19}$$

$$E_z = C_3 K_m \tag{2.20}$$

$$H_z = j \frac{\epsilon_2^{\frac{1}{2}}}{Z_o} C_4 K_m \tag{2.21}$$

$$E_\phi = \frac{a^2}{w^2}\left(\frac{\beta m}{r} C_3 K_m + k_o \epsilon_2^{\frac{1}{2}} C_4 K_m'\right) \tag{2.22}$$

$$H_\phi = \frac{j a^2 \epsilon_2^{\frac{1}{2}}}{Z_o w^2}\left(k_o \epsilon_2^{\frac{1}{2}} C_3 K_m + \frac{\beta m}{r} C_4 K_m'\right) \tag{2.23}$$

C_3, C_4 = constants

Matching the conditions at the boundary r = a will yield the characteristic equation

$$\frac{K_m'}{K_m} = \frac{G_i'}{G_i} \tag{2.24}$$

where i = 1 (i = 2) will, in the forthcoming expressions, correspond to upper (lower) sign.

2.2 Solution of the Characteristic Equation

The solution to 2.24 in terms of G_i presents difficulties. It is therefore advantageous to determine a transverse field function, F_i separately.

From 2.17 (or 2.18)

$$F_i = \frac{1}{k_0 \varepsilon_1^{\frac{1}{2}} (1 - h - \beta_1^2)} \left(\pm \beta_1 \frac{m}{r} G_i + G_i'\right) \tag{2.25}$$

$$\beta_1 = \beta/(k_0 \varepsilon_1^{\frac{1}{2}}) \tag{2.26}$$

Consequently G_i in terms of F_i

$$G_i = -\frac{1}{k_0 \varepsilon_1^{\frac{1}{2}}} \left(\frac{1 \mp \beta_1 m}{r} F_i + F_i'\right) \tag{2.27}$$

The right hand side of equation 2.24 then becomes

$$\frac{G_i'}{G_i} = \mp \beta_1 \frac{m}{a} + \frac{F_i \, w^2/a^2}{\frac{1 \mp \beta_1 m}{a} + F_i'} \tag{2.28}$$

By the combined use of 2.25 and 2.27, the differential equation for the transverse field may be deduced. Thus

$$F_i'' + \frac{F_i'}{r} + [k_o^2 \varepsilon_1 (1 - h - \beta_1^2) - (\frac{\beta_1 m \mp 1}{r})^2] F_i = 0 \quad (2.29)$$

with

$$x = r^2 \frac{k_o \gamma}{a} \quad (2.30)$$

$$W_i = x^{\frac{1}{2}} F_i$$

and setting $h(r) = 2\Delta(r/a)^2$, $\beta_1 = 1$, equation 2.29 is transformed into

$$\frac{d^2 W_i}{dx^2} + \frac{1}{4} [-1 + \frac{a(k_o^2 n_1^2 - \beta^2)}{k_o \gamma x} + \frac{1 - (m \mp 1)^2}{x}] W_i = 0 \quad (2.31)$$

where the solution is

$$W_i = e^{-x/2} x^{B_i/2} M_i (A_i, B_i, x) \quad (2.32)$$

M is known as the confluent hypergeometric function (Ref. Appendix B). The additional arguments are defined as

$$B_i = 1 + (m \mp 1) \quad (2.33)$$

$$A_i = \frac{B_i}{2} - \frac{a(k_o^2 n_1^2 - \beta^2)}{4 k_o \gamma} \quad (2.34)$$

On replacement into 2.24, 2.28, 2.30, 2.32, the modified version of the characteristic equation reads

$$-w \frac{K_m}{K_{m\mp1}} = V \left(\frac{2 A_i}{B_i} \frac{M_{i+1}}{M_i} - 1\right) + P_{ti} \tag{2.35}$$

$$P_{t\frac{1}{2}} = \begin{matrix} 2(m+1) \\ 2(m-1) \end{matrix} \tag{2.36a}$$

$$V = a k \gamma \tag{2.36b}$$

$$M_{i+1} = M_{i+1} ((A_i + 1), (B_i + 1), x) \tag{2.36c}$$

V is the so-called normalised frequency of the fibre.

Within the concept of modal analysis, the attenuation coefficient has to be recovered from the imaginary part of propagation constant β, since leaky modes allow a solution in complex notation only.

An approach previously formulated for step index fibres (2) will be pursued here. To this end, the conventional term u will be introduced where

$$u = a(n_1^2 k_o^2 - \beta^2)^{\frac{1}{2}} \tag{2.37}$$

Thus similar to w (equation 2.19), it describes the phase parameter inside the core.

After collecting all the terms in Equation 2.35 on one side and employing the alternative representation

$$X(u) = 0 \tag{2.38}$$

In practice, even for strongly leaky modes, the imaginary part of β will be small compared with the real part.

Hence, the following situations exist

$$\beta = \beta_r + j\,\beta_m \qquad \beta_m < \beta_r \text{ or } \beta_m << \beta_r \tag{2.39a}$$

$$u = u_r + j\,u_m \qquad u_m < u_r \text{ or } u_m << u_r \tag{2.39b}$$

$$w = w_r + j\,w_m \qquad w_m > w_r \text{ or } w_m >> w_r \tag{2.39c}$$

Equation 2.38 may be expanded as a Taylor Series

$$X(u_r + j\,u_m) = X(u_r) + j\,u_m \frac{d}{du_r} X(u_r) + (ju_m)^2 \frac{d^2}{du_r^2} X(u_r) + \ldots$$

$$\ldots \tag{2.40}$$

With the first two terms retained, the imaginary component is

$$X(u_r)_m + u_m \frac{d}{d\,u_r} X\,(u_r)_r = 0 \tag{2.41}$$

$$u_m = - \frac{X\,(u_r)_m}{\frac{d}{d\,u_r} X\,(u_r)_r} \tag{2.42}$$

To acquire $X\ (u_r)_m$, since w_m is large, it is more appropriate to invoke Hankel function H^2 (to be abbreviated by H henceforth) so that

$$\mathrm{Im}\ (w_m \frac{K_m}{\bar{K}_{m+1}}) = \frac{2}{\pi |\bar{H}_{m+1}|^2} \tag{2.43}$$

u is related to the parameters A_i, B_i via

$$u = (2V\ (B_i - 2\ A_i))^{\frac{1}{2}} \tag{2.44}$$

Thus if $u_r >> u_m$, the same will hold for A_i. The contribution from the confluent hypergeometric function to $X(u_r)_m$ may then be neglected.

Equation 2.44 will result in the partial differential operator

$$\frac{\partial}{\partial u_r} = \frac{u}{2V} (- \frac{\partial}{\partial A_i} + 2 \frac{\partial}{\partial B_i}) \tag{2.45}$$

when used on M, this will deliver

$$(- \frac{\partial}{\partial A_i} + 2 \frac{\partial}{\partial B_i})\ M_i\ (A_i, B_i, x) = U_i\ (A_i, B_i, x) \tag{2.46}$$

where, as shown in Appendix A, the function U may be expressed in a convenient form utilising the series representation of M. Together with the other details mentioned in the same Appendix, it is found that

$$\beta_m = \frac{\frac{2}{\pi} \frac{1}{|H_{m\mp1}|^2} \frac{1}{\beta_r a^2}}{\frac{A_i}{B_i} \frac{(U_{i+1} M_i - U_i M_{i+1})}{M_i^2} - \frac{B_i + 2A_i}{B_i^2} \frac{M_{i+1}}{M_i} + \frac{2}{V} + \left(1 - \frac{|H_{m\mp2} H_m|}{|H_{m\mp1}|^2}\right)} \tag{2.47}$$

2.3 Estimation of Error

On the derivation so far put forward, an estimate of the error involved is necessary.

Note that the characteristic equation was finally expressed using the transverse fields, therefore a more accurate representtation of the latter (in the core region) should establish the bases for such an analysis.

In the main the exact coupling between the transverse field will be governed by the pair chosen (i.e. E_ϕ, E_r or H_ϕ, H_r, refer to Appendix A). Assuming the case for the magnetic field

$$F_i'' + \frac{F_i}{r} + [k_o^2 \varepsilon - \beta^2 (\frac{m\mp1}{r})^2] F_i - \frac{\varepsilon'}{\varepsilon} (F_i' + \frac{1\mp m}{r} F_i) = 0 \tag{2.48}$$

The above differs from that of 2.29 via the last group of terms whose contribution would slightly alter the solution given earlier.

In order to predict what deviation ($\Delta\beta$) this would produce in the value of propagation constant, the following may be evaluated (3,4).

$$\Delta\beta = \frac{\int_0^{2\pi} \int_0^a F_i \frac{\varepsilon'}{\varepsilon} \left(F_i' + \frac{1 \mp m}{r} F_i\right) dr\, d\phi}{\int_0^{2\pi} \int_0^a F_i^2\, r\, dr\, d\phi} \qquad (2.49)$$

The integral as seen is to be carried out over the cross-section of the fibre.

Here the interest is with the perturbation in the imaginary part of β. If β_t and β_p are the propagation constants obtained from the reduced and perturbed form respectively, then

$$\beta_t^2 = (\beta_{tr} + j\,\beta_{tm})^2 \simeq \beta_{tr}^2 + 2j\,\beta_{tr}\,\beta_{tm}$$

$$\beta_p^2 = (\beta_{pr} + j\,\beta_{pm})^2 \simeq \beta_{pr}^2 + 2j\,\beta_{pr}\,\beta_{pm}$$

$$\beta_{pr} = \beta_{tr} + \Delta\beta_r \qquad (2.50)$$

$$\beta_{pm} = \beta_{tm} + \Delta\beta_m$$

$$\Delta\beta_m << \Delta\beta_r$$

Since the dependence of $e^{-jm\phi}$ was originally postulated, the integration over ϕ from both the numerator and the denominator will cancel. Additionally the conditions in 2.50 dictate that Re $(F_i) >>$ Im (F_i).
Therefore

$$\Delta\beta_m = \frac{1}{\beta_{tr}} \quad \frac{\int_0^a (P_1)_r \, r \, dr \int_0^a F_{ir} \, F_{im} \, r \, dr}{(\int_0^a F_i^2 \, r \, dr)^2} \tag{2.51}$$

where the whole of the upper line from 2.49 is now abbreviated by P_1. On replacement for F_i and changing to the variable x, this will read

$$\Delta\beta_m = \frac{1}{\beta_{tr}} \quad \frac{\{\int_0^V \frac{2\,\Delta(x/V)^{\frac{1}{2}} e^{-x} x^{B_i-1} M_i^2 [2 (\frac{k_o \gamma x}{a})^{\frac{1}{2}} (-\frac{1}{2} \cdot \frac{B_i-1}{2} + \frac{A_i}{B_i} \frac{M_{i+1}}{M_i}) + \frac{1 \mp m}{x^{\frac{1}{2}}} (\frac{k_o \gamma}{a})^{\frac{1}{2}}] \, dx\}}{(1-2\Delta x/V)}}{P_2}$$

$$\frac{(\int_0^V \frac{1}{2} e^{-x} x^{B_i-1} M_{ir} M_{im} \, dx)}{P_2} \tag{2.52}$$

$$P_2 = (\int_0^V \frac{1}{2} e^{-x} x^{B_i-1} M_i^2 \, dx)^2$$

2.4 Other Parameters of Mode Theory and Some Concepts

A particular mode of the fibre is designated by two letters, m, p (integers) where the former, as previously defined, shows the azimuthal variation. The second letter, p counts the number of zero crossings that a mode makes in the radial direction, hence the name radial order.

Apart from the usually known TE (transverse electric) and TM (transverse magnetic), hybrid modes HE and EH possessing longitudinal components both from E_z and H_z are also present in the fibre. Due to the weak guidance property however, the amplitude of the longitudinal fields is quite small compared with their transverse counterparts. From this the nearly circularly (linearly) polarized character of the fibre modes arises. As a result, the linearly polarized approximation has frequently been employed in the literature (5,6).

In the mathematical treatment in Section 2.1, the scalar function G_2 (or G_1) may alternately be set to zero to generate HE (or EH) modes while m = 0 will give TE (or TM).

On ignoring the cladding effects, the confluent hypergeometric function may be replaced by*

$$M(A_i, B_i, x) = \frac{-A_i\ !}{(1 + m \mp 1)_{-A_i}} L^{m\mp 1}_{-A_i}(x) \qquad (2.53)$$

L = Laguerre polynomial.

where A_i is now proportional to p and the connecting formula is

$$p = -A_i + 1 = \frac{A\,(k_o^2\, n_1^2 - \beta^2)}{4\, k_o \gamma} + \frac{(1 - m \pm 1)}{2} \qquad (2.54)$$

---

* Always $A_i < 0$, thus it turns positive on the R.H.S. For more detailed discussion on Laguerre polynomials, refer to Appendix B.

In the proper mode description p may be considered real, but the restriction integer values in this instance are due to extending the core medium to infinity (7).

Amongst the several modes supported by a fibre, a certain degree of degeneracy is to be observed especially when far from cut-off (cut-off is at $\beta = k_o \varepsilon_2^{\frac{1}{2}}$) meaning that the property of such modes will ultimately resemble each other. In general this degeneracy occurs between HE_{m+2p} and EH_{mp} as may also be verified analytically from 2.54.

In some cases, a process of mode counting may be desirable. This is to be accomplished by summing for each possible combination of p and m.

Noting the equivalence

$$\ell = ka\,\overline{l} = m \mp 1 \qquad (2.55)$$

as an approximation 2.54 may be converted into an integral over ℓ with limits from 0 to V/2 for guided modes and from 0 to V to include all modes. The propagation constant will simultaneously have

$$\beta = k_o n_2 \quad \text{guided modes}$$

$$\beta = (k_o^2 n_2^2 - (\tfrac{\ell}{a})^2)^{\frac{1}{2}} \quad \text{guided + leaky modes}$$

By further discarding the unistate polarization of TE and TM modes, the following may be obtained:

$$N_{guided} = \frac{V^2}{4} + V \qquad (2.56a)$$

$$N_{total} = \frac{V^2}{3} + 2V \qquad (2.56b)$$

2.5 Numerical Results (3)

As stressed in the opening remarks of this chapter, the mathematical complexity encountered within the context of mode analysis surpasses that of ray theory. Some of these are touched upon below. Computations will refer to HE modes unless specified otherwise.

In order to offer pictorial information on what happens in the fibre, the transverse fields are plotted in Figures 2.1, 2.2 for a selection of guided and leaky modes. The fields of the low order guided modes are well confined to the fibre axis, whereas the leaky modes have their fields extending strongly into the cladding.

As the prime target, equation 2.47 was evaluated numerically to obtain the attenuation coefficient (note that $\alpha = 2\ \beta_m$). The propagation constant decrements were the same as before. Additionally, for easier inspection, the $\overline{\beta}$ values from the ray analysis were retained (Table 2.1).

The large discrepancy immediately apparent is to be attributed to the following. In contrast to describing the propagation in terms of individual rays, mode theory requires the quantization of electromagnetic waves into discrete levels which are understandably labelled as modes. For the purpose of identifying these modes one by one, the characteristic equation that obeys the matching conditions at the interface is solved. Therefore, for a given set of fibre parameters, the propagation will only take place at certain values of β. Attempting to designate a propagation constant

other than those obtained directly from the solution of the characteristic equation violates the concept of matching, hence cannot represent a physically realizable mode.

Evidently, the equation derived in the preceding section assumed the prior knowledge of the real part of β. To facilitate this and also to substantiate the above claims, a simple method was resorted to.

The existence of turning points of rays were stated in Chapter 1. Thus, there would prevail a similar situation for the modes of the fibre. Using only the real part of β, the approximate location of the turning point was searched via the transverse field distribution function in the core. When this was found, the corresponding β_r value was perturbed till it yielded a smooth continuation of the fields on either side of the interface. This was initially done on a large scale graphing. Later the region around $0.95a \leq r \leq 1.05a$ was examined in greater detail.

The subsequent figures of the propagation constant were fed into equation 2.47. The results for some of the modes are displayed in Table 2.2.

Compared with the previous calculations, the agreement in this instance is excellent with the average error being 10%.

Finally the field distributions were replotted, this time taking into account both the real and imaginary components of β. The matching of the fields at the boundary was observed to be undisturbed, thus confirming that β_m would indeed be negligible in the majority of cases.

One remainder is that, to enable a fair basis of comparison, the azimuthal order was supplied to the ray analysis programme after subtracting 0.25 from the corresponding figure used here (i.e. $\ell^2 - 1/4$).

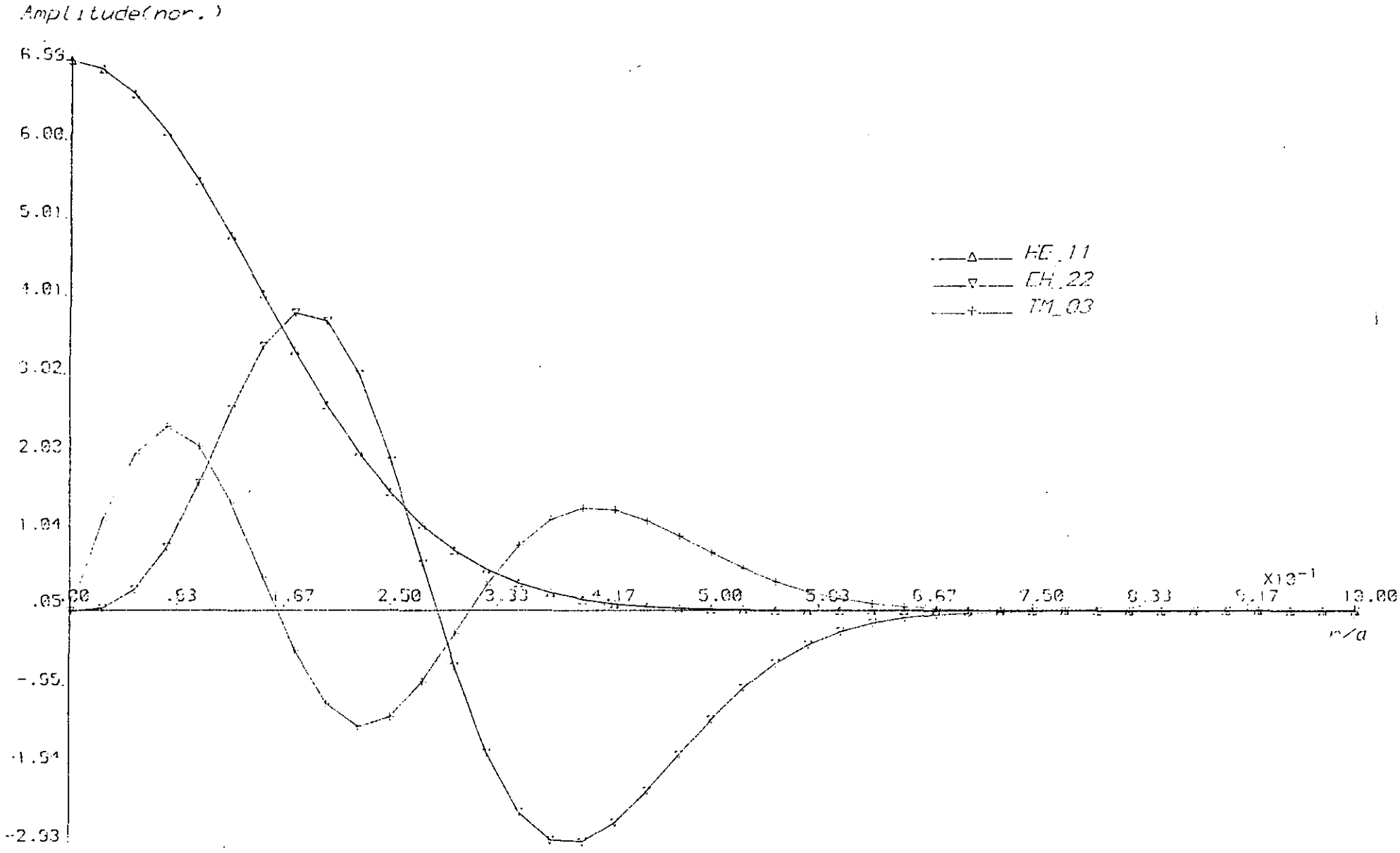

Fig. 2. 1 Transverse Field distributions of Guided Modes

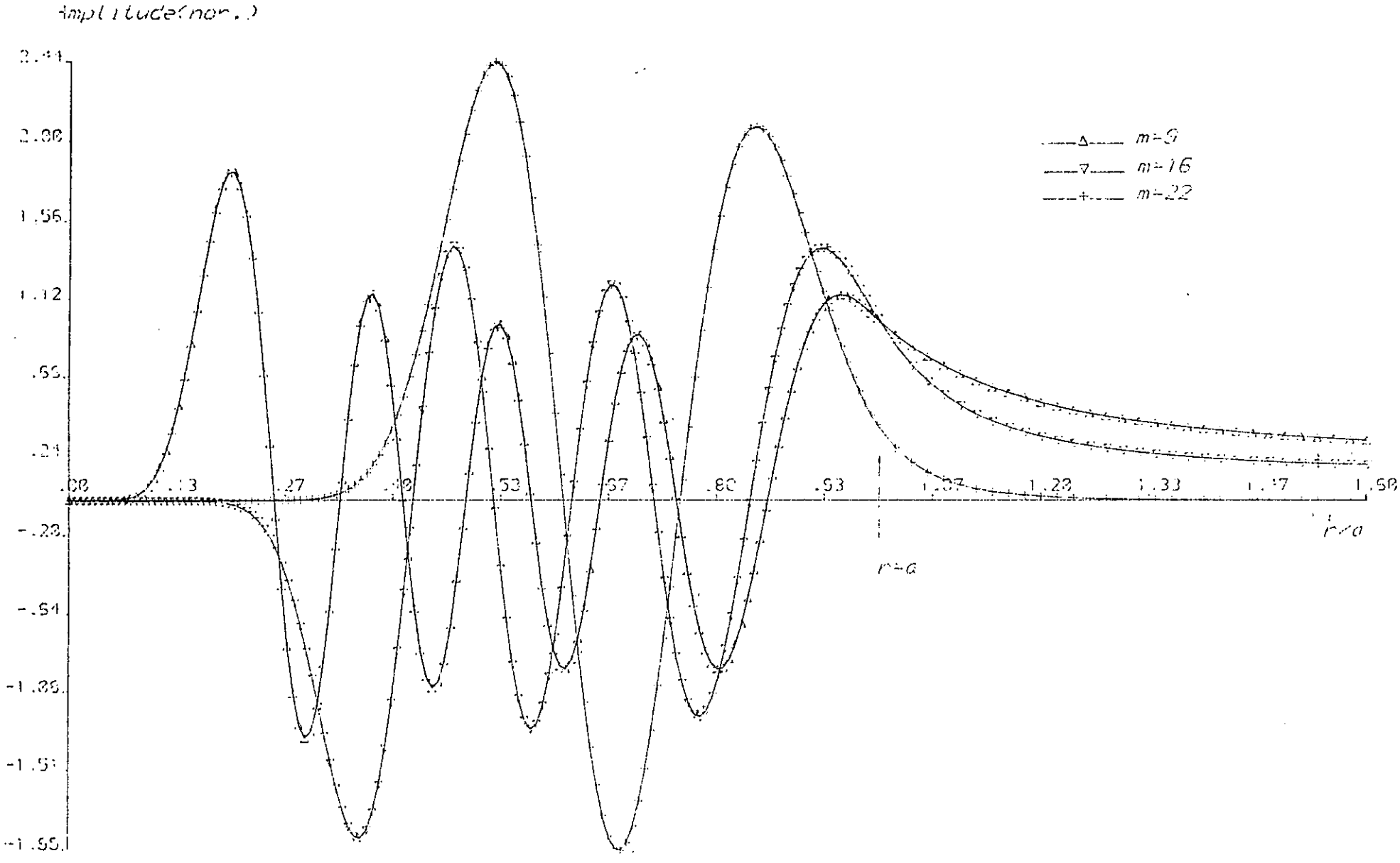

Fig. 2.2 Transverse field distributions of Leaky Modes

---------- TABLE (2.1) ----------

Comparison of Attenuation Coeff. for m = 10 q = 2.0

Ray An.	Ray wkb	Modal	Beta Sq.
0.1259D-32	0.1104D-32	0.1368D-31	2.1231
0.9455D-02	0.8483D-02	0.8650D-01	2.1229
0.2331D 01	0.2155D 01	0.1466D 02	2.1227
0.4002D 02	0.3959D 02	0.1680D 03	2.1225
0.2075D 03	0.2394D 03	0.7520D 03	2.1223
0.5184D 03	0.7548D 03	0.2348D 04	2.1221
0.8397D 03	0.1474D 04	0.6186D 04	2.1219

****

Comparison of Attenuation Coeff. for m = 14 q = 2.0

Ray An.	Ray wkb	Modal	Beta Sq.
0.4515D-53	0.3962D-53	0.2720D-51	2.1231
0.5427D-06	0.4757D-06	0.2578D-04	2.1228
0.2328D-02	0.2031D-02	0.7864D-01	2.1225
0.2300D 00	0.2003D 00	0.5250D 01	2.1222
0.4712D 01	0.4122D 01	0.6764D 02	2.1219
0.3911D 02	0.3514D 02	0.3568D 03	2.1216
0.1714D 03	0.1675D 03	0.1202D 04	2.1213
0.4486D 03	0.5189D 03	0.3334D 04	2.1210
0.7903D 03	0.1125D 04	0.8610D 04	2.1207
0.1077D 04	0.1698D 04	0.2258D 05	2.1204

---------- TABLE (2.2) ----------

Comparison of Attenuation Coeff. for chosen Beta values q = 2.0

m	Ray An.	Modal	Beta Sq.
7	0.6287D 03	0.5821D 03	2.1226
9	0.2083D 03	0.1591D 03	2.1225
11	0.1991D 02	0.1704D 02	2.1224
13	0.8513D 00	0.7541D 00	2.1223
14	0.5752D 03	0.5752D 03	2.1209
15	0.1050D-01	0.9717D-02	2.1222
16	0.8674D 02	0.8577D 02	2.1208
17	0.5164D-04	0.4875D-04	2.1222
18	0.4505D 01	0.4732D 01	2.1207
19	0.1150D-06	0.1023D-06	2.1222
20	0.8449D-01	0.9239D-01	2.1206
22	0.6786D-03	0.6613D-03	2.1206

TABLE (2.3)

A) Arbitary Beta :

Error Term in Imaginary part of Beta for m = 10

Rel. Error	Imaginary Beta	Beta Sq.
0.4960D-07	0.6838D-32	2.1231
0.3547D-07	0.4325D-01	2.1229
0.2375D-07	0.7330D 01	2.1227
0.6532D-07	0.8400D 02	2.1225

****

Error Term in Imaginary part of Beta for m = 22

Rel. Error	Imaginary Beta	Beta Sq.
-0.7079D-07	0.1281D-94	2.1231
0.8579D-07	0.3290D-12	2.1225
0.2378D-06	0.2367D-06	2.1219
0.4119D-06	0.3900D-03	2.1213

****

B) After Graphical matching :

Error Term in Imaginary part of Beta

Rel. Error	Imaginary Beta	Beta Sq.	m
0.1810D-07	0.2911D 03	2.1226	7
0.7003D-07	0.8520D 01	2.1224	11
0.9547D-07	0.2876D 03	2.1209	14
0.2360D-06	0.4288D 02	2.1208	16
0.2220D-06	0.2366D 01	2.1207	18
0.3095D-06	0.4619D-01	2.1206	20

The error term was evaluated employing the integral given in 2.52 A few examples are listed in Table 2.3. It is interesting to note that despite the difficulties mentioned above (i.e. whether β values were chosen randomly or not), the average error did not exceed 10^{-5} .

2.6 Mode Filtering

The former derivations of this chapter have assumed an infinite cladding. This is not practically feasible of course. Therefore a double boundary problem may be formulated for two reasons: (a) to assess how good the infinite cladding approximation is, and (b) to explore the filtering possibilities, a subject currently discussed in the ray analysis.

The previously stated equations for the core fields will remain unchanged. Due to the confinement of the cladding region, the fields here now consist of the combination of K and I. While the Bessel function K alone will describe the propagation in the newly added layer.

Hence, in the core

$$E_z = C_1 G_1 - C_2 G_2 \tag{2.57}$$

$$H_z = \frac{j \varepsilon_1^{\frac{1}{2}}}{Z_0} (C_1 G_1 + C_2 G_2) \tag{2.58}$$

$$E_\phi = - \frac{1}{k_0^2 \varepsilon - \beta^2} \left[\frac{\beta m}{r} (C_1 G_1 - C_2 G_2) + k_0 \varepsilon_1^{\frac{1}{2}} (C_1 G_1' + C_2 G_2')\right] \tag{2.59}$$

$$H_\phi = - \frac{j\,\varepsilon_1^{\frac{1}{2}}}{Z_o\,(k_o^2\varepsilon - \beta^2)} \left[\frac{\beta m}{r}\,(C_1\,G_1 + C_2\,G_2) + k_o\,\varepsilon_1^{\frac{1}{2}}(1-h).\right.$$

$$\left.(C_1\,G_1' - C_2\,G_2')\right] \qquad (2.60)$$

In the cladding

$$E_z = C_3\,K_m\,(wr/a) + C_4\,I_m\,(wr/a) \qquad (2.61)$$

$$H_z = \frac{j\,\varepsilon_1^{\frac{1}{2}}}{Z_o}\,(C_5\,K_m + C_6\,I_m) \qquad (2.62)$$

$$E_\phi = \frac{a^2}{w^2}\,\left[\frac{\beta m}{r}\,(C_3\,K_m + C_4\,I_m) + k_o\,\varepsilon_2^{\frac{1}{2}}\,(C_5\,K_m' + C_6\,I_m')\right] \qquad (2.63)$$

$$H_\phi = \frac{j\,\varepsilon_2^{\frac{1}{2}}\,a^2}{Z_o\,w^2}\,\left[\frac{\beta m}{r}\,(C_5\,K_m + C_6\,I_m) + k_o\,\varepsilon_2^{\frac{1}{2}}(C_3\,K_m' + C_4\,I_m')\right] \qquad (2.64)$$

In the jacket

$$E_z = C_7\,K_m\,(vr/a) \qquad (2.65)$$

$$H_z = \frac{j\,\varepsilon_3^{\frac{1}{2}}}{Z_o}\,C_8\,K_m \qquad (2.66)$$

$$E_\phi = \frac{a^2}{v^2}\,(\frac{\beta m}{r}\,C_7\,K_m + k_o\,\varepsilon_3^{\frac{1}{2}}\,C_8\,K_m') \qquad (2.67)$$

$$H_\phi = \frac{j\,\varepsilon_3^{\frac{1}{2}}\,a^2}{Z_o\,v^2}\,(\frac{\beta m}{r}\,C_8\,K_m + k_o\,\varepsilon_3^{\frac{1}{2}}\,K_m') \qquad (2.68)$$

where $v = a(\beta^2 - n_3^2 k_0^2)^{\frac{1}{2}}$, (refractive index of jacket) $n_3^2 = \epsilon_3$ (permittivity of jacket), C_1, C_2 ... C_8 = constants.

On matching at the respective interfaces i.e. r = a and r = b (cladding radius), the following characteristic equation may be deduced (refer to Appendix A).

$$\frac{G_i'}{G_i} = \frac{K_m'(I_{m1}' K_{m2} - I_{m1} K_{m2}') - I_m'(K_{m1}' K_{m2} - K_{m1} K_{m2}')}{K_m(I_{m1}' K_{m2} - I_{m1} K_{m2}') - I_m (K_{m1}' K_{m2} - K_{m1} K_{m2}')} \qquad (2.69)$$

$K_m = K_m(w)$, $I_m = I_m(w)$, $K_{m1} = K_m(wb/a)$, $I_{m1} = I_m(wb/a)$,

$K_{m2} = K_m(vb/a)$, $I_{m2} = I_m(vb/a)$

2.7 Solution of Characteristic Equation

To solve the characteristic equation, the approach adopted previously will be used.

By substituting the transverse field function for G_i in 2.69

$$V\left(\frac{2 A_i}{B_i} \frac{M_{i+1}}{M_i} + 1\right) + P_{ti}$$

$$+ w \frac{K_m(s I_{m1\mp1} K_{m2} + I_{m1} K_{m2\mp1}) - I_m(-s K_{m1\mp1} K_{m2} + K_{m1} K_{m2\mp1})}{K_{m\mp1}(s I_{m1\mp1} K_{m2} + I_{m1} K_{m2\mp1}) + I_{m\mp1}(-s K_{m1\mp1} K_{m2} + K_{m1} K_{m2\mp1})}$$

$$= X(u) \equiv 0 \qquad (2.70)$$

$s = w/v$

Since evenescence is expected to continue beyond the cladding into the jacket, the argument of I as well as that of K will have a dominant imaginary component. The counterparts J and H^2 may again be invoked.

Thus, the last term of the characteristic equation resolves to

$$\mp j w \frac{H_m H_5 + J_m H_6}{H_{m\mp 1} H_5 - J_{m\mp 1} H_6} \tag{2.71}$$

$$H_5 = s J_{m1\mp 1} H_{m2} - J_{m1} H_{m2\mp 1}, \quad H_6 = s H_{m1\mp 1} H_{m2} - H_{m1} H_{m2\mp 1}$$

The aim is then to find

$$u_m = - \frac{\mathrm{Im}\,[X(u_r)]}{\mathrm{Re}\,[\frac{X(u_r)}{d u_r}]} \tag{2.72}$$

$w_r << w_m$ and if the jacket is to disturb the fields slightly, the parameter s will therefore have

$$s = s_r + j s_m, \quad s_r \simeq \frac{w_m}{v_m}, \quad s_r >> s_m \tag{2.73}$$

so that its imaginary part too may be neglected.

On employing the rest of the approximations already mentioned, the numerator in 2.72 becomes

$$\mathrm{Im}(X(u_r)) = \frac{8 a^2/(\pi^3 v_m{}^2 b^2)}{[(Y_{m2\mp 1} H_1 - s_r Y_{m2} H_2)^2 + (J_{m2\mp 1} H_1 - s_r J_{m2} H_2)^2]} \tag{2.74}$$

with $H_1 = Y_{m\mp1}\, J_{m_1} - J_{m\mp1}\, Y_{m_1}$, $H_2 = Y_{m\mp1}\, J_{m_1\mp1} - J_{m\mp1}\, Y_{m_1\mp1}$

On the other hand

$$\frac{d}{d\, u_r}\ [w_m\ \frac{H_m\, H_5 + J_m\, H_6}{H_{m\mp1}\, H_5 - J_{m\mp1}\, H_6}]$$

$$= +\, u_r[\frac{(H_{m\mp2}\, H_5 - J_{m\mp2}\, H_6)(H_m\, H_5 + J_m\, H_6)}{(H_{m\mp1}\, H_5 - J_{m\mp1}\, H_6)^2}$$

$$- \frac{(H_{m\mp1}\, H_5 + J_{m\mp1}\, H_6)(H_{m\mp1}\, H_5 - J_{m\mp1}\, H_6)}{(H_{m\mp1}\, H_5 - J_{m\mp1}\, H_6)^2}\ ] \qquad (2.75)$$

When all the relevant elements are inserted into

$$\beta_m = \frac{u_r\, u_m}{\beta_r\, a^2} \qquad (2.76)$$

$$\beta_m = \frac{\dfrac{8/(\pi^3 \ v_m^{\,2} \ \beta_r \ b^2)}{[(Y_{m2\mp1} \ H_1 - s_r \ Y_{m2} \ H_2)^2 + (J_{m2\mp1} \ H_1 - s_r \ J_{m2} \ H_2)^2]}}{\dfrac{A_i}{B_i} \dfrac{U_{i+1}M_i - U_iM_{i+1}}{M_i^{\,2}} - \dfrac{B_i + 2A_i}{B_i^{\,2}} \ \dfrac{M_{i+1}}{M_i} + \dfrac{2}{V} + [\dfrac{|H_{m+2}\mp H_5 - J_{m+2}\mp H_6||H_mH_5 + J_mH_6|}{|H_{m+1} \ H_5 - J_{m\mp1} \ H_6|^2} - \dfrac{|H_{m+1}\mp H_5 + J_{m+1}\mp H_6|}{|H_{m\mp1}H_5 - J_{m\mp1}H_6|}]}$$

(2.76)

The resemblance of the above equation to the single boundary case may readily be concluded. The computed values follow.

TABLE (2.4)

Comparison of Attenuation Coefficient for n_3 = 1.4576

Ray wkb	Modal	Beta Sq.	m
0.2930D-07	0.2424D-09	2.1231	14
0.4229D-09	0.8970D-11	2.1231	16
0.4949D-11	0.4446D-12	2.1231	18
0.1230D-17	0.1380D-18	2.1231	24
0.2161D-15	0.1604D-15	2.1222	25

2.8 Numerical Results (4)

In this section, the results are again presented along with their counterparts from the ray analysis (Table 2.4). The restriction to a few values of the propagation constant was due to the functional forms adopted for the jacket region i.e. only those modes having a radiation point in the outer layer could be accounted for by Bessel functions of H, J.

Despite the cumbersome appearance of the final equation derived, the agreement is seen to be acceptable. For a major part of the discrepancy, the previously explained causes might be considered responsible.

2.9 Discussion (2)

This chapter described a detailed investigation of propagation in the fibre using the modal approach.

In line with the trend of the preceding chapter, firstly a single cladding was considered. Papers dealing with the derivation of a characteristic equation for such a situation are in references (6,7,8,9,10).

Normally the exact solution of the original Maxwell's equations is nearly impossible unless one makes the weak guidance assumption. Here the approximation was effected at the initial stages on reducing the coupled differential equations to the second order. It must be stated categorically however, there is no standard scheme yet available as to when and where the actual implementation should take place. Careless application will lead to inconsistent results.

The solution of the characteristic equation in the form illustrated was previously undertaken for step index fibres (2), while no complete analysis on parabolic index fibres has been reported,

with a few exceptions where the treatment is nevertheless by means of the WKB formula (11).

Choosing the physically existing modes of the fibre, the attenuation coefficient values obtained from the mode theory showed good agreement with those of the geometrical ray method.

One drawback however to the former case was its inability to account for general index profiles. At the moment such studies involve purely numerical techniques (12, 13, 14, 15).

Finally a double layer structure was examined. The characteristic equation deduced may be compared with the ones in references (6, 16, 17). Again the solution was produced employing the Taylor series expansion.

CHAPTER III

EXCITATION

Since optical communication first became technically viable, two main types of power source have developed, namely lasers and light emitting diodes (LEDs). Their characteristics as well as the nature of transmission they generate in the fibre differ.

3.1 Preview of Sources

Laser action is based on the maser principle which means that emission is stimulated rather than spontaneous (1). Thus the output of these sources exhibit a high degree of coherence. That is, the phase correlation at any point across the wavefront and also along the axis of propagation is maintained. Additionally the spectrum width is narrow.

The radiated beam from a laser can be made extremely directional. This aids to reduce the coupling losses on the launching side. Losses of merely 2 dB are common (2).

Amongst the various types available, semiconductor lasers have recently become popular because of their compact size and versatility. They have however yet to match the superiority of gas lasers in terms of output specifications. Since a HeNe laser was supplied for the project, the emphasis in the analysis will understandably be on the latter.

LEDs on the other hand are to be praised for their attractive features such as reliability and low power consumption. In contrast to lasers, the irradiance is lower and is less directional, hence LEDs are inefficient when coupling to a fibre. The output may almost be treated as incoherent with the spectrum

width being much wider. Although some of the drawbacks have been overcome by the newly constructed edge emitters (3,4), LEDs still remain for use in conjunction with multimode fibres where a laser would be luxurious.

Respective of their rise time, both devices are employed for different bit rate applications (2,5). In the main, amplitude modulation alone can be achieved requiring an optical feedback in some instances to improve the linearity (6).

In agreement with the theme of the last two chapters, it would seem logical to investigate the problem of excitation from the ray and mode points of view. In particular, the object will be to furnish the theoretical background for the forthcoming experiments.

3.2 LED Excitation

Figure 2.1 shows a ray impinging on the fibre front end face with its associated launching angles. The source may be assumed to be either butted against the fibre or some distance away from it. B_s defines the axial intensity and measures the amount of power falling onto unit area per unit solid angle.

The incident ray will enter the fibre according to

$$\text{Sin } \theta_o = n(r) \text{ Sin } \theta \tag{3.1}$$

One may then specify the total power in the following integral form

$$P = \int_r \int_{\theta_o} \int_{\phi} \int_{\psi} B_s \text{ Sin } \theta_o \; r \; dr \; d\theta_o \; d\phi \; d\psi \tag{3.2}$$

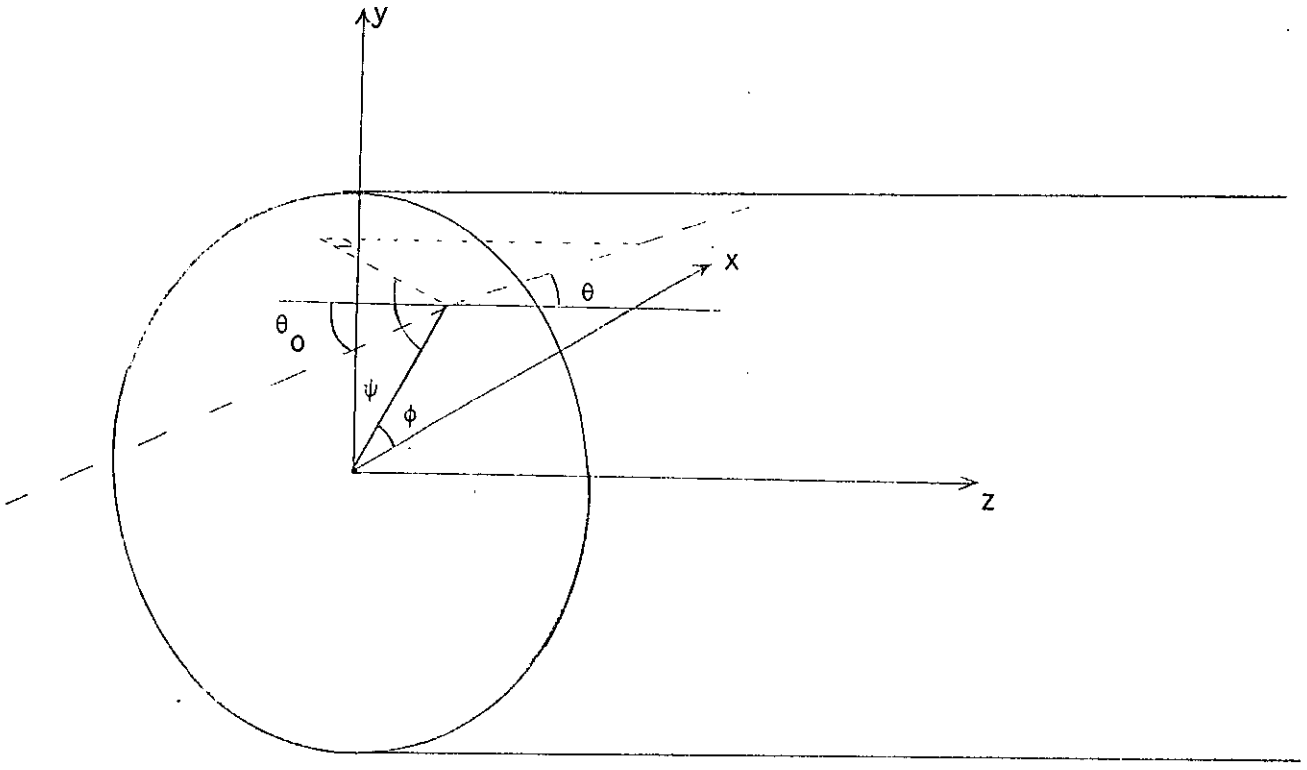

Fig. 3.1 Fibre Launching Arrangement (LED Excitation)

It is customary to ascribe a directionality to the source. A cosine term may be used for this purpose so that

$$B_s = B_o \, (\text{Cos } \theta_o)^g \qquad (3.3a) \quad \text{or} \quad B_s = B_o \, \text{Cos}\, g\theta_o \qquad (3.3b)$$

The case g = 1 gives what is frequently referred to as Lambertian source. Thus by taking either equation in 3.3, P is found to be

$$P_{tot} = \frac{2\pi^2 B_o \, a^2}{g + 1} \qquad (3.4)$$

where since the integration over r was performed to cover the entire core, P_{tot} denotes the total power incident on the fibre not the total power emitted by the source.

In order to calculate how the power is divided between different ray classes, the limits may be modified to (from Chapter I)

$$\text{Guided rays:} \quad 0 \rightarrow \text{Cos}^{-1} \frac{n_2}{n_1} = \theta_c \qquad (3.5a)$$

$$\text{Leaky rays:} \quad \theta_c \rightarrow \text{Sin}^{-1} \left[\frac{\text{Sin } \theta_c}{(1 - r_n^2 \, \text{Cos}^2 \, \psi)^{\frac{1}{2}}}\right] \qquad (3.5b)$$

Therefore for bound rays, when equation 3.5a is used

$$P_b = \frac{4\pi^2 B_o \, a^2}{g + 1} \int_0^1 r_n \left[1 - (1 - \gamma^2(1 - r_n^q))^{(q+1)/2}\right] dr_n \qquad (3.6)$$

In the above r has been normalized with respect to fibre radius. Recognizing the fact that $\gamma^2 << 1$, a first order expansion will yield

$$\frac{P_b}{P_{tot}} \simeq \frac{\gamma^2 q (g + 1)}{2 (q + 2)} \tag{3.7}$$

The tunnelling ray power on the other hand is

$$P_t = \frac{2\pi B_o a^2}{g+1} \int_0^1 r_r \, dr_n \int_0^{2\pi} [1 + n_2^2 - n^2 (r_n)]^{(g+1)/2} - [1 + \frac{n_2^2 - n^2(r)}{1 - r_n^2 \, Cos^2\psi}]^{(g+1)/2} d\psi \tag{3.8}$$

An analytic expression may likewise be deduced by expanding the terms in the brackets

$$\frac{P_t}{P_{tot}} \simeq \gamma^2 \frac{g+1}{2} [\frac{q+4}{q+2} - Be (\tfrac{1}{2}, \tfrac{q+2}{2})] \tag{3.9}$$

Be = Beta function.

Equations 3.7 and 3.9 suggest that P_b (also P_t) will increase indefinitely as the source directionality is increased. This is not physically realisable of course. The correct result will be retrieved from the integral forms remembering that the expansion process relies on $g < \infty$ besides γ^2 being small.

With the other source function * (i.e. $B_s = B_o \text{ Cos } g\ \theta_o$), the evaluation of the integrals proves to be more difficult.

For this situation P_b and P_t will be given by

$$\frac{P_b}{P_{tot}} = (g+1) \int_{r_n} \int_{\theta} \frac{\text{Cos } g\ [n(r_n)\ \text{Sin}\ \theta]}{\text{Cos } [n(r_n)\ \text{Sin}\ \theta]} n^2(r_n)\ \text{Sin}\ 2\theta\ .$$

$$r_n\ dr_n\ d\theta \qquad (3.10)$$

$$\frac{P_t}{P_{tot}} = \frac{g+1}{2\pi} \int_{r_n} \int_{\theta} \int_{\psi} \frac{\text{Cos } g\ [n(r_n)\ \text{Sin}\ \theta]}{\text{Cos } [n(r_n)\ \text{Sin}\ \theta]}\ n^2(r_n)\ \text{Sin}\ 2\theta\ .$$

$$r_n\ dr_n\ d\theta\ d\psi \qquad (3.11)$$

where $\text{Sin}^{-1}\ [n(r_n)\ \text{Sin}\theta]$ has been approximated to $n(r_n)\ \text{Sin}\theta$ which is justifiable since the range of integration extends over small values of θ.

Another case to consider is the variation of intensity with radial position on the LED surface (8).

Hence let B_s be

$$B_s = B_o\ (\text{Cos}\ \theta_o)^g\ e^{-f\ r_n^2} \qquad (3.12)$$

---

* It is worthwhile to note that such a description of source intensity has in the literature been attributed to semiconductor lasers (7). Mathematically however it might offer a more complete picture for LED radiation because $\text{Cos}g\theta$ may always be written in descending powers of $\text{Cos}\theta$.

f is the non-uniformity parameter.

On introducing the new term into the previous formulae, the normalized guided and leaky ray powers become

$$P_{bn} \simeq \frac{\gamma^2 \ (g+1)}{2(1 - e^{-f})} \ (1 - 2q \ D_{q-1}) \qquad (3.13)$$

$$P_{tn} \simeq \frac{2 \ \gamma^2 f \ (g+1)}{(1 - e^{-f})} \ [\frac{1}{2f} \ (q \ D_{q-1} - 1) + \frac{Da \ (f^{\frac{1}{2}})}{f^{\frac{1}{2}}}$$

$$- Db \ (q/2)] \qquad (3.14)$$

where the definitions of D_q, Da (Dawson's integral), Db (and Beta function) may be found in appendix A.

Similar equations (though not stated here) to 3.13 and 3.14 will be obtained by assuming the alternative type of intensity distribution, i.e. $Cosg\theta_o$.

Normally the reflection losses from the fibre end face are reported to be negligible. Their contribution may nevertheless be accounted for via the application of the well known Fresnel's Law (9).

Within the geometrical optic limits (i.e. for unpolarized light) the reflection coefficient is

$$T_f = \frac{Sin \ 2 \ \theta_o \ Sin \ 2\theta}{2 \ Sin^2 \ (\theta_o + \theta)} \ [1 + \frac{1}{Cos^2 \ (\theta_o - \theta)}] \qquad (3.15)$$

As long as the acceptance cone of the fibre is not too wide the dependence on θ_0, θ may be eliminated leaving (10).

$$T_f = \frac{4\, n(r)}{[1 + n(r)]^2} \qquad (3.16)$$

3.3 Numerical Results (5)

In this section the fibre parameters given earlier were used.

The first computation was to test the range of validity of the expansion appearing in equations 3.7 and 3.9.

Figure 3.2 displays the power accepted into guided and leaky rays as the source directionality is increased, where E and I are the expansion and integration methods respectively. Moreover B1 and B2 denote the two alternative forms of B_s (i.e. equation 3.3). Note that for the second intensity distribution direction integration only could be applied. The incremental deviation is seen to be larger for tunnelling rays when higher q values are considered.

It is interesting to observe that with the source brightness of $B_s = B_0 \cos g\theta$, the power launched into the fibre does not conform to the familiar linear pattern. This is to be attributed to the side lobe effects peculiar to this type of functional dependence.

In Figure 3.3 the normalized power is plotted for a non-uniform source. The small values of f do not produce any appreciable difference. As also expected the rising source non-uniformity concentrates more power into the bound ray domain whereas the opposite is true for leaky rays.

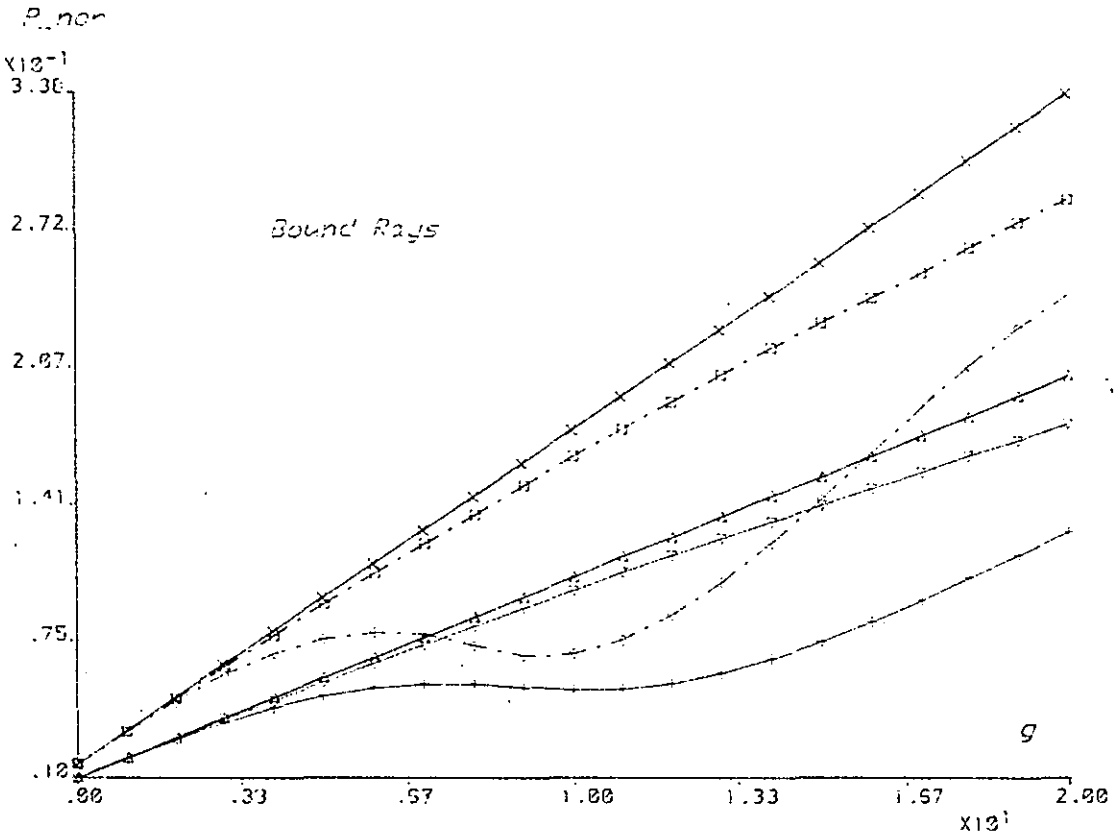

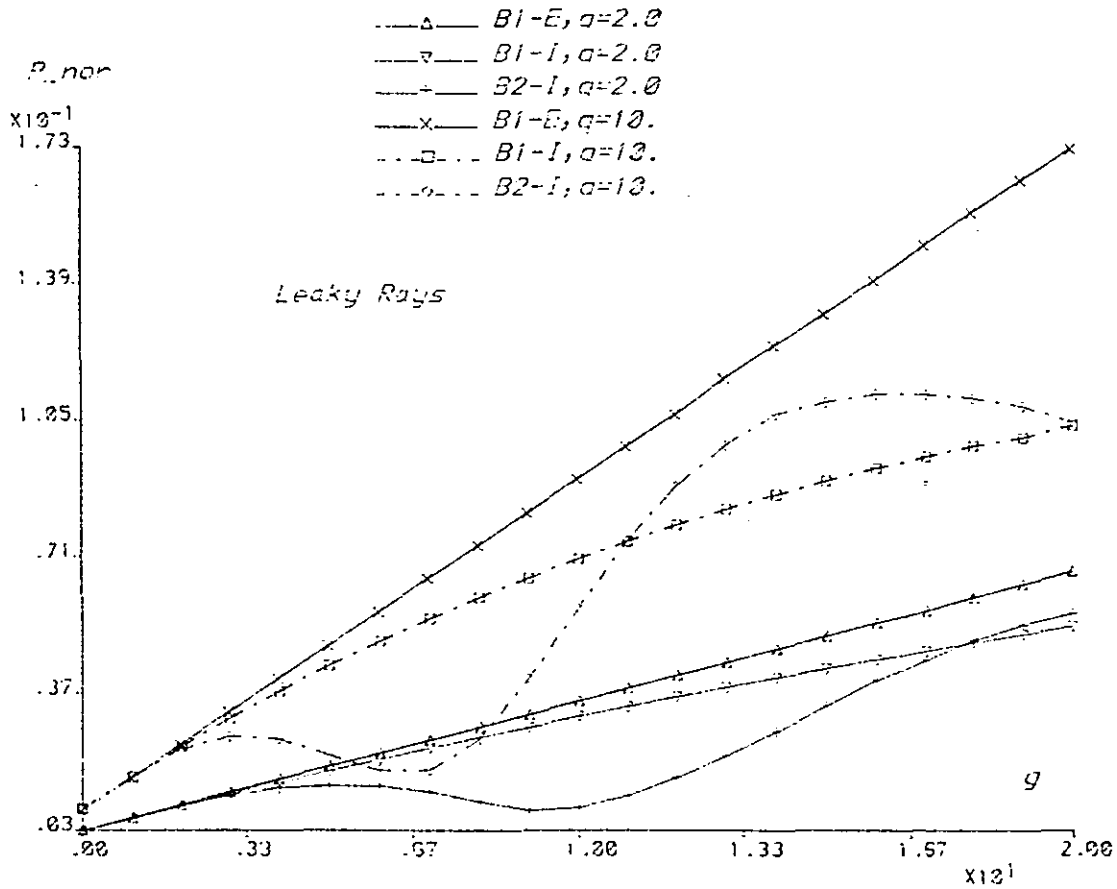

Fig. 3.2 Variation of normalized Power for Uniform source

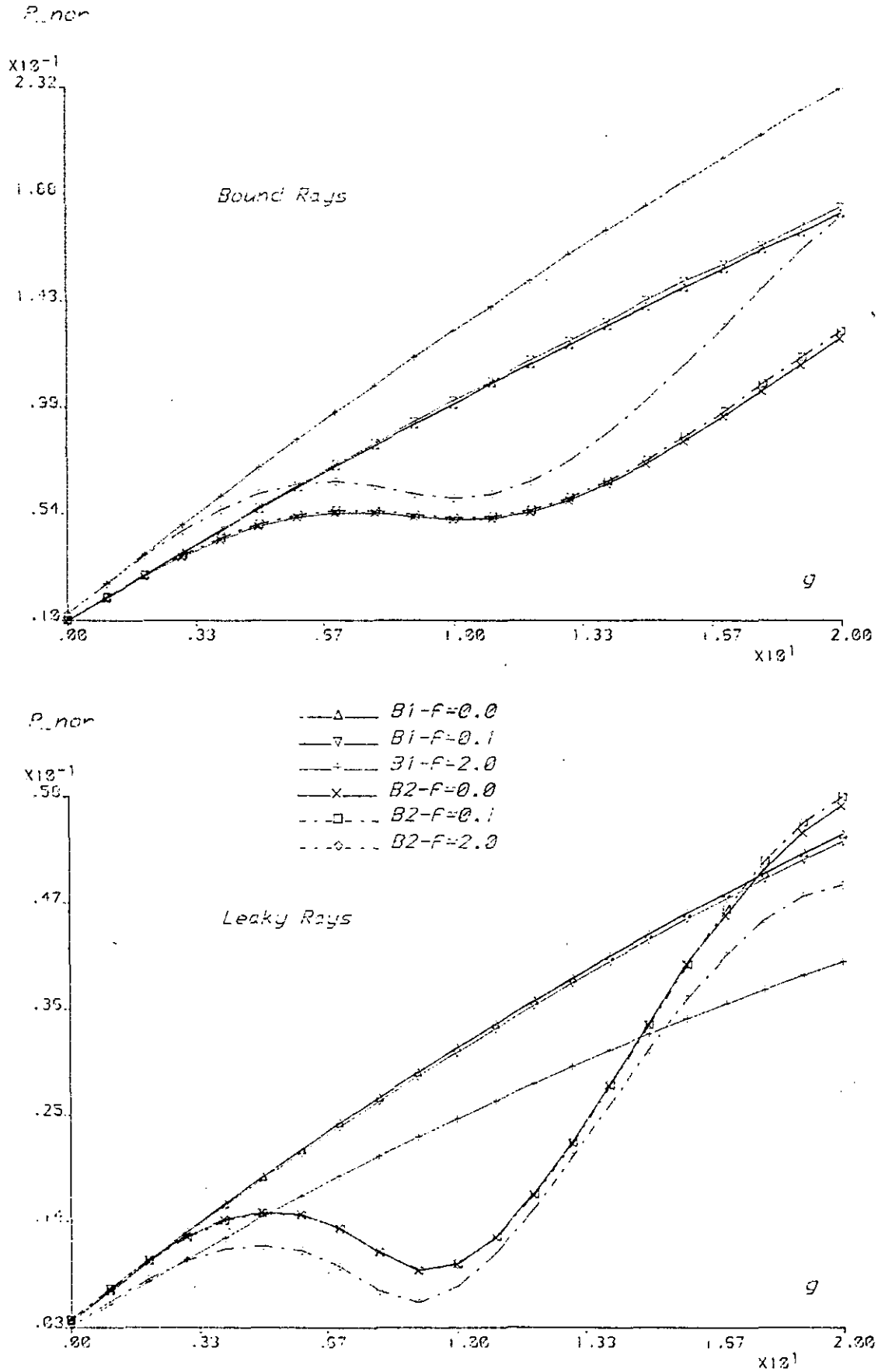

Fig. 3.3 Variation of P_nor for non-Uniform source (q=2.0)

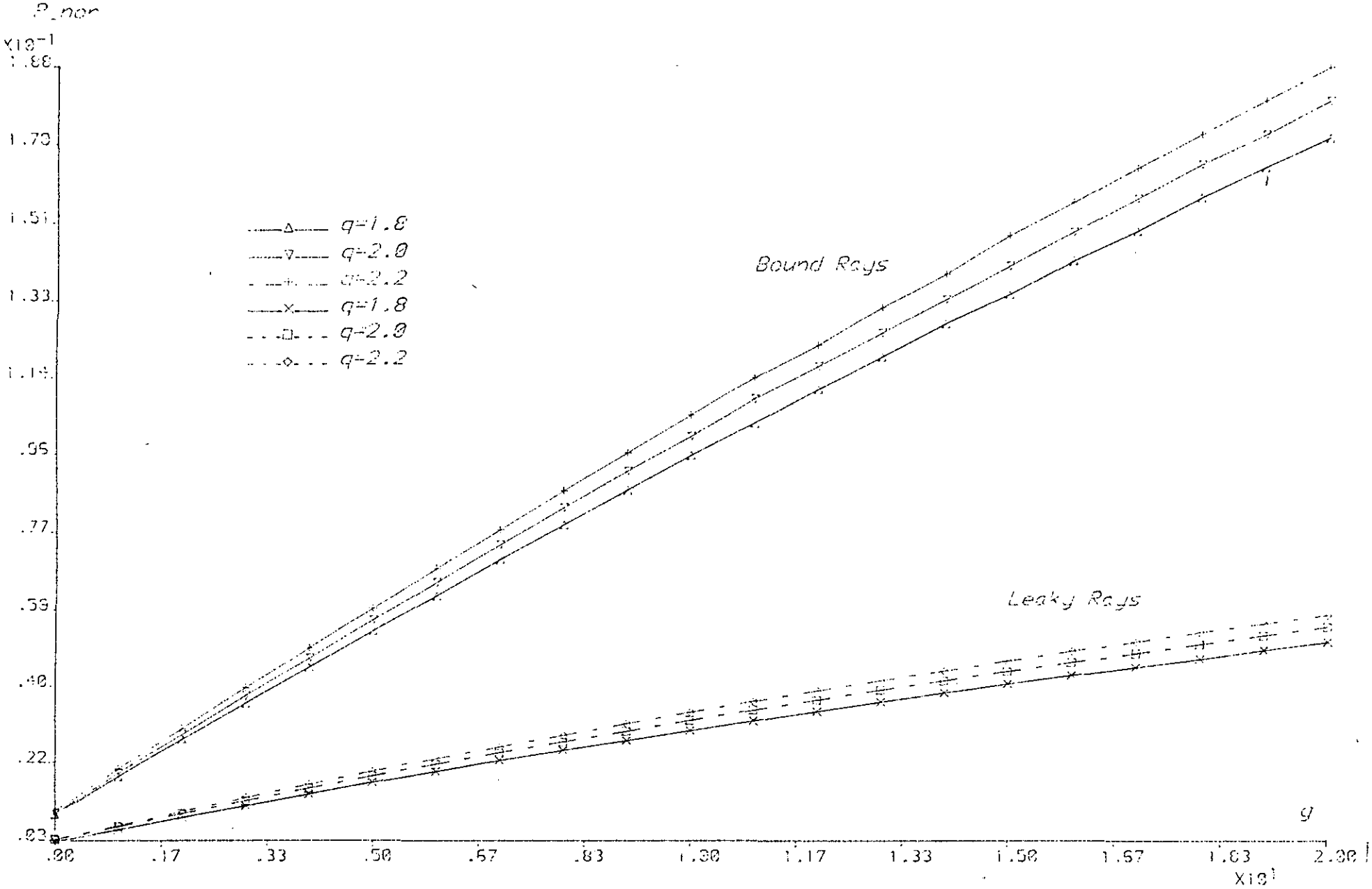

Fig. 3.4 Variation of P_nor For different rays (B_s=B_o(Cos0)**g)

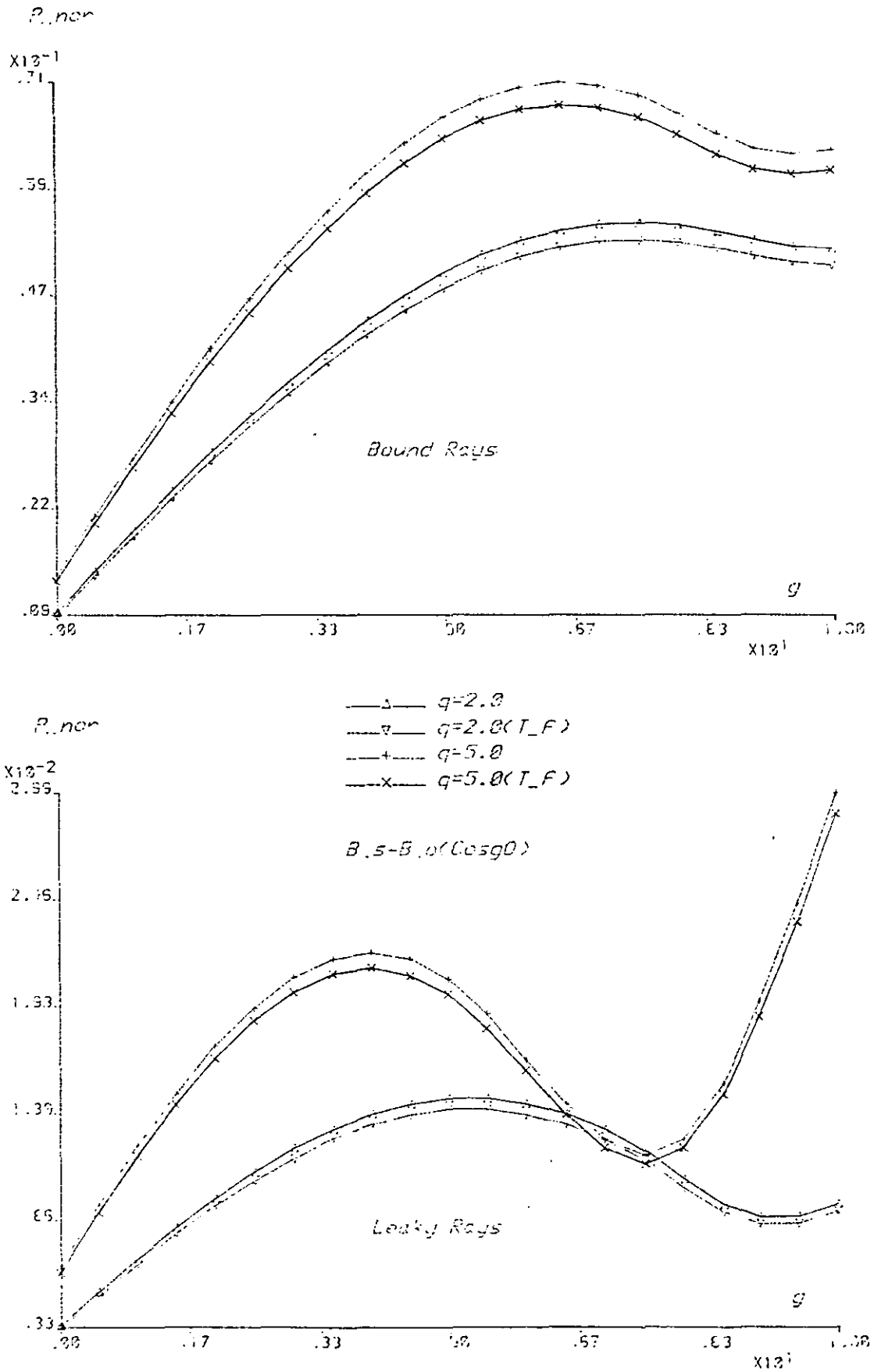

Fig. 3.5 Acceptance of rays when T_F taken into account

The effects of slight perturbations around the parabolic profile are examined in Figure 3.4.

Finally the contribution from reflection losses at the fibre entrance may be seen to be negligible (Figure 3.5).

3.4 Laser Excitation

High quality lasers are known to oscillate predominantly in the few lowest order modes TEM_{0n}. The representation follows from solving the Helmotz equation in Cartesian coordinates (11).

Hence, the electric field component in free space is*

$$E_{xn} = \left(\frac{2}{\pi}\right)^{\frac{1}{2}} \frac{1}{s} L_n \left(2r^2/s^2\right) e^{-(r/s)^2} e^{-j\psi} \qquad (3.17)^{**}$$

L_n = Laguerre Polynomial

where s is called the beam width of radiation and ψ indicates the phase angle. They are in turn defined by

$$s = s_o \left[1 + \left(\frac{2\,(z + d)}{k_o\, s_o^2}\right)^2\right]^{\frac{1}{2}} \qquad (3.18a)$$

---

* This result is based on the assumption that the variation in the z direction is slow so that $\partial^2 E_x / \partial^2 z$ can be neglected (11).

** The complete phase parameter is not explicitly shown here, refer to Appendix A.

$$\psi = \frac{k_o\, r^2}{2R} \tag{3.18b}$$

$$R = (z + d)\left[1 + \left(\frac{k_o\, s_o^{\,2}}{2\,(z + d)}\right)^2\right] \tag{3.18c}$$

d = distance from the centre of the beam.

s_o therefore measures the radius at the narrowest point. R on the other hand is the curvature of the beams as it travels along the z axis. These are illustrated in Figure 3.6. When launched axially into the fibre, such a beam gives rise to HE_{1p} modes only which are linearly polarised in the proper (12).

For a parabolic fibre, the HE_{1p+1} mode is described by

$$E_{xp+1} = \left(\frac{2}{\pi}\right)^{\frac{1}{2}} \frac{1}{s_f}\; L_p\,(2r^2/s_f^{\,2})\, e^{-(r/s_f)^2}\; e^{-j\beta z} \tag{3.19}$$

s_f = fibre spot size = $(2a/k_o\gamma)^{\frac{1}{2}}$

Noting that the incident field may be expanded at the entrance aperture of the fibre, the excitation coefficient for a particular mode becomes

$$\alpha_{np} = \int_0^a \int_0^{2\pi} E_{xn}\, E_{xp}\, r\, dr\, d\phi \tag{3.20}$$

Thus for instance, the fundamental mode of the fibre (HE_{11}) excited by TEM_{oo} or what is formally referred to as a Gaussian beam will have

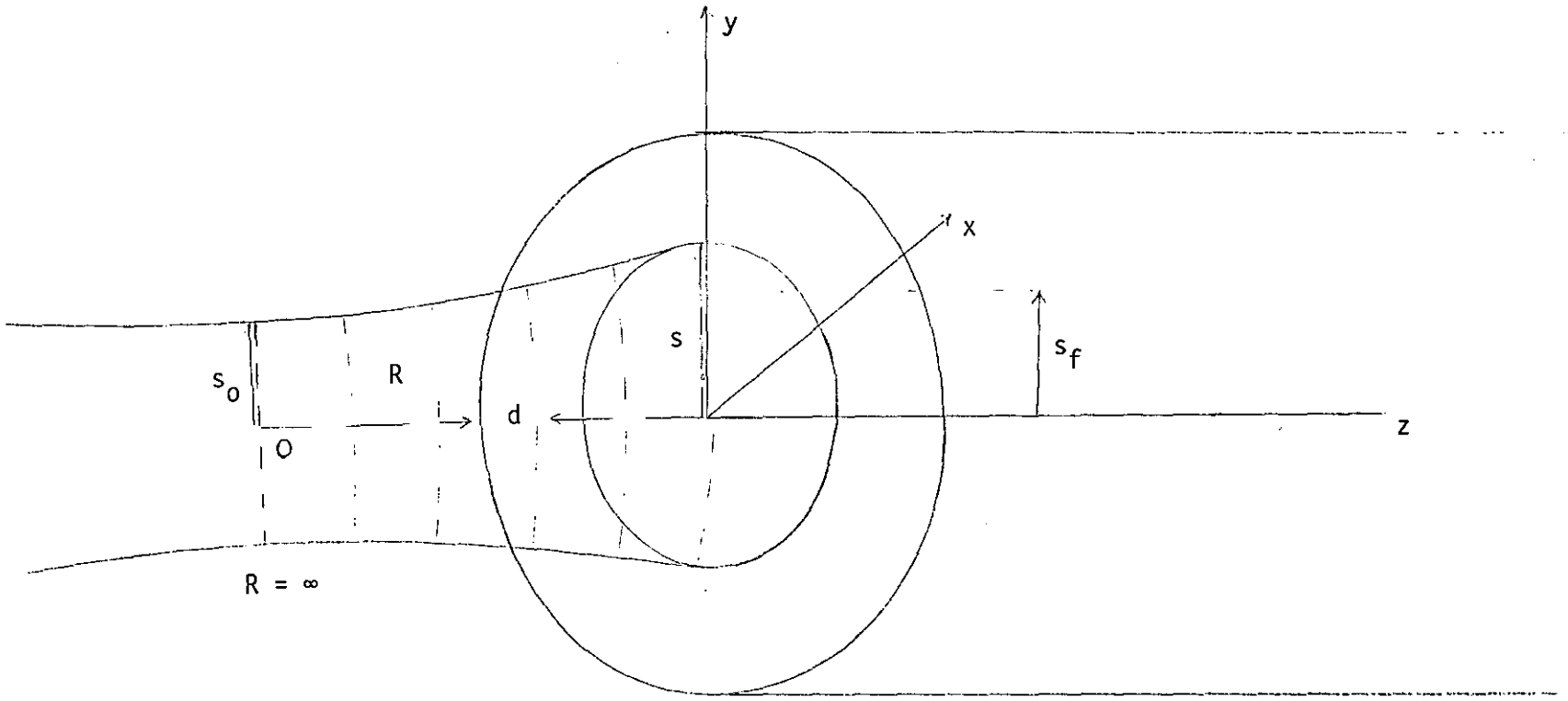

Fig. 3.6 Launching by a Laser Beam

$$\alpha_{oo} = 2\left(\frac{s_f}{s}\right) \frac{1}{P_1 + j\,P_2} \left[1 - e^{-P_1\,(a/s_f)^2}\right] \qquad (3.21)$$

parameters P_1 and P_2 are

$$P_1 = (s^2 + s_f{}^2)/s^2 \qquad (3.22a), \quad P_2 = k_o\, s_f{}^2/(2R) \qquad (3.22b)$$

which is arrived at by assuming $P_2 << P_1$. This condition is generally true and holds well as long as it is not too far away from the waist of the beam (point O in Figure 3.6).

The excitation coefficient for any mode amongst the HE_{1p+1} group may be shown to be*

$$\alpha_{o\ p+1} = 2\left(\frac{s_f}{s}\right)^2 \sum_{k=0}^{p} \frac{(-1)^k\, 2^k}{(P_1 + j\,P_2)^{k+1}} \left[C^{p}_{p-k} - e^{-P_1(a/s_f)^2}\, k\, L_{p-k}(2a^2/s_f{}^2)\right] \qquad (3.23)$$

C^{p}_{p-k} = Binomial coefficient

where L^{k}_{p-k} is now the generalized Laguerre polynomial of k th order.

Another case of interest is to examine excitation by other beam modes in the TEM_{on} group. A situation close to practical is to combine the TEM_{oo} with one or perhaps two of the higher order modes.

---

* Some brief accounts on these derivations may be found towards the end of Appendix A.

Due to its relevance (see next Chapter), the following choice is made

$$E_{xt} = TEM_{oo} + A_n\ TEM_{o1}\ e^{-j\ \psi_p}$$

$$= (\frac{2}{\pi})^{\frac{1}{2}}\ \frac{1}{s}\ e^{-(r/s)^2}\ [1 + (1 - 2r^2/s^2)\ A_n\ e^{-j\ \psi_p}]\ e^{-j\psi} \qquad (3.24)$$

In the above the amplitude of TEM_{o1} has been normalized w.r.t. the TEM_{oo}. Furthermore ψ_p governs the relative phase difference. The launching efficiency in this instance will be upon setting $\psi_p = 0$,

$$\alpha_{o+1\ p+1} = 2(\frac{s_f}{s})\ \{S_p + A_n\ [S_p - (p+1)(S_p - S_{p+1}) + p(S_{p-1} - S_p)]\} \qquad (3.25)$$

where the sum in 3.23 has been abbreviated to S_p.

To determine the overall efficiency, what is needed is to sum over all possible modes excited. It will be recalled from Chapter II that β and p were related by

$$\beta^2 = n_1^2\ k_o^2\ [1 - \frac{\sqrt{2\Delta}}{n_1\ k_o a}\ (4p+2)] \qquad (3.26)$$

Hence by taking the cut-off value, i.e. $\beta = n_2\ k_o$, an upper bound may be fixed for p

$$p_{max} = \text{Nearest int } (V/4 - 1/2) \qquad (3.27)$$

Therefore, the overall efficiency is η_t where

$$\eta_{tn} = \sum_{p=0}^{P_{max}} |\alpha_{n\ p+1}|^2 \qquad (3.28)$$

Prior to carrying out the actual summation however, one major simplification that may be effected is that for multimode fibres the characteristic spot size (s_f) is small compared to the radius of the core. The product involving the exponential in 3.23 may thus be removed all together.

Then for exclusive TEM_{oo} excitation

$$\eta_{to} = 4\ (\frac{s_f}{s})\ \frac{1}{P_1^2 + P_2^2} \sum_{p=0}^{P_{max}} \{ \frac{[(P_1^2 - 2P_1 + P_2^2) + 4\ P_2^2]^{\frac{1}{2}}}{P_1^2 + P_2^2} \}^{2p} \qquad (3.29)$$

Moreover in the limit

$$\eta_{to}\ P_2 \to 0 = 1 - (1 - \frac{2}{P_1})^{2\ (P_{max}+1)} \qquad (3.30)$$

and this result agrees with that of Ref. (12).

Using the same method when the excitation is composed of $TEM_{oo} + TEM_{01}$

$$|\alpha_{o+1\ p+1}|^2 = 4(\frac{s_f}{s})^2 \{|S_p|^2 + A_n^2[|S_p|^2 - (p+1)^2(|S_p|^2 - |S_{p+1}|^2)$$

$$+ p^2\ (|S_{p+1}|^2 - |S_p|^2)]\} \qquad (3.31)$$

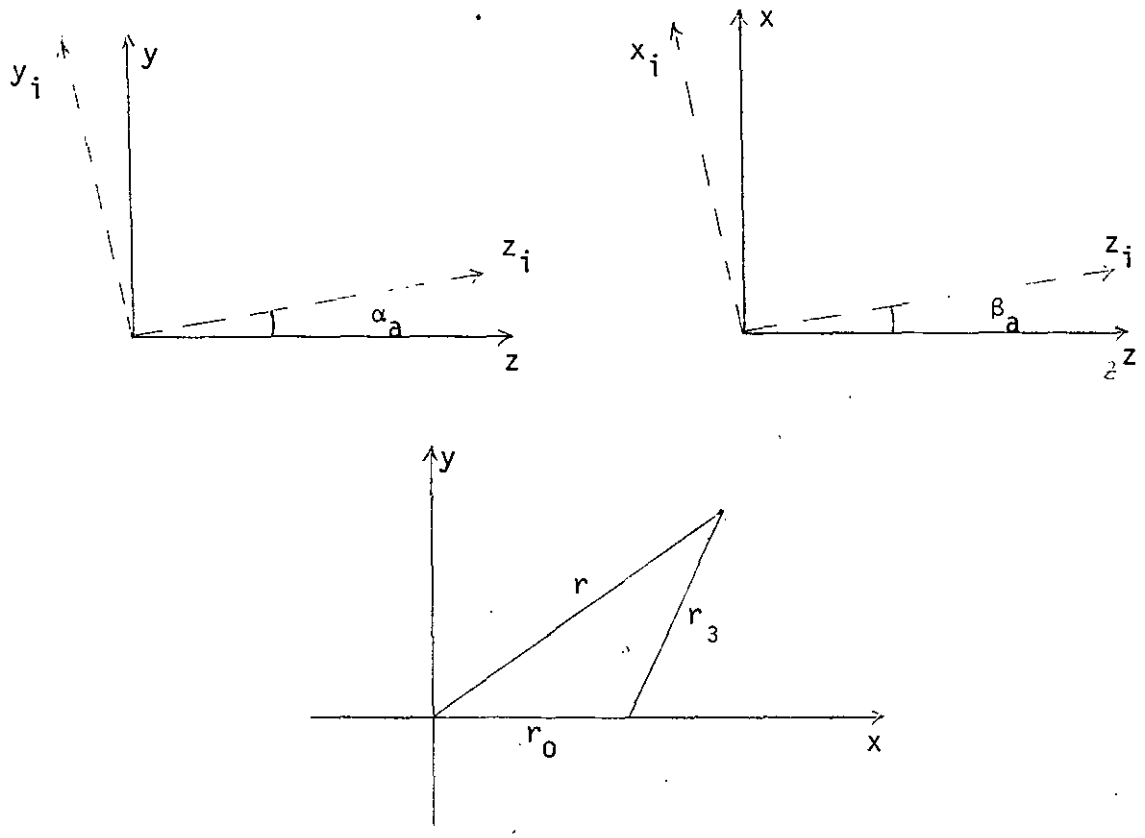

(a) Rotation of Coordinates

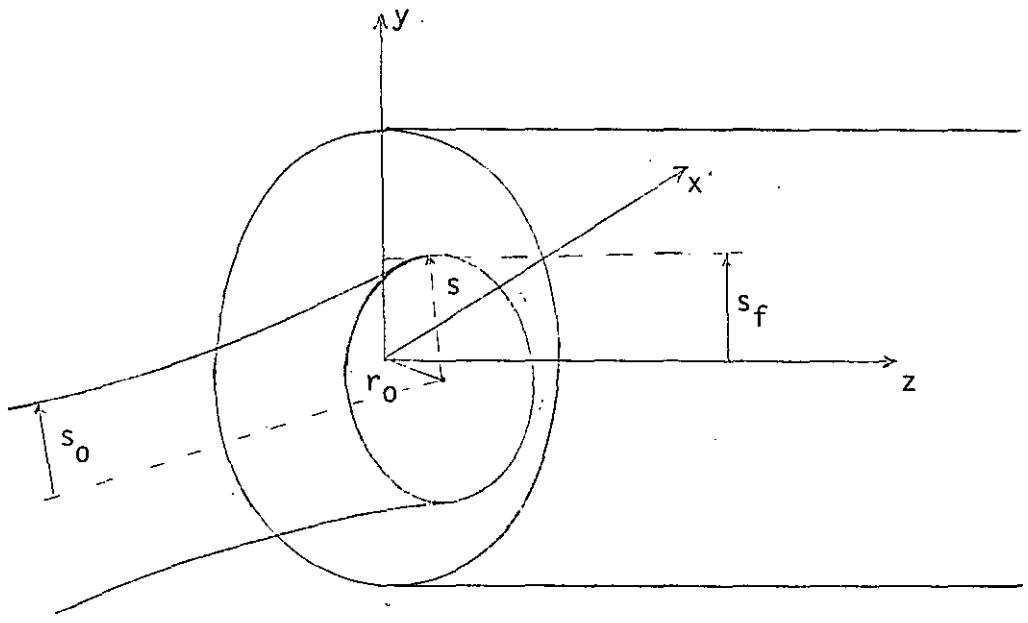

Fig. 3.7(b) Offset Launching by Laser Beam

and

$$\eta_{to+1} = \sum_{p=0}^{P_{max}} |\alpha_{o+1\ p+1}|^2/(1 + A_n^2) \qquad (3.32)$$

where on taking the modulus of S_p, S_{p-1}, S_{p+1} it has been assumed that $P_2 << P_1$, additionally the validity is restricted to $P_1 \neq 2$.

So far solely axial launching has been discussed. Inevitably, this conveys most of the power into the guided modes. Tilts and offsets must therefore be introduced to cause leaky mode generation. To this end, as shown in Figure 3.7, the y-z and x-z planes (of the incident beam) are rotated through the amounts α_a, β_a. Also the centre of the beam is displaced along the x axis to a position r_o.

Under the conditions that α_a, β_a, r_o all represent small quantities, the electric field expression at z = 0 is transformed into (see Appendix A)

$$E_{xn} = \left(\frac{2}{\pi}\right)^{\frac{1}{2}} \frac{1}{s_1} L_n\ (2\ r_3^2/s_1^2)\ e^{-r_3^2\ \left(\frac{1}{s_1^2} + \frac{jk_o}{2R_1}\right) - jk_o(r - r_o\ \cos\phi)\cdot}$$

$$(\beta_a\ \cos\phi + \alpha_a\ \sin\phi) \qquad (3.33)$$

$$r_3^2 = r^2 + r_o^2 - 2\ rr_o\ \cos\phi$$

With the shifted coordinates, the width and the curvature of the beam are altered to

$$s_1 = s_o\ \left[1 + 4\ \left(\frac{d + |r\ (\beta_a\ \cos\phi + \alpha_a\ \sin\phi)|}{k_o\ s_o^2}\right)^2\right]^{\frac{1}{2}} \qquad (3.34a)$$

$$R_1 = [d + |r\ (\beta_a\ \mathrm{Cos}\phi + \alpha_a\ \mathrm{Sin}\phi)|][1 + (\frac{k_o\ s_o^2}{2(d + |r\ (\beta_a\ \mathrm{Cos}\phi + \alpha_a\ \mathrm{Sin}\phi)|)})^2] \qquad (3.34b)$$

Contrary to the course of earlier theoretical development, overall efficiency will be formulated first. Using the Poynting vector, the power flowing through a surface S is given by*

$$P = \frac{1}{2}\ \mathrm{Re} \int_S E_x\ H_y^+\ dS \qquad (3.35)$$

H_y = magnetic field
$+$ = complex conjugate

On applying to equation 3.33, this induces, in the event of TEM_{oo} excitation η_t to be

$$\eta_{to} = \frac{2}{\pi} \int_0^a \int_0^{2\pi} \frac{1}{s_1^2}\ e^{-(r_3/s_1)^2}\ r\ dr\ d\phi \qquad (3.36)$$

For other types of excitation, the launching efficiency may suitably be written.

This analysis however ignores the phase mismatch between the oncoming beam and the fibre modes entirely. Since it asserts that the greater part of the incident power should be accepted into the core, it can only be regarded as a crude approximation.

For a rigorous treatment, an assessment of the coupling into the individual modes is necessary. This may be done in the manner described below (13).

---

* This notation is correct if the propagation medium is lossless.

The transverse field components from Appendix A are

$$E_{\phi} = \begin{bmatrix} F_i/F_i\ (a) \\ K_{m\mp1}/K_{m\mp1}(a) \end{bmatrix} \begin{bmatrix} \text{Sin } m\phi \\ \text{Cos } m\phi \end{bmatrix} \tag{3.37}$$

$$E_r = \pm \begin{bmatrix} F_i/F_i\ (a) \\ K_{m\mp1}/K_{m\mp1}(a) \end{bmatrix} \begin{bmatrix} \text{Cos } m\phi \\ \text{Sin } m\phi \end{bmatrix} \tag{3.38}$$

$$H_{\phi} = \mp \frac{1}{Z_o} \begin{bmatrix} \varepsilon_1^{\frac{1}{2}} F_i/F_i\ (a) \\ \varepsilon_2^{\frac{1}{2}} K_{m\mp1}/K_{m\mp1}\ (a) \end{bmatrix} \begin{bmatrix} \text{Cos } m\phi \\ \text{Sin } m\phi \end{bmatrix} \tag{3.39}$$

$$H_r = \frac{1}{Z_o} \begin{bmatrix} \varepsilon_1^{\frac{1}{2}} F_i/F_i\ (a) \\ \varepsilon_2^{\frac{1}{2}} K_{m\mp1}/K_{m\mp1}\ (a) \end{bmatrix} \begin{bmatrix} \text{Sin } m\phi \\ \text{Cos } m\phi \end{bmatrix} \tag{3.40}$$

The upper and lower lines in the first brackets express the normalized (w.r.t the amplitude at the interface) core and cladding fields respectively, whereas sine and cosine terms correspond to the freedom of adopting two independent states of polarization.

The incident field in the same coordinates is:

$$\vec{E}_{tn} = \vec{E}_{rn} + \vec{E}_{\phi n} = E_{xn}\,\text{Cos}\phi - E_{xn}\,\text{Sin}\phi \tag{3.41a}$$

$$H_{tn} = \vec{H}_{rn} + H_{\phi n} = \frac{E_{xn}}{Z_o}\,\text{Cos}\phi + \frac{E_{xn}}{Z_o}\,\text{Sin}\phi \tag{3.41b}$$

and when expressed in terms of fibre modes

$$\vec{E}_{tn} = \sum_m \sum_p \alpha^e_{mp} \vec{E}_{mp} \tag{3.42a}$$

$$\vec{H}_{tn} = \sum_m \sum_p \alpha^h_{mp} \vec{H}_{mp} \tag{3.42b}$$

$\vec{E}_{mp}$, $\vec{H}_{mp}$ may be expressed as the combination of

$$\vec{E}_{mp} = \vec{E}_r + \vec{E}_\phi \tag{3.43a}$$

$$\vec{H}_{mp} = \vec{H}_r + \vec{H}_\phi \tag{3.43b}$$

By means of equations 3.37 to 3.43, the coefficients α^e_{mp}, α^h_{mp} may be deduced. Reverting to scalar notation, they are given by

$$\alpha^e_{mp} = \int_r \int_\phi (E_{rn} H^+_\phi - E_{\phi n} H^+_r) \, r \, dr \, d\phi \tag{3.44a}$$

$$\alpha^h_{mp} = \int_r \int_\phi (H^+_{\phi n} E_r - H^+_{rn} E_\phi) \, r \, dr \, d\phi \tag{3.44b}$$

Finally the excitation coefficient of the mp th mode may be obtained from

$$\eta_{mp} = \mathrm{Re} \, (\alpha^e_{mp} \, \alpha^h_{mp}) \tag{3.45}$$

In order to enable a sound basis of comparison between the various modes, an appropriate scaling must be established. The power flow within a single mode of the fibre may be stated in the form

$$P_{mp} = \frac{1}{Z_o} \text{Re} \int_0^{\infty} \int_0^{2\pi} (E_{mp} H_{mp}^{+}) \, r \, dr \, d\phi \qquad (3.46)^*$$

After performing the integration over ϕ (and partially r), this will read

$$P_{mp} = \frac{a^2 \pi}{Z_o^2} \left[(\varepsilon_1^{\frac{1}{2}} \int_0^{V} \frac{e^{-x+V} \, x^{B_i - 1} \, M_i^2}{V^{B_i} \, M_i^2(a)} \, dx \right.$$

$$\left. + \varepsilon_2^{\frac{1}{2}} \left(\frac{K_{m-2} \, K_m}{K_{m-1}^2} - 1 \right) \right] \qquad (3.47)$$

η_{mp}, upon being divided by 3.47, will then be the required quantity.

When substituted for the electric and magnetic fields in 3.44, these become for a TEM_{oo} beam incidence (refer to next page).

---

* The factor Z_o is inserted to eliminate it from the final formula

$$\alpha^{e}_{mp} = \left(\frac{2}{\pi}\right)^{\frac{1}{2}} \frac{1}{Z_o} \int_0^{2\pi} \begin{matrix}\text{Cos}\\ \text{Sin}\end{matrix} (m\mp 1)\phi \, d\phi \int_0^{\infty} \frac{1}{s_1} e^{-(r^2 + r_o^2 - 2r\, r_o \text{Cos}\phi)\left(\frac{1}{s_1^2} + \frac{j\, k_o}{2\, R_1}\right)}$$

$$- j\, k_o\, (r - r_o\, \text{Cos}\phi)(\beta_a\, \text{Cos}\phi + \alpha_a\, \text{Sin}\phi) \begin{cases} \varepsilon_1^{\frac{1}{2}}\, F_i/F_i\,(a) & r \leq a \\ \varepsilon_2^{\frac{1}{2}}\, K_{m\mp 1}/K_{m\mp 1}\,(a) & r \geq a \end{cases} r\, dr \qquad (3.48)$$

$$\alpha^{h}_{mp} = \left(\frac{2}{\pi}\right)^{\frac{1}{2}} \frac{1}{Z_o} \int_0^{2\pi} \begin{matrix}\text{Cos}\\ \text{Sin}\end{matrix} (m\mp 1)\phi \int_0^{\infty} \frac{1}{s_1} e^{-(r^2 + r_o^2 - 2r\, r_o \text{Cos}\phi)\left(\frac{1}{s_1^2} - \frac{j\, k_o}{2\, R_1}\right)}$$

$$+ j\, k_o\, (r - r_o\, \text{Cos}\phi)\, (\beta_a\, \text{Cos}\phi + \alpha_a\, \text{Sin}\phi) \begin{cases} F_i/F_i\,(a) & r \leq a \\ K_{m\mp 1}/K_{m\mp 1}\,(a) & r \geq a \end{cases} r\, dr \qquad (3.49)$$

Unfortunately, it is somewhat tedious to invoke analytic solutions to the last three integrals presented. Some potentially useful approaches are nevertheless summarized in Appendix A. Here a numerical integration is undertaken.

3.5 Numerical Results (6)

The launching efficiencies for a selection of the low order modes are shown in Figure 3.8 both for TEM_{oo} and a $TEM_{oo} + TEM_{o1}$ combination. In this graph the results obtained on omitting the exponential term are superimposed and the difference is hardly visible. In fact for the modes considered the numerical values agreed up to the 6th significant digit.

For a closer investigation of excitation by various beams, Figure 3.9 is plotted. Any slight departure from a perfect TEM_{oo} beam disturbs the power division amongst the fibre modes. Thus, in such cases, the power accepted by HE_{11} will be reduced. That of the higher order modes on the other hand will rise. In the limit of the beam radius becoming very large all modes will be equally excited.

The overall efficiency that is obtained by summing over all the guided modes present in the fibre varies with the beam radius in the manner depicted in Figure 3.10. Here the plus and minus signs at the end of the symbols indicate whether the exponential term was included or ignored. The broadening of the beam appears to make its contribution somewhat more pronounced. It is worthwhile to point out that a $TEM_{oo} + TEM_{o1}$ mixture, unlike a pure TEM_{oo} mode, yields the maximum launching at approximately $s/s_f = 3.5$

In the last three computations presented the variation of the beam size was realised through z (i.e. equation 3.18a), hence the phase mismatch is readily accounted for. Practically this is more meaningful since, for a given source and focusing arrangement, the only way to alter the size of the beam would be to move the fibre axially.

The next step was the determination of overall efficiency under offset conditions (Figure 3.11). However as also stated in the derivations section, this formula did not properly express the effects of angular misalignment. Consequently a programme was devised employing the latter approach.

Figure 3.12 shows the results obtained. To give a concise interpretation of these graphs, one would expect the launching efficiency to reach maximum when the centre axis of the beam is orientated such that the respective angles satisfy equation 1.12 of Chapter I. In the event of m = 18, this was precisely the case (excluding the term n(r)). The same behaviour was not yielded however when m = 7 and m = 13 were considered. One reason might be the errors introduced during the computation, since each point on the curves had to be evaluated (with accuracy limits set to the minimum) to avoid exceeding the longest processing time allowed on the computer. To facilitate a quick recheck on the numerical values, it was then decided to reduce the accuracy limits below that specified in Appendix B. But it was found that even the peak displayed by the mode m = 18 disappeared. Thus, the overall conclusion is that, although the theoretical analysis does provide the correct approach, a more accurate computation should be undertaken to verify the consistency.

One final note is that the values of s and r_o in Figure 3.12 are normalized w.r.t. fibre parameters.

3.6 Discussion (3)

This chapter has dealt with excitation of fibres by various types of sources.

In contrast with conventional communication systems such as coaxial cables, a great deal of attention has to be paid to losses when coupling the optical sources to their transmission medium of fibres.

Basically, the aim would be to inject as much power as possible and furthermore to generate a few modes so as to minimize the dispersion problems. As also demonstrated by the computations, these requirements are easily met by lasers.

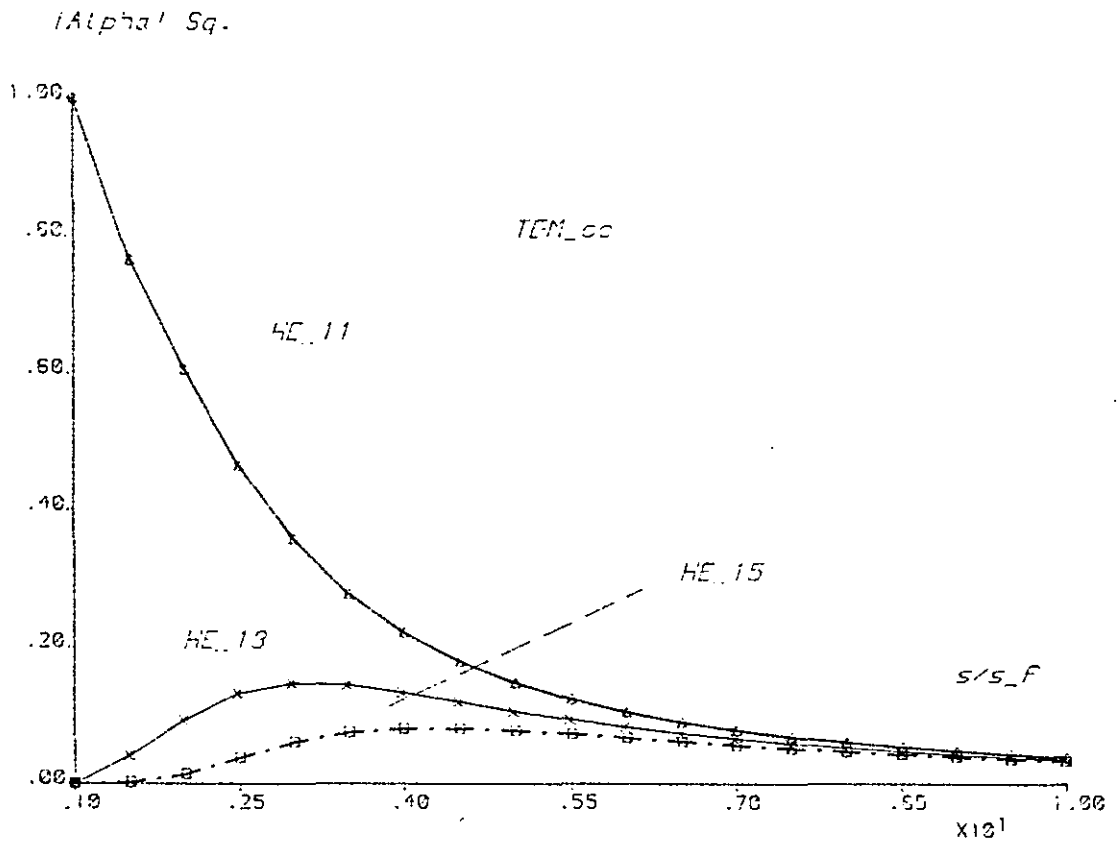

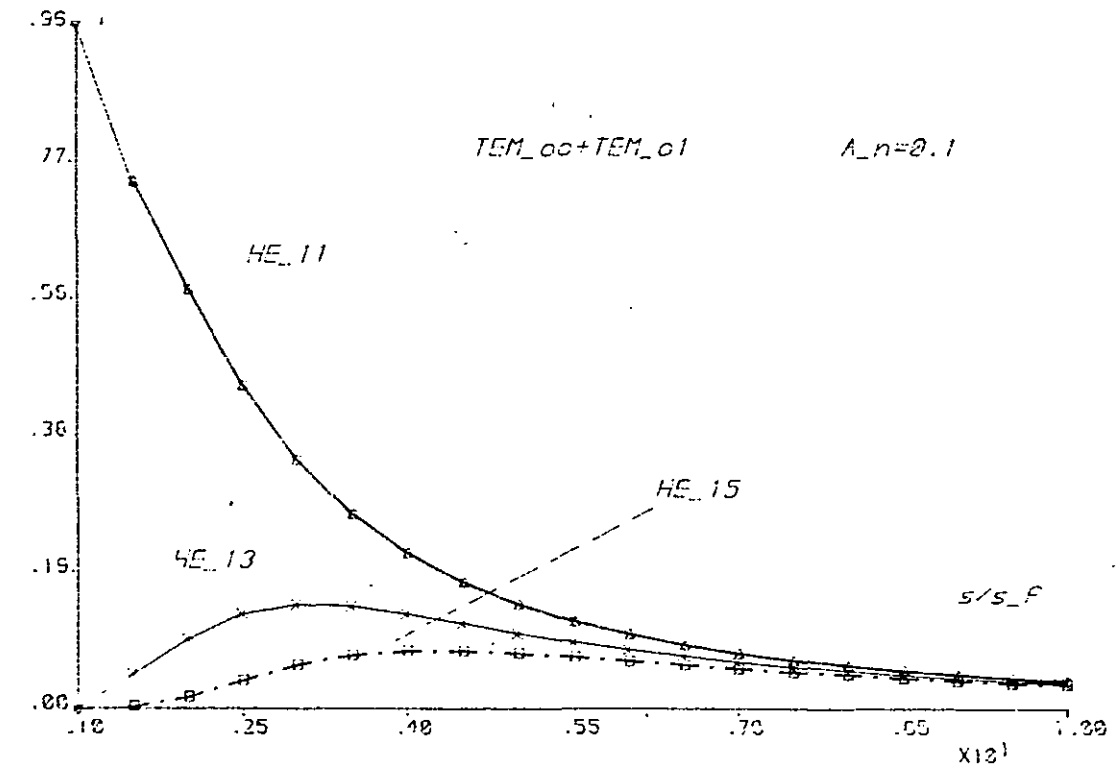

Fig. 3.8 Excitation Coefficients of various modes

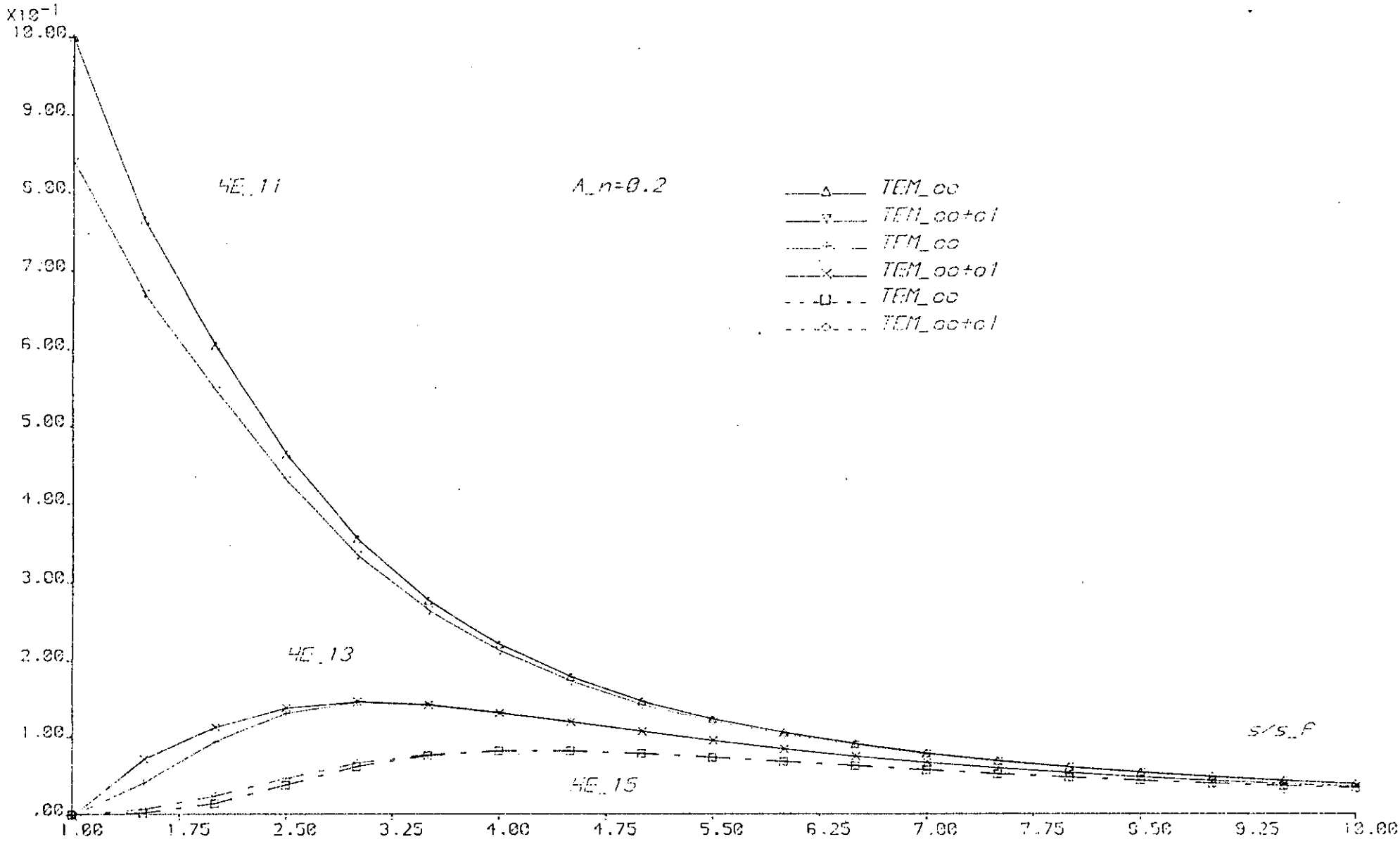

Fig. 3.9 Excitation Coefficients For different Beams

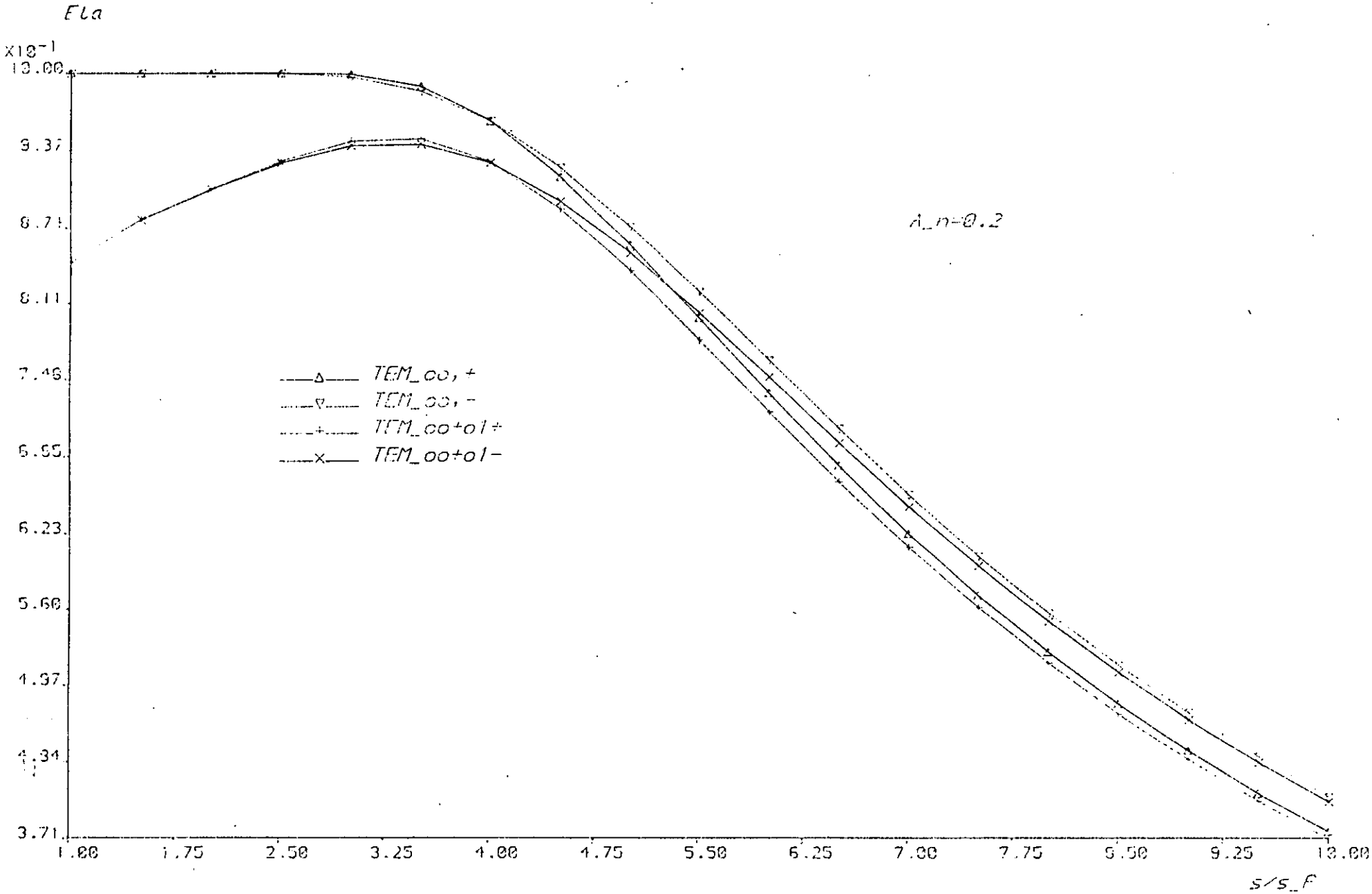

Fig. 3.10 Overall Launching Efficiency (V=48.84)

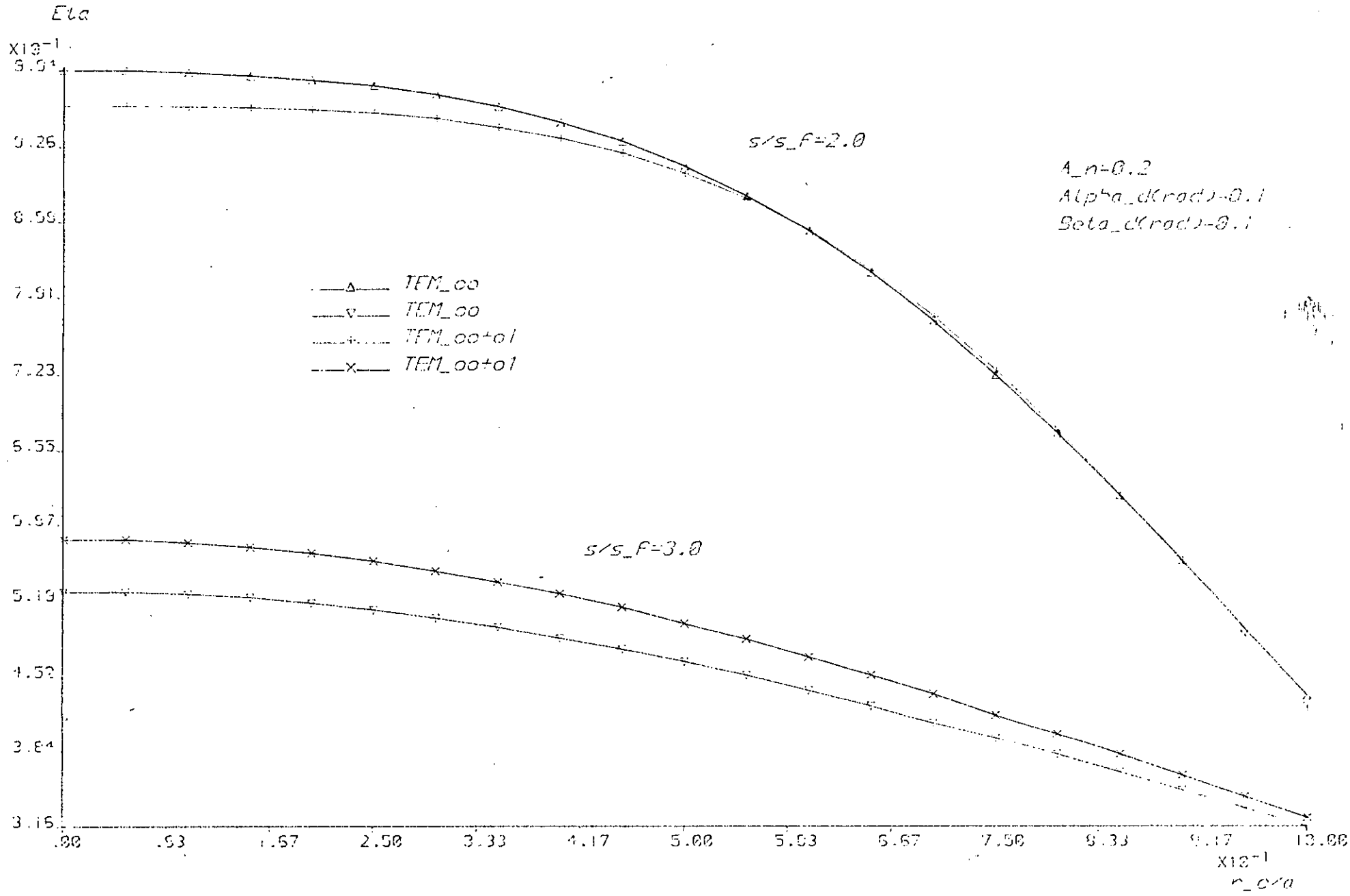

Fig. 3.11 Overall Launching Efficiency for various off-set conditions

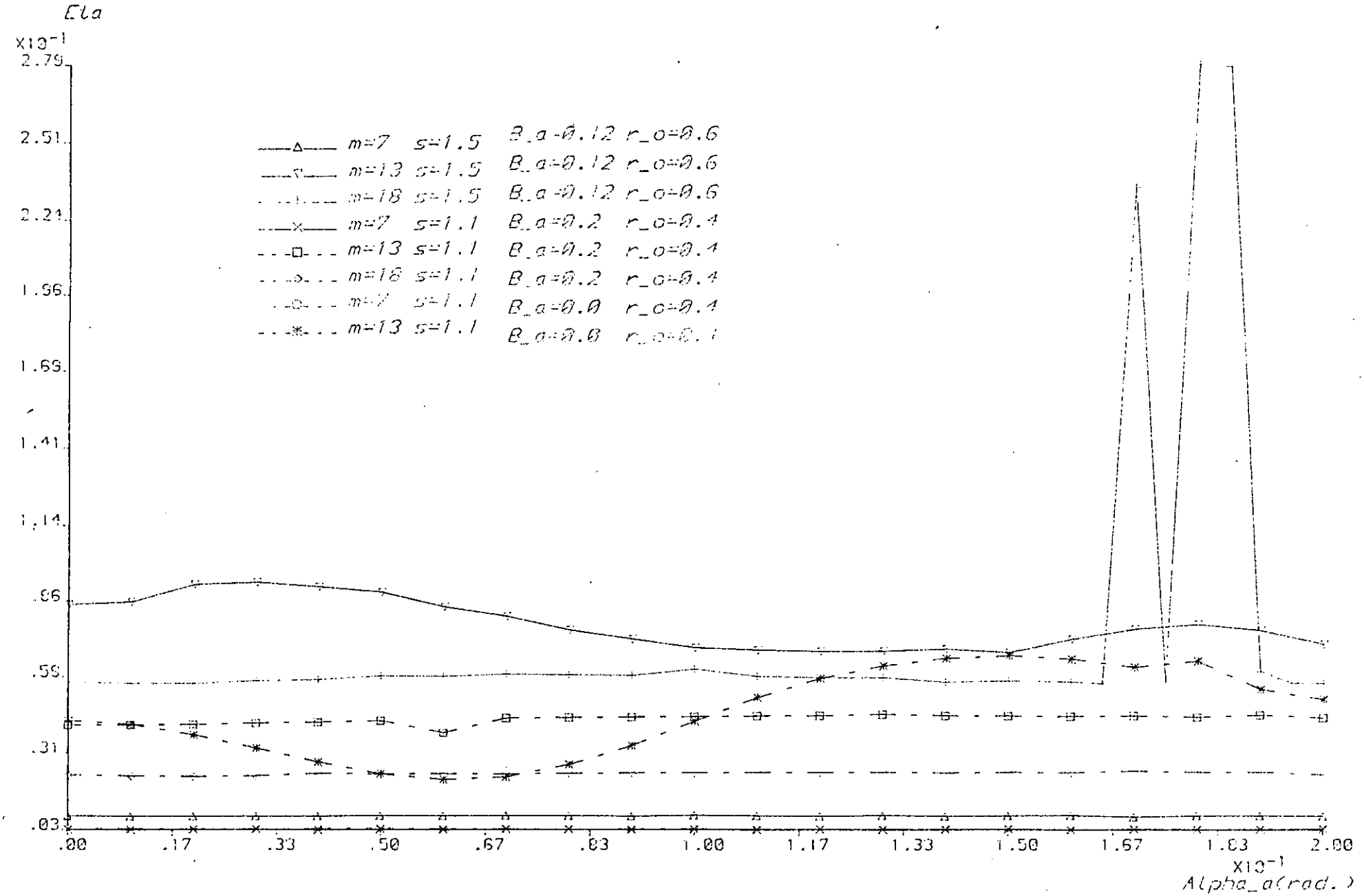

Fig.3.12 Excitation of Leaky modes For different offset conditions(TEM_00)

LED's tend to be rather poor in terms of excitation efficiency. This is because most of the power radiated by these sources constitute the refracting rays. Thus, on entering the fibre, they are filtered out within a fraction of a distance from the input.

No attempt was made here to examine the aspects of misalignments for LED's since even a perfectly aligned LED causes leaky mode generation. Reference (10) provides a comprehensive study in this direction.

Together with the associated integrals equation 3.44 furnishes the theoretical framework for the evaluation of coupling into individual modes of the fibre under the most general case of offset conditions. For completeness it is essential to incorporate the reflection losses occurring on the fibre front face. In the latter instance, the theoretical development is somewhat simpler since now a plane instead of a curved surface is to be considered. A detailed analysis is to be found in a recent publication (14).

CHAPTER IV

EXPERIMENTS

In this chapter some experimental results related to the theoretical content of the thesis will be reported.

It must be stated quite categorically that, although the cost of fibres has decreased drastically over the years, the act of experimenting with them still remains an expensive practice. This is primarily due to the high precision devices required for alignment etc. Additionally, much greater resolution than usual is needed to detect the effects of such parameters as non-uniformities in core diameter or the profile.

The available equipment for this project was rather limited for financial reasons. Justifiably therefore, not all the mathematical derivations could be tested experimentally.

Among the main research centres in the field of optical fibres in the UK are:

1. STL, Harlow
2. Post Office Research Centre, Ipswich.
3. Southampton University, Southampton.
4. Queen Mary College, London.

4.1 Fibre End Preparation

One of the most important criteria when dealing with fibres is the ability to obtain terminations of acceptable quality. This fact may be appreciated more if one bears in mind that optical fibres do not generate their own power, but instead have to be externally excited.

Throughout the development, two types of connections have come into existence. Fusion arc splicing which may be essentially regarded as the welding of fibres with index matching liquid in between, is used for mounting fibres permanently. By this method, it is possible to achieve extremely low loss levels, typically 0.5 dB (1).

The other type that provides more flexibility is to have the end of the fibre free and accomplish the coupling via precision alignment. Conventionally V grooves are employed for the task. Whether the fibre is protected by surrounding layers or lies bare would depend upon the particular requirement. Completely different processes of preparation are undertaken for the two.

A great deal of progress has been recorded in breaking fibres to produce reasonably flat termination. The mathematical equations developed (2) indicate that to avoid the occurrence of what is called a beak (see Figure 4.1a) a known stress must be applied to keep it under tension while simultaneously bending it over a curved surface with a certain radius as shown Figure 4.1b.

Normally of course, one would resort to a mechanically sound set-up to perform the above operation. The earlier types constructed consisted of curve shaped foam over which the fibre was stretched to the correct tension by a dial gauge. A knife fixed onto a pole would then come down and initiate a crack on the fibre. A more versatile version of this, as a hand held tool, that was manufactured in Japan, cost at the time of writing £500.

Another approach, less expensive, yet comparable in standard, is to tape the end of the fibre over any clean curved surface and pull it by hand. Touching it slightly with a chisel knife would then effect the cleavage.

The latter method was used here. Obviously without the knowledge of the stress applied and the radius of curvature, this was

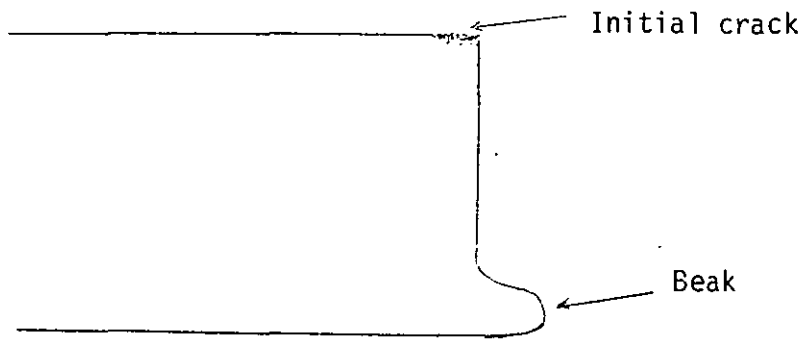

(a) Pictorial Representation of Beak for a Cleaved Fibre

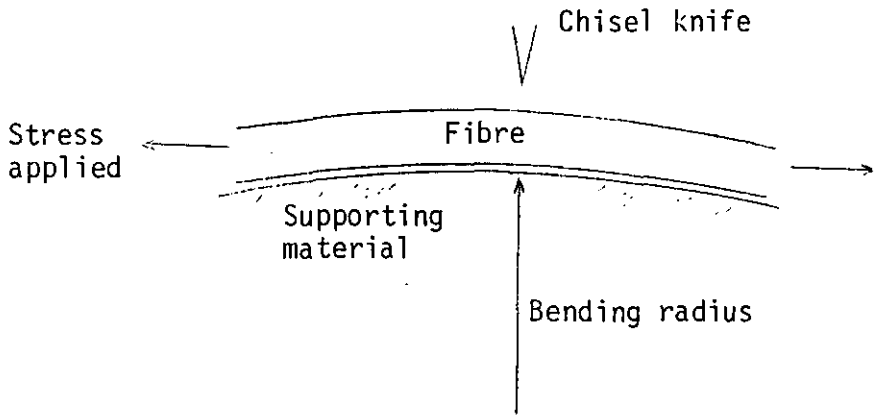

Fig. 4.1(b) Fibre Scoring

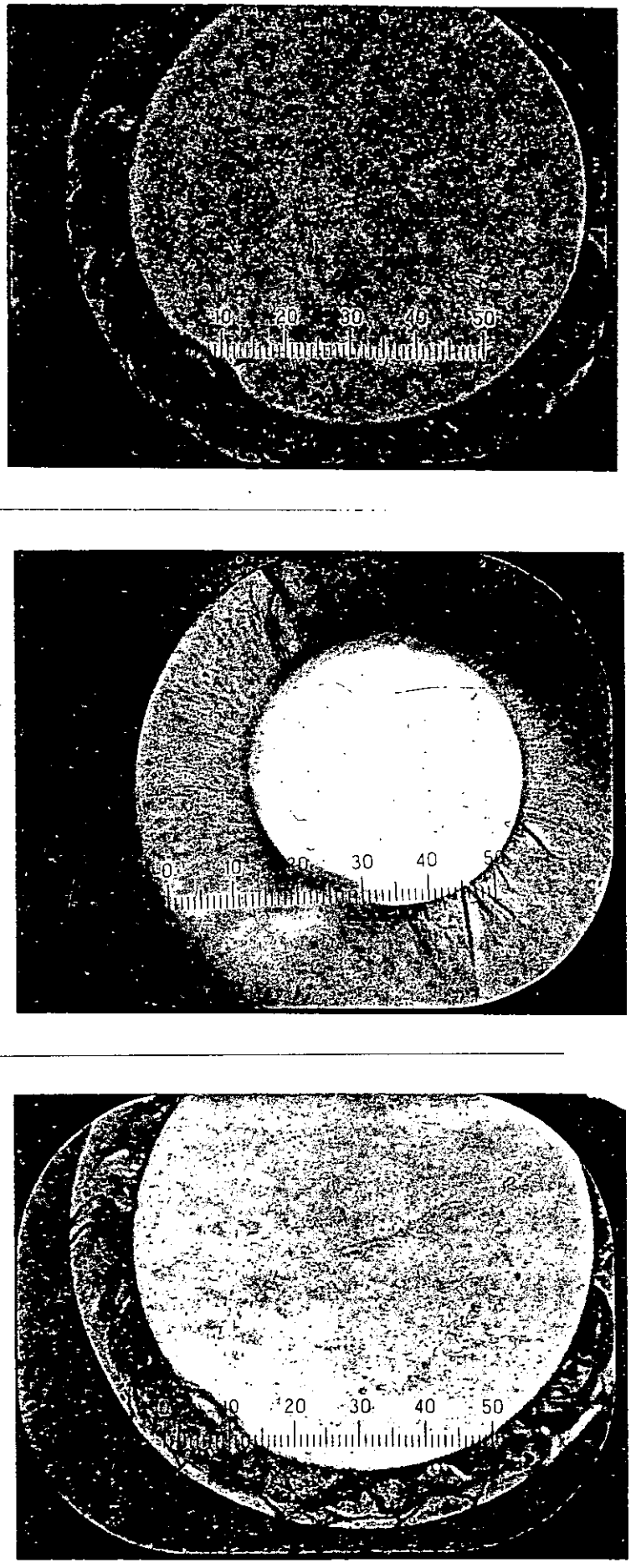

Fig. 4.2 Microphotographs of Cleaved Fibre Ends

more or less a trial and error task. The photographs in Figure 4.2 illustrate some of the high quality ends obtained by this procedure. The other type of termination requires more effort and time. It, however, offers the advantage of easier handling of the fibre.

The steps to be followed are described below.

After stripping the plastic coating from the fibre, it is immersed in concentrated H_2SO_4 to remove the silicon layer around the cladding. It is then washed in distilled water (note that these preparatory stages are also common to fibre cleaving).

Ferrules, one containing the jewel of the right size are cleaned in the ultrasonic bath while the fibre is mounted onto a clamp with the bare end directed upwards. Epoxy is injected into the larger ferrule and the other one is clipped around the fibre so that the upper edge rises up to the end of the plastic coating. The ferrule carrying the epoxy is then inserted over the fibre till the end has emerged out of the jewel and the ferrule has rigidly settled down. More epoxy is added to the top of the jewel and the whole assembly is left to dry. This usually takes two hours.

The excess fibre should then be removed by scoring it gently with a suitable knife. It is now ready for polishing. This is firstly done on a rough pad to reduce the protruding length and at the same time observing the process under the microscope. Care is called for here to maintain the fibre level flat with that of the jewel. When the above is completed, transferring to the fine polishing pad will finally yield the smooth surface desired.

Clearly, it is equally feasible to place protecting material around a broken fibre end. Conventionally however, if this is

to be undertaken it is more logical to adopt the polishing technique. Nevertheless bare terminations are known to suffer less from reflection losses (3).

4.2 Measurement

The equipment supplied for this project was as follows:

1. Optometer (analogue) plus a separate opto-detector from United Detector Technology.

2. Micro manipulators, three rotational and three translational stages with resolutions of 5 μm, from Unimatic Engineering Ltd.

3. Light sources (a) He-Ne laser, λ = 0.632 nm, (b) Two LEDs, λ_1 = 670 nm, λ_2 = 890 nm, from Spectra Physics and Rofin Math. Associates respectively.

4. An Ealing Beck microscope; additionally Kyowa viewing microscope.

5. Various convex and concave lenses, beam splitter (cube), from Ealing Beck.

6. Optical bench and a cast iron bed.

The hardware constructed was:

1. Mounting arrangement to fit onto the micro manipulators. These comprised two plates, the lower one was to join the assembly to the micro positioners (see photographs in Figures 4.3 and 4.4). The other plate would then be mounted on the top. Two further interchangeable plates would be placed on the upper part, one to take ferruled kinds of termination, the other being suitable for bare fibres. The V grooves on these were cut

accordingly. A clamping device with rubber attachment on the lower side was used to hold the fibre down.

2. A housing box and a drive unit for the LEDs. The circuit operated from a μ741 op. amp. and two intensity control buttons were provided.

3. A differential amplifier with variable gain, to facilitate a digital read-out from the output of the photodetector. This similarly used a μ741 amplifier.

4. Jewel pressing device. Various mounts for examining fibres under the microscope and to couple the fibre into the optometer head. These were cylindrical structures with holes bored through the middle. The mounting device for bare fibres was in two halves each one being individually V grooved. Additionally lens holders were constructed.

The various items supported on steel rods of appropriate height would then be lined up along the optical bench.

In addition to the above, a thin slice of fibre held by a copper plate was prepared. The length of it was approximately 500 μm, which was less than the ray period (582 μm) of the fibre. The required thickness and the flat surfaces on both sides were achieved by the polishing method. The sample served as a datum to some of the experimental data.

Measurements with the laser will be described first.

Initially an attempt was made to check the stability of the laser output. For this purpose, the two beams from the beam splitter were fed into the differential amplifier. It was found however that the chart recorder obtained heavily overloaded the input of the amplifier. This idea was therefore dropped. It was discovered later on that the laser would reach a reasonably stable point of operation after one hour of switch-on.

To determine the type of irradiance, the intensity distributions in two transverse planes were measured using a slit of 1 cm in length and 0.5 mm in width. The laser beam was broadened by passing it through a concave lens. Figure 4.5 shows the intensity patterns for various combinations of TEM_{oo+o1} modes. From these, the best selection was found to be $TEM_{oo} - 0.3\ TEM_{o_1}$ (Figure 4.6).

Axial displacement measurements were taken to observe the change in the launching efficiency against the variations in beamwidth and curvature. Since the utilization of a lens altered the natural propagation of the beam, the relevant parameters would have to be redefined. Assuming a thin lens, then, from the equations presented in Ref (4):

$$s_2 = \frac{(R_1 \pi s^2 + d\pi\ s^2)^2 + (d\ \lambda\ R_1)^2}{\pi^2\ R_1^{\ 2}\ s^2} \qquad (4.1)$$

$$R_2 = \frac{(R_1\ \pi\ s^2 + d\pi s^2)^2 + (d\ \lambda\ R_1)^2}{\pi^2 s^4\ (R_1 + d) + d\lambda^2 R_1^{\ 2}} \qquad (4.2)$$

where $R_i = \frac{fl\ R}{fl - R}$ (4.3)

fl = focal length of lens, d = distance from the lens.

From equation 4.3 it is seen that rapid variations of the beam curvature will be produced if lenses with short focal lengths are employed.

Hence, by using the above formulae, and the programmes of the previous chapter, the theoretical values for axial movements of the beam were calculated. These are displayed in Figure 4.7 along with the measured ones. The higher level of the power found

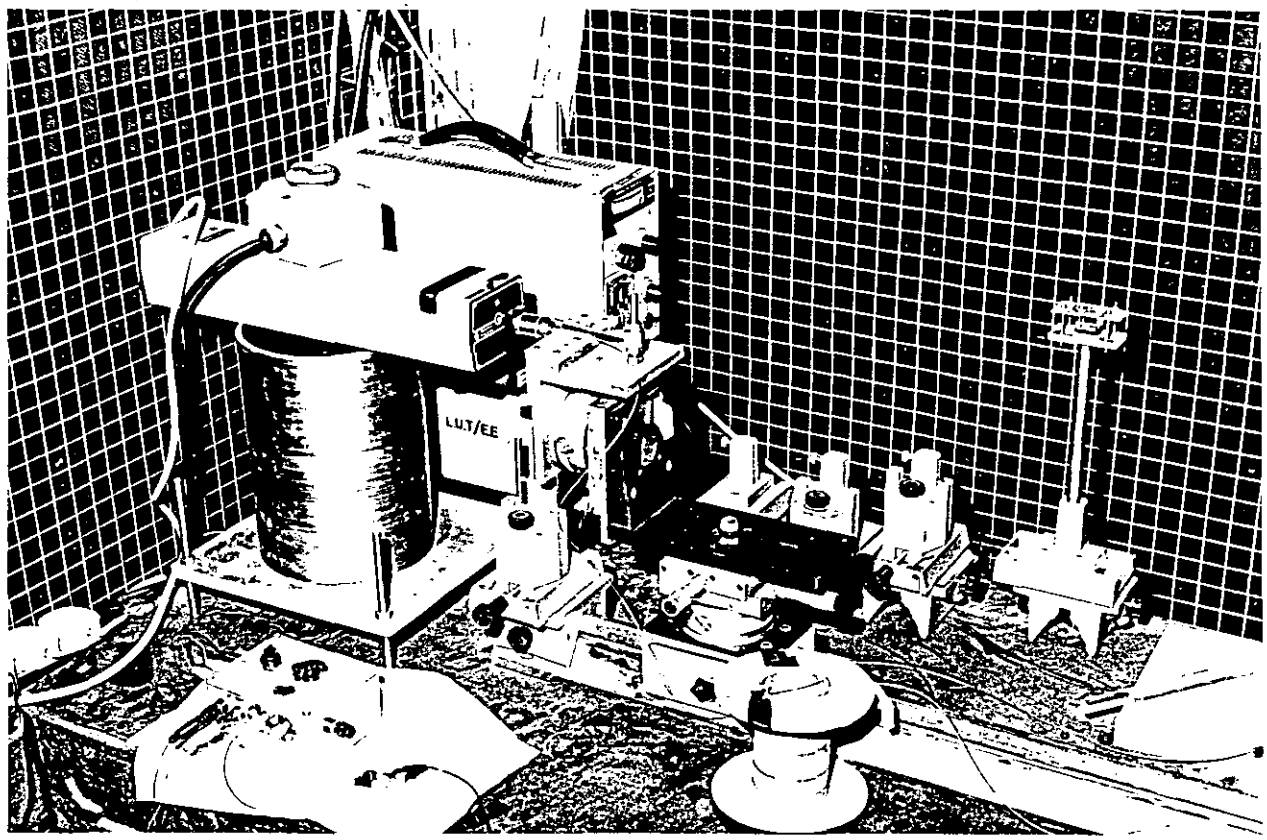

Fig. 4.3 General View of Experimental Assembly

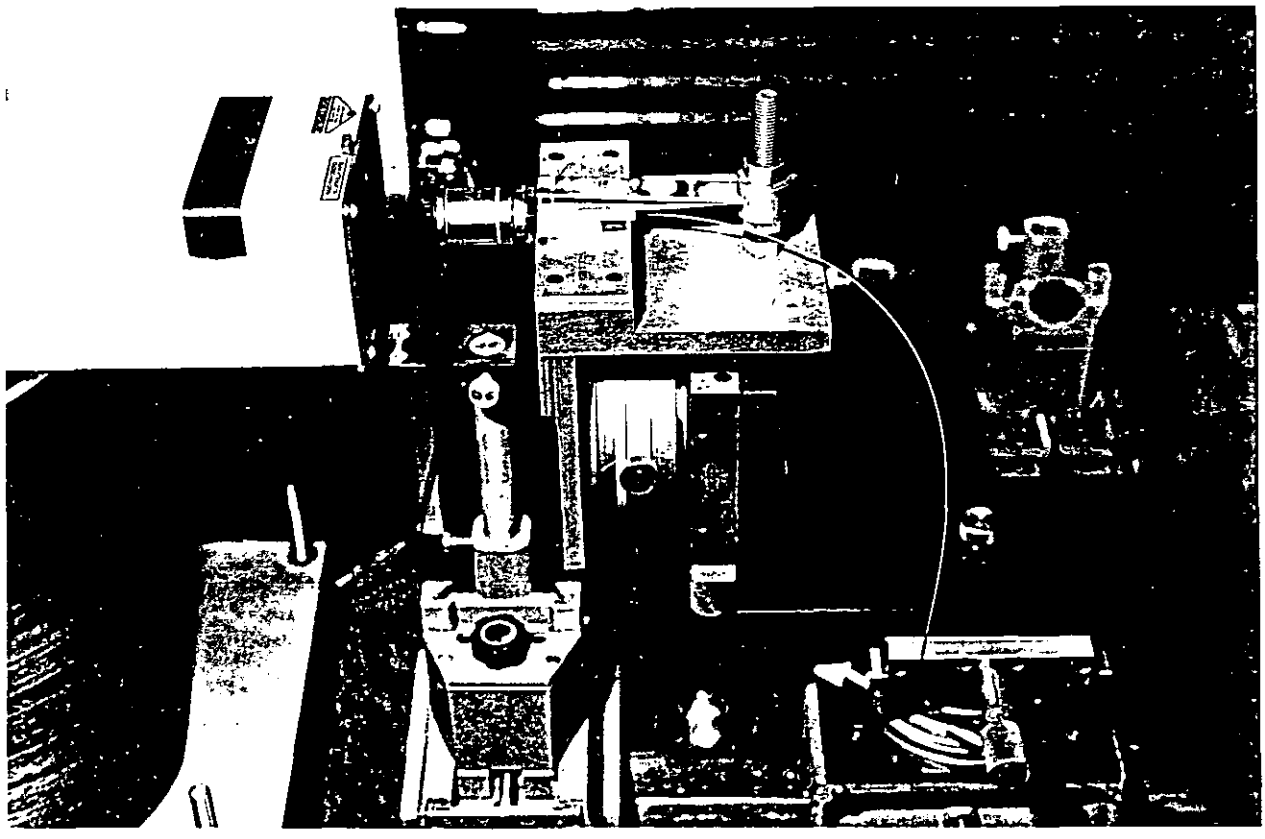

Fig. 4.4 Laser Launching Arrangement

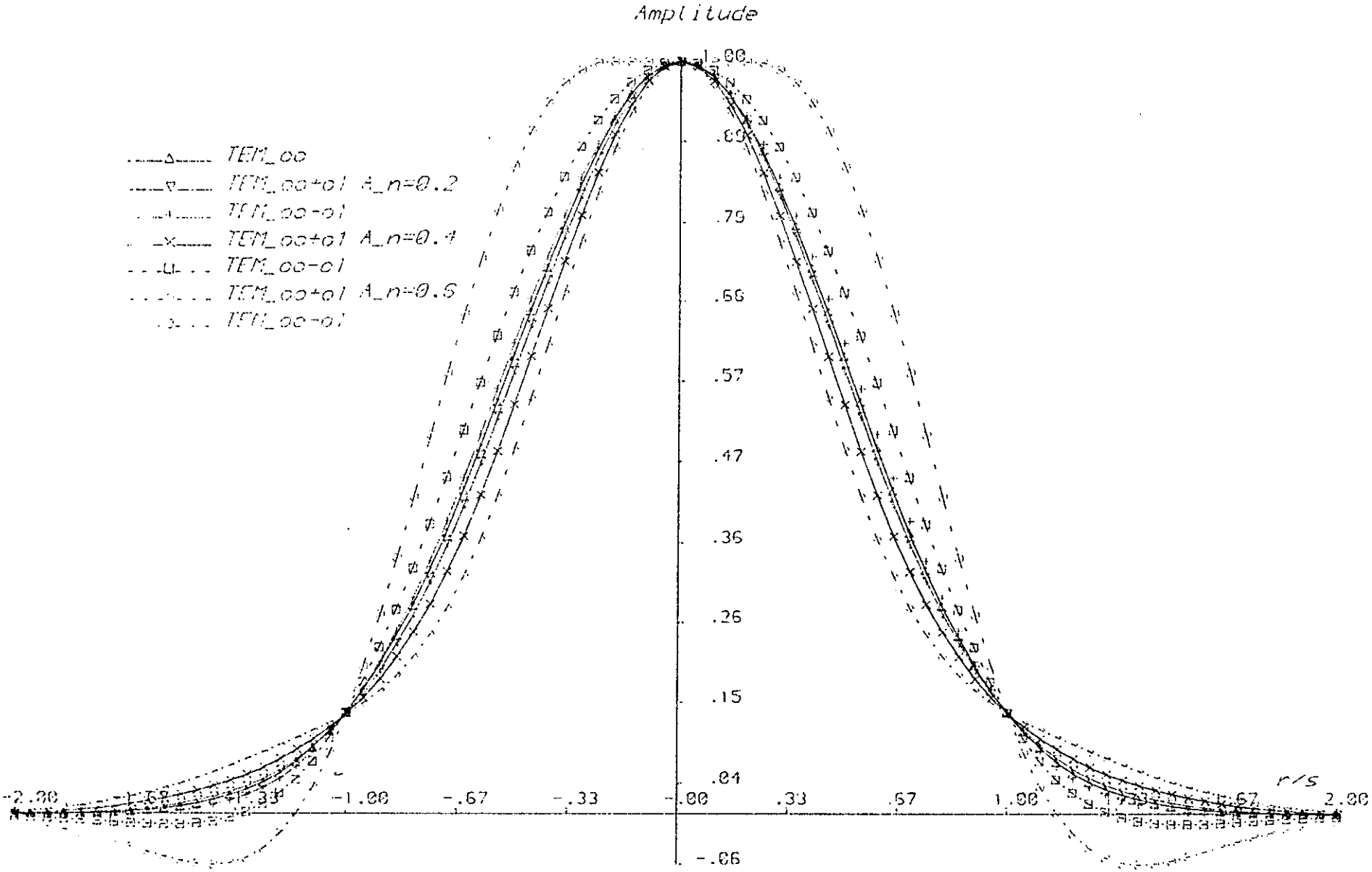

Fig 4.5 Intensity distributions For combinations of TEM_oo & TEM_o1 modes

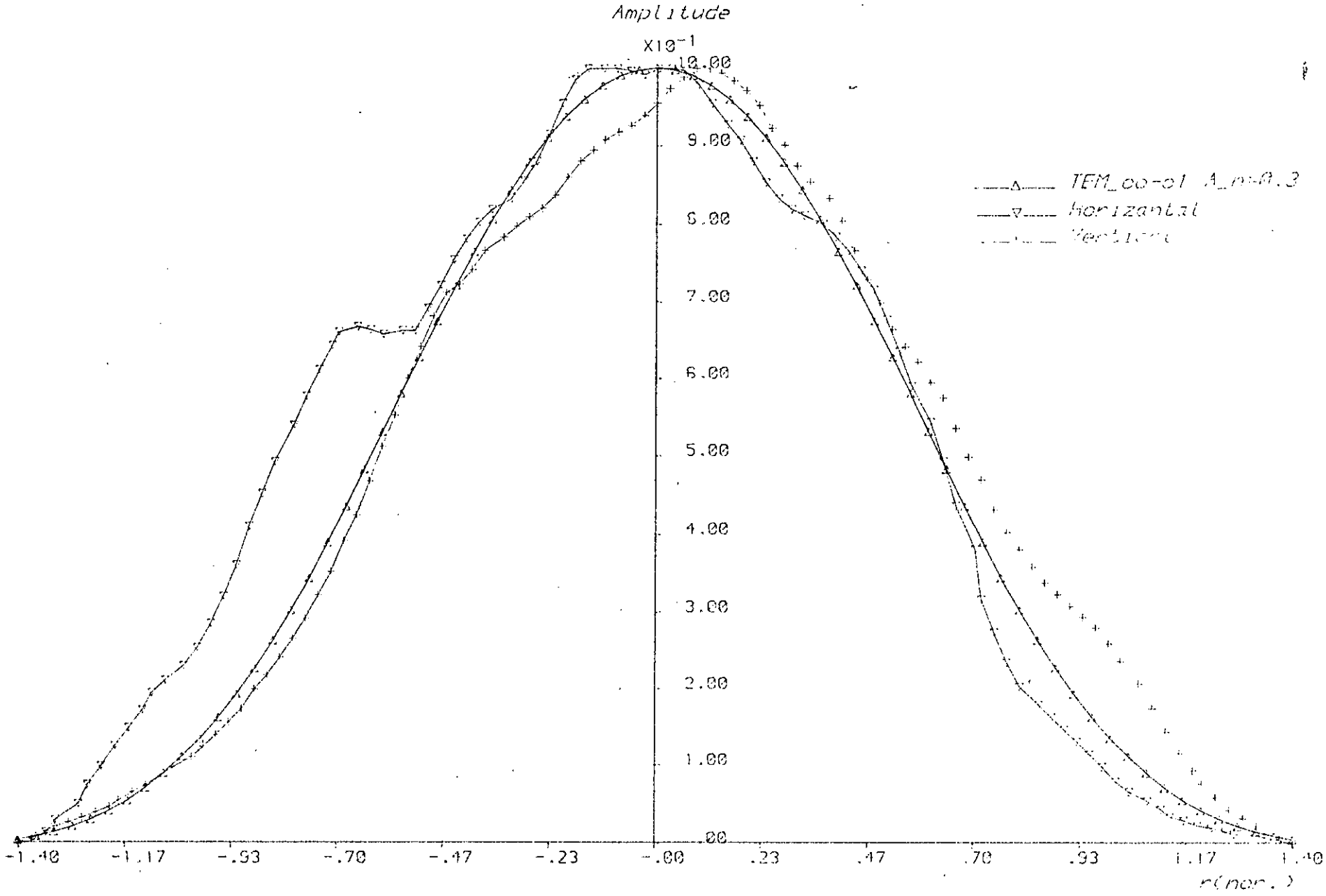

Fig. 4.6 Intensity distribution of Laser beam & its approximation by TEM_oo-o1 mode

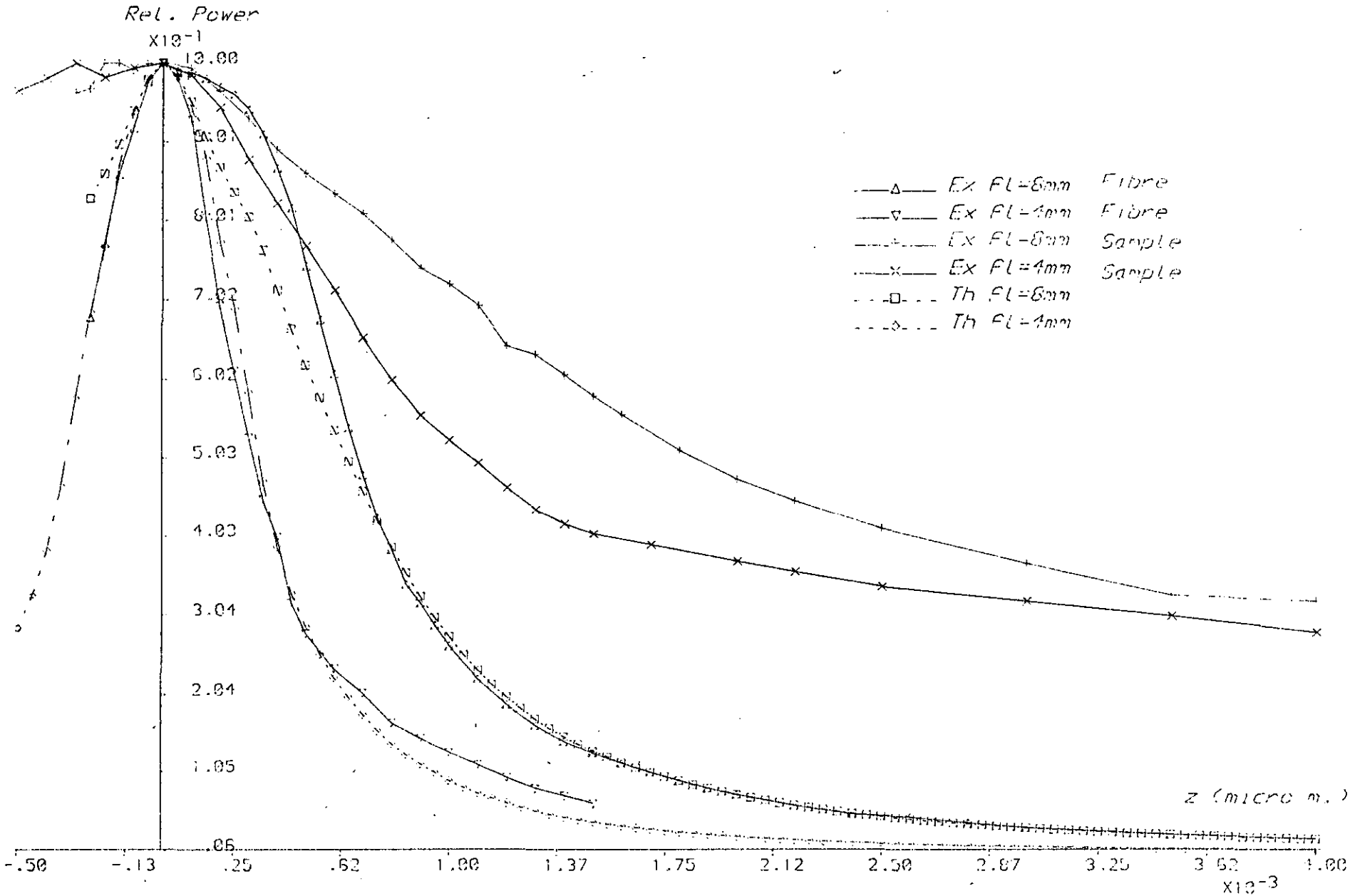

Fig. 4.7 Measurement of Axial displacement For Laser Beam

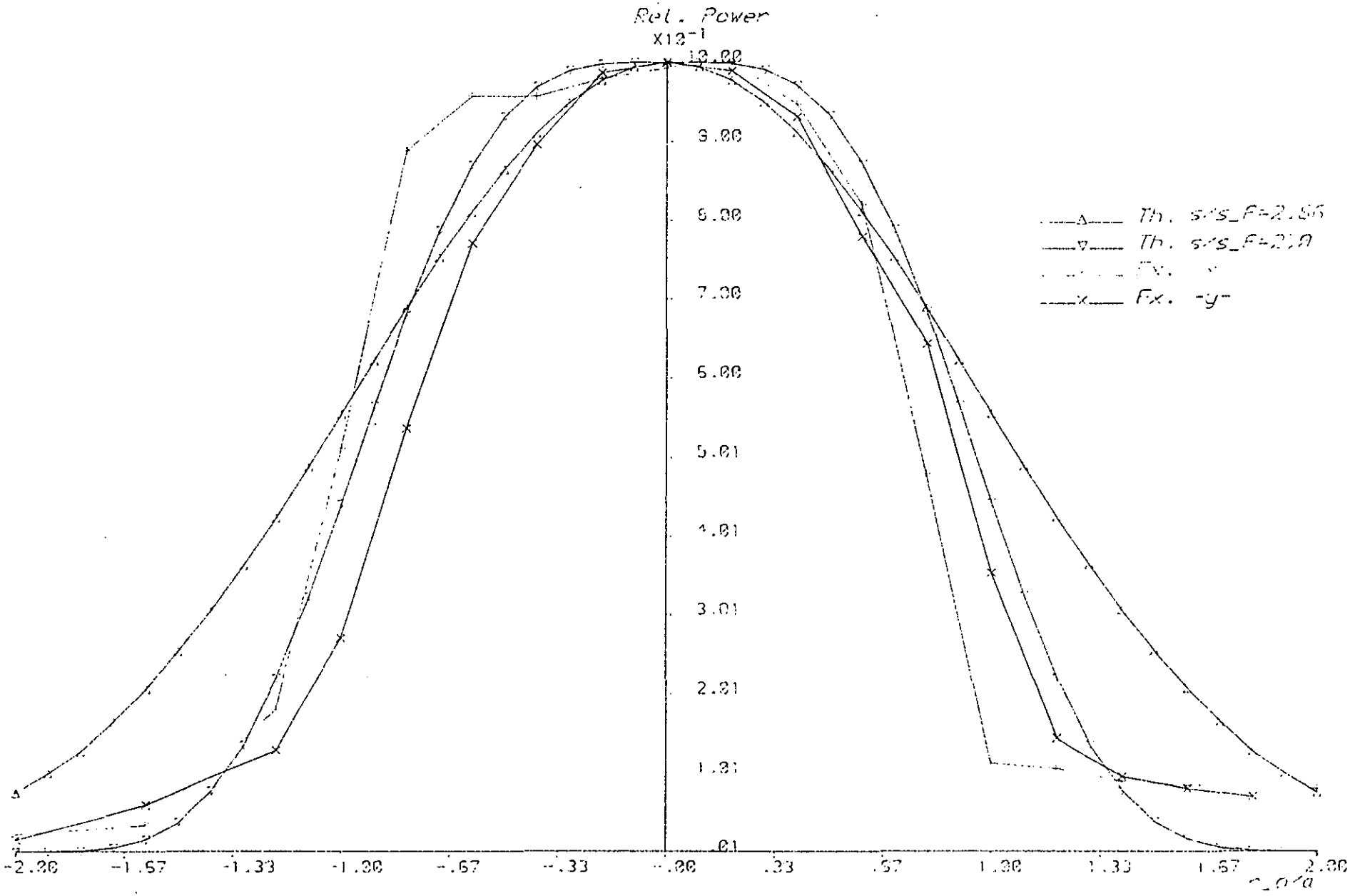

Fig. 4.8 Measurement of Transverse displacement For Laser Beam(Fibre)

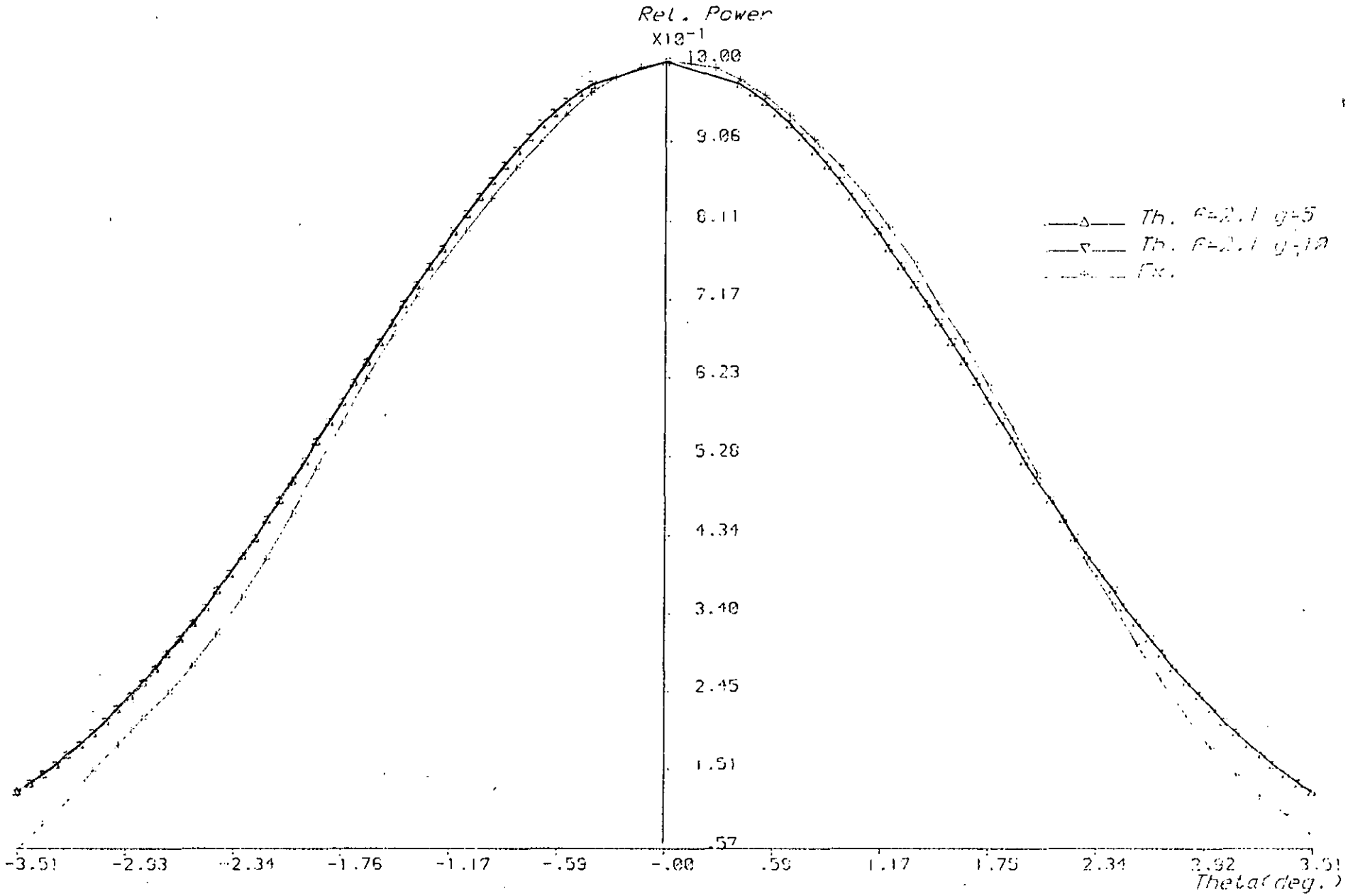

Fig. 4.9 LED intensity distribution plot

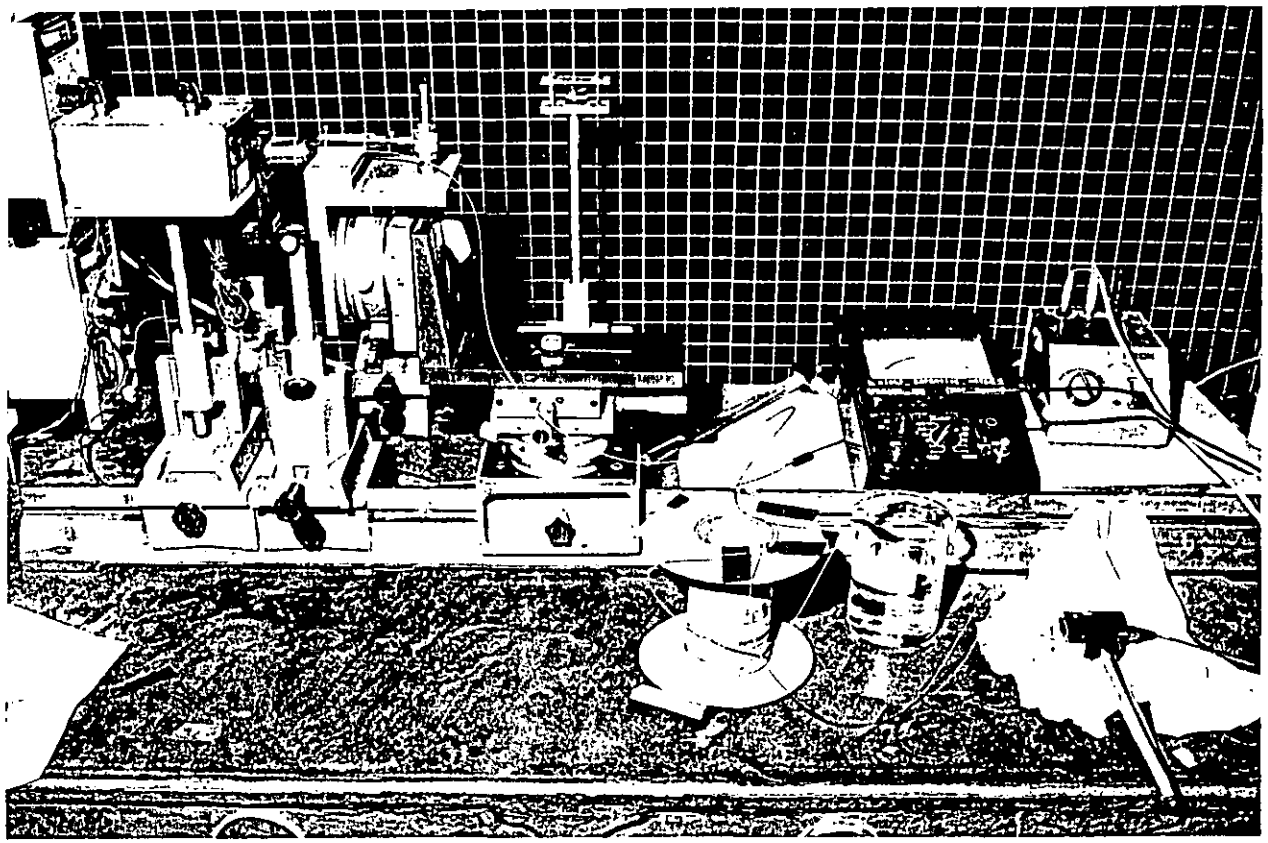

Fig. 4.10 Filtering Arrangement

far away from the focal point of the lenses (this was very nearly the zero point marked on the graph) in the case of the sample fibre, indicates the effect of the light intercepted by the cladding material.

The readings for offsets in the transverse directions were more difficult to handle. The use of a x5 objective yielded the optimum results and these are plotted in Figure 4.8. Again the theoretical figures are from Chapter III. It was found using equation 4.1 that at the narrowest point, the spot radius would be 14.47 μm. Choosing $s = 2\ s_f$ seems to fit the experimental data better. This discrepancy may be attributed to the inability of the theoretical derivation to account for the areas beyond the core periphery.

From the absolute values of the readings, the guided mode attenuation in the fibre was computed to be 35 dB/km.

The interpretation of intensity distribution measurements for the LED (λ = 670 nm) were somewhat different. The maximum expendable beam size without affecting the accuracy of the readings was comparable with the width of the slit or the optometer head. Therefore the numerical values obtained here were regarded as power falling into an area. Then a programme was devised to provide the irradiation pattern in a similar fashion. The respective graphs are plotted in Figure 4.9. It was rather difficult, however, to attain a closer match for the bottom parts. The distribution was highly sensitive to the non-uniformity parameter while the g values between five and ten could be selected without altering the shape of the curves by much.

It was intended to estimate the power levels of the different rays in the fibre via the sample prepared. This was not successful however since the light entering the cladding appreciably pre-dominated the readings. In fact it was discovered by adopting the figures of f and g that, this portion of the power constituted

slightly more than half of that accepted by the core.

Filtering experiments were carried out using carbon tetrachloride (see photograph in Figure 4.10). Firstly, to ascertain the reliability of the set-up, the stripped fibre (at ≃ 1m from the input) was immersed into the filtering liquid when the fibre was excited by the laser. Secondly it was immersed in water. No change was detected in both instances.

The table below shows the readings obtained and those of the theoretical predictions.

TABLE 4.1

LED	Power decrease due to filtering	Theoretical assuming full excitation		Theoretical using suitable values of f and g			
		q=2.0	q=2.2	q=2.0		q=2.2	
				f = 2.1			
				g=5	g=10	g=5	g=10
λ=670nm	0.8036, 0.7931	0.7595	0.7655	0.8594	0.8639	0.8595	0.8640
λ=890nm	0.8913 -						

As seen, unless the source parameters are properly taken into account, the theoretical analysis offers a figure lower than the measured one.

It was not possible to determine accurately the refractive index of the chemical fluid used. This is reported to be 1.459 (at λ = 589 nm) (5), but it is known that the index of refraction is susceptible to changes in wavelength (6).

4.3 Discussion (4)

The majority of the measurements were performed using the digital voltmeter, the only exception being the filtering experiment where the minimum power level detectable prevented the use of the differential amplifier.

Care was taken to keep fibres clean and free from dust. 'Inhibisol' solvent and 'Omit plus' sprays were used for this task.

The laserbeam exhibited strongly the presence of higher order modes. With a mode analyser not being currently available, one can only postulate what these higher order modes should be. A choice of -0.3 TEM_{01} was however seen to lead to consistent results. The irregularities in the beam were also reflected in the measurements. When, for instance, axial displacement readings were being recorded, it was noticed that an non-identical behaviour was experienced at symmetrical distances from the focal point of the lens. Although equation 4.1 also predicts this, its contribution would however be minimal.

Having no access to any other filtering liquid with a suitable index of refraction limited the exercise to one set of data only. In general it is logical to expect greater losses than the theoretically calculated ones. In this respect, the figures in Table 4.1 agree quite favourably. The effect of refractive index variation with wavelength is clearly seen from the readings obtained when the second LED was used, though another contributory factor here was the extremely low power provided by the source (ten times less than the first LED).

CHAPTER V

CONCLUSIONS

The major objective of this report was to study the attenuation of leaky rays (modes) and propose suitable filtering techniques.

Two familiar approaches whose theoretical basis have long been established by physicists were utilized.

It was shown in Chapter I that ray analysis is capable of furnishing an adequate description of the wave equation. Via its solution in terms of Airy functions, the behaviour of the individual rays in the entire $\bar{\beta}$-$\bar{l}$ domain was examined.

As a further step, the WKB formula was put forward to obtain the overall attenuation in the fibre due to tunnelling rays, which is perhaps the case of interest in the majority of practical situations.

The other powerful aspect of the WKB approximation lay in the fact that it enabled a quantitative assessment of the filtering phenomenon.

It was discovered that filtering is almost impossible by the methods known to date since surrounding the cladding with an ordinary jacket would affect the bound rays more than the leaky ones. Although the calculations verified that a graded jacket would offer some improvements, the overall effect was minimal. Thus, the main conclusion here was to suggest a reduced cladding thickness.

When using the geometrical ray approximation, variations in the core profile were considered in the greater part of the computer simulation work. That is probably the most appealing feature of this approach.

Mode theory, while being mathematically more complicated, revealed vital concepts of propagation which could not be afforded by its counterpart.

Starting with Maxwell's equations, the field expressions were deduced. The characteristic equation subsequently derived was employed to find the attenuation of leaky modes.

It was demonstrated that consistent results could be attained for the imaginary part of β by a simple procedure, namely graphical matching.

Through lengthy derivations, the characteristic equation for a fibre with an outer layer was obtained. This was solved in the same manner as that of the single boundary case. Its accuracy however could not be tested rigorously because of the nature of modal analysis. The numerical values nevertheless displayed close correlation with those evaluated from the WKB approximation.

The theory of excitation which plays an important role in the study of optical fibres was presented in Chapter III. Distinct analytic expressions were obtained to cover nearly all cases of LED excitation. Guided and leaky rays were investigated separately. Hence, given the source specifications, it is possible from the graphs plotted to determine the relative power level of each ray group.

When dealing with laser excitation, part of the work was similarly devoted to guided modes. The mathematical equations included launching by the TEM_{00} beam mode as well as the TEM_{00+01}. The variation of launching efficiency against the changes in the beam-waist were considered. The effects of tilts and offsets on the generation of leaky modes were studied. The results were however partially successful with the reasons outlined in the main text.

Fibre termination by various methods were described at the beginning of Chapter IV. The measurements, in general, showed good agreement with the theoretical predictions. Bearing in mind the crude set-up employed for the filtering experiments, the discrepancy was remarkably low.

Suggestions for Further Studies

1. From Chapter I it is apparent that filtering theory requires deeper investigation. In the main, the conventional concept that "a jacket with a refractive index higher than that of the cladding will remove radiating rays (modes)" must be revised. Ultimately, a more efficient process of filtration than the one put forward in this thesis is desirable.

2. One of the difficulties in the derivation of the field equations is the actual implementation of the weakly guiding approximation. As already explained, inconsistencies will arise unless care is exercised. At the moment there is no firmly established rule. Therefore one encounters odd cases of scaling factors (for example $\epsilon_1^{\frac{1}{4}}$ (instead of $\epsilon_1^{\frac{1}{2}}$ used here) employed by Kurtz and Streifer in Ref 1 of Chapter II). Additionally, if the analysis solely concerns leaky modes, it is more reasonable to assume $\beta \simeq k_o n_2$ rather than $\beta \simeq k_o n_1$.

   A formidable task that has confronted the researchers has been the solution of the characteristic equation. In the event of leaky modes, this difficulty is twofold since β becomes complex. To solve even the equation derived by means of Taylor Expansion, one needs to know (approximately at least) the real part. Here a graphical matching technique was used. Its disadvantages are obvious.

   It was hoped initially to solve the characteristic equation for the real and imaginary components of the propagation constant simultaneously. For this reason, all the relevant func-

tions were prepared accordingly. The non-availability of a stable algorithm however prevented this undertaking.

It was also the intention at the beginning to obtain the overall attenuation in the fibre via the mode counting procedure described in Chapter II. With the above aim not being realised however, this could not be carried out either.

Further attempts in these directions should therefore be made.

3. The formula presented in Chapter III for the most general case of misalignments in the laser beam may be developed further. By appropriate modifications, it would be of interest to apply it to semiconductor lasers in current use.

APPENDIX A

This appendix deals with the various analytic derivations encountered in the course of the report. The same meaning of the terms appearing in the text are preserved. Where unspecified, prime will indicated d/dr.

CHAPTER I

1) Epl and Ep2:

These are defined as follows:

$$Epl(+) = \{(3/2)\, k_o \int_{r_{tp}}^{a} [\bar{\beta}^2 + \bar{1}^2\,(a/r)^2 - n^2(r)]^{\frac{1}{2}} dr\}^{2/3} \qquad (1A)$$

$$Ep2(+) = \{(3/2)\, k_o \int_{a}^{r_{rad}} [\bar{\beta}^2 + \bar{1}^2\,(a/r)^2 - n_2^{\,2}]^{\frac{1}{2}} dr\} \qquad (2A)$$

where in the event of refracting rays, the sign inside the square root must be inverted. Denoting these Epl(-) Ep2(-), by standard integration techniques when q = 2

$$Epl(+) = \{\frac{3\, ak_o}{4} \left[P_1 + \frac{P_2^{\,2}}{2\gamma} \ln \frac{(P_2^{\,4} - 4\gamma^2 \bar{1}^2)^{\frac{1}{2}}}{(2\gamma P_1 + \bar{\beta}^2 - 2 n_2^{\,2} + n_1^{\,2})}\right.$$

$$\left. + \bar{1} \ln \frac{(P_2^{\,4} - 4\gamma^2 \bar{1}^2)^{\frac{1}{2}}}{(P_2^{\,2} - 2\bar{1}^2 - 2\bar{1}^2 P_1)}\right]\}^{2/3} \qquad (3A)$$

$$Ep2(+) = [\frac{3}{2} a k_o (\bar{1} \tanh^{-1} \frac{P_1}{\bar{1}} - P_1)]^{2/3} \qquad (4A)$$

$$Ep1(-) = \{\frac{3 a k_o}{2} [\frac{\pi}{2} (\frac{P_2^2}{2\gamma^2} - \bar{1}) - P_1 + \frac{P_2^2}{2\gamma} \cdot$$

$$\sin^{-1} \frac{(P_2^2 - 2\gamma^2)}{(P_2^4 - 4\gamma^2 \bar{1}^2)^{\frac{1}{2}}} + \bar{1} \sin^{-1} \frac{(P_2^2 - 2\bar{1}^2)}{(P_2^4 - 4\gamma^2 \bar{1}^2)^{\frac{1}{2}}}] \}^{2/3}$$

(5A)

$$Ep2(-) = [\frac{3}{2} a k_o (P_1 - \bar{1} \tan^{-1} \frac{P_1}{\bar{1}})]^{2/3} \qquad (6A)$$

$P_1^2 = (\bar{\beta}^2 + \bar{1}^2 - n_2^2)^{\frac{1}{2}}$ for Ep(+) and $(n_2^2 - \bar{\beta}^2 - \bar{1}^2)^{\frac{1}{2}}$ otherwise, $P_2^2 = n_1^2 - \bar{\beta}^2$

If the cladding is homogeneous, then Ep2 is always as given above. There is no general solution for Ep1 however, when q differs from 2 in which case a numerical evaluation has to be employed.

Alternatively, analytic approximations may be invoked. Consider Maclaurin's series about r = a

$$n^2(r) = n_1^2[1 - 2\Delta (r/a)^2] = n_2^2 + \frac{\gamma^2 q}{a} (r-a) + \frac{\gamma^2 q(q-1)}{2a^2} (r-a)^2 \ldots$$

(7A)

The terms containing γ^2 are small since $n_2 >> \gamma$. Another possibility is to expand $(r/a)^q$ in even powers of (r/a). This is claimed to offer the best fit for profiles obtained from the diffusion process (1).

Taking the first two terms in 7A corresponds to the linearization of Love and Winkler (2). Epl is then found to be

$$Epl(+) = \left(\frac{k_o \, a \, P_l^{\,3}}{q\gamma^2 - 2\bar{l}^2} \right)^{2/3} \qquad (8A)$$

2) Ray Period:
This is given by:

$$z_p = 2\bar{\beta} \int_{r_{min}}^{r_{tp}} [n^2(r) - \bar{\beta}^2 - \bar{l}^2 (a/r)^2]^{-\frac{1}{2}} \, dr \qquad (9A)$$

Again for a parabolic profile, the integration may readily be performed

$$z_p = \bar{\beta} \, a \, \pi/\gamma \qquad (10A)$$

It should be noted however that when $q \neq 2$, z_p does not significantly depart from 10A. The nominal figure for the ray period of the fibre investigated in this work was 582 μm.

3) Transmission Coefficient:

a) From

$$\frac{d^2 S_3}{d\ Ep^2} + Ep\ (1 + \frac{1}{4\ k_m^2})\ S_3 = 0 \qquad (11A)$$

the oncoming, outgoing and reflected rays may be represented as

$$S_3^{\,i} = Ai\ (-Ep) - j\ Bi\ (-Ep)$$

$$S_3^{\,r} = C_1\ [Ai\ (-Ep) + j\ Bi\ (-Ep)] \qquad (12A)$$

$$S_3^{\,t} = C_2\ [Ai\ (-Ep) + j\ Bi\ (-Ep)]$$

The boundary condition at r = a is

$$S_3^{\,i} + S_3^{\,r} = S_3^{\,t} \qquad (13A)$$

$$\frac{d}{dr}\ (S_3^{\,i} + S_3^{\,r}) = \frac{d}{dr}\ S_3^{\,t}$$

By noting for the derivatives

$$\begin{matrix} Ai' \\ Bi' \end{matrix}\ (Ep) = \frac{k_m}{Ep^{\frac{1}{2}}}\ \frac{d}{dEp}\ \begin{matrix} Ai \\ Bi \end{matrix}\ (Ep) \qquad (14A)$$

and the Wronskian expression

$$Ai\ (Ep)\ \frac{d}{dEp}\ Bi\ (Ep) - \frac{d}{dEp}\ Ai\ (Ep)\ Bi\ (Ep) = \frac{1}{\pi} \qquad (15A)$$

The transmission coefficient which is defined as

$$T = 1 - |C_1|^2 \tag{16A}$$

will be found via manipulation to be

$$T = \frac{4}{\pi^2} \frac{P_3}{P_4^2 + P_5^2} \tag{17A}$$

b) In order to derive T when Epl is approximate (linearized), it is more convenient to work with the field distribution function S_2.

Under these circumstances, two differential equations are produced.

$$\text{In the core } S_2'' + k_{mm}^2 S_2 = 0 \tag{18A}$$

$$\text{In the cladding } S_2'' + k_m^2 S_2 = 0 \tag{19A}$$

$$k_{mm} = k_0 [n_2^2 - \bar{\beta}^2 - \bar{l}^2 + (1 - r/a)(q\gamma^2 - 2\bar{l}^2)]^{\frac{1}{2}} \tag{20A}$$

18A reduces to the exact Airy equation, while 19A remains as before.

Thus on repeating the same procedure

$$T = \frac{4}{\pi^2} \frac{P_3}{P_4^2 + P_5^2} \tag{21A}$$

where P_3 and P_2 (present in P_4 and P_5, see Equation 1.28 in the main text) have the modified definitions

$$P_3 = \frac{P_1}{Ep2^{\frac{1}{2}}} \left(\frac{k_o\, a}{q\,\gamma^2 - 2\,\bar{1}^2}\right)^{1/3} \tag{22A}$$

$$P_2 = \left(\frac{\bar{1}^2}{2\,k_o\,a\,P_1^{\,2}} - \frac{P_1}{4\,Ep2^{3/2}}\right)\left(\frac{k_o\,a}{q\,\gamma^2 - 2\,\bar{1}^2}\right)^{1/3} \tag{23A}$$

c) Error Term:

Equation 11A may be rewritten without $(1/4\ k_m^{\,2})$

$$\frac{d^2\,S_3}{d\,Ep^2} + Ep\,S_3 = 0 \tag{24A}$$

or in terms of S_2

$$S_2'' + \left[k_m^{\,2} + \frac{5}{16}\,\frac{k_m^{\,2}}{Ep^3} - \frac{3}{4}\left(\frac{k_m'}{k_m}\right)^2 + \frac{1}{2}\left(\frac{k_m''}{k_m}\right)\right] S_2 = 0 \tag{25A}$$

Therefore, what lies to the right of $k_m^{\,2}$ in the parantheses is to be regarded as the error term.

This may be evaluated separately for the core and the cladding

$$ET\ (r \leq a) = \frac{5}{16}\ \frac{k_o^2\ P_1^2}{Ep1^3} - \frac{5}{16\ P_1^4}\ \left(\frac{q\ \gamma^2 - 2\ \bar{I}^2}{a}\right)^2$$

$$+ \frac{1}{4\ P_1^2}\ \left(\frac{q\ (q-1)\ \gamma^2 + 6\ \bar{I}^2}{a^2}\right) \qquad (26A)$$

$$ET\ (r \geq a) = \frac{5}{16}\ \frac{k_o\ P_1^2}{Ep2^3} - \frac{5}{4\ P_1^4}\ \left(\frac{\bar{I}^2}{a}\right)^2 + \frac{3\ \bar{I}^2}{2\ P_1^2\ a^2} \qquad (27A)$$

4) Filtering Equations:
Equation 1.48 may be split into

$$T = \exp\ \{-2\ [(\int_{r_{tp}}^{a} k_m\ dr) + (\int_{a}^{b} k_m\ dr) + (\int_{b}^{r_{tp}} k_m\ dr)]\}T_f \qquad (28A)$$

Such that the respective integrals denote the zone of evenescence in the core, cladding and the jacket. This is the most general situation. In the event of the radiation taking place before the jacket interface, the third integration vanishes and the upper limit of the second one has to be suitably adjusted.

It is possible to deduce analytic expressions for the last two integrals as demonstrated for Ep2

T_f is given by (3)

$$T_f = |4\ k_m\ (b-)\ k_m\ (b+)|/|[k_m\ (b-) + k_m\ (b+)]^2| \qquad (29A)$$

and it will hold reasonably well provided that the radiation point of the ray does not coincide with the outer boundary. -,+ indicate the two sides of the same interface.

The bound ray power without any filtering is

$$P_b = \left(\frac{1}{2+q}\right)^{\frac{2+q}{2q}} \frac{2^{\frac{2+5q}{2q}}}{2+3q} \tag{30A}$$

Upon the placement of the filtering material, it will be reduce to

$$P_{br} = \left(\frac{1}{2+q}\right)^{\frac{2+q}{2q}} \frac{2\left(2-\frac{2\gamma_1^2}{\gamma^2}\right)^{\frac{2+3q}{2q}}}{2+3q} \tag{31A}$$

For a graded jacket on the other hand

$$P_{br} = \left(\frac{1}{2+q}\right)^{\frac{2+q}{2q}} \frac{2^{\frac{2+5q}{2q}}}{2+3q} - \frac{4}{3q}\left(\frac{\gamma_1}{\gamma}\right)^2 \frac{2^{1/q}\, q^{\frac{1}{2}}}{(q+2)^{\frac{2+q}{2q}}} \tag{32A}$$

$$\gamma_1 = (n_3^2 - n_2^2)^{\frac{1}{2}}$$

In the latter case, the outside radius of the jacket may be determined from

$$c = \left(\frac{\gamma}{\gamma_1}\right) \frac{2^{1/q}\, q^{\frac{1}{2}}}{(q+2)^{\frac{q+2}{2q}}}\, a \tag{33A}$$

Chapter II

In the following lengthy derivations, the strict observance of the sign convention is essential. The reader is once again reminded that i = 1(2) is upper (lower) or correspondingly HE (EH) mode.

1) Field Expressions:

Maxwell's equations are

$$\nabla \times \vec{E} = -j\,\omega\,\mu_o\,\vec{H} \tag{34A}$$

$$\nabla \times \vec{H} = j\,\omega\,\varepsilon_o\,\varepsilon\,\vec{E} \tag{35A}$$

The curl operat or $\nabla\times$ in cylindrical coordinates

$$\nabla \times \vec{E} = \vec{r}\left(\frac{1}{r}\,\frac{\partial E_z}{\partial \phi} - \frac{\partial E_\phi}{\partial z}\right) + \vec{\phi}\left(\frac{\partial E_r}{\partial z} - \frac{\partial E_z}{\partial r}\right)$$

$$+ \vec{z}\left(\frac{1}{r}\,\frac{\partial (r\,E_\phi)}{\partial r} - \frac{1}{r}\,\frac{\partial E_r}{\partial \phi}\right) \tag{36A}$$

Thus with the dependence $e^{j(\omega t - m\phi - \beta z)}$ understood, the components of $\vec{E}$ and $\vec{H}$ may be derived

$$j\,\omega\,\varepsilon_o\,\varepsilon\,E_z = \frac{1}{r}\,\frac{\partial}{\partial r}\,(r\,H_\phi) + \frac{jm}{r}\,H_z \tag{37A}$$

$$j\,\omega\,\varepsilon_o\,\varepsilon\,E_\phi = -j\,\beta\,H_r - \frac{\partial}{\partial r}H_z \tag{38A}$$

$$j\,\omega\,\varepsilon_o\,\varepsilon\,E_r = j\,\beta\,H_\phi - \frac{jm}{r}H_z \tag{39A}$$

$$-j\,\omega\,\mu_o\,H_z = \frac{1}{r}\,\frac{\partial}{\partial r}(r\,E_\phi) + \frac{jm}{r}E_r \tag{40A}$$

$$-j\,\omega\,\mu_o\,H_\phi = -j\,\beta\,E_r - \frac{\partial}{\partial r}E_z \tag{41A}$$

$$-j\,\omega\,\mu_o\,H_r = j\,\beta\,E_\phi \qquad \frac{jm}{r}E_z \tag{42A}$$

From 39A, 41A, H_ϕ is found to be

$$H_\phi = \frac{k_o^2\,\varepsilon}{k_o^2\varepsilon - \beta^2}\left(-\frac{\beta m}{k_o^2\,\varepsilon r}H_z - \frac{j}{\omega\,\mu_o}E_z'\right) \tag{43A}$$

and its first derivative

$$H_\phi' = \frac{k_o^2\,\varepsilon'\,\beta^2}{(k_o^2\varepsilon - \beta^2)^2}\left(\frac{\beta m}{k_o^2\,\varepsilon r}H_z + \frac{j}{\omega\,\mu_o}E_z'\right) + \frac{k_o^2\,\varepsilon}{(k_o^2\varepsilon - \beta^2)}\cdot$$

$$\left[\frac{(\beta\,m\,\varepsilon' r + \beta\,m\,\varepsilon)}{k_o^2\,\varepsilon^2\,r^2}H_z - \frac{\beta m}{k_o^2\,\varepsilon r}H_z' - \frac{j}{\omega\,\mu_o}E_z''\right] \tag{44A}$$

while from 38A and 42A

$$H_r = \left(\frac{k_o^2 \varepsilon}{k_o^2 \varepsilon - \beta^2}\right)\left(\frac{m}{\omega \mu_o r} E_z - \frac{j\beta}{k_o^2 \varepsilon} H_z'\right) \tag{45A}$$

E_z may now be specified through the combined use of the last three equations since

$$E_z = -\frac{j}{r} H_\phi - j H_\phi' + \frac{m}{r} H_r \tag{46A}$$

Therefore, upon rearranging

$$E_z'' + \left[\frac{1}{r} - \frac{\varepsilon' \beta^2}{\varepsilon(k_o^2 \varepsilon - \beta^2)}\right] E_z' + \left(k_o^2 \varepsilon - \beta^2 - \frac{m^2}{r^2}\right) E_z$$

$$= -\frac{j \omega \mu_o \beta m \varepsilon'}{\varepsilon r (k_o^2 \varepsilon - \beta^2)} H_z \tag{47A}$$

It is important to note that the coupling between E_z and H_z is via the derivative of the gradient function.

A similar method to arrive at the differential equation for H_z reveals that

$$E_r = \left(\frac{k_o^2 \varepsilon}{k_o^2 \varepsilon \quad \beta^2}\right)\left(-\frac{m}{\omega \varepsilon_o \varepsilon r} H_z - \frac{j\beta}{k_o^2 \varepsilon} E_z'\right) \tag{48A}$$

$$E_\phi = \left(\frac{k_o^2 \varepsilon}{k_o^2 \varepsilon - \beta^2}\right)\left(-\frac{\beta m}{k_o^2 \varepsilon r} E_z + \frac{j}{\omega \varepsilon_o \varepsilon} H_z'\right) \tag{49A}$$

$$E_\phi' = \frac{k_o^2 \varepsilon' \beta^2}{(k_o^2 \varepsilon - \beta^2)^2}\left(\frac{\beta m}{k_o^2 \varepsilon r} E_z - \frac{j}{\omega \varepsilon_o \varepsilon} H_z'\right) + \frac{k_o^2 \varepsilon}{(k_o^2 \varepsilon - \beta^2)} \cdot$$

$$\left[\frac{(\beta m \varepsilon' r + \beta m \varepsilon)}{k_o^2 \varepsilon^2 r^2} E_z - \frac{\beta m}{k_o^2 \varepsilon r} E_z' - \frac{j \varepsilon'}{\omega \varepsilon_o \varepsilon^2} H_z' + \frac{j}{\omega \varepsilon_o \varepsilon} H_z''\right] \tag{50A}$$

and

$$H_z'' + \left[\frac{1}{r} - \frac{\varepsilon' k_o^2}{(k_o^2 \varepsilon - \beta^2)}\right] H_z' + \left(k_o^2 \varepsilon - \beta^2 - \frac{m^2}{r^2}\right) H_z$$

$$= \frac{j \omega \varepsilon_o \beta m \varepsilon'}{r(k_o^2 \varepsilon - \beta^2)} E_z \tag{51A}$$

A comparison of 47A and 51A will show that an equivalence can be achieved if the index variation is sufficiently smooth.

By defining the profile to be

$$\varepsilon(r) = \varepsilon_1(1 - h(r)) \tag{52A}$$

which obeys $h'/(1-h) \simeq 0$ and $1 - h \simeq 1$, then E_z and H_z will be related by the operator

$$D E_z = -j Z_o H_z \tag{53A}$$

$$D\ H_z = \frac{j\ \varepsilon_1^{\frac{1}{2}}}{Z_o}\ E_z \tag{54A}$$

where

$$D = \frac{r(k_o^2\varepsilon - \beta^2)}{k_o \beta\ m\ h'}\ \left[\frac{d^2}{dr^2} + \left(\frac{1}{r} - \frac{\varepsilon'\ k_o^2}{k_o^2\varepsilon - \beta^2}\right)\frac{d}{dr}\right.$$

$$\left. + (k_o^2\varepsilon - \beta^2 - \frac{m^2}{r^2})\right] \tag{55A}$$

In general a set consisting of four solutions are to emerge 53A and 54A. It is appropriate however, owing to the simplifications effected, to select only two of them which will be written as

$$E_z = C_1\ G_1 - C_2\ G_2 \tag{56A}$$

$$H_z = \frac{j\ \varepsilon_1^{\frac{1}{2}}}{Z_o}\ (C_1\ G_1 + C_2\ G_2) \tag{57A}$$

The transverse fields (radial component omitted) from 43A and 49A are

$$E_\phi = -\frac{1}{k_o^2\varepsilon - \beta^2}\ \left[\frac{\beta m}{r}\ (C_1\ G_1 - C_2\ G_2) + k_o \varepsilon_1^{\frac{1}{2}} (C_1\ G_1' + C_2\ G_2')\right]$$

(58A)

$$H_\phi = - \frac{j\,\varepsilon_1^{\frac{1}{2}}}{Z_o\,(k_o^2\varepsilon - \beta^2)} \left[\frac{\beta m}{r} (C_1\,G_1 + C_2\,G_2) + k_o\,\varepsilon_1^{\frac{1}{2}}\,(1-h)\cdot \right.$$

$$\left. (C_1\,G_1' - C_2\,G_2') \right] \qquad (59A)$$

Alternatively these may be expressed in terms of a new function, F_i $(i = \frac{1}{2})$

$$E_\phi = F_i \qquad (60A)$$

$$H_\phi = \mp \frac{j\,\varepsilon_1^{\frac{1}{2}}}{Z_o}\,F_i \qquad (61A)$$

The relationship between F_i and G_i will then be given by

$$F_i = \frac{1}{k_o\,\varepsilon_1^{\frac{1}{2}}\,(1 - h - \beta_1^2)} \left(\mp \beta_1 \frac{m}{r} G_i + G_i' \right) \qquad (62A)$$

Furthermore from 55A

$$G_i = - \frac{1}{k_o\,\varepsilon_1^{\frac{1}{2}}} \left(\frac{1 \mp \beta_1 m}{r}\,F_i + F_i' \right) \qquad (63A)$$

Thus by means of the last two formulae, the following differential equation is obtained

$$F_i'' + \frac{F_i'}{r} + \left[k_o^2\,\varepsilon_1\,(1 - h - \beta_1^2) - \frac{(\beta_1\,m \mp 1)^2}{r^2} \right] F_i = 0 \qquad (64A)$$

Assuming a homogeneous cladding, the fields will be described by

$$E_z = C_3 K_m (wr/a) \tag{65A}$$

$$H_z = \frac{j \varepsilon_2^{\frac{1}{2}}}{Z_o} C_4 K_m \tag{66A}$$

$$E_\phi = \frac{a^2}{w^2} \left(\frac{\beta m}{r} C_3 K_m + k_o \varepsilon_2^{\frac{1}{2}} C_4 K_m'\right) \tag{67A}$$

$$H_\phi = \frac{j a^2 \varepsilon_2^{\frac{1}{2}}}{Z_o w^2} \left(\frac{\beta m}{r} C_4 K_m + k_o \varepsilon_2^{\frac{1}{2}} C_3 K_m'\right) \tag{68A}$$

2) Characteristic Equation:

The conditions at the core-cladding boundary demand that all tangential components (i.e. E_z, H_z, E_ϕ, H_ϕ) be continuous.

Hence with the help of 56A, 57A, 58A, 59A, 65A, 66A, 67A, 68A this may be stated in the form of a 4x4 matrix (refer to next page).

For a nontrivial solution to exist, the determinant must vanish. On manipulation, this is seen to be

$$-K_m'^2 G_1 G_2 + K_m K_m' G_1 G_2' + K_m K_m' G_1' G_2 - K_m^2 G_1' G_2' = 0 \tag{70A}$$

$$\begin{bmatrix} G_1 & -G_2 & K_m & 0 \\ G_1 & G_2 & 0 & \delta K_m \\ \frac{\beta_1 m}{a} G_1 + G_1' & \frac{-\beta_1 m}{a} G_2 + G_2' & \frac{\beta_1 m}{a} K_m & \delta K_m' \\ \frac{\beta_1 m}{a} G_1 + \delta^2 G_1' & \frac{\beta_1 m}{a} G_2 - \delta^2 G_2' & \delta^2 K_m' & \frac{\delta \beta_1 m}{a} \end{bmatrix} \begin{bmatrix} C_1 \\ C_2 \\ C_3 \\ C_4 \end{bmatrix} = 0 \qquad (69A)$$

$$\delta = \varepsilon_2^{\frac{1}{2}} / \varepsilon_1^{\frac{1}{2}}$$

which will accept the following pairs of solutions

$$\frac{K_m'}{K_m} = \frac{G_1'}{G_1} \tag{71A}$$

$$\frac{K_m'}{K_m} = \frac{G_2'}{G_2} \tag{72A}$$

By the successive applications of 62A, 63A, the characteristic equation is converted into

$$\frac{K_m'}{K_m} = \mp \frac{\beta_1 \, m}{a} + \frac{F_i \, w^2/a^2}{F_i' + \frac{1 \mp \beta_1}{a} F_i} \tag{73A}$$

From the recurrence relationship of K_m

$$-\frac{K_m'}{K_m} \mp \frac{m}{a} = \frac{w}{a} \frac{K_{m\mp1}}{K_m} \tag{74A}$$

and using the differential properties of the function M that furnishes a solution to 64A in the case of a parabolic profile

$$\frac{\frac{d}{dx} M_i}{M_i} = \frac{A_i}{B_i} \frac{M_{i+1} (A_i+1, B_i+1, x)}{M_i (A_i, B_i, x)} \tag{75A}$$

the final form of the characteristic equation obtained is

$$- w \frac{K_m}{K_{m+1}} = V(2 \frac{A_i}{B_i} \frac{M_{i+1}}{M_i} - 1) + P_{ti} \qquad (76A)$$

Observe that after matching at the interface, x becomes equal to V (normalised frequency), hence a constant.

3) Solution of Characteristic Equation:

Let the characteristic equation be denoted by

$$X(u) = V(2 \frac{A_i}{B_i} \frac{M_{i+1}}{M_i} - 1) + P_{ti} + w \frac{K_m}{K_{m+1}} \equiv 0 \qquad (77A)$$

where the attenuation coefficient is to be evaluated from u which, with w, is related to the phase constant β in the manner

$$u = u_r + j\, u_m = a\, [n_1^2 k_o^2 - (\beta_r + j\, \beta_m)^2]^{\frac{1}{2}} \qquad (78A)$$

$$w = w_r + j\, w_m = a[(\beta_r + j\beta_m)^2 - n_2^2\, k_o^2]^{\frac{1}{2}} \qquad (79A)$$

For w

$$w_r = -a\, [P_1^2 - (P_1^4 + 4\, \beta_r^2\, \beta_m^2)^{\frac{1}{2}}]^{\frac{1}{2}}/2^{\frac{1}{2}} \qquad (80A)$$

$$w_m = a\, [P_1^2 + (P_1^4 + 4\, \beta_r^2\, \beta_m^2)^{\frac{1}{2}}]^{\frac{1}{2}}/2^{\frac{1}{2}} \qquad (81A)$$

$$P_1 = (n_1^2 k_o^2 + \beta_m^2 - \beta_r^2)^{\frac{1}{2}}$$

The parameter A_i that contains the β dependence in the confluent hypergeometric function will have

$$A_{ir} = \frac{B_i}{2} - \frac{a\,(k_o^2 n_1^2 - \beta_r^2 + \beta_m^2)}{4\,k_o\,\gamma} \tag{82A}$$

$$A_{im} = -\frac{2\,a\,\beta_r\,\beta_m}{4\,k_o\,\gamma} \tag{83A}$$

It aids the conceptual development of the solution to illustrate the respective components of w and A_i in the argand diagram (Figure 1A). Thus, as for β, A_i possesses a small imaginary part and a large real part whereas the reverse is true of w. A - $\pi/2$ rotation should therefore bring the latter into the first quadrant. Hankel function H^2 may then be employed:

$$\frac{K_m}{K_{m\mp1}} = \mp j\ \frac{H_m}{H_{m\mp1}} \tag{84A}$$

Using a two term Taylor series to expand equation 77A

$$X\,(u_r + j\,u_m) = X(u_r) + j\,u_m \frac{d}{d\,u_r} X(u_r) \equiv 0 \tag{85A}$$

imaginary part

$$X(u_r)_m + u_m \frac{d}{d\,u_r} X(u_r)_r = 0 \tag{86A}$$

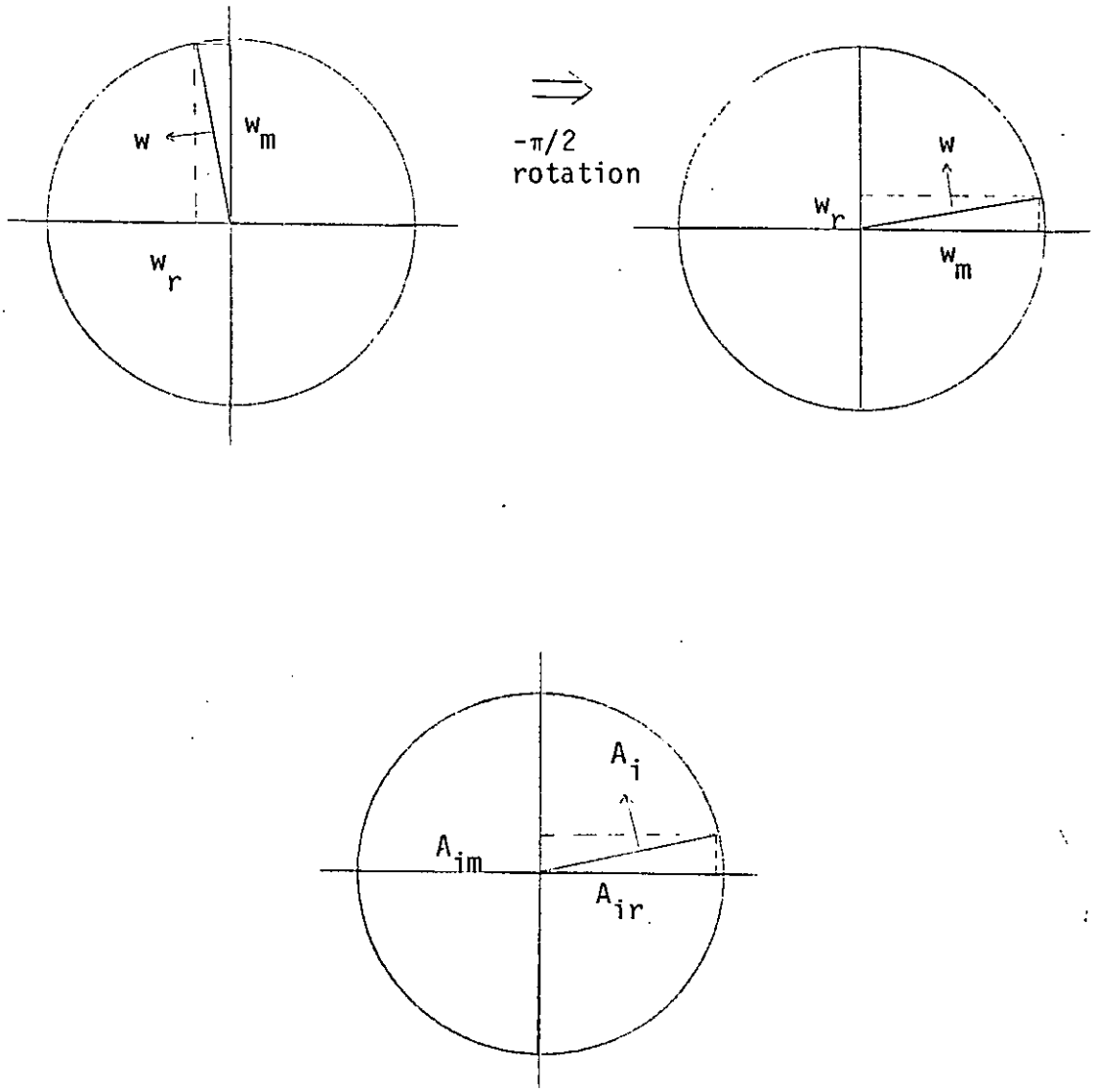

Fig. 1A Diagrams Showing the Respective Phases of w and A_i

or

$$u_m = - \frac{\dot{X}(u_r)_m}{\frac{d}{d u_r} X(u_r)_r} \tag{87A}$$

To find the relevant expression under the assumed conditions u_m and w_r are discarded completely.

By means of the wronskian

$$J_m Y_{\bar{m}+1} - J_{\bar{m}+1} Y_m = \pm \frac{2}{\pi w_m} \tag{88A}$$

$$X(u_r)_m = - \frac{2}{\pi} \frac{1}{|H_{\bar{m}+1}|^2} \tag{89A}$$

with A_i given as

$$A_i = \frac{B_i}{2} - \frac{u^2}{4V} \tag{90A}$$

$$\frac{\partial}{\partial u_r} = \frac{u_r}{2V} \left(- \frac{\partial}{\partial A_{ir}} + 2 \frac{\partial}{\partial B_i} \right) \tag{91A}$$

Additionally

$$u_r^2 - w_m^2 = V^2 \tag{92A}$$

$$\frac{d w_m}{d u_r} = \frac{u_r}{w_m} \tag{93A}$$

Hence

$$\frac{d}{d\,u_r} X(u_r)_r = \frac{u_r}{2V}\left(-\frac{\partial}{\partial A_{ir}} + 2\frac{\partial}{\partial B_i}\right)\left[V\left(2\frac{A_{ir}}{B_i}\frac{M_{i+1}}{M_i} - 1\right) + P_{ti}\right.$$

$$\left. + \frac{u_r}{w_m}\,\mathrm{Re}\,\frac{d}{d\,w_m}\left(\bar{+}\, w_m \frac{H_m}{H_{m+1}^{-}}\right)\right] \qquad (94A)$$

M has the representation

$$M(A,B,x) = \sum_{k=0}^{\infty} \frac{\Gamma(A+k)}{\Gamma(B+k)}\frac{\Gamma(B)}{\Gamma(A)}\frac{x^k}{k!} \qquad (95A)$$

Therefore, the derivation with respect to 91A will be

$$U(A_i,B_i,x) = \left(-\frac{\partial}{\partial A_{ir}} + 2\frac{\partial}{\partial B_i}\right) M_i = \sum_{k=0}^{\infty} \frac{\Gamma(A_i+k)}{\Gamma(B_i+k)}\frac{\Gamma(B_i)}{\Gamma(A_i)}\cdot$$

$$\left[\psi(A_i+k) + \psi(A_i) - 2\psi(B_i+k) + 2\psi(B_i)\right]\frac{x^k}{k!} \qquad (96A)$$

Furthermore, via the recurrence formula

$$\frac{1}{w_m}\,\mathrm{Re}\,\frac{d}{d\,w_m}\left(\bar{+}\, w_m \frac{H_m}{H_{m+1}^{-}}\right) = 1 - \frac{|H_{m+2}^{-}\, H_m|}{|H_{m+1}^{-}|^2} \qquad (97A)$$

Finally using (from 78A)

$$\beta_m = \frac{u_m u_r}{\beta_r a^2} \tag{98A}$$

will lead to the equation stated in the main text.

4) Derivation of Transverse Field Function

Admittedly, a concise relationship between E_ϕ and H_r (or H_ϕ, E_r) does not follow directly from Maxwell's equations. Therefore, the option would be to couple E_ϕ and E_r (or H_ϕ, H_r).

By sequential use of 37A, 41A, 39A, 40A, 42A, the differential equation for E_ϕ and E_r is attained

$$E_\phi'' + \frac{E_\phi'}{r} + (k_0^2 \varepsilon - \beta^2 - \frac{m^2+1}{r^2})E_\phi = (\frac{2m}{r^2} + \frac{m\varepsilon'}{\varepsilon r})E_r \tag{99A}$$

A similar procedure for H_ϕ and H_r will give

$$H_\phi'' + (\frac{1}{r} - \frac{\varepsilon'}{\varepsilon}) H_\phi' + (k_0^2\varepsilon - \beta^2 - \frac{m^2+1}{r^2} - \frac{\varepsilon'}{\varepsilon r})H_\phi$$

$$= (\frac{2m}{r^2} + \frac{m\varepsilon'}{\varepsilon r})H_r \tag{100A}$$

Upon setting the respective components as

$$E_\phi = F_i \quad , \quad E_r = \mp j F_i$$
$$H_\phi = \mp j F_i \quad , \quad H_r = F_i \tag{101A}$$

for the electric field

$$F_i'' + \frac{F_i'}{r} + [k_o^2\varepsilon - \beta^2 - \frac{(m\mp 1)^2}{r^2} \pm \frac{m\varepsilon'}{\varepsilon r}] F_i = 0 \tag{102A}$$

and for the magnetic field

$$F_i'' + \frac{F_i'}{r} + [k_o^2\varepsilon - \beta^2 - \frac{(m\mp 1)^2}{r^2}]F_i - \frac{\varepsilon'}{\varepsilon}(F_i' + \frac{1\mp m}{r} F_i) = 0 \tag{103A}$$

5) Derivation of Characteristic Equation with Jacket:

With the boundary conditions of r = a and r = b the equations 2.57 to 2.68 may be rearranged into an 8 x 8 matrix (refer to next page).

Utmost caution must be exercised when working out the matrix in question as it produces, prior to cancellations, 584 terms.

One method that is particularly useful in this instance is the Laplace expansion. To give brief accounts, if a line is drawn down the middle leaving four columns on each side, then selecting all possible combinations of 4 x 4 matrices belonging to L.H.S. and multiplying them with the corresponding cofactors of the R.H.S. will deliver the required result.

$$
\begin{bmatrix}
G_1 & -G_2 & 0 & 0 & K_m & I_m & 0 & 0 \\
G_1 & G_2 & 0 & 0 & 0 & 0 & \delta K_m & \delta I_m \\
\frac{\beta_1 m}{a} G_1 + G_1' & -\frac{\beta_1 m}{a} G_2 + G_2' & 0 & 0 & \frac{\beta_1 m}{a} K_m & \frac{\beta_1 m}{a} I_m & \delta K_m' & \delta I_m' \\
\frac{\beta_1 m}{a} G_1 + \delta^2 G_1' & \frac{\beta_1 m}{a} G_2 - \delta^2 G_1' & 0 & 0 & \delta^2 K_m' & \delta^2 I_m' & \delta \frac{\beta_1 m}{a} K_m & \delta \frac{\beta_1 m}{a} I_m \\
0 & 0 & K_{m2} & 0 & K_{m1} & I_{m1} & 0 & 0 \\
0 & 0 & 0 & \delta_1 K_{m2} & 0 & 0 & K_{m1} & I_{m1} \\
0 & 0 & \frac{\beta_2 m}{a} K_{m2} & \delta_1 K_{m2}' & \frac{\beta_2 m}{a} K_{m1} & \frac{\beta_2 m}{a} I_{m1} & K_{m1}' & I_{m1}' \\
0 & 0 & \delta_1^2 K_{m2}' & \delta_1 \frac{\beta_2 m}{a} K_{m2} & K_{m1}' & I_{m1}' & \frac{\beta_2 m}{a} K_{m1} & \frac{\beta_2 m}{a} I_{m1}
\end{bmatrix}
\begin{bmatrix} C_1 \\ C_2 \\ C_3 \\ C_4 \\ C_5 \\ C_6 \\ C_7 \\ C_8 \end{bmatrix}
= 0 \qquad (104A)
$$

$\beta_2 = \beta/(k_0 \varepsilon_2^{\frac{1}{2}})$ $\quad \delta_1 = \varepsilon_2^{\frac{1}{2}}/\varepsilon_3^{\frac{1}{2}}$

Further simplication is to be gained by transferring the last two columns in the place of the third and fourth. In this way thirty six pairs of 4 x 4 determinants are evaluated.

When the cross-cancellations have been implemented, the remaining terms are:

$$K_m'^2 \left[-I_{m1}'^2 + I_{m1} I_{m1}' \frac{K_{m2}'}{K_{m2}} (1 + \delta_1^2) - \delta_1^2 I_{m1}^2 \frac{K_{m2}'^2}{K_{m2}^2}\right]$$

$$+ I_m' K_m' \left[2 I_{m1}' K_{m1}' - (I_{m1}' K_{m1} + I_{m1} K_{m1}') \frac{K_{m2}'}{K_{m2}} (1 + \delta_1^2) + 2\delta_1^2 I_{m1} K_{m1} \frac{K_{m2}'^2}{K_{m2}^2}\right]$$

$$+ I_m'^2 \left[- K_{m1}'^2 + K_{m1} K_{m1}' \frac{K_{m2}'}{K_{m2}} (1 + \delta_1^2) - \delta_1^2 K_{m1}^2 \frac{K_{m2}'^2}{K_{m2}^2}\right]$$

$$+ K_m' K_m \left(\frac{G_1'}{G_1} + \frac{G_2'}{G_2}\right) \left[I_{m1}'^2 - I_{m1} I_{m1}' \frac{K_{m2}'}{K_{m2}} (1 + \delta_1^2) + \delta_1^2 I_{m1}^2 \frac{K_{m2}'^2}{K_{m2}^2}\right]$$

$$+ (I_m K_m' + I_m' K_m)\left(\frac{G_1'}{G_1} + \frac{G_2'}{G_2}\right) \left[-I_{m1}' K_{m1}' + (I_{m1}' K_{m1} + \delta_1^2 I_{m1} K_{m1}') \frac{K_{m2}'}{K_{m2}}\right.$$

$$\left. - \delta_1^2 I_{m1} K_{m1} \frac{K_{m2}'^2}{K_{m2}^2}\right]$$

$$+ I_m I_m' \left(\frac{G_1'}{G_1} + \frac{G_2'}{G_2}\right) \left[K_{m1}'^2 - K_{m1} K_{m1}' \frac{K_{m2}'}{K_{m2}} (1 + \delta_1^2) + \delta_1^2 K_{m1}^2 \frac{K_{m2}'^2}{K_{m2}^2}\right]$$

$$+ K_m^2 \frac{G_1' G_2'}{G_1 G_2} \left[- I_{m1}'^2 + I_{m1} I_{m1}' \frac{K_{m2}'}{K_{m2}} (1 + \delta_1^2) - \delta_1^2 I_{m1}^2 \frac{K_{m2}'^2}{K_{m2}^2} \right]$$

$$+ I_m K_m \frac{G_1' G_2'}{G_1 G_2} \left[2 I_{m1}' K_{m1}' - (I_{m1}' K_{m1} + I_{m1} K_{m1}') \frac{K_{m2}'}{K_{m2}} (1 + \delta_1^2) \right.$$

$$\left. + 2 I_{m1} K_{m1} \frac{K_{m2}'^2}{K_{m2}^2} \right]$$

$$+ I_m^2 \frac{G_1' G_2'}{G_1 G_2} \left[- K_{m1}'^2 + K_{m1} K_{m1}' \frac{K_{m2}'}{K_{m2}} (1 + \delta_1^2) - \delta_1^2 K_{m1}^2 \frac{K_{m2}'^2}{K_{m2}^2} \right] = 0$$

(106A)

On examining equation 106A closer, it may be detected that if the refractive index difference between the cladding and the jacket is ignored, the various terms will complete to perfect squares leading to*

$$\left\{ \left[K_m' \left(I_{m1}' - I_{m1} \frac{K_{m2}'}{K_{m2}} \right) - I_m' \left(K_{m1}' - K_{m1} \frac{K_{m2}'}{K_{m2}} \right) \right] \right.$$

$$\left. - \left[K_m \left(I_{m1}' - I_{m1} \frac{K_{m2}'}{K_{m2}} \right) - I_m \left(K_{m1}' - K_{m1} \frac{K_{m2}'}{K_{m2}} \right) \right] \frac{G_i'}{G_i} \right\} = 0 \qquad (107A)$$

---

* Actually it is equally permissible to achieve factorization without omitting δ_1. Under these circumstances, the characteristic equation (i.e. 107A) will have another bracket of the same terms (remember that 107A is a square) including δ_1 in front of each K_{m1} and I_{m1} so that one of G_i'/G_i will exhibit explicitly the refractive index ratio. However to conform to the single boundary situation, this is discarded.

Hence, the solution is

$$\frac{G_i'}{G_i} = \frac{K_m' \ (I_{m_1}' \ K_{m_2} - I_{m_1} K_{m_2}' \ ) - I_m' \ (K_{m_1}' \ K_{m_2} - K_{m_1} K_{m_2}' \ )}{K_m \ (I_{m_1}' \ K_{m_2} - I_{m_1} K_{m_2}' \ ) - I_m \ (K_{m_1}' \ K_{m_2} - K_{m_1} K_{m_2}' \ )} \qquad (108A)$$

6) Solution of Characteristic Equation:

By using the differential properties of I_m, K_m and replacing G_i by F_i, the characteristic equation may be represented as:

$$V \ (2 \frac{A_i}{B_i} \ \frac{M_{i+1}}{M_i} - 1) + P_{ti} =$$

$$-w \ \frac{K_m \ (w \ I_{m_1 \bar{+} 1} \ K_{m_2} + v \ I_{m_1} K_{m_2 \bar{+} 1}) - I_m (-w \ K_{m_1 \bar{+} 1} K_{m_2} + v \ K_{m_1} K_{m_2 \bar{+} 1})}{K_{m \bar{+} 1} (w \ I_{m_1 \bar{+} 1} K_{m_2} + v \ I_{m_1} K_{m_2 \bar{+} 1}) + I_{m \bar{+} 1} (- w \ K_{m_1 \bar{+} 1} K_{m_2} + v \ K_{m_1} K_{m_2 \bar{+} 1})} \qquad (109A)$$

Therefore by collecting everything on one side

$$X(u) = 0 \qquad (110A)$$

and the solution sought is

$$u_m = - \frac{X \ (u_r)_m}{\left[\frac{X \ (u_r)}{d \ u_r}\right]_r} \qquad (111A)$$

To convert from I and K into J and H

$$K_m(w) = -\frac{\pi}{2}(-j)^{m+1} H_m(-jw) \tag{112A}$$

$$I_m(w) = j^m J_m(-jw) \tag{113A}$$

such that the L.H.S. of 109A is transformed into

$$\mp j w \frac{H_m H_5 + J_m H_6}{H_{m\mp1} H_5 - J_{m\mp1} H_6} \tag{114A}$$

The real and imaginary parts of the above (excluding j w)

$$\text{Numerator} = Y_{m2\mp1} H_3 - s Y_{m2} H_4 + j(J_{m2\mp1} H_3 - s J_{m2} H_4) \tag{115A}$$

$$\text{Denominator} = Y_{m2\mp1} H_1 - s Y_{m2} H_2 + j(J_{m2\mp1} H_1 - s J_{m2} H_2) \tag{116A}$$

$$H_1 = Y_{m\mp1} J_{m1} - J_{m\mp1} Y_{m1}, \quad H_2 = Y_{m\mp1} J_{m1\mp1} - J_{m\mp1} Y_{m1\mp1} \tag{117A}$$

$$H_3 = Y_m J_{m1} + J_m Y_{m1}, \quad H_4 = Y_m J_{m1\mp1} + J_m Y_{m1\mp1} \tag{118A}$$

The imaginary component in the numerator when multiplied by the complex conjugate of the denominator and via the repeated applications of the recurrence relationship

$$J_{m\mp1}\, Y_m - J_m\, Y_{m\mp1} = \mp\, \frac{2}{\pi\, w_m} \tag{119A}$$

will be obtained in the form

$$\text{Im (Numerator)} = \pm\, \frac{8\, a^2}{\pi^3 v_m^{\,2}\, b^2} \tag{120A}$$

In order to determine the derivative of $X(u_r)$, similar to w, v will have

$$v^2 + u^2 = \text{constant} \tag{121A}$$

Hence*

$$\frac{d}{d\, u_r}\left(\frac{H_m\, H_5 + J_m\, H_6}{H_{m\mp1}\, H_5 - J_{m\mp1}\, H_6}\right) = \pm\, \frac{u_r}{w_m}\left\{\frac{H_{m\mp1}\, H_5 + J_{m\mp1}\, H_6}{H_{m\mp1}\, H_5 - J_{m\mp1}\, H_6}\right.$$

$$\left. - \frac{(H_{m\mp2}\, H_5 - J_{m\mp2}\, H_6)(H_m\, H_5 + J_m\, H_6)}{(H_{m\mp1}\, H_5 - J_{m\mp1}\, H_6)^2}\right\} - \frac{1}{w_m}\, \frac{H_m\, H_5 + J_m\, H_6}{(H_{m\mp1}\, H_5 - J_{m\mp1}\, H_6)}$$

---

* Note that for the term beginning with b/a it was assumed that $v_m \simeq w_m$. This is immaterial for the final result since the term concerned is eventually dropped.

$$- \frac{b}{a} \frac{H_{m2}(H_m J_{m+1}^{-} + J_m H_{m+1}^{-})[(H_{m1+1}^{-} H_5 - J_{m1+1}^{-} H_6) + H_{m2+1}(J_{m1} H_{m1+1}^{-} - H_{m1} J_{m1+1}^{-})]}{(H_{m+1}^{-} H_5 - J_{m+1}^{-} H_6)^2} \} \quad (122A)$$

Now under the assumed conditions, all the terms except extreme right hand one possess small phase angles and will therefore approximate to real quantities by themselves. The end term however is almost 90^{o} out of phase with the denominator and may thus be eliminated.

Upon replacement into

$$\beta_m = \frac{u_r u_m}{\beta_r a^2} \quad (123A)$$

β_m may be shown to have the form given in the main text.

CHAPTER III

1) Definition of Integrals contained in 3.2:

a) $$D_q(C_1) = \int_0^1 e^{-C_1 t^2} t^q dt \quad (124A)$$

or

$$D_q(C_1) = \frac{1}{2 C_1^{(q+1)/2}} \Gamma_1\left((q+1)/2, C_1^{\frac{1}{2}}\right) \quad (125A)$$

Γ_1 = Incomplete Gamma function

b) $$Da\ (C_1^{\frac{1}{2}}) = e^{-C_1} \int_0^{C_1^{\frac{1}{2}}} e^{t^2}\ dt \qquad (126A)$$

c) $$Db\ (q) = e^{-C_1} \int_0^1 (1 - t^2)^q\ e^{C_1 t^2}\ dt \qquad (127A)$$

d) $$Be\ (x,y) = \int_0^1 t^{x-1}\ (1-t)^{y-1}\ dt \qquad (128A)$$

or

$$Be\ (x,y) = \frac{\Gamma(x)\ \Gamma(y)}{\Gamma(x+y)} \qquad (129A)$$

2) Evaluation of Integral type:

$$I_{np} = \int L_p(t)\ e^{-C_1 t}\ dt \qquad (130A)$$

Continuous operation of integration by parts and employing the relationships

$$\frac{d^n}{dt^n}\ L_{p+n} = (-1)^n\ L_p^n, \quad L_o^n\ (t) = 1 \qquad (131A)$$

will yield

$$I_{np} = -\frac{e^{-C_1 t}}{C_1} \sum_{k=0}^{p} \frac{(-1)^k}{(C_1)^k}\ L_{p-k}^k\ (t) \qquad (132A)$$

3) Evaluation of Integral type:

$$I_{np1} = \int (1-t)\, L_p(t)\, e^{-C_1 t}\, dt \qquad (133A)$$

By writing

$$t\, L_p = (p+1)\,(L_p - L_{p+1}) - p(L_{p-1} - L_p) \qquad (134A)$$

The integral may be converted into a form similar to the above. The result is

$$I_{np1} = I_{np} - (p+1)(I_{np} - I_{np+1}) + p(I_{np-1} - I_{np}) \qquad (135A)$$

4) Derivation of Electric Field Component in Transformed Coordinates:

Consider the two successive rotations of the cordinate system (Figure 3.7), the first one about the x axis, the second about the y axis. Then by using the transformation matrix (for the former case for instance)

$$\begin{bmatrix} y_i \\ z_i \end{bmatrix} = \begin{bmatrix} \text{Cos } \alpha_a & \text{Sin } \alpha_a \\ -\text{Sin } \alpha_a & \text{Cos } \alpha_a \end{bmatrix} \begin{bmatrix} y \\ z \end{bmatrix} \qquad (136A)$$

all the coordinates may be determined w.r.t. the original ones. Lengthy expressions are to emerge of course, unless constraints are imposed on the relative magnitudes of α_a, β_a. Simplified forms

are attained, when they are both assumed to be small.

Hence, after carrying out the required conversion into cylindrical coordinates (subscript 2 indicates the two rotations applied)

$$r_2 = r - z\,(\beta_a \cos\phi - \alpha_a \sin\phi) \tag{137A}$$

$$\phi_2 = \phi - z\,(\beta_a \sin\phi - \alpha_a \cos\phi)/r \tag{138A}$$

$$z_2 = z - r\,(\beta_a \cos\phi + \alpha_a \sin\phi) \tag{139A}$$

The electric field (of the laser output) at an arbitrary point z, prior to any shifts in the coordinates with all the phase terms included (4)

$$E_{xn} = \left(\frac{2}{\pi}\right)^{\frac{1}{2}} \frac{1}{s} L_n\,(2\,r^2/s^2) e^{-r^2\left(\frac{1}{s^2} + \frac{jk_o}{2R}\right) - jk_o z}$$

$$+ j\,(2n+1)\tan^{-1}\left(\frac{2z}{k_o s^2}\right) \tag{140A}$$

Furthermore by moving the beam centre along the x axis to a position r_o, the r coordinate will become (see Figure 3.7)

$$r_3^2 = r_2^2 + r_o^2 - 2r_2 r_o \cos\phi \tag{141A}$$

A first order expansion* of the above will give

$$r_3 = r_2 - r_o \cos\phi \qquad (142A)$$

It is now feasible to rewrite the electric field subject to the new coordinates. For algebraic consistency however the signs in front of the paranthesis in equations 137A - 139A are to be inverted**. Also, since the coordinates still coincide with the core centre on the fibre end face, z may be equated to zero. To specify the distance of beam waist from the natural origin, it is convenient to insert the parameter d.

---

* An expansion containing the second order terms would reveal a singularity at $r_2 = 0$, i.e.

$$r_3 = r_2 + \frac{r_o^2 \sin^2\phi - 2 r_2 r_o \cos\phi}{2 r_2}$$

This is not surprising as the validity of the binomial series is based on $r_o < r_2$. Such occurrences are known as non-uniformity valid expansions (5). Despite the counter claim, the same degree of approximation was also employed in Ref (6).

** Another way of interpreting this is to consider the phase terms in equation 140A. When propagation is in the positive z diretion. one expresses it as

$$e^{-j k_o z}$$

The extra phase shift contributed from 137A would then reduce the total phase mismatch instead of reinforcing it if the minus sign were to be retained. In any case, the incident beam lies in the left hand plane of the coordinate system (i.e. where z is negative).

E_{xn} may eventually be shown to have the following form:

$$E_{xn} = \left(\frac{2}{\pi}\right)^{\frac{1}{2}} \frac{1}{s_1} L_n\ (2r^2/s_1^2) e^{-r_3^2 \left(\frac{1}{s_1^2} + \frac{jk_o}{2R_1}\right)}$$

$$- j\ k_o (r - r_o\ \mathrm{Cos}\phi)(\beta_a\ \mathrm{Cos}\phi + \alpha_a\ \mathrm{Sin}\phi) \qquad (143A)$$

where r_3^2 due to the aforementioned adjustments is now given by

$$r_3^2 = r^2 + r_o^2 - 2r\ r_o\ \mathrm{Cos}\phi \qquad (144A)$$

5) Coupling Efficiency Integrals:

The integral over the transverse field function in equation 3.46 by a change of variable from r to x may be rearranged into

$$\int_0^a F_i^2\ r\ dr = \frac{1}{2} \int_0^V e^{-x}\ x^{B_i - 1}\ [M(A_i, B_i, x)]^2\ dx \qquad (145A)$$

At this stage it is useful to introduce (7)

$$M(A_1, B, x)\ M(A, B, x)$$

$$= \sum_{k=0}^{\infty} \frac{(A)_k\ (A_1)_k}{(B)_k^2\ k!} M(A + A_1 - B, B + 2k, x)\ x^{2k} \qquad (146A)$$

and the Kummer's transformation

$$M(A, B, x) = e^{x} M(B-A, A, -x) \qquad (147A)$$

Thus with the help of 146A and 147A, the integral now reads

$$\int_0^a F_i^2 \, r \, dr = \frac{1}{2} \int_0^V \sum_{k=0}^{\infty} \left[\frac{(A_i)_k}{(B_i)_k} \right]^2 \frac{1}{k!} x^{B_i - 1 + 2k} \cdot$$

$$M_i \left(2(B_i + k - A_i), B_i + 2k, -x\right) dx \qquad (148A)$$

As an indefinite integral confluent hypergeometric function will satisfy

$$\int x^{B-1} M(A, B, -x) \, dx = \frac{x^B}{B} M(A, B+1, -x) \qquad (149A)$$

Therefore by using 149A and reverting to the case of positive argument

$$\int_0^a F_i^2 \, r \, dr = \frac{1}{2} \sum_{k=0}^{\infty} \left[\frac{(A_i)_k}{(B_i)_k} \right]^2 \frac{1}{k!} \frac{e^{-V} B^{B_i + 2k}}{B_i + 2k} \cdot$$

$$M_i \left(2A_i - B_i + 1, B_i + 2k + 1, V\right) \qquad (150A)$$

Further simplifications are hindered by the presence of $(B_i + 2k)$ in the denominator. One possible rearrangement would be

$$\int_0^a F_i^2 r\, dr = \frac{1}{2} e^{-V} V^{B_i-1} \{ \sum_{k=0}^{\infty} [\frac{(A_i)_k}{(B_i)_k}]^2 \frac{V^{2k}}{k!} \cdot$$

$$M_i (2A_i - B_i+1, B_i +2k, V) - [M_i(A_i, B_i, V)]^2\} \quad (151A)$$

The conventional technique adopted for the integrals of the latter type (i.e. α_{mp}^{e} , α_{mp}^{h}) is the use of Bessel generating functions, viz

$$e^{jz \, Sin\phi} = J_0(z) + 2 \sum_{k=1}^{\infty} J_{2k}(z) \, Cos \, (2k\phi)$$

$$+ 2j \sum_{k=1}^{\infty} J_{2k-1}(z) \, Sin \, (2k-1)\phi \quad (152A)$$

$$e^{jz \, Cos\phi} = J_0(z) + 2 \sum_{k=1}^{\infty} j^k J_k(z) \, Cos \, (k\phi) \quad (153A)$$

$$e^{z \, Cos\phi} = I_0 \, (z) + \sum_{k=1}^{\infty} I_k(z) \, Cosk\phi \quad (154A)$$

Upon replacement in 3.48, 3.49 the ϕ terms may be regrouped so as to enable the utilization of the orthogonal properties of the integration. Many terms however would be created in this way. Therefore here too, a numerical procedure was favoured.

APPENDIX B

This appendix describes the various mathematical functions used in the thesis and their simulation on the prime computer.

Fundamentally calculations of such functions is to be regarded as a specialized branch of numerical analysis. Selective methods have been devised, the most notable and also the oldest is the expansion in terms of Chebyshev polynomials (1). In fact the NAG Library subroutines which are in world wide usage employ this very technique exclusively.

It was thought however that a straightforward approach given in the text books would avoid the necessity of adopting a new representation, each time the range of the argument changed. This, unfortunately, is one of the complications inherent in Chebyshev polynomials.

A convergent series, for computational work merely requires a sufficient number of terms to be summed. One serious difficulty that might arise would be the instability, if the series was of oscillatory nature. In this instance, an integration formula which extracts the decaying part as an exponential or some other suitable function will probably recover the correct result. Therefore, depending on the capability, one of the two schemes was opted for.

Since the work on the thesis heavily relied on the evaluation of functions, the aim was to seek an accuracy to eight decimal places and this was often yielded.

Common to all series was the procedure that the largest term would first be located while adding up to that term, this would then be multiplied by 10^{-14} to obtain a lower bound, finally the computation would be terminated upon reaching this lower limit.

Simulation of integrals were carried out with less difficulty mainly thanks to a special subroutine kindly loaned by Dr G Evans

(Department of Mathematics, Loughborough University). Brief details of this routine may be found at the end of the appendix.

Double precision was used throughout, thus taking into account fourteen significant digits. However even with this declaration, it was found that surprisingly inaccurate results were returned for elementary functions, when compared to those of advanced pocket calculators (such as Texas TI58 owned by the author). This was especially true of sines and cosines whose arguments exceeded 2π. Therefore, these were either replaced by alternative definitions or the arguments were confined to lie in the range $\pi/2$ to $-\pi/2$ where some improvement was acquired.

All complex computations were undertaken as real in two parts, one reason being double precision complex declaration is not allowed. But secondly and more importantly, distinct analytic expressions enabled an easier process of inspection.

Along with the mathematical properties of functions, the performance of the associated computations are given below. Also contained towards the end are the notes on the general aspects of programmes.

1. AIRY FUNCTIONS

Definition: The solution of the differential equation

$$\frac{d^2W}{dz^2} + zW = 0 \qquad (1B)$$

are Ai(z) and Bi(z) known as Airy functions of the first and second kind respectively. In general z is complex. Because their use was restricted to ray analysis, only real values of the argument are considered.

Behaviour: The eight types namely Ai(z), Bi(z), Ai(-z), Bi(-z), Ai'(z), Bi'(z), Ai'(-z) and Bi'(-z) are shown in Figures 1B & 2B. Ai(z) and Ai'(z) decrease as the argument increases whereas Bi(z), Bi'(z) grow with increasing argument. The remainder are oscillatory.

Series Representation: (z arbitary)

$$Ai(z) = C_1 f_1(z) - C_2 f_2(z) \tag{2B}$$

$$Bi(z) = \sqrt{3}\ [C_1 f_1(z) + C_2 f_2(z)] \tag{3B}$$

$f_1(z)$ and $f_2(z)$ are

$$f_1(z) = \sum_{k=0}^{\infty} 3^k (C_3 + 1/3)_k \frac{z^{3k}}{(3k)!} \tag{4B}$$

$$f_2(z) = \sum_{k=0}^{\infty} 3^k (C_4 + 1/3)_k \frac{z^{3k+1}}{(3k+1)!} \tag{5B}$$

so that for the derivatives

$$f_1'(z) = \sum_{k=0}^{\infty} 3^k (C_3 + 1/3)_k \frac{z^{3k-1}}{(3k-1)!} \tag{6B}$$

$$f_2'(z) = \sum_{k=0}^{\infty} 3^k (C_4 + 1/3)_k \frac{z^{3k}}{(3k)!} \tag{7B}$$

The generalized coefficient has the definition

$$3^k (C + 1/3)_k = (3C + 1)(3C + 4) \ldots (3C + 3k - 2) \tag{8B}$$

C_3 and C_4 in the above are to be set to 0 and 1/3 respectively. C_1, C_2 are constants related to Gamma function (Γ) of

$$C_1 = 3^{-2/3}/\Gamma(2/3) \tag{9B}$$

$$C_2 = 3^{-1/3}/\Gamma(1/3) \tag{10B}$$

In a broader sense, Airy functions are classified as Bessel function of fractional order.

Hence, the following relations are available (2)

$$y = \frac{2}{3} z^{3/2}$$

$$Ai(z) = \pi^{-1} \sqrt{z/3}\ K_{1/3}(y) \tag{11B}$$

$$Ai'(z) = -\pi^{-1} (z/\sqrt{3})\ K_{2/3}(y) \tag{12B}$$

$$Bi(z) = \sqrt{z/3}\ [I_{-1/3}(y) + I_{1/3}(y)] \tag{13B}$$

$$Bi'(z) = (z/\sqrt{3})\ [I_{-2/3}(y) + I_{2/3}(y)] \tag{14B}$$

$$Ai(-z) = (\sqrt{z}/3)\ [J_{1/3}(y) + J_{-1/3}(y)] \tag{15B}$$

$$Ai'(-z) = -(z/3)\ [J_{-2/3}(y) - J_{2/3}(y)] \tag{16B}$$

$$Bi(-z) = \sqrt{z/3}\ [J_{-1/3}(y) - J_{1/3}(y)] \tag{17B}$$

$$B'(-z) = (z/\sqrt{3})\ [J_{-2/3}(y) + J_{2/3}(y)] \qquad (18B)$$

where K, I, J denote the Bessel functions which are dealt with in the next section.

A close study of equations from 2B to 8B will reveal that all except Bi(z) and Bi'(z) lead to infinitely oscillating series*. Thus, the series representation was solely reserved for Bi(z) and Bi'(z), while the rest were to be handled by Bessel functions.

The suitable integral form of modified Hankel function K is

$$K_\nu(y) = \frac{\pi^{\frac{1}{2}}\ (y/2)^\nu}{\Gamma(\nu + 1/2)} \int_1^\infty e^{-yt}\ (t^2 - 1)^{\nu-\frac{1}{2}}\ dt \qquad (19B)$$

The version used in simulation via $x = 1/t$

$$K_\nu(y) = \frac{\pi^{\frac{1}{2}}\ (y/2)^\nu}{\Gamma(\nu + 1/2)} \int_0^1 \frac{e^{-y/x}\ (1 - x^2)^{\nu-\frac{1}{2}}}{x^{2\nu+1}}\ dx \qquad (20B)$$

For J, the following representation was chosen

$$J_\nu(y) = \frac{1}{\pi} \int_0^T \text{Sin}\ (y\ \text{Sint} - \nu t)dt - \frac{\text{Sin}(\nu\pi)}{\pi} \int_0^\infty e^{-y\text{Sinh}t - \nu t}\ dt \qquad (21B)$$

Again by a similar transformation, $x = e^{-t}$ (for the second integral only)

$$J_\nu(y) = \frac{1}{\pi} \int \text{Sin}\ (y\ \text{Sint} - \nu t)dt - \frac{\text{Sin}\ (\nu\pi)}{\pi} \int_0^1 e^{-y(1/x - x)/2}\ x^{\nu-1}dx \qquad (22B)$$

---

* Actually the group series mentioned will evaluate Airy functions of all types satisfactorily (correct up to 5 digits at the worst) so long as mod z < 1.0.

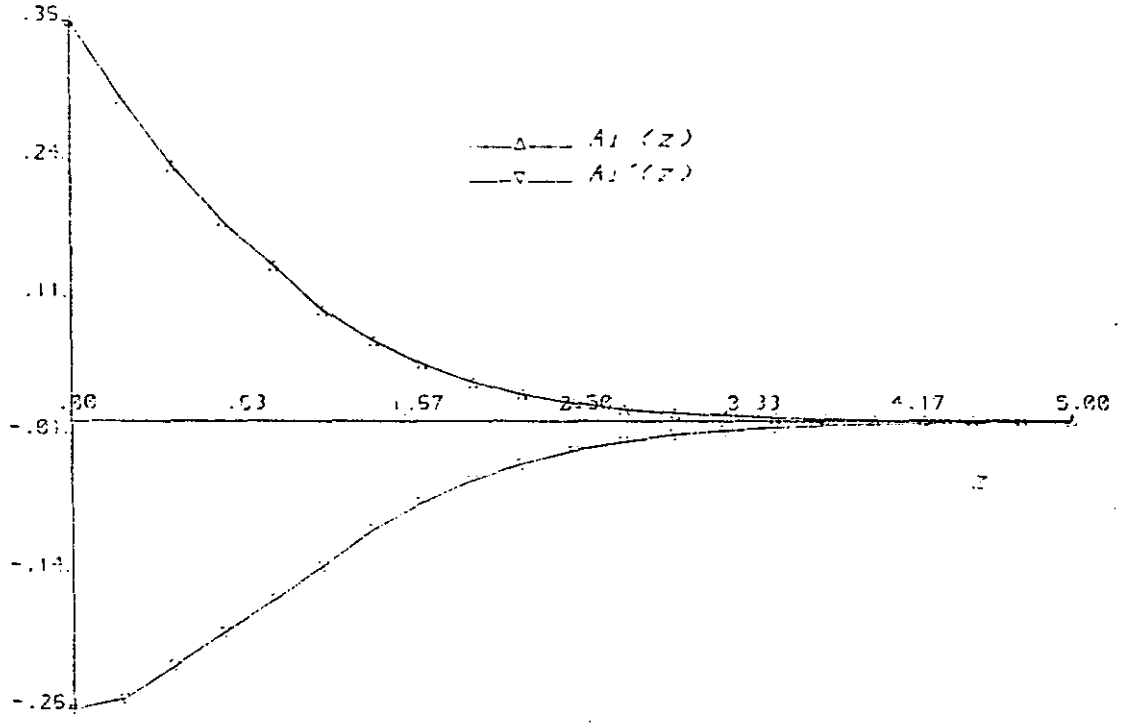

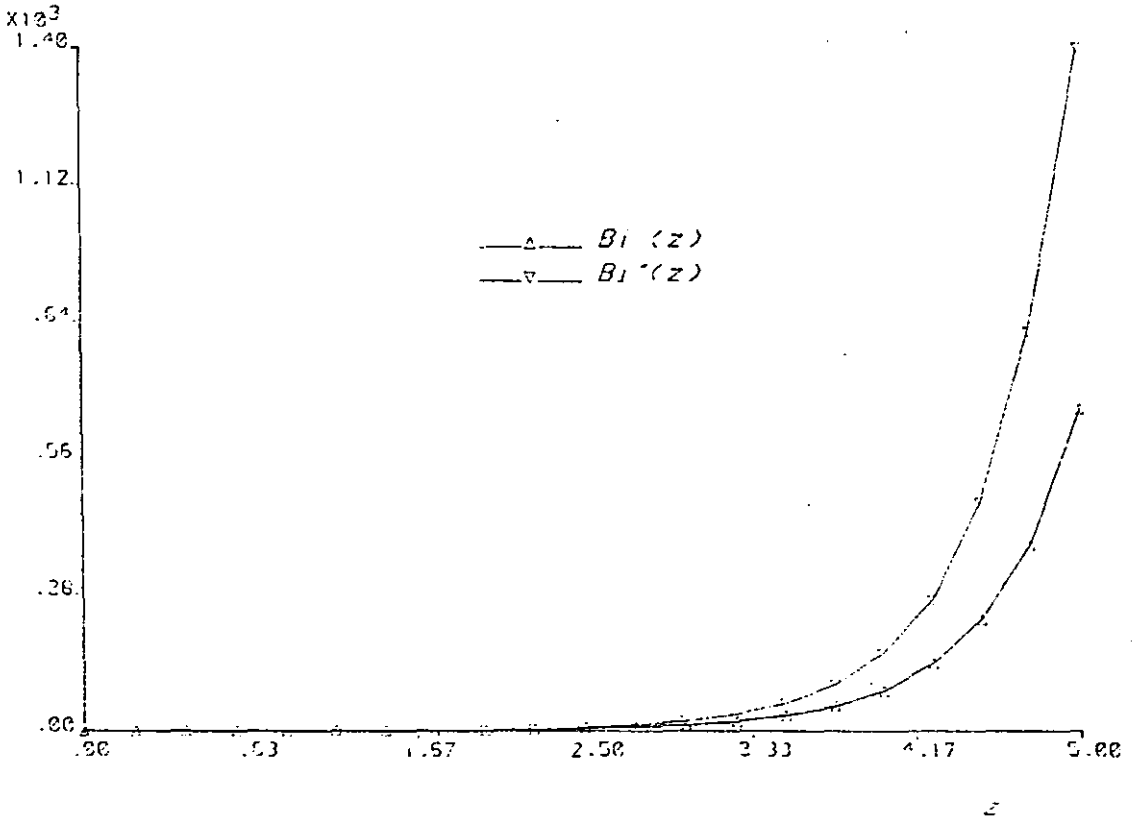

Fig. 1B *Airy Functions For pozitive Arguments*

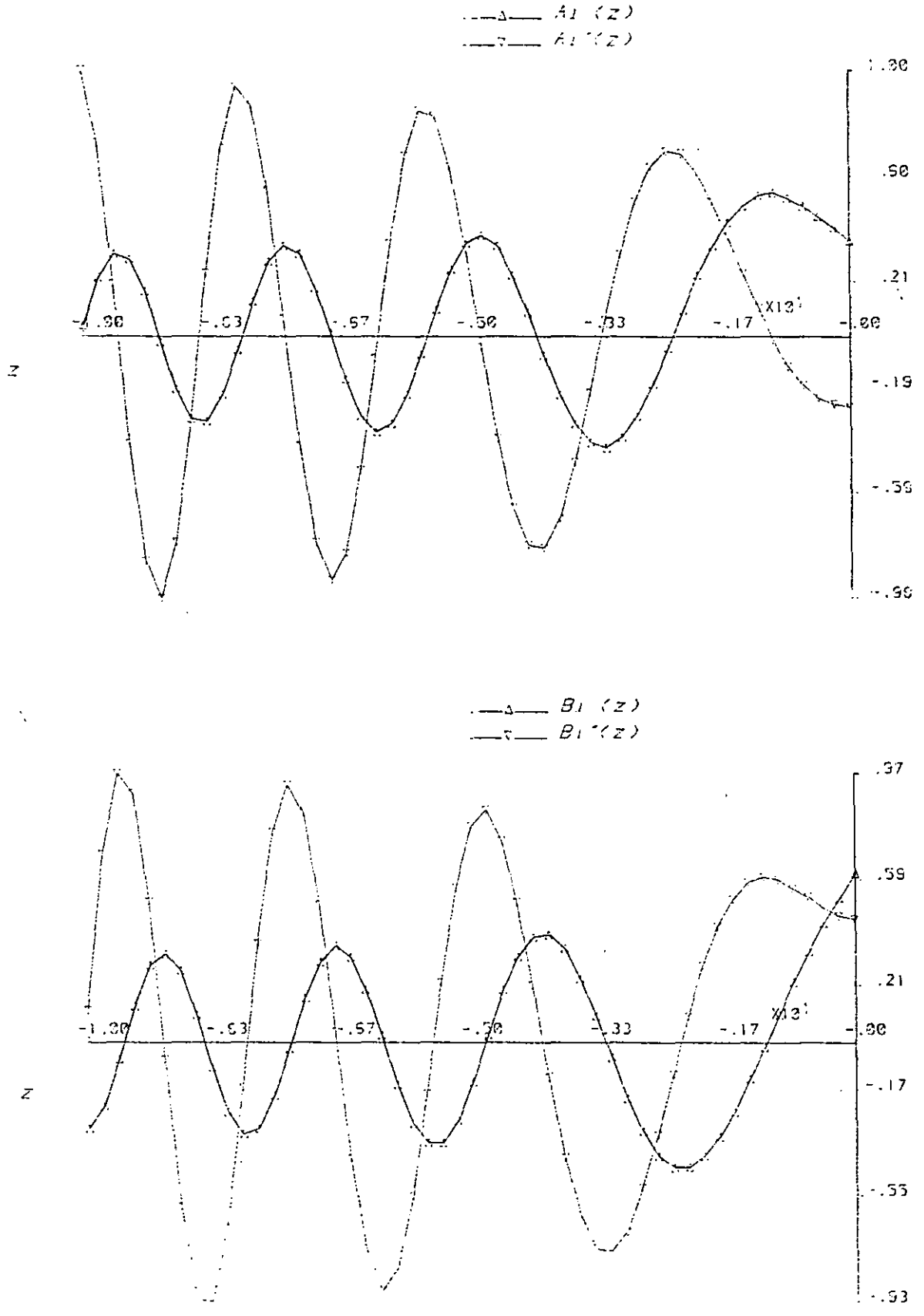

Fig. 2B *Airy Functions for negative arguments*

With a few examples the table below demonstrates the success and efficiency of algorithm routines constructed for Airy functions. The processing time for a single result was nominally 1 second, at the most rising to 3 seconds for large arguments.

2. BESSEL FUNCTIONS

Definition: The differential equation

$$z^2 \frac{d^2W}{dz^2} + z \frac{dW}{dz} \pm (z^2 + \nu^2)\, W = 0 \qquad (23B)$$

will accept as solutions the linearly independent combinations of $J_\nu(z)$, $Y_\nu(z)$ and $I_\nu(z)$, $K_\nu(z)$ with the first two corresponding to the case of plus sign in front of the parentheses. In general both z and ν may assume complex values.

Behaviour: The particular region of interest is where z is real and ν integer. Under these circumstances oscillatory behaviour is exhibited by J and Y. For a fixed order (ν) K decreases with increasing argument, and the opposite occurs with I.

Series Representation: Amongst the many which have been derived (3), the ones employed in simulation were

$$J_\nu(z) = (z/2)^\nu \sum_{k=1}^{\infty} \frac{(-1)^k\, (z^2/4)^k}{k!\, \Gamma(\nu + k + 1)} \qquad (24B)$$

$$Y_m(z) = (2/\pi)\, [\ln (z/2) - \Psi(m+1)]\, J_m(z)$$

$$- \frac{m!\, (z/2)^{-m}}{\pi} \sum_{k=0}^{m-1} \frac{(z/2)^k\, J_k(z)}{(m - k)\, k!}$$

TABLE (B1) : AIRY FUNCTIONS

Computed Figures	From Tables	Prog. Type
Ai (1.0) = 0.1352924163D 00	Ai (1.0) = 0.13529242D 00	(1)
Ai'(1.0) =-0.1591474413D 00	Ai'(1.0) =-0.15914744D 00	(1)
Bi (1.0) = 0.1207423595D 01	Bi (1.0) = 1.20742359D 00	(2)
Bi'(1.0) = 0.9324359334D 00	Bi'(1.0) = 0.93243593D 00	(2)
Ai (-1.0) = 0.5355608833D 00	Ai (-1.0) = 0.53556088D 00	(1)
Ai'(-1.0) =-0.1016056712D-01	Ai'(-1.0) =-0.10160570D-01	(1)
Bi (-1.0) = 0.1039973895D 00	Bi (-1.0) = 0.10399739D 00	(1)
Bi'(-1.0) = 0.5923756264D 00	Bi'(-1.0) = 0.59237563D 00	(1)
Ai (10.0) = 0.1104753255D-09	Ai (10.0) = 0.110475D-09 *	(1)
Ai'(10.0) =-0.3520633677D-09	Ai'(10.0) =-0.352062D-09 *	(1)
Bi (10.0) = 0.4556411535D 09	Bi (10.0) = 0.455679D 09 *	(2)

TABLE (B1)
(Continued)

Bi'(10.0) = 0.1429236134D 10	Bi'(10.0) = 0.142923D 10 *	(2)
Ai (-10.0) = 0.4024123849D-01	Ai (-10.0) = 0.40241240D-01	(1)
Ai'(-10.0) = 0.9962650441D 00	Ai'(-10.0) = 0.99626504D 00	(1)
Bi (-10.0) =-0.3146798296D 00	Bi (-10.0) =-0.31467983D 00	(1)
Bi'(-10.0) = 0.1194141134D 00	Bi'(-10.0) = 0.11941411D 00	(1)

Description of Programmes :

Type (1) : Method used - Integration

No of segments = 5 1) Main 2) Function subroutine for K_v(y) 3) Function subroutine for J_v(y) (first part) 4)Function subroutine for J_v(y) (second part) 5) Integral function subroutine .

Type (2) : Method used - Summation

No of segments = 1 , Main

* These values are by means of interpolation from the sub_tables given in Abramowitz(2)

$$- (2/\pi) \sum_{k=1}^{\infty} \frac{(-1)^k (m + 2k)}{k (m + k)} J_{m+2k}(z) \qquad (25B)$$

The subscript (m) used for Y implies that the validity of the series is limited to integer orders. Ψ is known as the logarithmic derivative of the Gamma function. The latter expansion is due to Neumann.

Similar series exist for I and K. The transformations invoked for this purpose and also referred to in the course of the report are:

$$-\pi/2 < \text{Arg } z < \pi$$

$$I_\nu(z) = e^{\nu\pi j/2} J_\nu (z e^{-\pi j/2}) \qquad (26B)$$

$$K_\nu(z) = - \frac{\pi j}{2} e^{-\nu\pi j/2} [J_\nu (z e^{-\pi j/2}) - j Y_\nu(z e^{-\pi j/2})] \qquad (27B)$$

$$= - \frac{\pi j}{2} e^{-\nu\pi j/2} H_\nu^2 (z e^{-\pi j/2}) \qquad (28B)$$

where the definition of Hankel function $H_\nu^2(z)$ can be readily understood from the third line of statement. (In this work unless the need arises to specifically distinguish between $H_\nu^1(z)$ and $H_\nu^2(z)$, the latter is written as $H_\nu(z)$).

Numerous integral representations may be cited in several sources on Bessel functions (2, 3, 5). A collection of these were initially attempted, and the overall experience gained suggests that those involving the dependence of the order inside the integrand

in terms of variables other than circular or hyperbolic function will easily attain 5 to 6 decimal places of accuracy.

However as z becomes complex, most of these integral formulae fail primarily because of the restrictions imposed on the argument of z. Even within the permitted range, proper convergence cannot be guaranteed. It may be said that there is no single routine which will uniformly evaluate the Bessel function concerned regardless of the position of z in the complex plane. The reason for switching from K, I to H, J in the section of modal analysis now becomes obvious.

One final note, Psi function (Ψ) present in 25B was obtained using the series

$$\Psi(m) = - Eu + \sum_{k=1}^{m-1} k^{-1} \qquad (29B)$$

Eu = Euler's constant.

The sum being finite, this did not present any problems.

The degree of success for computing Bessel function of complex arguments may be explored from the following numerical results. Since these could not be found in any mathematical tables, the test procedure was by means of the recurrence relationship.

$$J_{Y\,m-1}(z)\ J_{Y\,m+1}(z) = \frac{2m}{z}\ J_{Y\,m}(z) \qquad (30B)$$

The effect of oscillations in the series for Y were gradually felt as z increased. The integral

$$Y_m(x) = \frac{1}{\pi} \int_0^{\pi} \mathrm{Sin}\,(x\,\mathrm{Sin}t - mt)dt$$

$$- \frac{1}{\pi} \int_0^{1} (t^{m+1} + (-1)^m\, t^{-m+1})\, e^{-x(1/t-t)/2} dt \qquad (31B)$$

TABLE (B2) : BESSEL FUNCTIONS

A) FOR COMPLEX ARGUMENTS

	Computed Figures	Rel. Err.
J_10 (1.0 + j 0.1D-39)	= 0.2630615124D-09 + j 0.2618635056D-48	-0.654D-12 + j 0.397D-12
Y_10 (1.0 + j 0.1D-39)	=-0.1216180143D 09 + j 0.1209399938D-30	0.000D 00 - j 0.694D-12
J_10 (1.0 + j 0.1D 00)	= 0.1512432343D-09 + j 0.2315206016D-09	0.270D-11 + j 0.258D-11
Y_10 (1.0 + j 0.1D 00)	=-0.6336647071D 08 + j 0.9678440726D 08	-0.324D-12 + j 0.189D-12
J_50 (1.0 + j 0.1D-39)	= 0.2906004948D-79 - j 0.1452717545-117	0.000D 00 - j 0.811D-12
Y_50 (1.0 + j 0.1D-39)	=-0.2191142813D 78 + j 0.1095347797D 40	0.000D 00 - j 0.265D-11
J_50 (1.0 + j 0.1D 00)	= 0.9943179823D-80 - j 0.3591850101D-79	0.344D-10 + j 0.129D-10
Y_50 (1.0 + j 0.1D 00)	=-0.4557478951D 77 - j 0.1646588972D 78	-0.471D-10 + j 0.105D-10
J_10 (10.0 + j 0.1D-39)	= 0.2074861066D 00 + j 0.8436957863D-41	-0.164D-10 - j 0.847D-09
Y_10 (10.0 + j 0.1D-39)	=-0.3596497556D 00 + j 0.1607229758D-40	-0.285D-01 + j 0.355D-01
J_10 (10.0 + j 0.1D 00)	= 0.2075282178D 00 + j 0.8443594163D-02	0.428D-10 - j 0.353D-09
Y_10 (10.0 + j 0.1D 00)	=-0.3595710405D 00 + j 0.1605973821D-01	-0.283D-01 + j 0.354D-01
J_50 (10.0 + j 0.1D-39)	= 0.1784513608D-29 + j 0.8745935255D-69	-0.520D-11 - j 0.497D-11
Y_50 (10.0 + j 0.1D-39)	=-0.3641066496D 28 + j 0.1782975775D-11	-0.125D-08 - j 0.555D-09
J_50 (10.0 + j 0.1D 00)	= 0.1578483906D-29 + j 0.8421174694D-30	0.292D-11 + j 0.105D-10
Y_50 (10.0 + j 0.1D 00)	=-0.3205009184D 28 + j 0.1768148927D 28	-0.177D-08 - j 0.985D-09

TABLE (B2)
(Continued)

B) FOR REAL ARGUMENTS

Computed Figures	From Tables
J_10 (1.0) = 0.2630615124D-09	J_10 (1.0) = 0.2630615124D-09
Y_10 (1.0) =-0.1216180143D 09	Y_10 (1.0) =-0.1216180143D 09
J_50 (1.0) = 0.2906004948D-79	J_50 (1.0) = 0.2906004948D-79
Y_50 (1.0) =-0.2191142813D 78	Y_50 (1.0) =-0.2191142813D 78
J_10 (10.0) = 0.2074861066D 00	J_10 (10.0) = 0.2074861066D 00
Y_10 (10.0) =-0.3596497556D 00	Y_10 (10.0) =-0.3598141522D 00
J_50 (10.0) = 0.1784513608D-29	J_50 (10.0) = 0.1784513608D-29
Y_50 (10.0) =-0.3641066496D 28	Y_50 (10.0) =-0.3641066502D 28

Description of Programmes :

Y_m(z) : Method used - Summation

No of segments : 2 1) Main 2) Subroutine for J_m(z)

J_m(z) : Method used - Summation

No of segments : 1 , Main

TABLE (B2)
(Continued)

C) FOR LARGE ARGUMENTS OF $Y_m(x)$

Computed Figures	From Tables
$Y_{10}(10.0) = -0.3598141522D\ 00$	$Y_{10}(10.0) = -0.3598141522D\ 00$
$Y_{10}(50.0) = 0.5723897182D-02$	$Y_{10}(50.0) = 0.5723897953D-02$
$Y_{50}(10.0) = -0.3641066502D\ 28$	$Y_{50}(10.0) = -0.3641066502D\ 28$
$Y_{50}(50.0) = -0.2103165546D\ 00$	$Y_{50}(50.0) = -0.2103165558D\ 00$

Description of Programme :

Method used - Integration

No of segments : 4 1) Main 2) Function subroutine for $Y_m(x)$ (first part)

3) Function subroutine for $Y_m(x)$ (second part) 4) Integral function subroutine

was however able to cope with arguments up to x = 50.0 (x real).

3. CONFLUENT HYPERGEOMETRIC FUNCTION

Definition: The differential equation

$$z \frac{d^2W}{dz^2} + (B - z) \frac{dW}{dz} - AW = 0 \qquad (32B)$$

has solutions M(A,B,z) and Uh(A,B,z). Though M and Uh are functions of three variables A, B, z all of which may be complex, z is usually considered to be the main argument. In the hierarchy, of Transcendental functions, they constitute a special class of more general hypergeometric functions. Below only M will be discussed.

Behaviour: Depending on the magnitude and the sign of A and B a combination of oscillatory, decaying and growing types of behaviour are to be observed. Some of these are illustrated by the plots in Figure 3B.

Series Representation:

$$M(A,B,z) = \sum_{k=0}^{\infty} \frac{\Gamma(A+k)}{\Gamma(B+k)} \frac{\Gamma(B)}{\Gamma(A)} \frac{z^k}{k!} \qquad (33B)$$

Hence M fails to be defined when B takes on negative integer values, otherwise the series is convergent.

Within the context of this work, A was real or complex, B positive integer and z a variable being related to fibre parameters

as well as the radial dependence. The contrived routine additionally incorporated the trivial case of A being a negative integer.

Whittaker, by modifying the differential equation in 32B put forward a slightly different notation for M (4).

$$\text{Whittaker } M(A,B,z) = e^{-z/2}\, z^{B+\frac{1}{2}}\, M(\tfrac{1}{2} + B-A,\ 1+2B,z) \qquad (34B)$$

An integral representation that is relatively simple is

$$\text{Re } B > \text{Re } A > 0$$

$$M(A,B,z) = \frac{\Gamma(B)}{\Gamma(B-A)\ \Gamma(A)} \int_0^1 e^{zt}\, t^{A-1}\, (1-t)^{B-A-1}\, dt \qquad (35B)$$

Nevertheless, the stringent requirements on A and B render this approach somewhat futile. By the repeated application of the recurrence formula

$$M(A,B,z) = M(A+1,\ B,z) - \frac{z}{B}\, M(A+1,\ B+1,\ z) \qquad (36B)$$

and assuming B to be an integer, a series may be arrived at

$$M(A,B,z) = \sum_{k=0}^{Na+1} (-1)^k\, \frac{z^k\, M(A+Na+1,\ A+k,\ z)\ C_k^{Na+1}}{[(B+k-1)!/(B-1)!]} \qquad (37B)$$

$$Na = \text{Int}\,(\text{abs}(A)), \quad C_k^{Na+1} = \frac{(Na+1)!}{(Na+1-k)!\;k!} \quad \text{(Binomial coefficient)}$$

such that the necessary condition Re (A+Na+1) > 0 is now accounted for.

The initial calculations were performed using this method. However it was later abandoned since excessive computation time was required.

The second algorithm on confluent hypergeometric function involved the derivative with respect to:

$$-\frac{\partial}{\partial A} + 2\frac{\partial}{\partial B} \tag{38B}$$

Thus, when used on 33B:

$$U(A,B,z) = \left(-\frac{\partial}{\partial A} + 2\frac{\partial}{\partial B}\right) M(A,B,z)$$

$$= \sum_{k=0}^{\infty} \frac{(A)_k}{(B)_k} \left[-\Psi(A+k) + \Psi(A) - 2\Psi(B+k) + 2\Psi(B)\right] \frac{z^k}{k!} \tag{39B}$$

where for convenience $\Gamma(A+k)/\Gamma(A)$ is designated as $(A)_k$ and likewise for B.

In this implementation, it was discovered that an infinite series representation for $\Psi(A)$ did not produce the expected convergence. Instead the integral

$$\Psi(A) = -Eu + \int_0^1 \frac{1 - t^{A-1}}{1 - t}\,dt \tag{40B}$$

had to be assigned, then with the help of

$$\Psi(1-A) = \Psi(A) + \pi \mathrm{Cot}\ (\pi A) \tag{41B}$$

the results was converted into Psi function of negative argument. The values of $\Psi(A+k)$ were successively recovered from

$$\Psi(A+1) = \Psi(A) + \frac{1}{A} \tag{42B}$$

The kth derivative of M with respect to z may be inferred from 33B

$$\frac{d^k}{dz^k} M(A,B,z) = \frac{(A)_k}{(B)_k} M(A+k, B+k, z) \tag{43B}$$

One final remark is that the most asymptotic form quoted in some literature (2,5)

as $z \to \infty$

$$M(A,B,z) = \frac{\Gamma(B)}{\Gamma(A)} e^z z^{A-B} (1 + O(z^{-1})) \tag{44B}$$

O = order of

should have the constraint of Re $A > 0$.

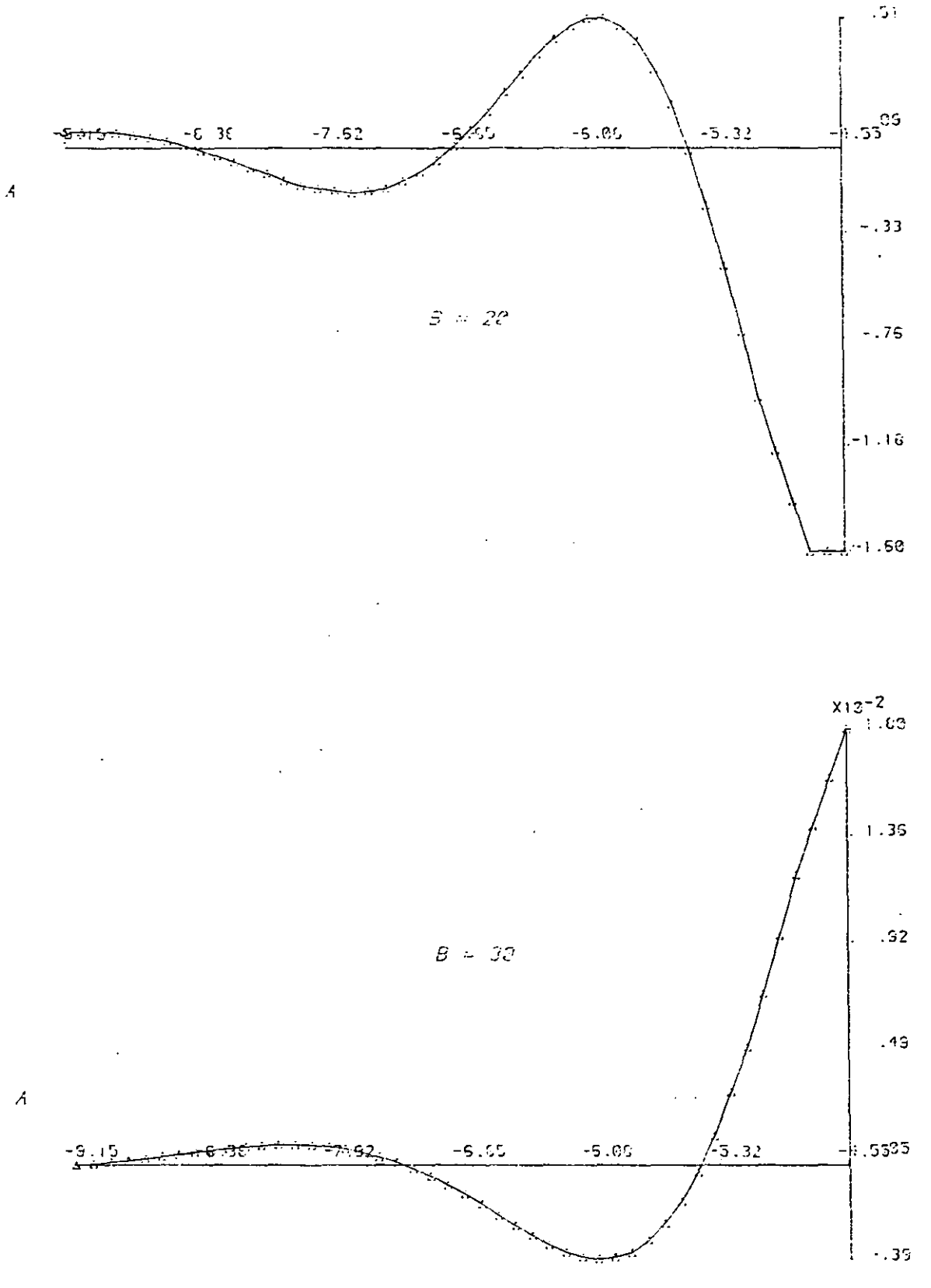

Fig. 3B Confluent Hypergeometric Function (z=48.84)

TABLE (B3) : CONFLUENT HYPERGEOMETRIC FUNCTION

1) FUNCTION ITSELF

A) WHEN - A - REAL

Computed Figures	Rel. Err.
M (-5.5 , 10 , 48.84) = 0.7390521206D 04	-0.123D-11
M (-1.5 , 30 , 48.84) = 0.7992837781D 00	-0.166D-11

B) WHEN - A - COMPLEX

Computed Figures	Rel.Err.
M (-5.5 - j 0.1D-39 , 10 , 48.84) = 0.7390521206D 04 - j 0.8291191180D-36	-0.123D-11 + j 0.170D-11
M (-5.5 - j 0.1D 00 , 10 , 48.84) = 0.7681402644D 04 - j 0.8689598562D 03	-0.118D-11 + j 0.162D-11
M (-1.5 - j 0.1D-39 , 30 , 48.84) = 0.7992837781D 00 - j 0.2005294715D-40	-0.166D-11 - j 0.128D-11
M (-1.5 - j 0.1D 00 , 30 , 48.84) = 0.8324309346D 00 - j 0.2470102051D-01	0.119D-13 - j 0.127D-11

TABLE (B3)
(Continued)

2) DERIVATIVE *

Computed Figures	Rel. Err.
M ' (-5.5 , 10 , 48.84) =-0.28246474 50D 05	-0.138D-10
M ' (-1.5 , 30 , 48.84) =-0.85450431 09D 00	-0.121D-09

Computed Figure	From tables
M (-0.9 , 1 , 10.0) =-0.5211212875D 02	M (-0.9 ,1 , 10.0) =-0.52112129D 02

Description of Programme :

Method used - Summation & Integration

No of segments : 3 1) Main a) Function & Derivative when - a - complex

b) Function when - a - negative integer 2) Function subroutine for Psi

3) Integral function subroutine

* This derivative is w.r.t. Eq.(38B)

The computed figures will now be presented. As earlier, the check on accuracy was via the known recurrence (36B). Only one example is attached at the end where the accompanying figure could be looked up in Ref 2.

Other Functions:

4. Gamma Function

This was evaluated using the formula

$$\Gamma(z) = \sum_{k=0}^{\infty} \frac{(-1)^k}{k!} \frac{1}{z+k} + \int_0^1 e^{-1/t}\, t^{-z-1}\, dt \qquad (45B)$$

where the characteristic of the representation (i.e. identifying the original part of the integration from 0 to 1 as a sum (6)) allows for negative values of the argument as well as positive.

5. Laguerre Polynomials

These are obtained when

$$M_{-A\to k}(-A,B,x) = C^{k}_{k+B-1}\, L_k^{B-1} \qquad (46B)$$

Since this case was readily included in the computation of M, no separate routine was devised for Laguerre polynomials. Some useful properties are

$$L_k^B(0) = \frac{(B+1)_k}{k!} \qquad (47B)$$

$$L_k^B(x) = (-1)^k \frac{d^k}{dx^k} L_{B+k}(x) \qquad (48B)$$

$$(k+B)\, L_k^{B-1}(x) = (k+1)\, L_{k+1}^B(x) - (k+1-x)\, L_k^B(x) \qquad (49B)$$

Integral Function Subroutine

This programme consisted of four segments:

1. 255 data points of an interlaced Gauss quadrature rule.
2. Function to detect singularities in the integral and remove them.
3. Subroutine to evaluate the integral to a specified accuracy.
4. Random number generator to test for convergence.

Based on a method proposed by Patterson (7) integrals with a semi-infinite range could be submitted to it, after creating a suitable singularity. The success of the output could be determined from the value of a returned parameter. No difficulties in this respect were experienced, as far as previously described mathematical functions are concerned.

Notes on Programmes in General

All together 25 programmes were constructed. A great majority of them operated in double precision, necessitated by the nature of computations undertaken.

Three main types of algorithms were encountered (a) summation, (b) integration, (c) root-finding.

Series, as already explained, could be handled easily provided that the oscillations decayed at a sufficiently rapid rate.

For the integral evaluations, the borrowed routine was employed for quite a number of instances other than the mathematical functions. Indeed, it was discovered that none of the NAG library subroutines would yield the kind of convergence demanded. In the case of the double and triple integrations performed, the final calculation was realized through this routine while the intermediate stages were implemented by the NAG library. The desired result was achieved as long as care was taken to supply the function in the tidiest analytic form.

Under exceptional circumstances however, to avoid exceeding the permitted processing time, some of the accuracy limits had to be reduced (10^{-4} in the worst case).

Solving non-linear equations was extremely tedious, since the NAG library programmes were used solely for this task, thus affording no external control. The NAG routines although some of them were quite powerful in approaching the root, possessed only one means of initial testing, which was to check the signs of the user prepared function at the respective ends of the defined interval. Clearly, if two roots lay close to each other, this procedure would hardly produce the expected result. Therefore strict consistency requirements (particularly relevant to Chapter One, Filtering Theory) had to be imposed prior to testing for sign changes.

REFERENCES

Introduction

1. J E Midwinter, *'Optical Communication Today and Tomorrow'*, Elect. & Power, Vol. 24, No. 6, pp. 442-447, 1978.

2. F P Kapron, *'Maximum Information Capacity of Fibre Optic Waveguides'*, Elect. Lett., Vol. 13, No. 4, pp. 96-97, 1977.

3. F R McDevitt et al, *'Optimized Designs for Fibre Optic Cable Television Systems'*, IEEE Trans. on Cable Television, Vol. 2, No. 4, pp. 169-194, 1977.

4. J G Farrington and M Chown, *'An Optical Fibre Multiterminal Data System for Aircraft'*, Fibre and Integrated Optics, Vol. 2, No. 2, pp. 173-193, 1979.

5. H T Eyyuboglu, *'A Preliminary Investigation into the Design of a Military Communication Network Using Optical Fibres'*, Ph.D. Initial Report, LUT, 1978.

6. L.Jeunhomme and J P Pocholle, *'Experimental Determination of the Radiation Pattern of Optical Fibres'*, Opt. Com. Vol. 12, No. 1, pp. 89-92, 1974.

7. D L Bisbee, *'Measurement of Loss Due to Offsets and End Separations of Optical Fibres'*, BSTJ, Vol. 50, No. 10, pp. 3159-3168, 1971.

8. A H Cherin and P J Rich, *'Measurement of Loss and Output Numetical Aperture of Optical Fibre Splices'*, Appl. Opt., Vol. 17, No. 4, pp. 642-645, 1978.

9. J A Kong, *'Theory of Electromagnetic Waves'*, John Wiley and Sons, New York, 1975.

10. A W Snyder, *'Asymptotic Expressions for Eigen-functions and Eigenvalues of a Dielectric or Optical Waveguides'*, IEEE Trans. MTT, Vol. 17, No. 12, pp. 1130-1138, 1969.

Chapter 1

1. L B Felson, *'Rays, Modes and Beams in Optical Fibre Waveguides'*, Opt. Quant. Elect. Vol. 9, No. 3, pp. 189-195, 1977.

2. P J Stevens, *'An Experimental Study of Propagation in Multimode Optical Waveguides using Spatially Incoherent Probe Techniques'*, Ph.D. Thesis, LUT, 1976.

3. A W Snyder and J D Love, *'Attenuation Coefficient for Tunnelling Leaky Rays in Graded Fibres'*, Elect. Lett., Vol. 12, No. 13, pp. 324-326, 1976.

4. J D Love and C Winkler, *'Refracting Leaky Rays in Graded Index Fibres'*, Appl. Opt. Vol. 17, No. 14, pp. 2205-2208, 1978.

5. J D Love and C Winkler, *'A Universal Tunnelling Coefficient for Step and Graded Index Multimode Fibres'*, Opt. Quant. Elect., Vol. 10, No. 4, pp. 341-351, 1978.

6. M Abramowitz and I A Stegun, *'Handbook of Mathematical Functions'*, Dover Publications, New York, 1968.

7. K Petermann, *'The Mode Attenuation in General Graded Core Multimode Fibres'*, Archiv. Electron. Ubertragungs-tech, Vol. 29, No. 7/8, pp. 345-348, 1975.

8. A H Hartog and M J Adams, *'On the Accuracy of the WKB Approximation in Optical Dielectric Waveguides'*, Opt. Quant. Elect., Vol. 9, No. 3, pp. 223-232, 1977.

9. C Pask, *'Equal Excitation of All Modes of an Optical Fibre'*, J. Opt. Soc. Am., Vol. 68, No. 5, pp. 572-576, 1978.

10. D J Carpenter and C Pask, *'Optical Fibre Excitation by Partially Coherent Sources'*, Opt. Quant. Elect., Vol. 8, No. 6, pp. 545-556, 1976.

11. J D Love and C Pask, *'Universal Curves for Power Attenuation in Ideal Multimode Fibres'*, Elect. Lett., Vol. 12, No. 10, pp. 254-255, 1976.

12. C Pask, *'Generalized Parameters for Tunnelling Ray Attenuation in Optical Fibres'*, J. Opt. Soc. Am., Vol. 68, No. 1, pp. 110-116, 1978.

13. K F Barrell and C Pask, *'Ray Launching and Observation in Graded Index Optical Fibres'*, ibid, Vol. 69, No. 2, pp. 295-301, 1979.

14. J D Love and C Winkler, *'Attenuation and Tunnelling Coefficients for Leaky Rays in Multilayered Optical Waveguides'*, ibid, Vol. 67, No. 12, pp. 1627-1633, 1977.

15. P Di Vita and R Vannucci, *'Loss Mechanism of Leaky Skew Rays in Optical Fibres'*, Opt. Quant. Elect., Vol. 9, No. 3, pp. 177-188, 1977.

16. K F Barrell and C Pask, *'The Effect of Cladding Loss in Graded Index Fibres'*, ibid. Vol. 10, No. 3, pp. 223-231, 1978.

17. J D Love and C.Winkler, *'The Effects of Material Absorption on Ray Power Attenuation in Multilayered Optical Waveguides'*, ibid, pp. 383-392.

18. J D Love and C Winkler, *'Generalized Fresnel Power Transmission Coefficients for Curved Graded Index Media'*, IEEE Trans. MTT, Vol. 28, No. 7, pp. 689-695, 1980.

19. D Gloge, *'Propagation Effects in Optical Fibres'*, ibid, Vol. 23, No. 1, pp. 106-120, 1975.

20. A Ankiewicz, *'Ray Theory of Graded Noncircular Optical Fibres'*, Opt. Quant. Elect., Vol. 11, No. 3, pp. 197-203, 1979.

21. D L Bisbee, *'Measurement of Loss due to Offsets and End Separations of Optical Fibres'*, BSTJ, Vol. 50, No. 10, pp. 3159-3168, 1971.

22. T C Chu and A R McCormick, *'Measurements of Loss Due to Offset, End Separation and Angular Misalignment in Graded Index Fibres Excited by an Incoherent Source'*, BSTJ, Vol. 57, No. 3, pp. 595-602, 1978.

23. F T Stone, *'Launch Dependent Loss in Short Lengths of Graded Index Multimode Fibres'*, Appl. Opt., Vol. 17, No. 17, pp.2825-2830, 1978.

24. V V Grigoryants et al, *'The Influence of the Cladding on Light Attenuation of Multimode Fibres'*, Opt. Quant. Elect., Vol. 11, No. 4, pp. 367-369, 1979.

25. N Kashima and N Uchida, *'Transmission Characteristics of Graded Index Optical Fibres with a Lossy Outside Layer'*, Appl. Opt., Vol. 17, No. 8, pp. 1199-1207, 1978.

Chapter II

1. C N Kurtz & W Streifer, *'Guided Waves in Inhomogeneous Focussing Media Part I'*, IEEE Trans. MTT, Vol.17, No. 1, pp. 11-17, 1969.

2. A W Snyder and D J Mitchell, *'Leaky Rays on Circular Optical Fibres'*, J. Opt. Soc. Am., Vol. 64, No. 5, pp. 599-607, 1974.

3. H Unger, *'Planar Optical Waveguides and Fibres'*, Oxford University Press, East Kilbridge, Scotland, 1977.

4. A W Snyder and W R Young, *'Modes of Optical Waveguides'*, J. Opt. Soc. Am., Vol. 68, No. 3, pp. 297-309, 1978.

5. D Gloge, *'Weakly Guiding Fibres'*, Appl. Opt., Vol. 10, No. 10, pp. 2252-2258, 1971.

6. B K Garside et al, *'Propagation Characteristics of Parabolic Index Fibre Modes: Linearly Polarized Approximation'*, J. Opt. Soc. Am., Vol. 70, No. 4, pp. 395-400, 1980.

7. M Hashimoto et al, *'Analysis of Guided Waves Along the Cladded Optical Fibre: Parabolic Index Core and Homogeneous Cladding'*, IEEE Trans.MTT Vol.25, No. 1, pp. 11-17, 1977.

8. Y Kokubun and K Iga, *'Mode Analysis of Graded Index Optical Fibres Using a Scalar Wave Equation Including Gradient Terms and Direct Numerical Integration'*, J. Opt. Soc. Am., Vol. 70, No. 4, pp. 388-394, 1980.

9. P Di Vita and U Rossi, *'A Modal Approach to Propagation in Graded Optical Fibres'*, Optica Acta, Vol. 27, No. 8, pp. 1117-1125, 1980.

10. T K Lim et al, *'Guided Modes in Fibres with Parabolic Index Core and Homogeneous Cladding'* Opt. Quant. Elect., Vol. 11, No. 4, pp. 329-344, 1979.

11. R Olshansky, *'Leaky Modes in Graded Index Optical Fibres'*, Appl. Opt., Vol. 15, No. 11, pp. 2773-2777, 1976.

12. M O Vassell, *'Calculation of Propagating Modes in a Graded Index Optical Fibre'*, Opto-Elect., Vol. 6, No. 3, pp. 271-286, 1974.

13. K Okamoto and T Okoshi, *'Vectorial Wave Analysis of Inhomogeneous Optical Fibres Using Finite Element Method'*, IEEE Trans. MTT, Vol. 26, No. 2, pp. 109-114, 1978.

14. T Okoshi and K Ukamoto, *'Analysis of Wave Propagation in Inhomogeneous Optical Fibres Using a Variational Method'*, ibid, Vol. 22, No. 11, pp. 938-945, 1974.

15. K Okamoto and T Okashi, *'Computer Aided Synthesis of the Optimum Refractive Index Profile for Multimode Fibre'*, ibid, Vol. 25, No. 3, pp. 213-220, 1977.

16. A S Belanov, *'Filtering of Higher Order Modes in Optical Waveguides'*, Radio Eng. and Elect. Phys., Vol. 23, No. 1, pp. 11-19, 1978.

17. A Yata and H Ikuno, *'Cutoff Frequencies of W Type Fibre with Polynomial Profile Core'*, Elect. Lett., Vol. 17, No. 1, pp. 9-11, 1981.

Chapter III

1. F T Anecchi and E O Schulz-dubois, *'Laser Handbook'*, Vol. I, North Holland, Amsterdam, 1972.

2. S Sugimoto et al, *'100 Mb/s 12 km and 400 Mb/s 8 km Optical Fibre Transmission Experiments'*, Elect. Lett., Vol. 13, No. 21, pp. 635-637, 1977.

3. M Ettenberg et al, *'Very High Irradiance Edge Emitting LED'*, IEEE J. Quant. Elect., Vol. 12, No. 6, pp.360-364, , 1976.

4. Y Horikashi et al, *'High Irradiance Light Emitting Diodes'*, Japan J. Appl. Phys., Vol. 15, No. 3, pp. 485-492, 1976.

5. W M Muska et al, *'Material Dispersion Limited Operation of High Bit Rate Optical Fibre Data Links Using LEDs'*. Elect. Lett., Vol. 13, No. 20, pp. 605-607, 1977.

6. D J Brace and I A Ravenscroft, *'Optical Fibre Transmission Systems: The 8.448 Mb/s Feasibility Trial'*, POEEJ, Vol. 70, No. 3, pp. 146-153, 1977.

7. F Albertin et al, *'Geometrical Theory of Energy Launching and Pulse Distorsion in Dielectric Optical Waveguides'*, Opto. Elect., Vol. 6, No. 4, pp. 369-386, 1974.

8. A Ankiewicz and C Pask, *'Geometric Optics Approach to Light Acceptance and Propagation in Graded Index Fibres'*, Opt. Quant., Elect., Vol. 9, No. 2, pp. 87-109, 1977.

9. M Born and E Wolf, *'Principles of Optics'*, Pergamon Press, Oxford, 1964.

10. P D Vita and R Vannucci, *'Multimode Optical Waveguides with Graded Refractive Index: Theory of Power Launching'*, Appl. Opt., Vol. 15, No. 11, pp. 2765-2772, 1976.

11. H Kogelnik and T Li, *'Laser Beams and Resomotors'*, Appl. Opt., Vol. 5, No. 10, pp. 1550-1567, 1966.

12. S Nemoto et al, *'Launching Efficiencies of the HE_{1m} Modes in a Self-Focussing Optical Fibre Waveguide'*, ibid, Vol. 14, No. 7, pp. 1543-1548, 1975.

13. M Imai and E H Hara, *'Excitation of Fundamental and Low Order Modes of Optical Fibre Waveguides by Gaussian Beams, I: Tilted Beams'*, ibid, Vol. 13, No. 8, pp. 1893-1899, 1974.

14. T Takenaka and O Fukumitsu, *'Some Wave Optics Considerations on an Optical Microdevice with Square Law Media'*, Elect. Com. Japan, Vol. 62, No. 4, pp. 97-104, 1979.

Chapter IV

1. D L Bisbee, *'Optical Fibre Joining Technique'*, BSTJ, Vol. 50, No. 10, pp. 3153-3158, 1971.

2. D Gloge et al, *'Optical Fibre End Preparation for Low Loss Splices'*, ibid, Vol. 52, No. 9, pp. 1579-1588, 1973.

3. J Leach, private communication, STL.

4. A Yariv, *'Introduction to Optical Electronics'*, Holt Rinehart and Winston, New York, 1976.

5. R C Weast, *'CRC Handbook of Chemistry and Physics'*, CRC Press, Florida, 1980.

6. I H Malitson, *'Interspecimen Comparison of the Refractive Index of Fused Silica'*, J. Opt. Soc. Am., Vol. 55, No. 10, pp. 1205-1209, 1965.

Appendix A

1. Reference 3 of Chapter II.

2. Reference 4 of Chapter I.

3. Reference 14 of Chapter I.

4. D Marcuse, *'Excitation of Parabolic Index Fibres with Incoherent Sources'*, BSTJ, Vol. 54, No. 9, pp. 1507-1530, 1975.

5. H A Nayfeh, *'Perturbation Methods'*, John Wiley and Sons, New York, 1973.

6. M Imai, *'Some Considerations of Idealized Gas Lens by Wave Optics'*, Elect. Com. Japan, Vol. 51, No. 5, pp. 69-77, 1968.

7. Reference 5 of Appendix B.

Appendix B

1. L Fox and I B Parker, *'Chebyshev Polynomial in Numerical Analysis'*, Oxford University Press, Belfast, Northern Ireland, 1968.

2. Reference 6 of Chapter I.

3. G N Watson, *'Theory of Bessel Functions'*, Cambridge University Press, Cambridge, 1958.

4. E T Whittaker and G N Watson, *'A Course of Modern Analysis,'* Cambridge University Press, Cambridge 1927.

5. A Erdelyi et al, *'Higher Transcendental Functions'*, Volume I, McGraw-Hill Book Co. Inc., New York, 1953.

6. N Lebedev, *'Special Functions and Their Applications'*, Prentice-Hall, New Jersey, 1965.

7. T N L Patterson, *'The Optimum Addition of Points to Quadrature Formulae'*, Math. Comp., Vol. 22, pp. 847-856, 1968.